POLY(AMIDOAMINE) DENDRIMER BASED NANOMATERIALS FOR DELIVERY OF ANTICANCER AGENTS

Ph.D. THESIS

by

ISHITA MATAI

CENTRE OF NANOTECHNOLOGY
INDIAN INSTITUTE OF TECHNOLOGY ROORKEE
ROORKEE-247667 (INDIA)
MAY, 2016

POLY(AMIDOAMINE) DENDRIMER BASED NANOMATERIALS FOR DELIVERY OF ANTICANCER AGENTS

A THESIS

Submitted in partial fulfilment of the requirements for the award of the degree

of

DOCTOR OF PHILOSOPHY

in

NANOTECHNOLOGY

by

ISHITA MATAI

CENTRE OF NANOTECHNOLOGY
INDIAN INSTITUTE OF TECHNOLOGY ROORKEE
ROORKEE-247667 (INDIA)
MAY, 2016

INDIAN INSTITUTE OF TECHNOLOGY ROORKEE
ROORKEE

CANDIDATE'S DECLARATION

I hereby certify that the work which is being presented in this thesis entitled **"POLY(AMIDOAMINE) DENDRIMER BASED NANOMATERIALS FOR DELIVERY OF ANTICANCER AGENTS"** in partial fulfilment of the requirements for the award of the Degree of Doctor of Philosophy and submitted in the Centre of Nanotechnology of the Indian Institute of Technology Roorkee, Roorkee is an authentic record of my own work carried out during a period from July, 2013 to May, 2016 under the supervision of Dr. P. Gopinath, Associate Professor, Department of Biotechnology, Indian Institute of Technology Roorkee, Roorkee.

The matter presented in this thesis has not been submitted by me for the award of any other degree of this or any other Institute.

(Ishita Matai)

This is to certify that the above statement made by the candidate is correct to the best of my knowledge.

Date: _____

(P. Gopinath)
Supervisor

Dedicated

to my Beloved Parents

ACKNOWLEDGEMENTS

I still remember the day when I joined Centre of Nanotechnology, IIT Roorkee as a research scholar, I had no idea that the experience I was about to gain in the following years would turn out to be a life-changing one. I can now understood the actual meaning of a doctoral degree. Today, when I sit back and amass the memories of the time I spent at IIT Roorkee, my heart is pounding with emotions and gratitude towards numerous people without whom, I would not be able to complete this wonderful journey of my Ph. D degree.

Before thanking anyone, I owe my everything to the Almighty, for it was 'His ultimate wish' that helped me cross all the barriers to reach this pleasant day. Thank you God for granting me the wisdom, health and strength to undertake this research task and enabling me to its completion.

I am extremely glad and grateful to my research supervisor, Dr. P.Gopinath, who happily accepted me as his Ph.D. student after completing my M.Tech dissertation under his able guidance. Undoubtingly, it was his unconditional belief in me which motivated me to pursue Ph.D. and surpass all the challenges I faced over these years. He was always there for me in difficult times with his valuable advice, patience, and guided me in the right direction. I have learnt a lot from him, and will always cherish my decision to work under him. Thank you Sir, for all your help, support and freedom.

Besides my supervisor, I am also indebted to Prof. S.K Nath, Prof. Anil Kumar, Prof. Vijaya Agarwala and Prof. R. Jayaganthan (Former and present Heads of Centre) and Prof. Ramesh Chandra (Head Institute Instrumentation Centre, IIT Roorkee) for their continuous motivation, support and for providing the necessary research facilities.

I owe my sincere thanks to my SRC committee, Prof. R.P Singh (Chairman SRC), Prof. G.D Verma, Prof. Partha Roy (External expert) and Dr. M. Sankar (Internal expert) who guided me through all these years. I am thankful for their encouragement, insightful comments, and precious suggestions.

My special thanks to the office staff of the Centre of Nanotechnology, Mr. Rawan pal, Mr. Vinod, Mr. Naresh, Mr. Riyaz, and Mr. Satinder, for they always welcomed me with smiling faces and helped me in every possible ways.

It is said that one can fight all the life's battles if he/she has an understanding and a loving family. My heartfelt thanks to my lab colleagues and my friends as a part of my IIT Roorkee family especially Abhay, Deepika, Dr. Mini, Vijayesh, Rajesh, Raj Kumar and Akshay for their research

help in the form of experiment planning and execution, data interpretation, scientific discussions and continuous encouragement. Their positive attitude, motivation, unending love and appreciation, served as my inner strength which only family and true friends can bestow. They were indeed the pillars of strength for both my personal and professional life all these years. I wish them happiness and success for life.

I also express my deep thanks to my other lab mates, Uday, Bharat, Poornima, Shanid, Raj Kumar, Dr. Saba, Vinay and Vaibhavi who were always there for me in my difficult times and helped me with their valuable suggestions, and immense support. I am really overwhelmed with their joyous behavior and encouragement which helped me complete my research work.

I would reserve as special place for Dr. S. Chockalingam, who joined our Nanobiotechnology group as a post-doctoral fellow, even though for a short duration, provided me the essence of research. I truly thank him for being a dear friend a guide for, without his direction this thesis would have never been possible. Thank you Chocks!!

I am deeply moved as I bow to my lovable parents for giving me existence in this world and for all their sacrifices which they happily did throughout my life just to see me happy. I still remember when I used to feel frustrated while work and my parents used to encourage me over the phone, their words were enough for me to regain my temperament. Relation of a brother and a sister is unique in its own way. I am thankful to my brothers Ashutosh and Akshay, for their unlimited love, support and blessings for my career.

The financial assistance provided by Ministry of Human Resource Development (MHRD) from July 2013 to May 2016 that made my research work very smooth and prompt, is gratefully acknowledged.

In the end, I feel privileged and owe deep respect to my alma mater IIT Roorkee, for providing me a wonderful platform to work and turn my dreams to a reality. I salute my nation and take an oath to serve for the mankind and the whole world with whatever knowledge and wisdom I possess and will acquire in future by virtue of furtherance of my research work and results thereof.

(Ishita Matai)

ABSTRACT

Cancer is still notorious to create havoc in the modern society despite considerable advancements in field of medical technology. Though commendable efforts and improvements have been done to better the lives of cancer patients, still the ultimate goal to eradicate this dreadful disease demands inspection of new smart materials. In this fight towards cancer, nanotechnology based materials are certainly valuable. Lately, polymer based nanoscale drug delivery systems (DDS) as 'nanomedicines' have garnered much attention for the chemotherapeutic drug delivery in cancer treatment. With a suitable design and structural versatility, they provide biocompatibility, controlled drug release profiles, and increased drug circulation times. Such advantages suggest the pre-eminence of nanoscale drug carriers over traditional drugs. Among the available polymers, dendrimers especially poly(amido amine) (PAMAM) dendrimers offer numerous advantages such as distinct molecular architecture, monodispersity, enhanced solubility of hydrophobic drugs, reduced toxicity and tumor selectivity by enhanced permeability and retention (EPR) effects. Therefore, the present thesis is an endeavour to develop dendrimer based nanomaterials as delivery systems for anticancer agents.

With this perspective, PAMAM dendrimer based multicomponent therapeutic agents have been developed for *in vitro* cancer therapy applications. Firstly, G5.0 PAMAM dendrimers stabilizing silver nanoparticle surface (DsAgNPs) were synthesized to encapsulate anticancer drug 5-fluorouracil (5-FU) to attain anticancer synergism. The formation of 5-FU loaded DsAg nanocomposites (5-FU@DsAgNCs) was confirmed by various characterization techniques. These NCs were taken up effectively by cells and elicited synergistic antiproliferative effects in A549 (human lung cancer) and MCF-7 (human breast cancer) cells at low doses. When the therapeutic outcomes were investigated in detail by different cell-based experiments, 5-FU@DsAgNCs induced apoptosis in cancer cells. The therapeutic effects of 5-FU@DsAgNCs were more pronounced in MCF-7, when compared to A549 cells.

Another smart dendrimer nanoformulation i.e. chemically cross-linked nanogels of G5 PAMAM dendrimers and sodium alginate (AG) have been prepared as delivery systems. The integration of PAMAM dendrimer with alginate and formation of AG-G5 hybrid nanogels was confirmed by different microscopic and spectroscopic techniques. Chemo-drug epirubicin (EPI) was entrapped in the nanogels interiors. When evaluated *in vitro*, these nanogels released EPI slowly

and steadily in tumor environment. Fluorescence imaging, study of nuclear and morphological deformations in EPI⊂AG-G5 nanogels treated MCF-7 indicated apoptosis induction and subsequently cell death.

Subsequently, the impact of hydrophobic modification of G5 PAMAM dendrimer surface on delivery of anticancer agents has been studied. Lipid-like myristic acid (My) chains were introduced on the dendrimer surface, to augment the delivery profile of anti-estrogen tamoxifen (TAM) in MCF-7 (ER+) cells. The successful grafting of My chains on PAMAM dendrimers (My-*g*-G5) and formation of My-*g*-G5/TAM nanocomplexes was confirmed with several characterization experiments. This dendrimer nanoformulation of TAM demonstrated good water-solubility, stability and cell death inducing ability.

Finally, the theranostic (*therapeutic* and *diagnostic*) applications of partially surface acetylated G5 PAMAM dendrimers towards cancer therapy have been elucidated. Luminescent carbon dots (CQDs) with anionic terminus and cationic acetylated G5 PAMAM dendrimers were combined to form self-assembled fluorescent hybrids. The fluorescence of CQDs in hybrids was enhanced in the vicinity of primary amine groups of dendrimers, making them suitable as cellular imaging probes. When EPI was entrapped in the dendritic architecture, CQDs@EPI⊂G5-Ac85 hybrids demonstrated anticancer potential. Moreover, these hybrids served as a dual-emission delivery system to track the intracellular distribution and cytotoxic effects of EPI. Further *in vitro* assays implicate apoptosis induction in hybrid treated MCF-cells.

In a nutshell, different PAMAM dendrimer based nanomaterials are presented as nanomedicines to efficaciously deliver various anticancer agents especially to breast cancer cells to inhibit their proliferation and induce cell death.

Keywords: Drug delivery, PAMAM dendrimers, nanomaterials, cancer therapy, silver nanoparticles, nanocomposites, apoptosis, nanogels, hydrophobic modification, theranostics, hybrids.

LIST OF PUBLICATIONS

I. In Refereed Journals

1. **I. Matai** and P.Gopinath. Chemically Cross-linked Hybrid Nanogels of Alginate and PAMAM Dendrimers as Efficient Anticancer Drug Delivery Vehicles. *ACS Biomaterials Science & Engineering*, 2016, 2, 213-223.
2. **I. Matai** and P.Gopinath. Hydrophobic Myristic Acid Modified PAMAM Dendrimers Augment the Delivery of Tamoxifen to Breast Cancer Cells. *RSC Advances*, 2016, 6, 24808-24819.
3. **I. Matai**, A. Sachdev and P. Gopinath. Self-Assembled Hybrids of Fluorescent Carbon Dots and PAMAM Dendrimers for Epirubicin Delivery and Intracellular Imaging. *ACS Applied Materials & Interfaces*, 2015, 7, 11423-11435.
4. **I. Matai**, A. Sachdev and P. Gopinath. Multicomponent 5-fluorouracil Loaded PAMAM Stabilized-Silver Nanocomposites Synergistically Induce Apoptosis in Human Cancer Cells. *Biomaterials Science*, 2015, 3, 457-468 *(Cover page of the issue)*.
5. A. Sachdev**, I. Matai** and P. Gopinath. Carbon Dots Incorporated Polymeric Hydrogels as Multifunctional Platform for Imaging and Induction of Apoptosis in Lung Cancer Cells. *Colloids and Surfaces B: Biointerfaces***,** 2016**,** 141, 242-252 *(Highlighted in Atlas of Science)*.
6. A. Sachdev, **I. Matai** and P. Gopinath. Dual-Functional Carbon Dots-Silver@Zinc Oxide Nanocomposite: *In Vitro* Evaluation of Cellular Uptake and Apoptosis Induction. *Journal of Materials Chemistry B*, 2015, 3, 1208-1220 *(Cover page of the issue)*.
7. P. Dubey, **I. Matai**, S. Uday Kumar, A. Sachdev, B. Bhushan and P. Gopinath. Perturbation of Cellular Mechanistic System by Silver Nanoparticle Toxicity: Cytotoxic, Genotoxic and Epigenetic potentials. *Advances in Colloid and Interface Science*, 2015, 221, 4-21.
8. P. Dubey, B. Bhushan, A. Sachdev, **I. Matai**, S. Uday Kumar and P. Gopinath. Silver Nanoparticles Incorporated Composite Nanofiber for Potential Wound Dressing Applications. *Journal of Applied Polymer Science*, 2015, 132, 42473 *(Cover page of the issue)*.

9. B. Bhushan, P. Dubey, S. Uday Kumar, A. Sachdev, **I. Matai** and P. Gopinath. Bionanotherapeutics: Niclosamide Encapsulated Albumin Nanoparticles as a Novel Drug Delivery System for Cancer Therapy. *RSC Advances*, 2015, 5, 12078-12086.
10. A. Sachdev, **I. Matai** and P. Gopinath. Implications of Surface Passivation on Physicochemical and Bioimaging Properties of Carbon Dots. *RSC Advances*, 2014, 4, 20915-20921.
11. S. Uday Kumar, **I. Matai**, P. Dubey, B. Bhushan, A. Sachdev and P. Gopinath. Differentially Cross-Linkable Core-Shell Nanofibers for Tunable Delivery of Anticancer Drugs: Synthesis, Characterization and its Anticancer Efficacy. *RSC Advances*, 2014, 4, 38263-38272.
12. B. Bhushan, S. Uday Kumar, **I. Matai**, A. Sachdev, P. Dubey and P. Gopinath. Ferritin Nanocages: A Novel Platform for Biomedical Applications. *Journal of Biomedical Nanotechnology*, 2014, 10, 2950-2976.

II. Book and Book Chapters

1. P. Gopinath, S.U. Kumar, **I. Matai**, B. Bhushan, D. Malwal, A. Sachdev and P. Dubey. Cancer Nanotheranostics, *Springer Briefs in Applied Science and Technology, Springer, Singapore* (2015), ISBN: 978-981-287-434-4, 1-93.
2. **I. Matai**, A. Sachdev, S. Uday Kumar, P. Dubey, B. Bhushan and P. Gopinath. 'Dendrimer: A Promising Nanocarrier for Cancer Therapy' in book titled "*Nanotechnology: Recent Trends, Emerging Issues and Future Directions" Nova publishers* (2014) chapter 7, page no. 127-155, ISBN: 978-1-63117-561-9.

III. Conferences

1. **I. Matai**, A. Sachdev and P. Gopinath, "Chitosan as a Nanocarrier for Intracellular Delivery of Lysozyme", poster presentation in *International Conference on Nano Science and Technology (ICONSAT 2014)*, Mohali, India, 3-5 March, 2014.
2. A. Sachdev, **I. Matai** and P. Gopinath, "Synthesis of Carbon Dots-Ag/ZnO Nanocomposites for Theranostic Applications", poster presentation in *Tech Connect World Innovation Conference & Expo*, Washington DC, USA, 15-18 June, 2014.

CONTENTS

LIST OF FIGURES

LIST OF TABLES

ABBREVATIONS

%.....	Percent
θ.....	Theta
λ_{ex}.....	Excitation Wavelength
λ_{em}.....	Emission Wavelength
µg.....	Microgram
µm.....	Micrometre
µM.....	Micromolar
µL.....	Microlitre
^{o}C.....	Degree Celsius
5-FU.....	5-Fluorouracil
5-FU@DsAg.....	5-Fluorouracil loaded Dendrimer Stabilized Silver
Å.....	Angstrom
a.u.....	Arbitrary Unit
A549.....	Human Lung Adenocarcinoma Cells
AAS.....	Atomic Absorption Spectroscopy
ABC.....	ATP-Binding Cassette
Ag.....	Silver
AG.....	Sodium Alginate
AG-G5.....	Alginate-PAMAM Dendrimer Hybrid
$AgNO_3$.....	Silver Nitrate
Au.....	Gold
AO.....	Acridine Orange
Bad.....	Bcl-2 Associated Death Promoter
Bax.....	Bcl-2 Associated X Protein
Bcl-2.....	Basal Cell Lymphoma 2
Bcl-xl.....	Basal Cell Lymphoma-Extra Large
BET.....	Brunauer-Emmett-Teller
Caspases.....	Cysteine-Aspartic Acid Proteases
C6.....	Coumarin-6
$CaCl_2$.....	Calcium Chloride
cDNA	Complementary Deoxyribonucleic Acid
CI.....	Combination Index

COOH…….	Carboxyl
CQDs.....	Carbon Dots
CQDs@EPI⊂G5-Ac.....	Carbon dots Anchored Epirubicin loaded Partially Acetylated dendrimers
Ch.....	Channel
cm…….....	Centimetre
cm^{-1}.....	Wavenumber
CNT…..……	Carbon Nanotube
CSCs……...	Cancer Stem Cells
CT…….……...	Computed Tomography
Cu.....	Copper
D_2O.....	Deuterium Oxide
DCFH-DA.....	2',7'-dichlorofluorescin diacetate
DDS.....	Drug Delivery Systems
DLE…….	Drug Loading Efficiency
DLS.....	Dynamic Light Scattering
DMEM.....	Dulbecco's Modified Eagle's Medium
DMPC…….	1,2-dimyristoyl-sn-glycero-3-phosphocholine
DMSO.....	Dimethyl Sulfoxide
DOX.....	Doxorubicin
dsDNA…….....	Double Stranded DNA
EA…….....	Early Apoptosis
EB…….....	Ethidium Bromide
EDTA.....	Ethylenediaminetetraacetic Acid
EE…….....	Entrapment Efficiency
EDA……	Ethylenediamine
EDS…….....	Energy Dispersive X-ray Spectrometry
EDC…….	N-Ethyl-N′-(3-dimethylaminopropyl)Carbodiimide
EPI……...	Epirubicin
EPI⊂AG-G5…….....	Epirubicin Loaded Alginate-G5 PAMAM dendrimer hybrid
EPR…….....	Enhanced Permeability and Retention
ER…….....	Estrogen Receptor
FBS.....	Fetal Bovine Serum
FDA...……..…….…....	Food and Drug Administration

FE-SEM.....	Field Emission Scanning Electron Microscopy
FA.....	Folic Acid
FTIR.....	Fourier Transform Infrared Spectroscopy
g.....	Gram
G5.....	Generation 5
Gd.....	Gadolinium
h.....	Hour
^{1}H NMR.....	Proton Nuclear Magnetic Resonance
H_2O.....	Water
HCl.....	Hydrochloric acid
10-HCPT……	10-hydroxycamptothecin
HER-2.....	Human Epidermal Growth Factor Receptor 2
IC_{50}.....	Half Maximal Inhibitory Concentration
ICP-MS.....	Inductively Coupled Plasma Mass Spectrometry
i.v……	Intravenous
JCPDS…….	Joint Committee on Powder Diffraction Standards
keV.....	Kilo electron Volt
KBr.....	Potassium Bromide
LA…….……....	Late Apoptosis
M……..……...	Molar
mg.....	Milligram
min.....	Minute
mL……..……	Millilitre
mM.....	Millimolar
mm.....	Millimetre
mV.....	Millivolt
M_w……....	Molecular Weight
MPa	Megapascal
MCF-7.....	Human Breast Adenocarcinoma Cells
MDR……...	Multidrug Resistance
MMP……...	Mitochondrial Membrane Potential
MNPs.....	Multifunctional Nanoparticles
MRI.....	Magnetic Resonance Imaging
mRNA.....	Messenger RNA

MTT.....	3-(4,5-Dimethyl-2-thiazoyl)-2,5-diphenyltetrazolium bromide
MWCO.....	Molecular Weight Cut Off
My.....	Myristic Acid
My-*g*-G5/TAM……...	Tamoxifen loaded Myristic Acid grafted G5 PAMAM
N.....	Newton
NCs.....	Nanocomposites
nm.....	Nanometer
NPs……..……...	Nanoparticles
ns.....	Nanosecond
$NaBH_4$.....	Sodium Borohydride
NaCl……....	Sodium Chloride
NaOH.....	Sodium Hydroxide
NIH.....	National Institute of Health
NIH 3T3.....	Mouse Embryonic Fibroblast Cells
NHS……	N-Hydroxysuccinimide
NIR.....	Near-infrared
NSCLC……...	Non-Small Cell Lung Cancer
OH……..	Hydroxyl
PAMAM…….	Poly(amidoamine)
p……..	Probability value
pg.....	Picogram
P-gp…….……	P-glycoprotein
pH.....	Potential of Hydrogen
PI.....	Propidium Iodide
PL.....	Photoluminescence
ppm.....	Parts per million
PBS…….....	Phosphate Buffer Saline
PCR……..……...	Polymerase Chain Reaction
PDT.....	Photodynamic Therapy
PEG..……...	Polyethylene Glycol
PPI……...	Propylene imine
RES…….	Reticuloendothelial System
RGD……	Arginyl-glycyl-aspartic acid
ROS...……....	Reactive Oxygen Species

RNA.....	Ribonucleic Acid
RNase…….…….....	Ribonuclease
rpm.....	Revolutions Per Minute
R.T.....	Room Temperature
RT-PCR…..……....	Reverse Transcriptase-Polymerase Chain Reaction
s.....	Second
SAED…….…….....	Selected Area Electron Diffraction
SEC…….	Size-Exclusion Chromatography
SEM……	Standard Error Mean
SPR…….	Surface Plasmon Resonance
TAM……...	Tamoxifen
TEM.....	Transmission Electron Microscope
TGA…….....	Thermogravimetric Analysis
Tris-HCl.....	Tris (hydroxymethyl) aminomethane hydrochloride
UTS.....	Ultimate Tensile Strength
UV.....	Ultra Violet
V.....	Volts
v/v%.....	Volume Percent
Wt. %.....	Weight Percent
XRD.....	X-Ray Diffraction

CHAPTER 1

INTRODUCTION

This chapter gives a brief introduction to the present status and requisite of nanomedicine in cancer therapy. The objectives, significance of the work and organisation of thesis are also included.

CHAPTER 1

INTRODUCTION

Ever since its realization, cancer is considered one of the top 'killers' of the modern society following cardiovascular diseases (Liu et al., 2007). According to global cancer statistics, around 14.1 million new cancer cases were identified worldwide in 2012. Nearly 8.2 million deaths are projected to occur which include ~2.9 million in economically developed countries and ~5.3 million in economically developing countries. Unfortunately, this global burden is expected to reach 21.7 million new cancer cases by 2030 (ACS 2015). Among different cancer types- lung, female breast, bowel (including anus) and prostate are the most frequently diagnosed cancers worldwide and account for 42% (four in ten) of all new cases. In economically developing countries including India, lung cancer is most common in males (~13%) and breast cancer in females (~25%) (Torre et al., 2015, Siegel et al., 2015, www.cancerresearchuk.org and http://globocan.iarc.fr/Pages/fact_sheets_cancer.aspx).

Basically, cancer is a group of diseases as a consequence of uncontrolled growth and spread of abnormal cells. Cells which fail to undergo their natural dying process termed as 'apoptosis' or programmed cell death eventually develop abnormalities and form tumors which if left untreated causes death (Hengartner, 2000). Occurrence of cancer is driven by external factors including tobacco, infectious organisms, unhealthy lifestyle, chemicals, and radiations and, internal factors such as inherited genetic mutations, hormones, and immune conditions (ACS 2014). These factors can act either together or in a sequence to trigger cancer initiation and development. In essence, cancer is multifactorial and multitargeted in which all the targets are interrelated and interdependent, which makes it complex (Kumar et al., 2013). Current cancer treatment involves administration of chemotherapeutic drugs to cancer patient combinatorial with surgery and radiation therapy. Although many forms of cancer are treatable with these therapies, but inability of chemo-drugs to differentiate diseased and healthy tissues and emergence of multi-drug resistance have failed to improve the cancer survival rate. In the quest to strengthen the conventional chemotherapeutic agents, novel agents have been identified and worked upon, but they usually suffer from non-specific tissue distribution leading to insufficient therapeutic index. Moreover, emergence of a rare class of cells called 'cancer stem cells' (CSCs) bearing stem

cell-like properties can stimulate tumor growth and exhibit different features compared to differentiated tumor cells has aggravated the condition. Above all, cancer patients treated with the current systemic therapies suffer extreme side-effects ranging from nausea to infertility. Thus, there is a high risk of genetic disorders in children born to cancer patients treated with such therapies due to germ line mutations (Malecki et al., 2012). Availability of alternative treatment options to improve the quality of cancer patients is highly desirable.

Nanotechnology is an advanced multidisciplinary field which brings together physicists, chemists, biologists and material chemists to design and engineer materials in nanometer (nm) scale (Silva, 2004 and Whiteside, 2005). The prefix ‘nano’ refers to one-billionth on a metric scale. The developed nanoparticles are expected to exhibit distinct and improved physical and chemical properties as their size is scaled down to atomic levels (Saikia et al., 2013 and Saha et al., 2015). Nanotechnology has exhibited quite promising advancements in various fields including optoelectronics, device fabrication, sensing, medicine etc. (Whiteside, 2005). It offers immense potential in not only amending the present technologies but also providing entirely new tools and capabilities. Application of nanoscale technologies as innovative tools for disease diagnosis, therapy, and prevention has recently referred to as ‘nanomedicine’ by the National Institute of Health, USA. Research into the rational delivery and targeting of pharmaceutical, therapeutic, and diagnostic agents is at the forefront of projects in nanomedicine (Moghimi et al., 2005 and Liu et al., 2007). In line with this, great efforts are being laid in the design and engineering of nanoparticulate systems as effective tools for prognosis and treatment of critical diseases such as cancer, infectious or neurological disorders (Nicolas et al., 2013).

Nanomedicine in cancer has provided impulse to the development of ‘smart’ delivery systems to transport anticancer drugs to the target sites in an effective manner. Primarily, it deals with anchoring chemotherapeutics to colloidal nanoscale delivery systems with the aim to traverse the non-cellular and cellular barriers and increase the selectivity more towards cancerous cells, sparing damage to healthy tissues (Brigger et al., 2002 and Nair et al., 2011). Such drug delivery systems (DDS) can lower the requisite drug doses eventually diminishing the non-specific toxicity, protects the drug from premature inactivation and enhances its solubility and bioavailability at the tumor site surpassing multi-drug resistance in cancer cells. (Allen et al., 2004 and Kutty et al., 2015). Nanoparticles as attractive DDS can target cancer tissues in a passive or active manner. In passive targeting, nanoparticles take advantage of their small size can easily penetrate the leaky and distorted tumor vasculature (100 nm to 2 μm size) to preferentially accumulate therein by the well-known ‘enhanced permeability and retention effect

(EPR)'to release the drug in a sustained manner (Maeda et al., 2000). This unique pathophysiology of tumor cells is absent in normal tissues which trigger selective targeting by nanoparticles. Attaching specific affinity ligands on the nanoparticle surface for specific recognition and uptake by cancer cells is the rationale of active/ligand-mediated targeting. In this strategy, ligands are selected to recognize and bind specifically to the surface molecules or receptors overexpressed in cancerous cells (Allen et al., 2002 and Bertrand et al., 2014). Commonly used ligands for tumor targeting include antibodies and their engineered fragments, peptides, aptamers, proteins such as transferrin, lactoferrin, and lectins, and small molecules including folates and mannose derivatives (Mathew et al., 2015 and Toporkiewicz et al., 2015). For maximal benefit, the actively targeted nanoparticle should be in close proximity to identify and bind to its target. Furthermore, the release of drug in the tumor microenvironment can be tailored by controlling the nanocarrier structure and the mode of drug association. Drugs can either be adsorbed or physically encapsulated or covalently attached to the nanocarrier.

Keeping above points in mind the prime challenge is identification of a suitable and versatile nanocarrier which can solubilise, stabilize and release the drug cargo in an effective manner. Polymeric materials of either natural or synthetic origin are being explored (Holland et al., 2007 and Mo et al., 2009). Numerous nanoparticulate systems which have been tested so far for their biomedical applications include liposomes (Cattel et al., 2003 and Teo et al., 2014), micelles (Rapoport., 2007 and Kedar et al., 2010) , solid-lipid nanoparticles (SLNs) (Uner et al., 2007 and Pardeike et al., 2009), protein nanoparticles (Elzoghby et al., 2012 and Bhushan et al., 2014), dendrimers (Lee et al., 2005 and Matai et al., 2014b), magnetic nanoparticles (Besenius et al., 2012 and Balasubramanian et al., 2015), nanowires (Hong et al., 2011 and Peng et al., 2014), nanotubes (Ji et al., 2010 and Adeli et al., 2013), nanorods (Ahlers et al., 2014 and Appel et al., 2015) and nanofibers (Mortimer et al., 2013 and 2015) etc. Many of such nanotherapeutics have already been approved by Food and Drug Administration (FDA) for cancer treatment while others are in clinical trials. The two notable examples of FDA-approved cancer nanomedicines that are clinically successful include Doxil (liposomal doxorubicin HCl injection, Janssen) and Abraxane (paclitaxel protein-bound particles for injectable suspension, Celgene) (Morigi et al., 2012 and Ventola et al., 2012). However, most of the DDS available till date suffer from low stabilities, low drug loading capacities, immunogenicity, size and structural constraints etc. which serve as roadblocks to safe and desirable cancer therapy. As a solution, 'dendrimers' have recently become a topic of research as potential nanocarriers for biomedical applications, especially for cancer diagnosis and therapy. These are the newly introduced members in the family of polymeric systems. The unique structural characteristics of dendrimers proposes their

candidature to deliver anticancer and imaging agents with minimal toxicity. Moreover, dendrimers are highly renowned as 'drug solubility enhancers' for both hydrophilic and hydrophobic drugs (Milhem et al., 2000). These key features necessitates to gain an insight to the utility of dendrimers as nanocarriers for cancer therapy for future clinical applications. In this thesis, various dendrimer based nanomaterials have been worked upon to assess their ability to deliver therapeutic modalities to cancer cells.

1.1. Objectives

The chief objectives of the present work are as follows:

- Development of a poly(amidoamine) (PAMAM) dendrimer based multicomponent therapeutic agent for *in vitro* cancer therapy applications.
- Formulation of PAMAM dendrimer based nanogels for sustained delivery of chemotherapeutic agents.
- Examination of the surface modification of PAMAM dendrimers with hydrophobic entities for delivery of anticancer agents.
- Evaluation of the theranostic potential of PAMAM dendrimers *in vitro*.

1.2. Significance of the present work

The significance and salient features of the present research work are mentioned underneath:

- A novel G5 PAMAM dendrimer based multicomponent system for simultaneous delivery of silver nanoparticles (AgNPs) and anticancer drug, 5-fluorouracil (5-FU) to cancer cells has been synthesized.
- This is the first instance wherein, dual functionality of PAMAM dendrimer as a stabilizer to synthesize amine terminated AgNPs and a delivery system for 5-FU has been explored.
- This multicomponent therapeutic system (5-FU@DsAgNCs) was designed to attain synergistic antiproliferative effects in cancer cells, such as A549 (Lung cancer) and MCF-7 (Breast cancer).
- Next, chemically cross-linked hybrid nanogels of alginate and G5 PAMAM dendrimers (AG-G5) were synthesized via carbodiimide chemistry.
- Fluorescent drug epirubicin (EPI) was entrapped within these AG-G5 nanogels interiors to endow them with therapeutic potential.
- The formulated AG-G5 nanogels were proficient to enhance the loading capacities of EPI molecules and then subsequently deliver it to MCF-7 cells in a sustained manner.

- Further, G5 PAMAM dendrimers were hydrophobically modified by grafting lipid- like myristic acid (My) tails at periphery by EDC/NHS chemistry.
- These My-*g*-G5 dendrimers were evaluated as a delivery system for tamoxifen (TAM), an estrogen agonist to MCF-7 cells.
- In another attempt, luminescent carbon dots (CQDs) were anchored to partially surface acetylated G5 PAMAM dendrimers (with entrapped EPI) through self-assembly to formulate fluorescent CQDs@EPI⊂G5-Ac hybrids for theranostic applications.
- This complete system can serve as a dual-emission delivery system to track the intracellular distribution and cytotoxic effects of anticancer agents such as EPI.
- These CQDs@EPI⊂G5-Ac hybrids were taken up by MCF-7 cells effectively and there was an augment in fluorescence of CQDs as a part of hybrids, making them suitable cellular imaging probes.
- Various cell-based experiments were performed to evaluate the inhibitory and cytotoxic effects of G5 PAMAM dendrimer based nanoformulations *in vitro*.
- These four nanomaterials including 5-FU@DsAgNCs, EPI⊂AG-G5 nanogels, My-*g*-G5/TAM complexes and CQDs@EPI⊂G5-Ac hybrids, resolves the inherent toxicity issues of pristine G5 PAMAM dendrimers and can effectively induce apoptosis in breast cancer cells.

1.3. Organisation of thesis

Keeping in view the above mentioned objectives, the complete efforts in the present research work have been described in form of eight chapters. An introductory section to the present status and need of nanomedicine in cancer treatment is presented in chapter 1. A background to dendrimers as prospective anticancer polymeric nanocarriers is described as literature survey in chapter 2. The materials and methods adopted for the work have been described in chapter 3. In chapter 4, the ability of multicomponent 5-FU loaded PAMAM stabilized-silver nanocomposites (5-FU@DsAgNCs) to induce synergistic anticancer effects *in vitro* have been demonstrated. Chapter 5 describes the formulation of chemically cross-linked hybrid nanogels of sodium alginate and PAMAM dendrimers for delivery of fluorescent anticancer drug EPI. In chapter 6, the effect of surface modification of PAMAM dendrimers with hydrophobic myristic acid for the enhanced delivery of TAM, an anti-estrogen has been described. In chapter 7, the theranostic potential of hybrids of EPI loaded partial surface acetylated PAMAM dendrimers and CQDs has been investigated. In chapters 4-7, after synthesis, the PAMAM dendrimer based nanomaterials were subjected to different characterization techniques and were subsequently evaluated for their anticancer potential. Finally, in chapter 8, the complete work has been summarized and the future scope has been discussed.

CHAPTER 2

LITERATURE REVIEW

This chapter provides an insight to the updated review on dendrimers as prospective polymeric nanocarriers for the delivery of anticancer agents.

CHAPTER 2

LITERATURE REVIEW

2.1. Nanomedicine in cancer therapy

The famous talk of Richard Feynman "There's Plenty of Room at the Bottom", introduced the concept of smart nanodrug delivery devices which can interact with biological systems at the cellular level (Feynman, 1960). Till date i.e. after five decades of his talk, nanotechnology has ushered the interest of researchers and medical oncologists to find feasible and promising cancer nanomedicines. The biggest challenge for an oncologist is to search for a potential agent that is cytotoxic and kills the neoplastic cells while preserving the healthy host cells and their normal functions. If in case the hurdles in the form of drug resistance or, lack of selectivity would not exist, fighting cancer with conventional chemotherapeutics would be highly appreciated. Nanomedicines are being scrutinised for their use in anticancer therapies to improve drug delivery, increase the efficacy of treatment, reduce side effects, and overcome drug resistance (Markman et al., 2013).

Nanocarriers are key ingredients for nanomedicine in cancer treatment. They have unique features of nanoscale size, high surface-to-volume ratio, and favourable physicochemical characteristics (Goswami et al., 2014, Uday et al., 2014 and Sarkar et al., 2015a). Additionally, they can upgrade the drug therapeutic index by modulating its pharmacokinetic and pharmacodynamics profile. Drug loaded nanocarriers have improved *in vivo* stability, extended blood circulation times, and controlled drug release characteristics (GuhaSarkar et al., 2010). Hence, nanomedicines can alter the biodistribution by sequestering the drug molecules to enter through the tumor fenestrations and preferentially accumulate therein (by EPR effect) (Moghimi et al., 2005 and Peer et al., 2007). Nanoplatforms such as liposomes, lipid nanoparticles, micelles, dendrimers and gold nanoparticles can address the problems associated with cancer diagnostics and therapy (Muthu et al., 2014). Multifunctional nanoparticles (MNPs) integrating therapeutic and imaging agents, referred to as 'Theranostic agents' are specifically being developed for personalized nanomedicine (Swierczewska et al., 2016). Amidst various nanoplatforms, the polymeric nanocarriers carrying chemotherapeutic agents can overcome drug resistance. Multidrug resistance (MDR) is a common problem related to cancer chemotherapy.

P-glycoprotein (P-gp) belongs to ATP-binding cassette (ABC) superfamily of membrane transporters is generally over-expressed in tumor cells than drug-sensitive parent cell lines. Tumor cells acquire MDR owing to drug efflux by this P-gp. Most of the clinically used anticancer drugs are substrates of P-gp. Thus in order to overcome MDR, drugs can be loaded in nanocarriers to enhance the efficiency of drug delivery to tumor cells by by-passing the efflux pump and can enter the cells through alternate routes such as endocytosis (Dong et al., 2010 and Markman et al., 2013). Currently, many of the nanotechnology-driven therapeutic and diagnostic entities are undergoing clinical trials and some have received the FDA approval for treating cancer patients. Some of the FDA approved cancer nanomedicines are described below:

Doxil (PEGylated liposomal doxorubicin)

This liposomal based DDS is the first nanodrug formulation approved by FDA in 1995 and is used to treat some specific cancers, including metastatic ovarian cancer and AIDS-related Kaposi's sarcoma. Basically, it comprise of doxorubicin (Adriamycin), an anthracycline drug enclosed in a 80-90 nm unilamellar liposome with PEG coating. Such PEG stabilized liposomes, termed as 'stealth liposomes' allows the doxorubicin molecules to stay in the bloodstream for longer duration (mean residence time ~ 4 days) when injected intravenously to exhibit therapeutic effects. Doxil was actually formulated as a midway between the therapeutic and side-effects of doxorubicin. Doxorubicin is known to inhibit the cell proliferation by either intercalation into DNA and disruption of topoisomerase II-mediated DNA repair and generation of reactive species (free radicals) that can eventually damage the cellular machinery (Gordan et al., 2000). Unfortunately, patients receiving doxorubicin therapy are highly prone to life-threatening heart problems (eg, heart failure). But when administered in liposomal formulation, it has fewer side-effects on normal cells (Gordan et al., 2001, O'Brian et al., 2004 and Rahman et al., 2007). The other popular names of this liposomal doxorubicin are Doxil (Johnson & Johnson, USA), Caelyx (Janssen-Cilag, Europe), Evacet (Liposome company INC.,) and lipodox (Sun Pharma).

Myocet (Non-PEGylated liposomal doxorubicin)

This liposome based nanoformulation received Canadian regulatory approval in December 2001, as first line treatment for metastatic breast cancer in combination with cyclophosphamide. It has also been approved in Europe but, the approval is still pending for United States. At present, myocet is used in a combination form with herceptin (trastuzumab) and taxol (paclitaxel) against HER2-positive metastatic breast cancer (Baselga et al., 2014). Myocet has been identified as a better alternative to conventional doxorubicin in terms of less cardiotoxicity and anticancer efficacy. The half-life for myocet is reported to be 16-50 hours, significantly more than the

conventional doxorubicin. Commercially, Myocet is made by Enzon Pharmaceuticals for Cephalon in Europe and for Sopherion Therapeutics in the United States and Canada.

Abraxane (Paclitaxel albumin bound)

This protein based nanoformulation of paclitaxel (Taxol, Bristol-Myers Squibb) was approved by FDA in January 2005 for treating metastatic breast cancer and in October 2012 as a first line treatment for advanced non-small cell lung cancer (NSCLC) in combination with carboplatin. In 2013, Abraxane had received approval for treating advanced pancreatic cancer. Basically, Abraxane involves human albumin nanospheres (~130 nm in diameter) holding paclitaxel, an insoluble drug. Initially, paclitaxel was solubilized in a combination of polyethoxylated castor oil (cremophore EL, a non-ionic surfactant) and ethanol (50:50 v/v) (Desai et al., 2006). However, the adverse side-effects and dose-limiting issues of solvent were a major drawback. Nanoparticle albumin bound (Nab) paclitaxel suspension is usually administered intravenously (260 mg/m^2 as infusion for 30 min) to cancer patients. The half-life of Abraxane is around 27 hours compared to 5.8 hours for paclitaxel. In short, Albumin is a suitable carrier for delivering paclitaxel for its availability, biodegradability, non-immunogenic nature and lack of toxicity. Interestingly, it can be taken up by a unique Gp60 (albondin, a glycoprotein) - mediated pathway in endothelial cell walls of tumor cells (Desai et al., 2004).

A summarized description of FDA approved cancer nanomedicines and ones in clinical trials till date are mentioned in **table 2.1.**

Drug Product	Active Nanomedicine ingredient	Manufacturer	Targets	FDA approved status/stage of clinical trial
Doxil(Caelyx)	Pegylated liposomal doxorubicin	Orthobiotech, Schering-Plough	Ovarian/breast cancer	November 1995
Abraxane	Albumin-bound paclitaxel nanospheres. Nab paclitaxel in combination with gemcitabine	Abraxis Bioscience, Astrazeneca Celgene	Various cancers Metastatic pancreatic cancer	Jan-2005 September 2013
Myocet	Liposome encapsulated doxorubicin	Elan Pharmaceuticals / Sopherion Therapeutics	Breast cancer	2000, Approved in Europe and Canada

DepoCyt	Liposomal cytarabine	Skye Pharma, Enzon	Lymphomatous meningitis	Apr-1999
DaunoXome	Liposome encapsulated daunorubicin	Gilead Science	HIV-related Kaposi sarcoma	Apr-1996
Genexol-PM	Paclitaxel-loaded polymeric micelle	Samyang	Breast cancer/small cell lung cancer	Marketed in Europe, Korea
Oncaspar	PEG asparaginase	Enzon	Acute lymphocytic leukemia	Feb-1994
Marqibo	Vincristine	Talon Therapeutics	Philadelphia chromosome negative lymphoblastic leukemia	Aug-2012
Onco-TCS	Liposomal vincristine	Inex	Non-Hodgkin Lymphoma	In clinical phase I/II
SPI-77	Stealth liposomal cisplatin	Alza	Head & Neck cancer/Lung cancer	In clinical Phase III
EndoTAG-I	Paclitaxel	Medigene/SynCore Biotechnology	Breast cancer/Pancreatic cancer	In clinical phase II
OSI-211	Liposomal lurtotecan	OSI	Lung/ Ovarian cancer	In clinical phase II
ThermoDox	Doxorubicin	Celsion Corporation	Hepatocellular carcinoma	In clinical phase III
Lipoplatin	Liposomal cisplatin	Regulon	Pacreatic/ Head and Neck/breast cancer	In clinical phase III
Paclical	Paclitaxel micelles	Oasmia Pharmaceutical AB	Ovarian cancer	Phase III, April-2015 received marketing authorization in the Russian Federation.
Atragen	Liposomal all transretinoic acid	Aronex Pharmaceuticals	Acute promyelocytic leukemia	In clinical phase II
Narekt -102	Irinotecan, PEGylated liposome	Nektar Therapeutics	Breast /Colorectal cancer	In clinical Phase III
NC-6300 (K-912)	pH sensitive polymeric micelle incorporating epirubicin	NanoCarrier	Solid tumors	In clinical Phase I

Aurimmune (CYT-6091)	TNF-α bound to colloidal gold nanoparticles	Cytimmune Sciences	Head and Neck cancer	In clinical phase II
Auroshell	Gold nanoshells	Nanospectra Biosciences	Aurolace therapy of cancer	In clinical Phase I

Table 2.1. FDA approved cancer nanomedicines and ones in clinical trials. (Source: FDA website, websites of pharmaceutical companies supplying/developing these drugs and Pillai, 2014).

2.2. Dendrimers

2.2.1. Background and structural characteristics

With the progress in polymer science, the variations in compositions and architectures of macromolecules has also steadily increased. The ability to tailor the size, topology, chemistry and ultimately the properties of polymeric molecules synthesized *via* the chemical route inevitably has paved way to their biological applications. Amidst a myriad of chemically synthesized molecules, 'dendrimers' are of significant interest to researchers. These synthetic molecules are the newly introduced members in the family of polymeric systems.

Dendrimers have derived their name from the Greek word '*dendron*' which means tree and '*meros*' meaning part, which indicate their architecture to be three-dimensional and tree-shaped with a regular branched structure (Lee et al., 2005 and Abbasi et al., 2014). From the view of polymer chemistry, dendrimers are defined to be nearly defect-free, monodisperse (meaning consistent size and form), multivalent, and globular molecules with diameter of 2-10 nm. These hyperbranched molecules were first discovered by Vogtle in 1978, independently by Tomalia, Newkome and Denkewalter in the early 1980s. Vogtle and co-workers, studied the controlled synthesis of dendritic arms by repetitive reactions of mono- and diamines with a central core to produce polymeric branching units with large molecular cavities and termed them as "*cascade molecules*" (Buhleier et al., 1978). Tomalia and group described the iterative coupling of ethylene diamine to a central ammonia core to form series of branched macromolecules and named them as "*starburst dendrimers*" (Tomalia et al., 1985) Newkome's group called them "*arborols"* (Latin word '*arbor*' which translates to a tree) (Newkome et al., 1985). Denkewalter with co-workers reported the first dendritic wedge using lysine residues as branching units (Denkewalter et al., 1981).

In structure, dendrimers comprise of multiple branched monomers attached to a common root which constitutes the "core" in the center. These branched monomers with identical fragments are called the "dendrons". The number of dendrons present in a complete dendrimer molecule depends on the multiplicity of the core (2, 3, 4 or more). The "branches" which emanate radially from the central core are composed of repeating chemical units with branch junctions (at least one). The number of branch points faced upon moving outward from the core of dendron towards the periphery (end groups) defines its 'generation' (G1, G2, G3). The end groups present on the dendrimer surface forms the "exterior" **(Figure 2.1)** (Newkome et al., 1985, Dufès et al., 2005, Lee et al., 2005 and Kesharwani et al., 2014). The nature and extent of these terminal functional groups confer dendrimers with distinct physiochemical and biological properties. These end groups provide flexibility for chemical modification to modulate the properties of dendrimer macromolecules.

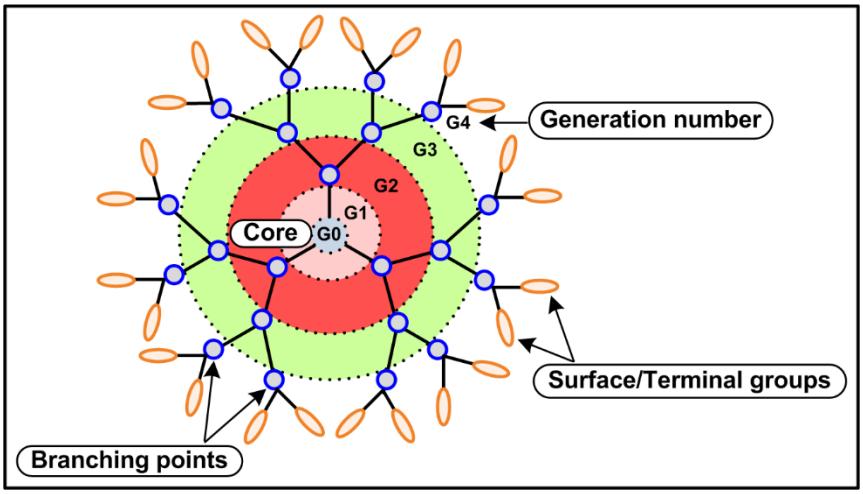

Figure 2.1. Structural components of dendrimer.

Moreover, the branching style of dendrimers mediate formation of nano-cavities whose environment determines its encapsulating properties while the external groups are responsible for its solubility and chemical behavior (Jolly et al., 2014 and Liang et al., 2016). Therefore, dendrimers are suitable polymeric materials in the field of catalysis (Bhyrappa et al., 1996, Gopidas et al., 2003 and Niu et al., 2003a), supramolecular chemistry or host-guest chemistry (Elemans et al., 2002, Al-Jamal et al., 2005 and Jolly et al., 2015), light harvesting (Adronov et al., 2000 and Bradshaw et al., 2011), pollution control (Xu et al., 2005 and DeFever et al., 2015), unimolecular micelles (Liu et al., 2000 and Cao et al., 2011), disease diagnostics (McCarthy et al., 2005 and Tomalia et al., 2007), drug (Agashe et al., 2007, Cheng et al., 2007 and Caminade et al., 2014) and gene (Chen et al., 2013a and Sarkar et al., 2015b) delivery.

Advancement in synthetic chemistry has led to formation of numerous dendritic nanoconstructs with distinct features. By far, poly (amido amine) dendrimers (PAMAM) and the poly (propylene imine) (PPI) are the two most prevalent and commercially available dendrimers (Sigma-Aldrich and Dendritic Nanotechnologies). A lot many variations in the core and peripheral functionalities of different generations of these dendrimers have been tested in various applications.

2.2.2. Synthesis of dendrimers

Dendrimers are chemically synthesized macromolecules having a symmetric and a highly-branched structure. The synthesis of dendrimers by specific chemical reactions is an appropriate example of controlled-hierarchical synthesis, an approach that enables 'bottom-up' creation of intricate systems. Predominantly, the synthesis of dendrimers involves a two-step reaction sequence which include a (i) coupling or generation growth step, and (ii) an activation step. To obtain pure dendrimers in high yields with no structural distortions, these steps should move in a clean manner to generate minimal side-products. Generally, two distinct synthesis schemes are adopted for preparation of dendrimers: convergent approach developed by Hawker and Fréchet (Hawker et al., 1990) and divergent approach developed by Tomalia et al (Tomalia et al., 1985) and Newkome et al (Newkome et al., 1985). Both of these schemes are well-documented and aim to obtain monodisperse and defect-free dendrimers as the end product. The difference in the two strategies lies in the direction of dendrimer growth **(Figure 2.2)**.

2.2.2.1. Convergent synthesis

The convergent strategy involves step by step growth of dendrimer in a controlled manner which is initiated by the molecules which ultimately forms the exterior of the final macromolecule. (Liu et al., 1999, Grayson et al., 2001). In simple words, dendrimer growth begins at the chain ends and moves inwards to the core through successive addition of dendrimer parts to a single monomer unit (what ultimately forms the dendron). Since this strategy is based on uniting the monomeric units to the functional core to form a globular structure, this scheme is mostly limited to synthesize low generation dendrimers.

2.2.2.2. Divergent synthesis

In this approach, the dendrimer growth originates from the reactive core functionality and proceeds towards the periphery with step-wise addition of successive generations as arms or building blocks. For instance, well-known PAMAM dendrimers also called 'Tomalia type dendrimers' or 'starburst dendrimers' have been successfully synthesized by divergent approach. The entire synthesis scheme of PAMAM dendrimers is an iteration of reaction steps which

involve (i) Michael addition of methyl acrylate ester to the amine core and (ii) exhaustive amidation with ethylenediamine to obtain terminal amine functionalities. Completion of this sequence gives a full generation (G=1.0). The entire procedure is repeated several times to add further concentric layers or generations to the dendrimer molecule. The number of generations present in the final dendrimer structure equates to the number of repetitive cycles performed. (Tomalia et al., 1985). Each newly added generation arranges itself around the core to form an ellipsoidal or globular structure. **Figure 2.3** illustrates the synthesis of ethylenediamine core (EDA) PAMAM dendrimers with terminal amine groups by divergent strategy. The other most common PPI dendrimers are also synthesized using this strategy. With this procedure, it is possible to synthesize high generation dendrimers (≤ G10) with high molecular weights (>25000 g/mol) and abundant terminal groups. This is beneficial for large-scale production of dendrimers for commercial purposes. However, in this strategy a large-influx of chemical reagents are required to drive the reaction steps to completion. Also, sometimes different molecular weights of dendrimers get synthesized which demand multiple purification steps, which is often a tedious and a time-consuming procedure. If the chemical reagents could be made available in high amounts, then divergent approach is the best available strategy as the number of end product i.e. dendrimer doubles after each successive reaction and the terminal functional groups increase in an exponential manner.

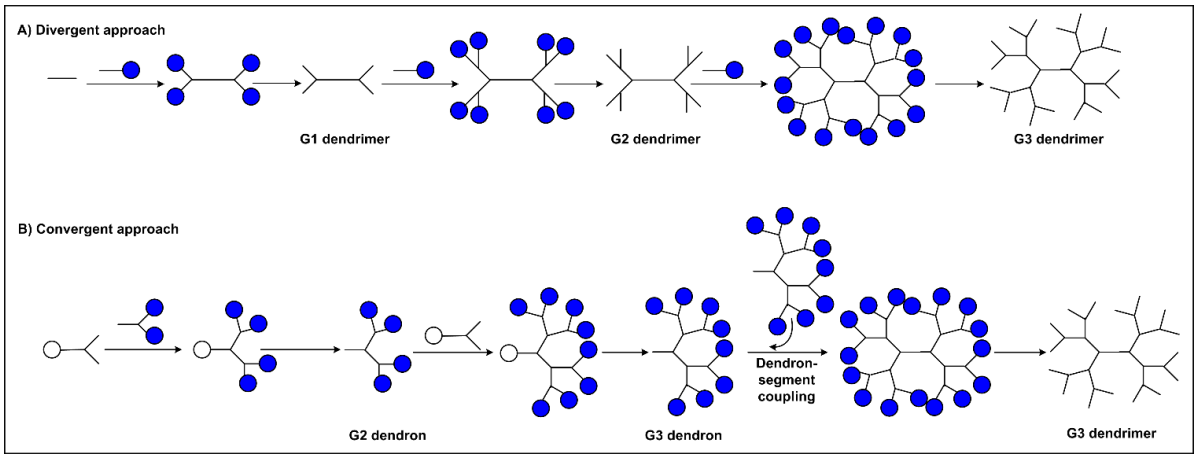

Figure 2.2. Different approaches to synthesize dendrimers (schematically depicted).

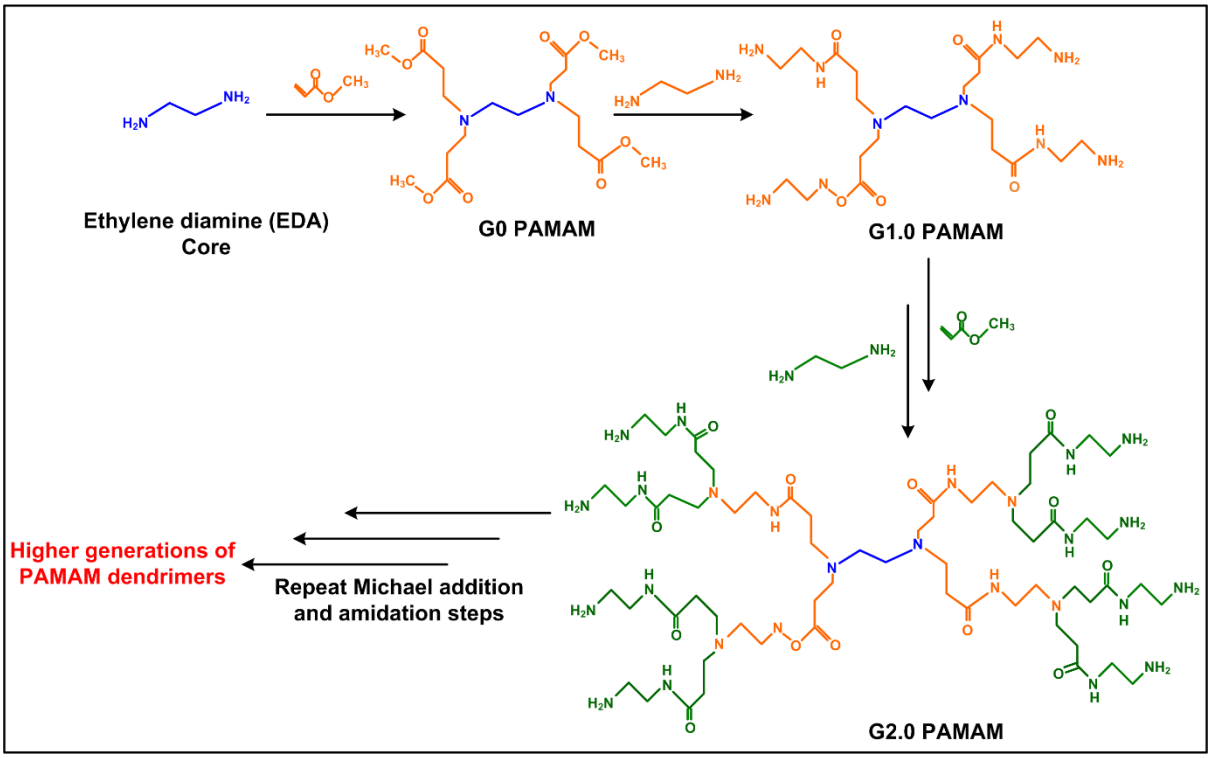

Figure 2.3. Divergent approach strategy to synthesize PAMAM dendrimers.

2.2.3. Dendrimers as biological mimics

Interestingly, the dendritic architecture is among the most pervasive topologies observed in biological systems (Esfand et al., 2001). These are three-dimensional, globular shaped structures which mimic the natural proteins in dimensional length scale and are hence regarded as 'artificial proteins' (Jiang et al., 1996, Dandliker et al., 1997, Weyermann et al., 1999, Hecht et al., 2001, Tomalia et al., 2002, Tomalia et al., 2003). Within the PAMAM family of dendrimers, they mimic certain important proteins and their assemblies. For instance, G3, G4, G5 PAMAM dendrimers with ammonia core are similar in shape and scale to insulin (≈ 30 Å), cytochrome C (≈ 40 Å) and haemoglobin (≈ 55 Å) proteins, respectively. Furthermore, the diameter of G5 and G6 PAMAM dendrimers is approximately equivalent to the thickness of biological lipid bilayers (~ 5.5 nm) and the size of G2 PAMAM dendrimer matches the DNA duplexes (2.4 nm). Although dendrimers resemble closely to biological proteins, there exists some significant differences also. Globular proteins hold a tertiary structure with densely packed interiors owing to the intricate folding of linear protein sequences. Moreover, they are extremely fragile and sensitive to the denaturing conditions such as pH, temperature, and light. On the contrary, dendrimers are robust, covalently-linked, three-dimensional structures with a well described interior core and a exterior surface functionality (nanoscaffold) (Tomalia, 2005, Svenson et al., 2012, Noriega-Luna et al., 2014)

2.2.4. Properties of dendrimers

2.2.4.1. Monodispersity

Unlike linear polymers, dendrimers are a new class of dendritic polymers which are synthesized step-wise and have regular structures with very low polydispersity ($M_w/ M_n < 1.01–1.05$). From the application point of view, monodisperse products are chiefly demanded not only for their synthetic reproducibility but also to minimise the experimental and therapeutic variability. The experimental evidence of the monodisperse nature of dendrimers has been provided by mass spectrometry, size-exclusion chromatography (SEC), gel electrophoresis and transmission electron microscopy (TEM). Mass spectrometry have described PAMAM dendrimers produced by divergent method to be highly monodisperse. Moreover, dendrimers obtained by convergent scheme are the most monodisperse products, for it purifies dendrimers at each step and eradicates the products generated by erroneous couplings. (Tomalia., 2005)

2.2.4.2. Nano-size and shape

Dendrimers with nanoscale dimensions and uniform shape are desirable for their biological applications. Typically, nano-sized dendrimers can cross the biological barriers with ease and the chances of premature clearance by the reticuloendothelial system (RES) are significantly diminished. All these benefits of dendrimers can be credited to their unique dendritic architecture, which makes them an ideal carrier. The earlier generation i.e. (G= 0-3) do not exhibit any well-defined internal characteristics and tend to adopt an ‘open’ conformation and exhibit ellipsoidal shapes. While in intermediate and higher generations i.e. (G= 4-10) the internal networks are well-developed to form cavities and they have roughly ‘spherical’ shapes. When incorporated, drug molecules get entrapped in these nanoscopic networks. (Tomalia, 2005 and Kesharwani et al., 2014). During the growth as the generation increases, the diameter and the number of surface functional groups also increase **(Table 2.2)**. The unique topology of dendrimers grants access to their several surface functional groups for chemical transformations. To simplify, the multivalent and multifunctional surface of dendrimers can be manipulated for some specific functions. These surface groups can either be chemically modified or attached with some targeting moieties or ligands such as antibodies, peptides, carbohydrate molecules or their derivatives, etc. This salient feature of dendrimers is mostly exploited to attain target specificity or to change their external environment.

Dendrimer Generation	No. of Surface groups	Molecular formula	Molecular weight (g/mol)	Diameter (nm)
0	4	$C_{22}H_{48}N_{10}O_4$	517	1.5
1	8	$C_{62}H_{128}N_{26}O_{12}$	1,430	2.2
2	16	$C_{142}H_{288}N_{58}O_{88}$	3,256	2.9
3	32	$C_{302}H_{608}N_{122}O_{60}$	6,909	3.6
4	64	$C_{622}H_{1248}N_{250}O_{124}$	14,215	4.5
5	128	$C_{1282}H_{2528}N_{508}O_{252}$	28,826	5.4
6	256	$C_{2542}H_{5088}N_{1018}O_{508}$	58,048	6.7
7	512	$C_{5102}H_{10208}N_{2042}O_{1020}$	116,493	8.1
8	1024	$C_{10222}H_{20448}N_{4090}O_{2044}$	233,383	9.7
9	2048	$C_{20462}H_{40928}N_{8188}O_{4092}$	467,162	11.4

Table 2.2. Structural characteristics of PAMAM dendrimers. (Source: Tomalia et al., 1985, http://www.dendritech.com/pamam.html,http://www.sigmaaldrich.com/materials science/nanomaterials/dendrimers/properties.html)

2.2.4.3. Solubility and reactivity

The solubility properties are mainly governed by dendrimer generation, concentration, pH, and structural components which comprise the surface functional groups and the central core. Dendrimers show excellent solubility in water and a large number of solvents. Moreover, these macromolecules have been crowned as ‘solubility enhancers’ for several hydrophobic guest molecules, similar to cyclodextrins and micelles. Dendrimers with hydrophobic core and hydrophilic exterior exhibit micelle-like properties in solution. They can incorporate hydrophobic entities (M_w <800 Da) in their internal cavities rendering them water-soluble. (Milhem et al., 2000, Yiyun et al., 2005 and Gupta et al., 2006). Upon surface functionalization of poorly-water soluble nanomaterials such as carbon nanotubes (CNTs), dendrimers can enhance their aqueous solubility tremendously (Sun et al., 2011). The high-density of dendrimer functional groups (–OH, –COOH and $–NH_2$) on the surface can be conjugated to certain biologically relevant molecules. Hence, these solubility and reactivity features of dendrimers unanimously suggest development of dendrimer based multifunctional nanodevices for biomedical applications.

2.2.4.4. Pharmacokinetics

For any drug delivery system to be effective its circulation times, organ uptake and tissue biodistribution are of paramount importance (Wolinsky et al., 2008). As such, the pharmacokinetic profile of dendrimers can be modulated by tailoring its polymeric architecture, physiochemical properties, and interactions with the cellular surfaces. The biodistribution characteristics of dendrimers is strongly influenced by the generation number and PEGylation degree including arm length and molecular weight. (Kaminskas et al., 2008 and Kim et al., 2008). Gillies et al., 2005a reported the pharmacokinetic profile of uniquely designed "bow-tie" polyester dendrimers with G3 hydroxyl terminated dendrimers on one side and G1, G2, or G3 dendrons with PEG chains of 5000, 10000 and 20000 MWs on the opposite side. All these dendrimers regardless of molecular weight were non-toxic to MDA-MB-231 breast cancer cells. While performing the degradation studies, [G3]-$(PEG5k)_8$-[G3]-$(OH)_8$ dendrimers were incubated in buffer solutions of pH 5.0 and 7.4. Over a period of 15 days, different MWs were detected by size exclusion chromatography (SEC), indicating carbamate chain hydrolysis and cleavage of PEG chains from dendrimer. PEGylated ^{125}I-labeled dendrimers when injected intravenously (i.v.) in mice demonstrated differential retention and excretion times depending on the MWs of PEG chains attached. These radiolabelled dendrimers [G3]-$(PEG5k)_8$-[G3]-$(OH)_8$, [G3]-$(PEG10k)_8$-[G3]-$(OH)_8$, and [G3]-$(PEG20k)_8$-[G3]-$(OH)_8$,respectively) had long circulation times, with elimination half-lives of 31, 40, and 50 h, respectively. Urinary clearance of these dendrimers decreased with increasing PEG molecular weight. After 48 h of incubation, < 4 % of these were excreted in urine and 7-16 % in faeces (Yamaoka et al., 1993). PEGylated PAMAM dendrimers with lysine residues (G=4, 5) with or without acetylation exhibited variable blood retention capacities. Ac-Lys-PAMAM (G4) dendrimers when injected i.v. in nude mice were clearly after 24 h while, PEG2k-Lys-PAMAM (G5) and PEG5k-Lys-PAMAM (G4) with M_w~300 Da exhibited longer blood circulation than PEG2k-Lys-PAMAM (G4) dendrimers (with low M_w) (Kojima et al., 2010). Following systemic administration in neonatal rabbits, G4 PAMAM-OH dendrimers labelled with Cy5 dye (D-Cy5) showed fast renal clearance with relatively high accumulation in kidneys and bladder after 24 h, than free Cy5 (Lesnaik et al., 2013). The effect of surface charge of G5 PAMAM dendrimers on its biodistribution was studied in B16 melanoma and DU145 prostate tumor models. Cationic dendrimers showed higher tissue deposition and accumulated in mainly lungs, liver and kidneys with ~3% of initial dendrimer-loading within 1 h post i.v. injection. The urine clearance of neutral dendrimers was three times faster than positively-charged dendrimers (48.3 % and 29.6 %, respectively). Excretion via faeces was comparatively very less for neutral and positive dendrimers (5.4 % and 2.9 %, respectively) over 7 days. The long-term distribution studies till 12 weeks in non-tumor mice revealed that

dendrimers were detected in all organs tested, with minimal levels in brain (Nigavekar et al., 2004).

2.2.4.5. End groups and toxicity

Dendrimers hold immense potential as nanocarriers or 'smart delivery systems' as they can cross the cell barriers by both paracellular and transcellular pathways. After gaining entry, they can circulate in the mainstream for the time needed to exert the clinical effect (Menjoge et al., 2010). To be used for pharmaceutical applications, dendrimers need to be evaluated as biologically safe materials. In recent years, several reports point out the toxicity concerns related to cationic macromolecular systems such as cationic PAMAM dendrimers. The cytotoxicity contributed by dendrimers is found to be concentration, generation and surface-charge dependent. Anionic and neutral-charged surfaces of dendrimers display biocompatibility compared to positively-charged surfaces which show strong toxicities. Moreover, lower generation anionic dendrimers (with carboxylate surface groups) (G=0,1) are not much permeable to biological membranes than higher generation dendrimers (G=2-5) (Boas et al., 2006, Najlah et al., 2007 and Klajnert et al., 2007). While, amine groups bearing dendrimers (G=3-7) bearing positive charges are known to strongly interact and permeate the negatively-charged cell membranes. The order of cytotoxicity of PAMAM dendrimers when tested on human intestinal adenocarcinoma Caco-2 cells is hydroxyl-terminated < carboxyl-terminated < amine-terminated systems. (Sadekar et al., 2012). Byrne and co-workers have reported the cytotoxic response of successive generations of PAMAM dendrimers (G4, G5 and G6) with increasing number of surface amine groups using different *in vitro* and *in vivo* models. The cytotoxicity of PAMAM dendrimers was determined by various biological assays whereby, G6>G5>G4 (Naha et al., 2009, Naha et al., 2010, Mukherjee et al., 2010 and Naha et al., 2013). Further investigations on amine-terminated PAMAM dendrimer interactions with 1,2-dimyristoyl-sn-glycero-3-phosphocholine (DMPC) lipid bilayers and KB and Rat2 cell membranes revealed interesting observations. G7 PAMAM dendrimers (10-100 nM) form holes of 15-40 nm diameter in aqueous lipid bilayers, while G5 PAMAM dendrimers did not initiate hole formation but expanded holes at the existing defects (Hong et al., 2004). The hole formation could be due to removal of lipids or direct insertion of dendrimers into the membrane (Mecke et al., 2005 and Lee et al., 2008). These amino-terminated PAMAM dendrimers are also identified to induce generation and dose-dependent haemolytic effects (Malik et al., 2000 and Klajnert et al., 2010). Besides, PAMAM dendrimers exhibit low toxicity in comparison to amino-functionalized linear polymers probably due to lesser interaction of globular dendrimers with the cellular surfaces. This suggests that toxicity also depends on type of amine functionality and degree of substitution with primary amines being more toxic than

secondary or tertiary amines (Fischer et al., 2003). With this context, surface engineering of the amino-terminated dendrimers to manipulate their overall positive charges has been implemented. By attaching poly (ethylene glycol) (PEG) chains to the dendrimer surfaces (PEGylation) the circulation times for dendrimers in the body can be increased manifold and its cytotoxicity can be suppressed (Bhadra et al., 2003, Chen et al., 2004, Guillaudeu et al., 2008 and Kaminkas et al., 2014). Surface amidation by introducing neutral acetyl groups can be another way to by-pass the cytotoxicity issues of dendrimers without touching their unique advantages (Kolhatkar et al., 2007, Waite et al., 2009 and Fant et al., 2010).

2.2.5. Biological applications of dendrimers

Keeping the mind the magnificent architecture and structural versatility of dendrimers they have been reviewed by researchers as potent nanocarriers for anticancer therapeutics. Their multifunctional exterior and multivalency can be used to either attach or encapsulate drug molecules, targeting moieties and solubilizing groups to the periphery in a precise manner. Moreover, the low polydispersity of dendrimers contrarily to some linear polymers with distinct molecular weight can provide reproducible pharmacokinetic behavior. Such interesting properties make dendrimers highly suitable for biological applications (Nishikawa et al., 1996).

2.2.5.1. Dendrimers as drug carriers

Phenomenal properties of dendrimers such as high water solubility, monodisperse size and uniform composition (Sezaki et al., 1989, Singer et al., 2001, Winne et al., 2005 and Shi et al., 2006) are exuberant especially for anticancer drug delivery and imaging (D'Emanuele et al., 2005, Gillies et al., 2005b and Kobayashi et al., 2005). These properties impart batch to batch consistency in anticancer activity achieved by dendrimer based delivery systems. The three-dimensional structure and high density of surface functional groups can be exploited to either encapsulate or conjugate large number of therapeutic agents to be selectively transported to the cytoplasm of cancer cells to exhibit therapeutic effects (Ooya et al., 2004 and Wu et al., 2004). Inside the core of dendrimers the environment differs than the one at the periphery. The globular shape and highly branched dendrimers offer potential routes to encapsulate various guest molecules by weak supramolecular host-guest interactions. Guest molecules can be entrapped and stabilized in the internal cavities based on the idea of "dendritic box". This concept is based on the presence of large number of functional groups at the periphery of high generation dendrimers which formulate a stearic shell thereby separating the core from the bulk allowing the guest molecules to accommodate inside the core of the macromolecular host (Jansen et al.,

1994). Drugs can either be non-covalently encapsulated in the interiors or attached to the surface to form dendrimer-drug conjugates **(Figure 2.4)**.

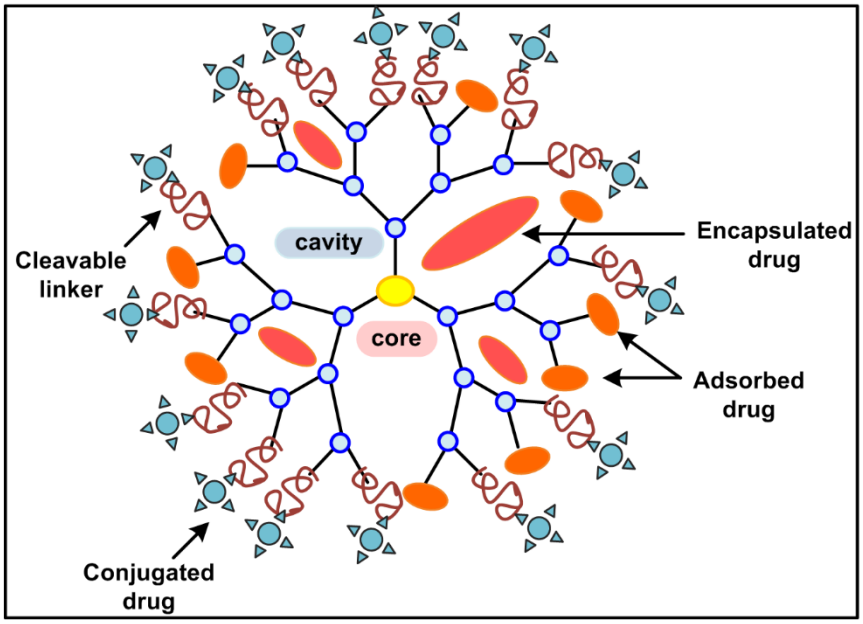

Figure 2.4. Different ways of attachment of drug molecules to dendrimers.

2.2.5.1.1. Drug-encapsulated dendrimers

In recent years numerous reports are available wherein high generation dendrimers have been used for accommodation of anticancer drugs under physiological conditions. Poly(glycerol succinic acid) dendrimers, or PGLSA dendrimers were evaluated for delivery of camptothecins (group of naturally derived hydrophobic compounds with anticancer activity). In earlier studies G4-PGLSA dendrimers with hydroxyl (G4-PGLSA-OH) or carboxylate (G4-PGLSA-COONa) termini were investigated to encapsulate and deliver 10-hydroxycamptothecin (10-HCPT) to cancer cells. Approximately, 10-fold increase in the water solubility was observed when 10-HCPT was encapsulated in G4-PGLSA-COONa dendrimers. When exposed to cancer cells, dendrimers alone were not cytotoxic at the tested concentrations. While, dendrimer encapsulated 10-HCPT drastically reduced the cell viability with lower IC_{50} values compared to free 10-HCPT in DMSO. For instance, the IC_{50} values of encapsulated 10-HCPT was 10, 16.7, and 4.6 nM, and for free 10-HCPT it was 72, 32.4 and 13.1 nM, respectively in MCF-7 (breast cancer), NCI-H460 (lung cancer) and SF-268 (glioblastoma) cells. This indicates the 7.1, 1.9 and 2.8-fold potency of dendrimer encapsulation over free drug. Uptake studies performed in MCF-7 cells revealed a 16-fold increment in the cellular uptake of dendrimer encapsulated 10-HCPT (Morgan et al., 2003, 2005 and 2006). In another study, G4 PAMAM-NH_2 dendrimers demonstrated increased

permeability and cellular uptake of 7-Ethyl-10-hydroxy-camptothecin (SN-38), an antitumor agent across the Caco2 cell monolayers (Kolhatkar et al., 2008).

A similar trend in the cytotoxicity profile was observed with dendrimer-cisplatin complexes. The IC_{50} values of G4 PAMAM-NH_2 dendrimer-cisplatin complexes were significantly lower than free cisplatin in OVCAR-3, SKOV-3, A2780 (wild-type ovarian cancer) and CP70 (A2780/CP70, cisplatin-resistant) cells. Moreover, the platinum content of G4 PAMAM-NH_2 dendrimer-cisplatin detected by HPLC was 10-times more in the cisplatin-resistant ovarian cancer cells (Yellipeddi et al., 2011). Hence dendrimers were proficient to deliver cisplatin to even resistant cancer cells. Also, PEGylated PAMAM dendrimers loaded with 5-FU and DOX, enhance their intracellular uptake with slow release rates and high inhibitory effects (Bhadra et al., 2003 and Liao et al., 2014). In another study by Hu and group, the interior pockets of fully acetylated G4, G5 PAMAM and G4 PPI dendrimers were functionalized with 1,3-propane sultone (PS) (this generates zwitterions) for improved encapsulation and sustained release of methotrexate sodium (anticancer drug). While evaluating the cytotoxic effects in MCF-7 cells, Ac-G4-PS/drug complex with 20 µM methotrexate showed much lower inhibition (~ 31.9 %) than 5 µM free methotrexate (~ 45.5 %). This indicated that Ac-G4-PS PAMAM/drug formulations can augment the maximum tolerance dose of drug in clinical trials due to a sustained release mechanism (Hu et al., 2011).

By anchoring ligands to the dendrimer surface, the anticancer efficacy of the encapsulated therapeutic drugs can be improved. He and group synthesized DOX loaded dual-targeting drug carrier G4 PAMAM-PEG-WGA-Tf with transferrin (Tf) and wheat germ agglutinin (WGA) on the periphery against brain gliomas. After 2 h, the nanocarrier delivered 13.5 % of DOX compared to 8 % for PAMAM-PEG-WGA, 7 % for PAMAM-PEG-Tf and 5 % for free DOX. Tf and WGA enhanced the targeting effect of the carrier causing increased accumulation of DOX at the tumor site leading to the complete breakage of the avascular C6 glioma spheroids (He et al., 2011). Further, G5 PAMAM /FA (folic acid)/FI (fluorescein isothiocyanate)-multiwalled carbon nanotubes (MWCNTs) loaded with DOX showed targeted and pH responsive delivery to KB cells over expressing folic acid receptor (FAR). The modified CNTs showed high drug payload and encapsulating efficiency of 97.8 %. MWCNT/G5.NHAc-FI-FA in itself did not generate any cytotoxicity (concentrations 1-4 µM) while, when loaded with DOX decreased the KB cell viability to 67 % (Wen et al., 2013a). In a recent attempt by Wei and co-workers, amphiphilic dendrimer-based nanomicelles were synthesized by molecular self-assembly to encapsulate anticancer drugs with small size and high payload. The amphiphilic dendrimer

(AmDM) comprise of a small hydrophilic PAMAM dendron and two hydrophobic C_{18} alkyl chains bridged via click chemistry. AmDM nanosystem were used to form supramolecular micelles in solution to encapsulate DOX with high loading capacity (> 40%). AmDM/DOX micelles in both DOX-sensitive MCF-7S cells and resistant MCF-7R cells demonstrated lower IC_{50} values (0.62 and 2.0 μM, respectively) than those of free DOX (6.1 and >100 μM) and Caelyx (>100 μM). Hence, they were more effective than free drug DOX and nanodrug Caelyx in reducing cell proliferation in both drug-sensitive and drug-resistant cell lines, eventually leading to apoptosis induced anticancer activity. Upon i.v. injection of AmDM/DOX micelles in NOD scid gamma (NSG) mice bearing tumors derived from MCF-7R cells, significant tumor inhibition was seen (at 2.5 and 5.0 mg/kg) than free DOX. Moreover, fluorescence based biodistribution studies in mice, revealed deeper tumor penetration of AmDM nanosystem due to the EPR effect (Wei et al., 2015).

2.2.5.1.2. Dendrimers-drug conjugates

Another strategy could be covalent conjugation of drug molecules with the dendrimer external functional groups. In this approach, the covalently bound drugs can be released via chemical or enzymatic cleavage of hydrolytically labile bonds. Complexation of drugs with the dendrimer molecules by simple encapsulation or via electrostatic interactions can retain the chemical integrity and pharmacological properties of drug molecules, while covalent conjugation of drugs to the surface functional groups of dendrimers through chemical linkages can enable controlled drug release which cannot be achieved by simple encapsulation/electrostatic complexation approaches (Wolinsky et al., 2008 and Caminade et al., 2014).

Patri and co-workers compared the release kinetics of covalently conjugated and hydrophobically complexed methotrexate (MTX) drug to G5 PAMAM dendrimers. The activity of MTX complexed within dendrimer was comparable to free drug *in vitro* while the covalently conjugated drug was better suited for targeted drug delivery as it inhibits the premature release the drug under biological conditions (Patri et al., 2005). Another study suggested stochastic functionalization of MTX and TAMRA (tetramethylrhodamine) fluorophore conjugated to PAMAM dendrimers by copper-free click chemistry. The reaction involves esterase stable amide linkages and the conjugate exhibited comparatively less toxicity than free MTX towards B16–F10 (melanoma) cells (Thomas et al., 2012). In another attempt, biotinylated poly (L-glutamic acid) dendrimers with OAS cores (oligomeric silsesquioxane) carrying DOX were investigated for anticancer effects against mice breast cancer 4T1 cells. The formulated nanocarrier showed reduced the systemic toxicity of DOX and enhanced the inhibition activity

to the xerograft breast cancers in mice. The tumor inhibition rates increased from 43.8 % in OAS-G3-hyd-DOX to 60.6 % OAS-G3-hyd-DOX/Biotin nanoparticles (Pu et al., 2013). However, covalent conjugation of active drugs through stable bonds can alter its efficiency (Goller et al., 2001). In a comparative study, DOX was conjugated to G4 PAMAM dendrimers either through a non-cleavable amide group (a PEG-PAMAM-succinic-DOX (PPSD) conjugate) or an amide group cleavable under acidic conditions (a PEG-PAMAM-cis-aconityl-DOX (PPCD) conjugate). PEG derivative was utilized to enhance the water solubility of conjugates, reduce their toxicity towards healthy cells and enhance their tumor uptake. Although both conjugates were internalized by SKOV-3 cells but only cleavable PPCD conjugates were able to release DOX to induce cell death while PPSD conjugates displayed no toxic effects (Zhu et al., 2010). Use of Janus dendrimers (two types of terminal functions in two different areas of the surface of the dendrimer) for dendrimer-drug conjugates has been described (Caminade et al., 2014). An asymmetric biodegradable polyester dendrimer (modified with PEG derivatives) conjugated to DOX with cleavable acyl hydrazone linkages has been used *in vivo* in mice bearing C-26 colon tumors. A single i.v. injection of the Janus dendrimer-DOX conjugates was able to release DOX (through cleavage of pH sensitive acyl hydrazone linker) caused complete tumor regression and 100 % survival of mice, whereas with DOX alone or Janus dendrimer- DOX conjugate linked through stable carbamate bond, no cure was achieved. Ability of dendrimer to favourably modulate the pharmacokinetics of conjugated DOX can be held worthy of the remarkable antitumor activity. All the above stated examples of dendrimer-drug conjugates involve use of pH sensitive linkages, i.e. release of attached drug occurs specifically under acidic conditions. Such linkers are expected to be cleaved more rapidly in cancer cells (with low pH conditions) than normal cells, which is still a hypothetical condition (Tannock et al., 1989 and Griffiths et al., 1991). Generally, as stated before, covalent attachment of drugs to the dendrimer periphery (wherein the release of drug can be controlled) can exert more antitumor activity compared to free drug or dendrimer-entrapped drug under similar biological conditions. However, the complexity of reaction which involve use of chemical linkers to conjugate anticancer drugs to the dendrimer functional groups can complicate the entire therapeutic procedure. Moreover as described, drugs can be released by cleavage of chemical linkages in tumor milieu which can sometimes result in low drug release and can prove incompetent in tumor inhibition and therapy.

2.2.5.2. Dendrimers for cancer diagnostics

Availability of imaging agents that can detect and quantitatively estimate *in vitro* and *in vivo* cellular events can prove useful for early cancer diagnosis and therapeutics (Sahoo et al., 2014). The ideal molecular imaging agent would be specifically directed towards the target organ and

should deliver the imaging payload without any alteration in its functionality. Structural flexibility and availability of multiple attachment sites on the dendrimer surface has opened up avenues for development of dendrimer based Computed Tomography (CT), nuclear medicine, optical imaging and Magnetic Resonance Imaging (MRI) agents. The targeting ligands can be attached to dendrimer exterior termini and contrast agents can either be conjugated with the peripheral groups or can be resided in the core (Longmire et al., 2008). Two classes of dendrimers with MR imaging proficiencies have been developed: dendrimers incorporating gadolinium (Gd) chelates and magneto-dendrimers (i.e. dendrimers containing paramagnetic iron oxide particles). Dendrimer based MRI agents offer better relaxivity and increased circulation times than conventional low molecular weight (LMW) contrast agents such as Gd-DTPA (DTPA = diethylenetriaminepentaacetic acid) and Gd-DOTA (DOTA = 1,4,7,10-tetraazacyclododecane-1,4,7,10-tetraacetic acid). Gd-based dendrimer agents for MRI are 'positive' contrast agents as compared to iron oxide-based agents which produce a differential enhancement by signal reduction (Barrett et al., 2009). Chiral dendrimer–triamine-coordinated Gd complexes as contrast agents for MRI imaging offer longitudinal relaxivity (r1) 3 times higher than that of clinically used Gd-DTPA (Miyake et al., 2012). PEGylated Gd-loaded dendrimer-entrapped gold nanoparticles (Gd-Au-DENPs) with two radiodense imaging elements AuNPs and Gd(III) in a single system display both CT/MR imaging capabilities with increased circulation times. They were able to image heart, liver, kidney, and bladder of rat or mouse within a time frame of 45 min (Wen et al., 2013b). Chen et al., 2013b developed FA conjugated- Gd-Au-DENPs as nanoprobes for targeted CT/MR imaging of cancer cells. Lactobionic acid (LA)-modified dendrimer-entrapped gold nanoparticles (LA-Au DENPs) have been used for *in vitro* and *in vivo* targeted CT imaging of human hepatocellular carcinoma. LA-Au DENPs imaging probes were injected both intravenously and intraperitonealy to the mice. The results suggested that the tumor CT values of the targeted group injected with LA-Au DENPs was much more than the non-targeted group at same time points. Additionally, intravenous injection enabled much more sensitive CT imaging of the tumor model compared to intraperitoneal injection (Liu et al., 2014b).

Biodegradable polydisulfide dendrimer nanoclusters (DNCs) labelled with Gd chelates have been tested as MRI contrast agents. Accumulation of Gd was tested in various organs of mice including heart, lung, liver, kidney, spleen, and blood 24 h post-injection with the highest uptake observed in the kidney (5.68 ± 2.32 % I.D./g) followed by liver (4.52 ± 1.93 % I.D./g) and then the spleen (2.95 ± 1.36 % I.D./g). Polydisulfide DNCs exhibited a circulation half-life of > 1.6 h in mice with significant contrast enhancement in the abdominal aorta and kidneys for around

4 h. A significant contrast enhancement in T1-weighted images was seen in kidneys and abdominal aorta at 15 min and 1 h post-injection of Polydisulfide DNCs compared to G3 PAMAM dendrimers (Huang et al., 2012). All the above stated examples clearly implicate that the road towards improvement of efficiency in dendrimer-based contrast agent synthesis will increase their availability for clinical applications. Perhaps the most exciting new horizon could be combining the molecular contrast agents and therapeutic payloads in a single dendrimer molecule to achieve imaging of malignant tissue for therapeutic benefit.

2.2.5.3. Dendrimers for cancer theranostics

The term "theranostics" was coined by Funkhouser in 2002 which combines *therapeutic* and *diagnostic* agents in a single material is a significant advancement in personalised therapy (Funkhouser et al., 2002, Janib et al., 2010 and Veeranarayanan et al., 2015). Development of dendrimer based nanocarriers for simultaneous deliver of therapeutic and imaging modalities to cancer cells can undoubtedly tailor the conventional treatment options. These nanosized tightly packed cargos can overcome the undesirable differences in biodistribution and selectivity that exists with distinct therapeutic and diagnostic modalities. In brief, when administered in cancer cells dendrimer based theranostic nanoplatforms can mediate concurrent imaging of the outcomes of therapeutic agents (Kelkar et al., 2011, Muthu et al., 2014 and Sk et al., 2015).

Literature supports various studies which claim beneficial use of dendrimers for simultaneous drug delivery and imaging for cancer therapy. Majoros and colleagues developed PAMAM dendrimer based theranostic nanodevices for cancer therapy. G5 PAMAM dendrimers with anticancer drugs methotrexate (MTX) and paclitaxel (PTX) were modified with fluorescent dye (FI) and targeting ligand FA (Majoros et al., 2005 and 2006). They also evaluated saccharide-terminated G3 PAMAM dendrimer for theranostic applications. The conjugates demonstrated efficient cellular internalization and cytotoxicity in FA-overexpressing cells (Zhang et al., 2011). Chang and group designed non-conjugated and FA conjugated PEG-modified PAMAM dendrimers with PTX, Cy5.5 fluorophore and superparamagnetic iron oxide (IONPs) (FA-PEG-G3.5-PTX-Cy5.5@IONPs) for their antiproliferative effects and MRI imaging of tumors. After 2 h incubation, FA-PEG-G3.5-PTX-Cy5.5 and mPEG-G3.5-PTXCy5.5 conjugates sufficiently accumulated in cytoplasm of MCF-7 cells described by the red coded fluorescence of Cy5.5. In MRI evaluation studies, after 24 h post-injection tumor areas were observed as hyper-intense regions owing to IONP conjugates accumulation (Chang et al., 2013). Zhu and co-workers synthesized alpha-tocopheryl succinate (α-TOS) conjugated multifunctional dendrimer-entrapped gold nanoparticles (Au DENPs) for targeted cancer theranostic applications. When

tested in U87MG (brain gliomas), the cancer cell inhibition efficacy of Au-TOS-FA DENPs was significantly higher than free α-TOS (at α-TOS conc. >12.5 μM). IC_{50} of Au-TOS-FA DENPs (19.2 μM) was far less than free α-TOS (30.6 μM) after 24 h. Similarly, Au-TOS-FA DENPs-treated mice showed superior tumor inhibition effect (5.23 ± 0.72 times tumor growth) than free α-TOS (7.37 ± 0.65 times tumor growth) and Au-TOS DENP-treated group (6.65 ± 1.00 times tumor growth). When tested for CT imaging application, the CT images of mice injected with Au-TOS-FA DENPs after 24 h were brighter than non-targeted groups (Zhu et al., 2014). Recently, Zhao and co-workers synthesized chlorotoxin (CTX)-conjugated multifunctional PAMAM dendrimers labelled with radionuclide ^{131}I as nanoprobes for targeted single photon emission computed tomography (SPECT) imaging and radiotherapy of MMP2-overexpressing gliomas (Zhao et al., 2015). In another study by Zhu and co-workers, G5 PAMAM dendrimers were modified with chelator/gadolinium (Gd) complexes and FA via a PEG spacer to deliver DOX and for MR imaging of KB cancer cells (Zhu et al., 2015). He et al., 2015 prepared a multifunctional G5 PAMAM dendrimer conjugated with PEG, arginyl-glycyl-aspartic acid (RGD) peptide and FI for DOX delivery to integrin $\alpha_v\beta_3$-overexpressing glioblastoma U87MG cancer cells. The dendrimer conjugates released DOX in a sustained manner and were internalized in cells by receptor-mediated endocytic pathway. Further efforts are being laid on development of asymmetric dendritic structures with high structural complexity to provide multiple functionalities for delivery of theranostic agents. Ornelas et al., 2011 synthesized a Janus-like multifunctional dendrimer comprising of 9 azide termini, 9 amine termini and 54 terminal acid groups as next generation of materials for cancer theranostics. Aptamer-conjugated PAMAM dendrimer-modified quantum dots have been used for imaging of U251 (glioblastoma) cells (Li et al., 2010). Peptide conjugated PEGylated-PPI dendrimer with numerous hydrophobic pockets can encapsulate photosensitizers such as phthalocyanines (Pc) for fluorescence image-guided drug delivery and non-invasive treatment of deep tumors by photodynamic therapy (PDT). Such Pc based theranostic modalities allow visualization of malignant tissue by fluorescence imaging when accumulated and thereafter near infrared (NIR) light can be precisely applied on the detected cancer tissue for PDT leaving the healthy organs untouched (Taratula et al., 2013).

2.2.6. Dendrimers as templates or stabilizers for metal nanoparticle synthesis

The use of dendrimer molecules as templates to control the size, stability and solubility of metal NPs is an attractive area. They are well-suited to host metal ions precursors which can later be converted by reduction to NPs in the size range 1-5 nm. The chief reasons for which dendrimers can serve as hosts or templates for metal NP synthesis include: (a) dendrimer have a uniform

composition and architecture and can facilitate synthesis of NPs with minimal size deviations, (b) Since the metal NPs are stabilized within dendrimer cavities, chances of agglomeration are considerably reduced, (c) Because the surface of dendrimer-entrapped metal NPs is passivated by the dendrimer branching groups, the solubility properties of NPs can be tailored by amending the peripheral surface and (d) importantly, when considered for biological applications the undesirable toxicity associated with non-passivated metal NPs are subsided with use of dendrimer entrapped or stabilized nanoparticles. All these advantages stems from the unique structural and chemical properties of dendrimers (Crooks et al., 2001). The size and properties of metal NPs synthesized heavily depend on the generation, and surface functionality of dendrimer used. By using G3-G5 PAMAM.NH_2 dendrimers, gold (Au) NPs in size range 1.5-4.0 nm were obtained wherein their size decreased with increasing concentration as well as generation number of the dendrimers (Esumi et al., 2000). With G5 PAMAM.NH_2 dendrimers as templates, the size of Au DENPs (~ 2.2 nm) remained unaffected after surface acetylation, only the surface charges changed. Contrarily, the size of Ag NPs obtained using pristine dendrimers increased from ~ 2.9 nm to 11 nm after complete acetylation of terminal dendrimer amines (Shi et al., 2007). By changing the reaction conditions, G5 PAMAM dendrimers are known to spontaneously form Au, Ag and Au-Ag binary dendrimer stabilized NPs (DSNPs), wherein one NP is surrounded by multiple dendrimers (Garcia et al., 1999, Endo et al., 2005, Shi et al., 2009, Liu et al., 2010a, Liu et al., 2013 and Yuan et al., 2013). Platinum (Pt) NPs in size regime 2.4-3.0 nm were obtained with G3-G5 PAMAM dendrimers and their sizes were insensitive to concentration and generation of dendrimer templates (Esumi et al., 2000). Palladium (Pd) NPs with size ~ 3.2 nm were synthesized using G4-OH PAMAM dendrimers as templates (approximate diameter = 4.5 nm) (Pittelkow et al., 2003).

2.2.7. Dendrimers for nanogels synthesis

Nanogels are nanoscale-sized hydrogel particles formulated by physically or chemically cross-linked hydrophilic polymers (Kabanov et al., 2009 and Li et al., 2015b). They have recently been exploited in various fields including diagnostics, chemical and biochemical sensing, tissue engineering, cancer imaging, and especially drug delivery (Oishi et al., 2007, Wu et al., 2010, Peng et al., 2010, Miyahara et al., 2012 and Banerjee et al., 2016). Compared to existing nanocarriers, nanogels offer several advantages in therapeutic delivery applications which include (i) high drug loading capacity, (ii) high storage stability than liposomes and micelles, (iii) controlled and sustained drug release, (iv) ease of synthesis, (v) response to external stimuli, and (vi) low inherent toxicity (Chiang et al., 2012 and Eckmann et al., 2014). When dispersed in aqueous media, swollen nanogels are soft with high water absorption capacities. Their flexibility

and versatility have offered them prime focus as potent DDS. Till date, they have been synthesized by either polymerization of monomers or by cross-linking of pre-synthesized or natural polymers by microemulsion or inverse microemulsion techniques (Liu et al., 2014a).

Nanogels prepared using natural polymers such as collagen, chitosan, alginate, pullulan, gelatin, dextran, cellulose, hyaluronic acid, and polypeptides are inherently biocompatible and biodegradable (Park et al., 2012, Kim et al., 2013, Maciel et al., 2013, Morimoto et al., 2013, Zhou et al., 2013a, Gandhi et al., 2014, Bendtsen et al., 2015, Dutta et al., 2016 and Natarajan et al., 2016). PAMAM dendrimers are also known to act as key ingredients in nanogels preparation. However, very few papers are available which have reported use of PAMAM dendrimers as it is a relatively new topic. In a study by Goncalves and co-workers, dual-cross-linked dendrimer/alginate fluorescent nanogels (AG/G5) were synthesized using $CaCl_2$ as a cross-linker and G5 PAMAM dendrimers as co-cross-linkers through emulsion technique. During synthesis, dendrimers were found to significantly reduce the size of nanogels. AG nanogels synthesized in absence of dendrimers were ~ 873 nm in size, while AG/G5 nanogels were of ~ 433 nm. These AG/G5 nanogels were used for DOX encapsulation and were able to deliver it to CAL-72 cells (a human osteosarcoma cell line) for a prolonged time (Goncalves et al., 2014).

In summary, the literature review elaborated the phenomenal potential of nanomedicine in revolutionizing the present cancer treatment options and some of the commercially available nanomedicines for treating cancer patients. Considering the tremendous advantages associated with polymeric nanomedicines, a special focus is being laid to identify new nanocarriers that can surpass all the challenges and emerge as effective delivery systems of anticancer agents. With this background, the structure, properties and biological properties of dendrimers as prospective nanocarriers for cancer therapy were studied in detail. With the observations and understanding from the literature, the scope for further research on dendrimer based nanomedicines was identified, as listed in section 1.1. The experimental investigations, analysis and inferences drawn to achieve the targeted goal are mentioned in detail in the following chapters.

CHAPTER 3

MATERIALS AND METHODS

This chapter includes the materials section and the methodology adopted for synthesis and in vitro testing of different PAMAM dendrimer based nanomaterials.

CHAPTER 3

MATERIALS AND METHODS

3.1. MATERIALS

3.1.1. Reagents

- PAMAM dendrimer, ethylenediamine core, generation 5.0 solution (Sigma-Aldrich, cat.no. 536709) **NOTE:** MeOH content in PAMAM solution was removed by rotary evaporation under reduced pressure.
- 5-FU, ≥99 % (5-Fluorouracil) (Sigma-Aldrich, cat. no. F6627)
- $AgNO_3$ (silver nitrate) (Merck, cat. no. 1.93200.0027)
- $NaBH_4$, ≥95 % (sodium borohydride) (Merck, cat. no. 61792701001730)
- Triton X-100 (Merck, cat. no. RM845)
- NaOH (sodium hydroxide) (SRL, cat.no. 1949181)
- HNO_3 (nitric acid) (Rankem, cat.no. N0060)
- CH_3-CH_2-OH (ethanol) (Amresco, cat.no. E193)
- Sodium alginate (from brown algae) (Sigma-Aldrich, cat.no. W201502)
- EDC (N-(3-Dimethylaminopropyl)-N′-ethylcarbodiimide hydrochloride) (Sigma-Aldrich, cat.no. E7750)
- EPI.HCl, ≥90 % (epirubicin hydrochloride) (Sigma-Aldrich, cat.no. E9406)
- $CaCl_2$ (anhydrous calcium chloride) (Himedia, cat. no. GRM710)
- CH_3COONa (sodium acetate) (VETEC, cat.no. V800363)
- KBr (potassium bromide) (Merck, cat. no. 1.04907.100)
- Myristic acid ($CH_3(CH_2)_{12}COOH$) (SRL, cat.no. 134932)
- N-hydroxysuccinimide (NHS) (Sigma-Aldrich, cat.no. 130672)
- Tamoxifen (TAM, ≥99 %) (Sigma-Aldrich, cat.no. T5648)
- Coumarin-6 (≥98 %) (Sigma-Aldrich, cat.no. 442631)
- DMSO-D6 (Euriso-top, cat. no. D310ES)
- $(CH_3CO)_2O$ (acetic anhydride) (Thomas Baker, cat. no. 0750)
- $(CH_3)_3N$, >99 % (triethylamine) (Thomas Baker, cat. no. 121-44-8)
- MeOH (anhydrous or dry methanol) (SDFCL, cat.no. 39193 L10)

- Chitosan (low molecular wt.) (Sigma-Aldrich, cat.no. 448869)
- PEG-4000 (poly (ethylene glycol)) (SRL, cat.no. 1647131)
- CH_3COOH (glacial acetic acid) (SRL, cat.no. 0129168)
- Glutaraldehyde (Sigma-Aldrich, cat. no. 340855)
- PTA (phosphotungstic acid) (Sigma-Aldrich, cat. no. P4006)
- A549 (lung cancer), MCF-7 (breast cancer) and NIH3T3 (mouse embryonic fibroblast) cells (NCCS Pune)
- DMEM (Dulbecco's minimum essential medium) (Himedia, cat. no. AT007)
- FBS (fetal bovine serum) (Gibco, cat. no. 10270-106)
- Penicillin-streptomycin (Gibco, cat. no. 10378-016)
- DPBS, Ca^{2+} and Mg^{2+} free (Dulbecco's phosphate buffer saline) (Sigma-Aldrich, cat. no. D5652)
- Trypsin-EDTA, 0.25 % (Sigma-Aldrich, cat. no. 25200-072)
- MTT (3-(4,5-Dimethyl-2-thiazoyl)-2,5-diphenyltetrazolium bromide) (Amresco, cat no. 0793)
- AO (Acridine orange) (Himedia, cat. no. TC262)
- EtBr (ethidium bromide) (SRL, cat. no. 054817)
- DCFDA (2′,7′-dichlorofluorescin diacetate) (Sigma-Aldrich, cat. no. D6883)
- Hoechst 33342 (Sigma-Aldrich, cat. no. 14533)
- Rhodamine B (Sigma-Aldrich, cat. no. 83689)
- Rhodamine 123 (Sigma-Aldrich, cat. no. R8004)
- Lysotracker Green (Life Technologies, L7526)
- Lysotracker Red (Life Technologies, L7528)
- PI (Diamino-5-[3-(diethylmethylammonio) propyl]-6-phenylphenanthridinium diiodide) (Sigma-Aldrich, cat. no. P4170)
- Tri reagent (Sigma-Aldrich, cat. no. T9424)
- Agarose (SRL, cat. no. 83404)
- Tris buffer (SRL, cat. no. 2044122)
- EDTA (Ethylenediaminetetraacetic Acid) (SRL, cat. no. 054448)
- Ultrapure water (18 MΩ cm) (Millipore)

3.1.2. Equipments

- UV–Visible spectrometer (Lasany double-beam L1 2800)
- Transmission electron microscope (TEM) (FEI TECHNAI G2)
- X-ray diffractometer (XRD) (Bruker AXS D8 Advance)

- Zetasizer (Malvern Zetasizer Nano ZS90)
- Nuclear magnetic resonance (NMR) spectrometer (Bruker 500 MHz)
- Atomic absorption spectroscope (AAS) (Avanta M, GBC)
- Fourier transform infrared spectrometer (FTIR) (Thermo Nicolet)
- Thermogravimetric Analyzer (TGA) (TG/DTA SII 6300 EXSTAR)
- Brunauer–Emmett–Teller (BET) Analyzer (Quantachrome NOVA 2200e)
- Mechanical tensile tester (Bose ElectroForce 3230 Series III)
- Fluorescence spectrophotometer (Hitachi, F-4600)
- Fluoro Cube Fluorescence Lifetime System (Horiba Jobin Yvon)
- Micro volume spectrophotometer (Denovix)
- Inverted fluorescent microscope (EVOS FL Color, AMEFC 4300)
- Field emission-scanning electron microscope (FE-SEM) (Ultra plus-Carl Zeiss)
- Microplate reader (Cytation3, Biotek)
- Flow cytometer (Amnis Flowsight)
- Thermal cycler (Veriti, Applied Biosystems, ThermoFisher Scientific)
- Gel documentation System (Gel Doc) (BioRad)
- Automated cell counter (Invitrogen)
- Centrifuge (Beckman Coulter)

3.2. PROCEDURE

3.2.1. Synthesis of G5 PAMAM dendrimer stabilized silver nanoparticles (DsAgNPs)

1. Weigh 2.8 mg $AgNO_3$ in a 1.5 mL mini centrifuge tube and dissolve it in 125 µL ultrapure water (18 MΩ cm).

CRITICAL: $AgNO_3$ is very sensitive to light, cover the tube with aluminium foil.

2. Dissolve 8.31 mg G5 PAMAM dendrimer in 500 µL water in another vial.
3. Carefully add $AgNO_3$ solution to PAMAM aqueous solution under vigorous magnetic stirring at 660 rpm.
4. Weigh 2.2 mg $NaBH_4$ and dissolve it in 200 µL ice-cold water/methanol (v/v 3:1) mixture.

CRITICAL: $NaBH_4$ solution gets oxidised quickly, always prepare the solution fresh.

5. After 30 min, add the $NaBH_4$ solution to PAMAM-$AgNO_3$ solution very slowly.

NOTE: The colour of the solution immediately turns dark yellow upon $NaBH_4$ addition.

6. Leave the reaction undisturbed for 2 h, away from light.
7. Dialyze the obtained solution using regenerated cellulose membrane (MWCO 10 kDa) against PBS (3 times, 4 L) and water (6 times, 4 L) for 3 days to remove excess reactants.

8. Lyophilize the dialyzed solution to obtain brown-colored DsAgNPs powders and store at -20 °C until use.

NOTE: DsAgNPs can also be stored at 4 °C for immediate use.

9. The concentration of Ag can be estimated by ICP-MS or AAS before 5-FU entrapment.

3.2.2. Preparation of 5-FU loaded DsAg nanocomposites (5-FU@DsAgNCs)

1. Take aqueous solutions of 5-FU and DsAgNPs (100:1 molar ratio) in a dark colored glass vial and magnetically stir at 100 rpm.
2. After 24 h, transfer the solution to a dialysis bag (MWCO 10 kDa) and dialyze the solution against water twice under strict sink conditions for 20 min.
3. Then, lyophilize the solution to obtain 5-FU@DsAgNCs in powdered form and re-dissolve in water prior to use.
4. The amount of 5-FU loaded in 5-FU@DsAgNCs can be estimated from the dose-absorption curve of free 5-FU in PBS (0-50 μg mL^{-1}) at 265 nm using a UV-Vis spectrometer.
5. Drug loading efficiency (DLE, wt. %) of 5-FU in 5-FU@DsAgNCs can be calculated according to following formula:

$$DLE\ (\%) = [(\text{Amount of loaded 5-FU}/\text{Amount of initial 5-FU})] \times 100$$

3.2.3. Preparation of EDC activated alginate

1. 50 mg sodium alginate (0.001785 mmol) powder was weighed on butter paper and dissolved in 2 mL water in a capped glass vial.

NOTE: Sodium alginate powder is sticky in nature, so either Al foil or butter paper is preferred.

2. The mixture was vigorously stirred at 700 rpm for 30 min at 37 ºC to form a clear and homogenous hydrogel.
3. 20 mg EDC (0.1043 mmol) powder was thereafter added at once to above alginate solution.

NOTE: EDC was added to activate the carboxylic (–COOH) groups of alginate.

4. The reaction was allowed to continue for 1 h at 37 ºC.

3.2.4. Preparation of Alginate-PAMAM dendrimer hybrid nanogels (AG-G5)

1. 25 mg G5 PAMAM dendrimer (0.00086 mmol) was dissolved in 2 mL water.
2. This solution was added dropwise to the EDC activated alginate mixture.

NOTE: Viscosity of the solution progressively increased with the PAMAM addition, due to cross-linking of PAMAM molecules with alginate chains.

3. The solution was initially magnetically stirred at 250 rpm, and then very slowly for 1 h at room temperature.
4. 100 mg $CaCl_2$ was dissolved in 1 mL water, and added very slowly over 15 min to the alginate-PAMAM solution.
5. The solution was thereafter left for overnight incubation
6. The AG-G5-Ca^{2+} gels were washed with water (2 times) and centrifuged at 10,000 rpm for 5 min.
7. The supernatant was discarded to obtain pure AG-G5 nanogels.
8. The AG-G5 nanogels were then lyophilized to fetch AG-G5 nanogels in dried form and stored at -20 ºC.

3.2.5. Preparation of EPI ⊂AG-G5 nanogels

1. 25 mg G5 PAMAM dendrimer (0.00086 mmol) was dissolved in 2 mL water.
2. This solution was added dropwise to the EDC activated alginate mixture.
3. The solution was initially magnetically stirred at 250 rpm, and then very slowly for 1 h at room temperature.
4. 200 µL of EPI.HCl (1 mg) in methanol was very slowly added to the above AG-G5 solution.

NOTE: When EPI solution was added the color of the mixture turned deep purple.

5. The reaction was allowed to proceed for 1 h and then $CaCl_2$ solution (100 mg mL^{-1}) was added.
6. The obtained gels were left for overnight incubation.
7. The gels were then washed with water twice, centrifuged at 10,000 rpm for 5 min.
8. The amount of entrapped EPI in EPI ⊂AG-G5 nanogels was estimated indirectly by measuring the absorbance at 481 nm of free EPI in supernatant after centrifugation.
9. The encapsulation efficiency (EE, %) was calculated as follows:

$$\text{EE}\ (\%) = \frac{\text{Weight of initial EPI} - \text{Weight of free EPI in supernatant}}{\text{Weight of initial EPI}} \times 100$$

10. Different concentrations of EPI in water were used to make the calibration curve. For the data fitting, the least-squares approach was used (the regression equation and correlation coefficient at 481 nm were $y = 0.01664x - 0.0155$ and 0.9996, respectively).
11. Similar procedure was followed to prepare EPI⊂AG nanogels, except for adding PAMAM dendrimer and EDC.

3.2.6. Synthesis of myristic acid grafted G5 PAMAM (My-*g*-G5) dendrimers

The myristic acid chains were introduced on the periphery of G5 PAMAM dendrimers through EDC/NHS chemistry.

1. 10 mg myristic acid (0.043 mmol) was dissolved in 3 mL DMSO under N_2 atmosphere in a round-bottomed flask.
2. Then, 8.3 mg EDC (0.043 mmol) and 5 mg NHS (0.043 mmol) powders were added at once to myristic acid–DMSO solution.
3. The solution was thereafter magnetically stirred for 12 h astray from light to activate the terminal carboxyl groups (–COOH) of myristic acid.
4. Meanwhile, 20 mg G5 PAMAM dendrimers (0.7 mmol) were separately dissolved in 3 mL DMSO in amber colored glass vials.
5. After 12 h, the activated myristic acid solution was added drop-wise to the G5 PAMAM–DMSO solution under N_2 atmosphere.
6. The mixture solution was left undisturbed for 24 h at room temperature.
7. Thereafter, the myristic acid–G5 PAMAM solution was dialyzed against PBS (2 L) for 1 day followed by water (2 L) for 3 days.
8. The dialyzed solution was then freeze dried to obtain pale-yellow colored My-*g*-G5 dendrimers. The samples were stored in powdered form at -20 °C until use.

3.2.7. My-*g*-G5/TAM complexation

1. 10 mg My-*g*-G5 dendrimers were dissolved in 1.5 mL double distilled water through high-speed vortexing.
2. Meanwhile, 1.28 mg TAM (10 molar equivalents of My-*g*-G5 dendrimers) was dissolved separately in 300 µL methanol and added very slowly to the My-*g*-G5 aqueous solution.
3. The mixture solution was kept uncovered under magnetic stirring to evaporate methanol for 24 h at room temperature.
4. Then, My-*g*-G5/TAM solution was passed through nylon filter (pore size: 0.22 mm) to remove precipitates related to non-complexed free TAM.
5. The concentration of TAM bound to My-*g*-G5 PAMAM dendrimers was estimated spectrophotometrically at 278 nm.
6. An absorbance versus concentration calibration curve was generated using different concentrations of TAM. For data fitting, the least squares approach was used (the regression equation at 278 nm was $y = 0.035x - 0.068$, $R^2 = 0.994$).
7. Similar procedure was adopted to complex TAM within the pristine G5 PAMAM dendrimers.

8. All the samples were stored at -20 °C in dark.
9. For tracking the *in vitro* cellular uptake of My-*g*-G5 PAMAM dendrimers, a fluorescent dye coumarin-6 was complexed using above procedure instead of TAM.

3.2.8. Surface acetylation of G5 PAMAM dendrimers

The ratio between acetic anhydride and dendrimer was adjusted to convert 70 % primary amines on the surface to acetamide groups. The stoichiometric ratio of primary amines: acetic anhydride was kept 1:1 to achieve desired extent of surface acetylation.

1. 31.7 mg of G5 PAMAM dendrimer (1.1×10^{-3} mmol) was dissolved in 10 mL of dry methanol under stirring conditions in a two-necked round-bottomed flask.
2. 15×10^{-3} mL of triethylamine (10 % molar excess of acetic anhydride) was added to the above PAMAM solution under argon (Ar) atmosphere.
3. Separately, 9.4×10^{-3} mL of acetic anhydride (9.9×10^{-2} mmol) was dissolved in 4 mL of dry methanol.

CRITICAL: Acetic anhydride is very sensitive to light and air and gets converted to acetic acid. Keep the solution in an air-tight amber colored vial.

4. After 30 min, the acetic anhydride solution was added very slowly to the PAMAM-triethylamine mixture solution.

NOTE: Triethylamine was added to quench acetic acid, a side product formed in the reaction.

5. The reaction was allowed to continue for 24 h in dark.
6. The methanol content was removed under vacuum to obtain white colored polymer residue.
7. The polymer residue was re-dissolved in 3 mL water and dialyzed against PBS (1 L) followed by water for 3 days using dialysis membrane (MWCO = 10 kDa).
8. The dialyzed solution was then lyophilized to obtain polymer residue and stored at -20°C for further use.
9. The number of primary amines acetylated were determined by ^{1}H NMR analysis and were found to be 85 groups.

3.2.9. Encapsulation of EPI within G5-Ac85 interiors

1. 10 mg G5-Ac85 dendrimers (0.3×10^{-3} mmol) were dissolved in 1.5 mL water in a glass vial under magnetic stirring.
2. 1.75 mg EPI.HCl (3×10^{-3} mmol) was weighed in a mini-centrifuge tube and diluted with 300 µL methanol.
3. 5 µL triethylamine was carefully added to the EPI solution.

NOTE: This will make EPI insoluble in water.

4. The EPI solution obtained after step 3, was added to aqueous solution of G5-Ac85 dendrimers under vigorous stirring conditions.
5. The above mixture solution was kept undisturbed for 18-24 h.

NOTE: The vial was left uncovered to allow evaporation of methanol.

6. Centrifuge the solution at 7000 rpm for 10 min at 4 ºC.

NOTE: This step was done to remove precipitates related to free or non-complexes EPI.

7. The supernatant was collected and analyzed spectrophotometrically at 481 nm using an UV−vis spectrometry for indirect determination of EPI encapsulation efficiency.
8. The encapsulation efficiency (E.E, %) was calculated as follows:

$$\text{E. E (\%)} = \frac{\text{Weight of EPI in G5−Ac(85) dendrimers}}{\text{Weight of EPI fed initially}} \text{ X } 100$$

9. Different concentrations of EPI (2.5 to 25 µM) were used to make the EPI calibration curve. For the data fitting, least-squares approach was used (the regression equation and correlation coefficient at 481 nm were y = 0.0135x -0.0465 and 0.9985, respectively).
10. The supernatant was lyophilized for 3 days to obtain EPI⊂G5-Ac85 inclusion complexes and kept at -20 °C for further study.

3.2.10. Hydrothermal synthesis of hydroxyl-functionalized CQDs

For the synthesis, chitosan was used as the carbonaceous source and PEG-4000 as the passivating agent.

1. 400 mg chitosan powder was weighed, and dissolved in 60 mL of water under stirring conditions in a flask.
2. 300 µL of acetic acid was added to enable dissolution of chitosan.
3. 400 mg PEG-4000 powder was added to the above solution and stirred for 2-3 h to obtain a homogenous solution.
4. The solution was then shifted to the hydrothermal reactor and sealed.
5. The reactor was heated at 200 ºC for 8 h under nitrogen (N_2) atmosphere.
6. After cooling, the dark colored solution was centrifuged at 9000 rpm for 20 min at room temperature to remove insoluble precipitates.
7. The pure CQDs solution was taken and stored at room temperature.

3.2.11. Preparation of CQDs@EPI⊂G5-Ac85 fluorescent hybrids

1. 50 µL of aqueous CQD stock solution (1.33 mg mL^{-1}) was taken in a 1.5 mL mini-centrifuge tube.

2. Different volumes of EPI⊂G5-Ac85 dendrimers corresponding to varied concentrations of EPI (0.625, 1.25, 2.5, 5 and 10 µM) were added to the CQD solution.
3. The mixture solution was thereafter diluted with 250 µL ultrapure water.
4. The tubes were left for shaking at 150 rpm for 18-24 h at 4 °C in an orbital shaker.

3.3. Characterization techniques

(A) UV−Visible spectroscopic measurements: For recording the absorption spectra (200-800 nm), samples were dissolved in their respective solvents (such as water or methanol) in required concentrations.

(B) TEM experiments: 20 µL of aqueous solution of samples was dropped onto non-shining carbon coated copper grid and subsequently air dried before measurements. Size distribution histogram of the nanoparticles was analysed with ImageJ (http://rsb.info.nih.gov/ij/download.html). 5-FU@DsAgNCs, EPI⊂AG-G5 nanogels, CQDs@EPI⊂G5-Ac85 hybrids, and My-*g*-G5/TAM complexes were viewed after negative staining with 2 % PTA (phosphotungstic acid) under TEM operating at 200 kV.

(C) XRD measurements: The samples were coated on to glass slides by drop-casting technique and analyzed after drying using X-ray diffractometer (Cu-K_α radiation, λ= 1.5406A˚) in the range of 20–80˚ at a scan speed of 0.05˚/min.

(D) NMR experiments: For ^{1}H NMR spectra, the G5 PAMAM complexes were dissolved in D_2O or DMSO-d_6 solvent in millimolar concentrations.

(E) FE-SEM experiments: The freeze-dried samples were placed directly over double-sided carbon tape. The morphology of the samples was then analyzed after gold sputtering using FE-SEM operating at 5.0 kV.

(F) Zeta and Dynamic light scattering (DLS) measurements: For experiment, samples (1 mg mL^{-1}) were dissolved in their solvents and their zeta potential and hydrodynamic diameter were then estimated using Zetasizer operating at 25°C.
For nanogels sample preparation, nanogels (1 mg mL^{-1}) were dispersed in PBS (pH 7.4) by sonication (5 sec ‘on’ and 2 sec ‘off’) for 10 min.

(G) FTIR measurements. The FTIR spectrum were obtained by mixing samples with KBr pellets and recorded by spectrometer in the range 4000–400 cm^{-1}.

(H) TG analysis. Thermal stability of nanogel samples was correlated with their respective weight losses evaluated by thermograms obtained from thermal analyzer. Around 10 mg of nanogel powders were heated up to 800 °C at a constant rate of 10 °C/min under N_2 atmosphere.

(I) Swelling studies: A predetermined amount of dried nanogels were immersed in sodium acetate (20 mM, pH 5.5) and PBS (20 mM, pH 7.4) buffer at room temperature for 24 h. After incubation, the swollen gels were carefully removed and placed on a piece of tissue paper (to remove excess water from surface). Weights of gels were then measured using a weighing balance. % Swelling was expressed as follows:

$$\% \text{ Swelling} = \frac{W2 - W1}{W1} \times 100$$

Where, W1 is the initial weight of dried nanogels
and W2 is the weight of nanogels after swelling.

(J) BET measurements. The surface area and pore volume of freeze dried nanogels were estimated from N_2 adsorption-desorption isotherms recorded using a high speed automated surface area analyser.

(K) Tensile testing. The mechanical properties of as-synthesized nanogels were assessed using a small scale mechanical tensile tester machine. For measurements the nanogels were cut in thin, uniform rectangular slices and their dimensions were measured using Vernier callipers. Further, the samples were clamped on a 450 N load cell and a maximum load of 200 N was applied at a speed of 0.1 N/s. Signals related to force and displacement were recorded throughout the experiments. The ultimate tensile strength (UTS) and elongation at break were calculated from the stress-strain plots.

(L) Fluorescence measurements. For acquiring the fluorescence spectra, 10-15 µL CQDs (from the stock solution) were diluted to 500 µL volume with water. The fluorescence spectra of CQDs@EPI⊂G5-Ac85 hybrids with equivalent concentration of CQDs were also recorded using fluorescence spectrophotometer for comparison. For lifetime measurements, 50 µL CQDs and 105 µL CQDs@EPI⊂G5-Ac85 hybrids (~ CQDs content) were diluted to 5 mL water (final volume) and then subjected to data acquisition with a fluorescence lifetime system equipped with Nano LED (635 nm) source. The decay curves were analyzed with IBH decay analysis v 6.1 software.

3.4. *In vitro* drug release studies

3.4.1. *In vitro* release of 5-FU from 5-FU@DsAgNCs

The release studies were performed using dialysis bag method. 5-FU@DsAgNCs were prepared with a 5-FU concentration of 0.4 mg mL^{-1}. 3 mL of sample solution was placed in a dialysis bag (MWCO 10 kDa), hermitically tied and placed in 200 mL PBS (pH 7.4) at 37 ˚C with mild agitation (70 rpm). Subsequently, 1.0 mL of dissolution medium was withdrawn at specific time intervals up to 48 h and replaced with same volume of fresh PBS. Pure 5-FU in water at an equivalent concentration was applied as control to monitor its permeation through dialysis bag. The cumulative 5-FU release was determined by measuring absorbance at 265 nm using calibration curve.

% Release was calculated as:

$$5-\text{FU release}\ (\%) = \frac{\text{Concentration of drug aliquot X Volume of release medium}}{\text{Initial drug concentration}}\ \text{X}\ 100$$

3.4.2. *In vitro* release of EPI from nanogels

The pH dependent release of EPI from EPI⊂AG and EPI⊂AG-G5 nanogels was studied in acetate buffer (20 mM, pH 5.5) and PBS (20 mM, pH 7.4) at predetermined time intervals. Around 5 mg nanogels were added to 1 mL acetate or PBS buffer in mini centrifuge tubes and incubated at 37 °C for 48 h. After each time interval i.e. 1, 3, 6, 9, 12, 24, 36 and 48 h, the sample were centrifuged at 10,000 rpm for 2 min, supernatant were collected and fresh buffer was added. The amount of EPI in supernatant was determined from the dose-absorption curve of EPI by measuring the absorbance at 481 nm. The percentage of EPI released was quantitated according to following equation:

$$\%\ \text{Cumulative release} = \frac{\text{EPI released in supernatant}}{\text{Total amount of EPI loaded in nanogels}}\ \text{X}\ 100$$

3.4.3. *In vitro* release of TAM from My-*g*-G5/TAM complexes

The release of TAM from My-*g*-G5 dendrimers was monitored in sodium acetate buffer (pH 5.5) and PBS (pH 7.4) using a Slide-A-Lyzer™ MINI dialysis device (10 kDa MWCO). Briefly, 1 mL of My-*g*-G5/TAM solution was added to the dialysis tube and the outer compartment was filled with 45 mL of buffer. The dialysis devices were mildly agitated at 100 rpm at 37 ºC. At scheduled time intervals of 3, 6, 9, 12, 24, 36 and 48 h, 500 µL of buffer was withdrawn from the outer medium and replaced with equal volume of fresh buffer. The cumulative TAM in the medium was quantitated from its dose-absorption curve by measuring its absorbance at 278 nm. The % release was calculated as follows:

$$\text{TAM release (\%)} = \frac{\text{Concentration of TAM aliquot}}{\text{Initial TAM concentration}} \text{ X } 100$$

3.4.4. *In vitro* release of EPI from CQDs@EPI⊂G5-Ac85 hybrids

The release of EPI from hybrids was studied under different pH conditions using acetate buffer (20 mM, pH 5.5) and PBS (20 mM, pH 7.4) at same time intervals. 2 mL of CQDs@EPI⊂G5-Ac85 hybrid solution was placed equally in two dialysis bags (MWCO 3500 Da) and the receptor compartment were filled with 10 mL acetate or PBS buffer with mild agitation (70 rpm). After each interval, that is 1, 2, 3, 4, 5, 6, 8, 10, 12, 24, 48 h, 5 µL of each buffer solution was withdrawn and measured for EPI absorbance at 481 nm by micro volume spectrophotometer. The concentration of EPI was estimated from the dose-absorption curve of EPI. Percentage of EPI released was quantitated as follows:

$$\text{EPI release (\%)} = \frac{\text{EPI released in medium}}{\text{EPI loaded in CQDs@EPI} \subset \text{G5} - \text{Ac85 hybrids}} \text{ X } 100$$

3.5. Cell culture

A549 (human lung adenocarcinoma), MCF-7 (human breast adenocarcinoma) and NIH3T3 (mouse embryonic fibroblast) cells were cultured in DMEM comprising of 10 % (v/v) FBS supplemented with 1 % (v/v) penicillin-streptomycin and maintained at 37 °C in a humidified incubator with 5 % CO_2 atmosphere. Cells were subcultured every 48 h and harvested from subconfluent cultures (60-70 %) using 0.25 % trypsin-EDTA.

3.5.1. MTT assay

Cytotoxicity was evaluated by MTT, a mitochondrial based cell viability assay. Cell viability was assessed on the ability of cells to transform tetrazolium salt to purple formazon crystals. Cells at a density of 10^4 cells/well were seeded in 96 well plate (Corning, Costar, NY) and were allowed to attach overnight. The cells were then exposed to different concentrations of G5 PAMAM samples for stipulated times. After exposure, medium with PAMAM complexes was removed and PBS wash was given twice. Fresh 100 µL DMEM medium with MTT dye (5 mg mL^{-1}) was added per well and cells were incubated for another 4 h. To dissolve the formazon crystals formed, medium was aspirated and 100 µL of lysis solution (DMSO) was added. By measuring the color intensity of formazon solution we can estimate the cell growth condition or cell viability. The soluble formazon product was measured using microplate reader at 570 nm and the background control at 690 nm. Cell viability (%) was expressed as:

$$\text{Cell Viability (\%)} = \frac{(\text{A570} - \text{A690}) \text{ treated cells}}{(\text{A570} - \text{A690}) \text{control cells}} \text{X } 100$$

While testing nanogel samples, MCF-7 and NIH3T3 cells were seeded in 24-well assay plate at a density of $3x10^4$ cells/well for 24 h. Then after attachment, sterile pieces of EPI⊂AG and EPI⊂AG-G5 nanogels (0.1, 0.25 and 0.5 mg) were added to fresh DMEM medium for 48 h incubation at 37 °C. Blank AG and AG-G5 nanogels (with equivalent weights) and free EPI solution (with equivalent concentration) were also added to cells for comparative analysis. The subsequent steps were similar as described above.

3.5.2. Synergy analysis and combination index (CI) value determination for 5-FU@DsAgNCs

The synergistic inhibitory effect of 5-FU and AgNPs loaded in the PAMAM nanocarrier was evaluated by the isobologram method (Tallarida et al., 2001). Briefly, a straight line was formed by plotting the IC_{50} value of 5-FU-D and DsAgNPs on the x- and y- axes, respectively. The data point in the isobologram correspond to the actual IC_{50} value of 5-FU@DsAgNCs. If the data point lies on or near to the line, it indicates additive treatment effect, whereas the position of data point below or above the line suggests synergism or antagonism, respectively. Moreover, CI value was also determined to examine the interaction between the two components by Chou Talalay's method (Chou et al., 2006).

The equation used to compute the CI value

$$CI = \frac{(D)1}{(Dx)1} + \frac{(D)2}{(Dx)2}$$

CI is a dimensionless quantity and a CI =1, <1 or >1 indicates additive effect, synergism, and antagonism, respectively. In the denominator (Dx) is for concentration of drug D1 "alone" that inhibits the cell growth by 50 %, and (Dx)2 is for drug D2 "alone" to inhibit the growth, respectively. In the numerators, (D)1+ (D)2 "in combination" to inhibit the same 50 % growth. In this study, D1 and D2 refers to DsAgNPs and 5-FU, respectively. (D)1+ (D)2 refers to the concentration of 5-FU@DsAgNCs in a combinatorial form required to achieve the similar inhibitory effect. For an effective treatment, synergism reflected by a CI value < 1 is desirable.

3.5.3. *In vitro* cellular uptake studies

3.5.3.1. For 5-FU@DsAgNCs

Quantitative estimation of uptake of Ag by A549 and MCF-7 cells was done by AAS. For the experiment, A549 and MCF-7 cells were seeded separately in a 6-well plate ($2x10^5$ cells/well) for overnight attachment. Cells were then exposed to different concentrations of 5-FU@DsAgNCs (2.5, 5 µg mL^{-1} Ag equivalent) for 3 h. After exposure, cells were thoroughly

washed with PBS to remove the unbound Ag, harvested and counted. 1 mL of 0.5 % triton X-100 in 0.2 N NaOH solution was added to lyse the cells completely. Samples were further acidified with 65 wt. % HNO_3 to ensure complete digestion of Ag complexes before measurement. Parallel blanks (untreated cells) were set to calculate the net cellular uptake. Results were expressed in form of cellular dose i.e. mean amount of Ag in pg/cell.

3.5.3.2. For EPI⊂AG-G5 nanogels

For imaging cellular uptake of nanogels, MCF-7 cells (2x 10^5 cells/well) were seeded in 35 mm culture dishes for overnight attachment. Different doses of EPI⊂AG-G5 nanogels and free EPI (with equivalent EPI concentration as in EPI⊂AG-G5 nanogels) were then added to 1 mL DMEM medium for 24 h at 37 °C. After that, medium was removed and PBS wash was given once. Then, 3 µL Hoechst 33342 dye (10 mg mL^{-1}) was added to PBS and images were captured using an inverted fluorescent microscope. For time dependent cell uptake studies, MCF-7 cells were treated with EPI⊂AG-G5 and EPI⊂AG nanogels for 1, 3 and 6 h. After treatment, the cellular localization of EPI was visualized by staining with 1 µL lysotracker green dye (100 µM) for 10-15 min at 37 °C. PBS wash was given to remove excessive dyes. The images were then acquired at 40 X magnification using fluorescent microscope under different filters.

3.5.3.3. For My-*g*-G5/C6 complexes

The uptake of My-*g*-G5/C6 complexes by MCF-7 cells was examined qualitatively using fluorescence microscopy and quantitatively through flow cytometry. MCF-7 cells (2 x 10^5 cells) were cultured in 6-well plates and incubated with My-*g*-G5/C6 (0.75 and 1 µM) complexes for 6 h. Unexposed MCF-7 cells were used as internal control. Subsequently, cells were observed under fluorescence microscope in the GFP filter. For quantitating green positive cells (%), the cells were washed with PBS, trypsinized carefully and harvested by centrifugation at 600 *g* for 6 min at 4 °C. The attained cell pellets were then dispersed in 200 µL PBS and analyzed for green fluorescent signals in Ch. 02 (505−560 nm) by flow cytometer. A total of 10,000 events were acquired per sample and analyzed using Amnis Ideas software.

The cellular location of My-*g*-G5/C6 complexes was also determined in a time dependent manner. For this, MCF-7 cells (2 x 10^5 cells) were seeded and cultured in 35 mm plates and exposed to My-*g*-G5/C6 (0.75 µM) for 1, 2, 4 and 6 h. Thereafter, cells were given a PBS wash followed by staining with 2 µL of Hoechst 33342 dye (10 mg mL^{-1}) and 2 µL of lysotracker red (100 µM) for 10-15 min at 37 °C. Images were then recorded under various filters of an inverted fluorescence microscope.

3.5.3.4. For CQDs@EPI⊂G5-Ac85 hybrids

For cellular imaging, MCF-7 cells (1 x 10^5 cells/ mL) were seeded in 35 mm culture dishes and cultured overnight. Following attachment, free CQDs, free EPI, EPI⊂G5-Ac85 and CQDs@EPI⊂G5-Ac85 hybrids with final EPI concentration (5 µM) were added to fresh DMEM medium and left for 12 h incubation at 37 °C. After treatment, cells were washed with PBS twice and nucleus was stained with 2 µL Hoechst 33342 dye (10 mg mL^{-1}) for 10 min. Cells were then analyzed for fluorescent signals using inverted fluorescent microscope. For imaging, the filters used were DAPI (λ_{ex} 360 nm, λ_{em} 447 nm), GFP (λ_{ex} 470 nm, λ_{em} 525 nm) and RFP (λ_{ex} 530 nm, λ_{em} 593 nm), respectively.

Quantitative estimation of cellular uptake of CQDs@EPI⊂G5-Ac85 hybrids was done using a flow cytometer. CQDs exhibit bright green fluorescence with 488 nm excitation laser in Channel 02 (505-560 nm) and this enables tracking distribution of hybrids inside the cells. MCF-7 cells (2 x 10^5 cells/ mL) were plated in 35 mm culture dishes and cultured overnight. Subsequently, medium was removed and fresh DMEM medium containing CQDs, EPI⊂G5-Ac85 and CQDs@EPI⊂G5-Ac85 hybrids were added to cells. After 3 h of incubation, cells were washed, trypsinized and centrifuged at 600 *g* for 6 min at 4 ºC. The cell pellet obtained, was re-dispersed in 200 µL PBS and analyzed by flow cytometer. 10,000 events were recorded per sample and analyzed by Amnis Ideas software.

3.5.4. Acridine orange/ethidium bromide (AO/EB) dual staining

Apoptotic effects of various test samples against cancer cells was examined by AO/EB staining. Briefly, 2x10^5 cells/well seeded in a 6-well tissue culture plate and were allowed to attach overnight. Cells were then exposed to different concentrations of samples for around 24 h. Following treatment, ice cold PBS wash was given and cells were incubated with AO/EB (10 µg mL^{-1} working concentration) at 37 ˚C for 15 min. Subsequently, once PBS wash given to remove excessive dyes. Images were captured under different filters using EVOS cell imaging system.

3.5.5. Time dependent morphological examination by Hoechst-Rho B staining

Nuclear chromatin compaction and alteration in cytoskeleton can be assessed with a combination of fluorescent dyes-Hoechst 33342 and rhodamine B (Rho B). MCF-7 and A549 cells (2x10^5 cells/well) seeded in a 6-well plate were treated with 5-FU@DsAgNCs for 6, 12, and 24 h. Following treatment, DMEM medium was removed and mild PBS wash was given to remove dead floating cells. Cells were then incubated with 2 µL Hoechst dye (10 mg mL^{-1}) and 5 µL

Rho B (1 mg mL^{-1}) for 10-15 min at 37 ˚C. An overlay of images acquired under DAPI and red filters was taken.

3.5.6. Cell cycle analysis

Induction of apoptotic mode of cell death was determined by PI staining and subsequent analysis by flow cytometry. Cells at a density of 2 x 10^5 cells/ mL were seeded in 35 mm culture plates for overnight attachment. Test samples in different concentrations were then added to fresh cell culture medium. After incubation, medium was carefully removed to prevent loss of floating cells, washed with PBS, trypsinized and harvested by centrifugation at 200 *g* for 5 min at 4 ºC. Cells were fixed with 70 % alcohol in ice for 15 min. Next, fixed cells were stained with PI staining solution (50 µg mL^{-1} PI, 1 mg mL^{-1} RNase A, and 0.05 % triton X-100) for 45 min at 37 °C in dark. The amount of PI-labelled DNA was then measured from the cell cycle distribution using a flow cytometer. 10,000 cells were analyzed for fluorescent signals per sample. The cell cycle distribution was studied from the obtained histograms after statistical analysis using Amnis Ideas software.

3.5.7. Cell morphology analysis by FE-SEM

Cells were seeded on sterile glass coverslips in 35 mm culture plates and nursed for 24 h. After that, test samples were added to the cells and kept for scheduled time intervals. Cells without test samples were also cultured in media and used as control sample. After treatment, the cells were washed with PBS and fixed in 2 % glutaraldehyde solution for 10 min followed by ethanol gradient fixation (20 %, 40 %, 60 %, and 80 %). The air dried samples were then gold sputtered and examined by FE-SEM operating at 10 kV.

Further, elemental mapping was done to verify the elemental distribution of elements ‘F’ (Fluorine in 5-FU) and ‘Ag’ in 5-FU@DsAgNC treated cells.

3.5.8. Monitoring the intracellular ROS generation

Cells ($2x10^5$ cells/well) grown in 6 well plate were treated with appropriate concentrations of samples for particular times. Thereafter, cells were supplemented with 1 mL fresh DMEM containing 20 µM DCFH-DA dye and incubated for 10 min at 37 °C. Following incubation, cells were harvested and resuspended in PBS. DCFH-DA is a cell permeant fluorogenic dye used to measure ROS activity within the cell. Upon cellular diffusion, cleavage of the acetate groups by intracellular esterases occurs and DCFH-DA is converted to the highly fluorescent 2, 7-dichlorofluorescein (DCF) upon oxidation. DCF has an excitation and emission maxima at 495 nm and 529 nm, respectively. Immediately after incubation, samples were analyzed for DCF

fluorescence using flow cytometer (Amnis Flowsight). Amnis Ideas software was used to analyze the acquired data for 10000 events per sample and ROS generation was expressed in terms of percentage of cells with green (DCF) fluorescence.

3.5.9. Determination of mitochondrial membrane potential (MMP)

Alterations in MMP ($\Delta\Psi$) in MCF-7 cells was evaluated by rhodamine 123 staining. MCF-7 cells (2×10^5 cells/well) were seeded in 6-well plates for overnight attachment. Cells were then exposed to G5/TAM and My-*g*-G5/TAM (0.75 and 1 μM) complexes for 24 h. Untreated MCF-7 cells were also kept as control. After exposure cells were washed twice with PBS, trypsinized and harvested by centrifugation at 600 *g* for 6 min at 4°C. The cell pellet was then resuspended with 200 μL PBS containing rhodamine 123 (5 μg mL^{-1}) and kept for 30 min at 37 °C. The fluorescence intensities of rhodamine 123 in cells were quantitated by flow cytometry. For fluorescent microscopy, in parallel treated MCF-7 cells (seeded in another plate) were washed with PBS and stained with equivalent concentration of rhodamine 123 (5 μg mL^{-1}) for 30 min. Images were captured for red fluorescent signals under RFP filter (λ_{ex} 530 nm, λ_{em} 593 nm) at 40 X magnification of fluorescent microscope.

3.5.10. Gene expression studies

For gene expression studies, MCF-7 cells were plated in 35 mm culture plates and subsequently treated with test samples for scheduled times. Differential expression of apoptotic signaling genes was determined by RT-PCR analysis. Housekeeping β-actin gene was used as an internal control. Total RNA was isolated from cells using Tri-reagent. After that, cDNA was generated from total denatured RNA (1 μg) by reverse transcription performed at 42 °C for 50 min using Super Script II Reverse Transcriptase (Life Technologies, India) in a total mixture of 20 μL. The steps include an initial denaturation (94 °C for 3 min) followed by PCR cycle of denaturation (94 °C for 30 s), annealing (60 °C for 30 s), extension (72 °C for 1 min) and a final extension (72 °C for 10 min). Finally, the PCR products were resolved on a 1.2 % agarose gel and visualized by ethidium bromide staining under UV light. The fold difference was calculated using Image lab 4.0 software in the same instrument.

The forward and reverse primer sequences used are mentioned in **Table 3.1.**

Gene	Primers
Beta-actin	Forward: 5’ CTGTCTGGCGGCACCACCAT 3’ Reverse : 5’ GCAACTAAGTCATAGTCCGC 3’
p53	Forward: 5’ TGGCCCCTCCTCAGCATCTTAT 3’ Reverse : 5’ GTTGGGCAGTGCTCGCTTAGTG 3’
Caspase 3	Forward : 5’ TTCAGAGGGGATCGTTGTAGAAGTC 3’ Reverse : 5’ CAAGCTTGTCGGCATACTGTTTCAG 3’
C-myc	Forward : 5’ CCAGGACTGTATGTGGAGCG 3’ Reverse : 5’ CTTGAGGACCAGTGGGCTGT 3’
Bax	Forward : 5’ AAGCTGAGCGAGTGTCTCAAGCGC 3’ Reverse : 5’ TCCCGCCACAAAGATGGTCACG 3’
Bad	Forward : 5’ CCTTTAAGAAGGGACTTCCTCGCC 3’ Reverse : 5’ ACTTCCGATGGGACCAAGCCTTCC 3’
Bcl-xl	Forward : 5’ ATGGCAGCAGTAAAGCAAGC 3’ Reverse : 5’ CGGAAGAGTTCATTCACTACCTGT 3’
Bcl-2	Forward : 5’ TCCGCATCAGGAAGGCTAGA 3’ Reverse : 5’ AGGACCAGGCCTCCAAGCT 3’

Table 3.1. Forward and reverse primer sequences used in the gene expression studies.

3.5.11. Statistical analysis

The values were expressed as mean ± standard error mean (SEM) for all experiments. The data were analyzed via student’s *t* test or via two-way ANOVA with Bonferroni/Tukey’s multiple comparisons test to determine the statistical comparison within the group means using GraphPad Prism software (version 6.0).

CHAPTER 4

Development of Multicomponent 5-fluorouracil Loaded PAMAM Stabilized-Silver Nanocomposites to Synergistically Induce Apoptosis in Human Cancer Cells

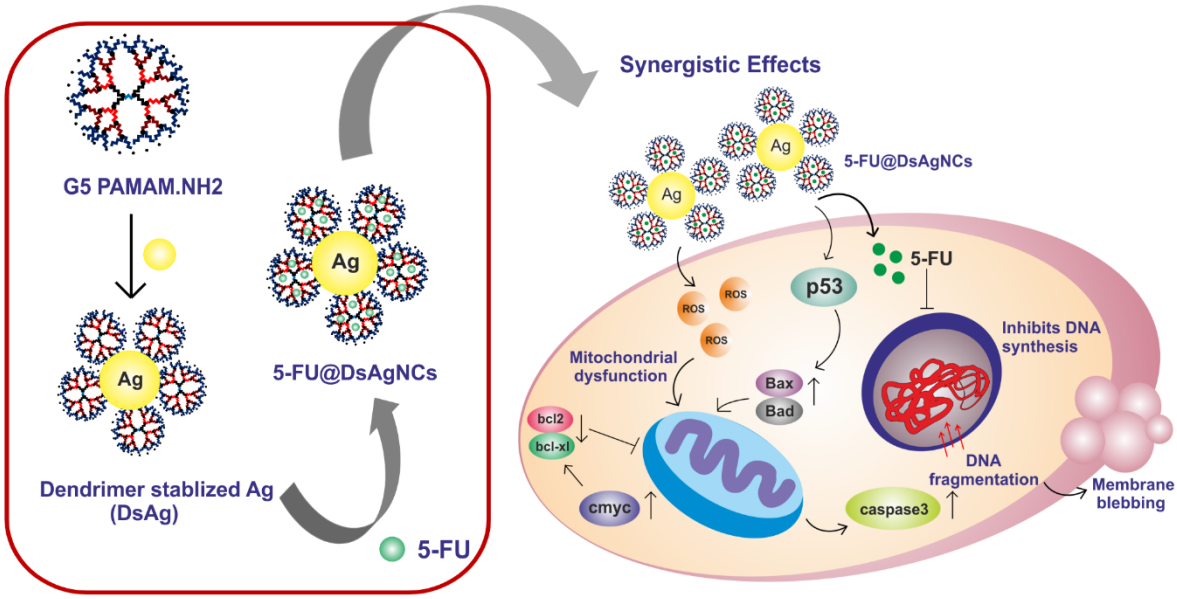

CHAPTER 4

DEVELOPMENT OF MULTICOMPONENT 5-FLUOROURACIL LOADED PAMAM STABILIZED-SILVER NANOCOMPOSITES TO SYNERGISTICALLY INDUCE APOPTOSIS IN HUMAN CANCER CELLS

4.1. Overview

As described in chapter 1, lung cancer is the most recurrent cause of cancer-related deaths worldwide followed by breast cancer (Siegel et al., 2015 and Torre et al., 2015) Till date, chemotherapy is the most evolved treatment for cancer which relies on administration of bolus doses of drugs systemically to cancer patients (Brannon-Peppas et al., 2004). Combinatorial therapy including multiple drugs or potential drug candidates with distinct signalling pathways, enhanced therapeutic effects against specific targets and routes to overcome mechanisms of resistance is a promising alternative to single-agent chemotherapy (Kolishetti et al., 2010 and Jain et al., 2014). In this regard, nanotechnology mediated delivery of anticancer agents under a single therapeutic platform can prove to be an effective strategy. Lately, pertinence of amine terminated PAMAM dendrimers as templates or stabilizers for metal nanoparticle synthesis have been reported (Shi et al., 2008, 2009 and Yuan et al., 2013). High generation PAMAM dendrimers comprising of abundant terminal amines and amide linkages are contemplated to reduce and stabilize metal nanoparticles. Many groups have reported the role of G5 PAMAM dendrimer terminal groups in formation of dendrimer entrapped /stabilized gold and silver nanoparticles (Shi et al., 2008 and 2009). Use of G5 PAMAM dendrimer stabilized gold, silver and gold-silver alloy nanoparticles as potential computed tomography (CT) imaging agents have been reported (Liu et al., 2010a, 2013 and Wang et al., 2013a). However, use of such PAMAM based metal nanoparticles as drug carriers for cancer therapeutics is not yet studied. Pre-existing literature suggests the use of silver nanoparticles (AgNPs) as apoptosis (programmed cell death) inducing agents (AshaRani et al., 2009, Gopinath et al., 2010, Sanpui et al., 2011, Gliga et al., 2014, and Sharma et al., 2014). Moreover, 5-FU is an established cytotoxic drug used in the treatment of lung, breast, skin, liver, colon, bladder, pancreatic, head and neck cancers

(Liu et al., 2012b). 5-FU is known to inhibit the activity of thymidine synthetase (TS) enzyme involved in DNA synthesis and arrests cell growth. However, its limited tissue and cell biodistribution profiles with side effects in form of liver damage and digestive discomfort limits its usage (Visser et al., 1990 and Raveendran et al., 2015). 5-FU has been used in conjunction with anticancer drugs, such as curcumin, cisplatin as well as nanoparticles of silver and selenium to exhibit synergistic anticancer effects (Lynch Jr. et al., 1993, Gopinath et al., 2008, Liu et al., 2012b and Kumar et al., 2014). In addition, some groups have shown the anticancer potential of 5-FU loaded PAMAM dendrimers *in vitro*. Tran and co-workers demonstrated the antiproliferative activity of 5-FU grafted Pegylated PAMAM dendrimers (G3) against MCF-7 (breast cancer) cells and obtained IC_{50} of 9.92 ± 0.19 μg mL^{-1} (Tran et al., 2013). Mei and co-workers studied the inhibitory effects of 5-FU PAMAM dendrimer in combination with antisense micro-RNA 21 gene therapy to enhance the chemo sensitivity of 5-FU in MCF-7 cells (Mei et al., 2009). However, the strategy to combine nanoparticles and anticancer drugs with different action mechanisms within PAMAM based carriers still remains unexplored. The present study introduces a new dimension wherein, dual functionality of PAMAM dendrimer, as a stabilizer for amine terminated AgNPs and carrier for 5-FU for cancer therapy has been exploited. Combinatorial therapy of AgNPs and 5-FU drug in a single PAMAM nanocarrier enable their co-delivery in sufficient amounts to cancer cells *in vitro* for attaining synergistic anticancer effects. To the best of our knowledge, this is the first instance employing dual functionality of PAMAM dendrimer as a stabilizer and a drug carrier to further investigate its *in vitro* anticancer effects. The rationale behind is to kill the cancer cells by combination of two separate mechanistic pathways: caspase activation pathway and reactive oxygen species (ROS) induction for efficient apoptosis. We have tested the ability of 5-FU loaded dendrimer stabilized silver nanocomposites (5-FU@DsAgNCs) to induce apoptosis in human lung and breast adenocarcinoma cell lines i.e. A549 and MCF-7. Interestingly, MCF-7 cells were found to be more susceptible to 5-FU@DsAgNC treatment than A549 cells.

4.2. RESULTS AND DISCUSSION

4.2.1. Synthesis and characterization of 5-FU@DsAgNCs

The objective of this work is to construct a PAMAM based therapeutic agent wherein it serves the dual role of a stabilizer for AgNPs and as a delivery system for 5-FU. To achieve this, dendrimer stabilized AgNPs were synthesized using dendrimer terminal amine/Ag salt molar ratio 100:1 and $NaBH_4$ reduction to obtain one AgNP stabilized by multiple dendrimers (Yuan et al., 2013). Next step was to entrap partially insoluble drug 5-FU in the internal PAMAM cavities. The interactions responsible in 5-FU-PAMAM dendrimer complexation include

(i) mainly hydrogen bond formation, (ii) weaker hydrophilic interactions (with polar internal PAMAM groups – tertiary amine and amide) and (iii) much weaker hydrophobic interactions. (Buczkowski et al., 2012a) **(Scheme 4.0).**

UV-vis spectrometry was first used to qualitatively confirm the formation of amine terminated AgNPs and successful loading of 5-FU in the PAMAM G5 interiors **(Figure 4.1).** Appearance of two absorption peaks in 5-FU@DsAgNCs (black line): one at 410 nm is attributed to typical surface plasmon resonance (SPR) band of AgNPs (Shi et al., 2008, Liu et al., 2010a and Sarkar et al., 2015c) while the other at 266 nm is the typical absorption peak of 5-FU (Mei et al., 2009). In contrast, amine terminated AgNPs (red line) display only one peak at 419 nm corresponding to SPR band of AgNPs. Inset in **Figure 4.1** shows photographs of pure G5 PAMAM dendrimer (colorless, 1), DsAgNPs (yellow, 2) and 5-FU@DsAgNCs (golden yellow, 3). The transition in color confirms the formation of 5-FU@DsAgNCs. Next, the concentration of Ag in the PAMAM complexes estimated by ICP-MS was 175 µg mL^{-1}. Drug loading efficiency (DLE, wt. %) of 5-FU in 5-FU@DsAgNCs estimated from the standard curve (y = 0.047x+ 0.02; r^2 0.999) was 25.9 ± 3.5 % i.e. around 26 molecules of 5-FU were loaded per dendrimer. This is in accordance with the previous findings of Buczkowski et al., 2012a.

Further, TEM analysis was done to characterize the formed DsAgNPs and 5-FU@DsAgNCs. It was clear that the formed DsAgNPs were spherical in shape with an average size distribution of 8.32 nm (± 1.13 nm) much bigger than the PAMAM G5 size (5.4 nm) indicating formation of dendrimer stabilized AgNPs and not entrapped nanoparticles **(Figure 4.2 a)**. Size distribution histogram of DsAgNPs is shown in **Figure 4.2 b**. Negative staining with PTA enabled view of homogenous distribution of DsAgNPs loaded with 5-FU **(Figure 4.2 c)** and its corresponding selected area diffraction pattern (SAED) is depicted in **Figure 4.2 d.** Bright spots in SAED pattern are ascribed to crystalline silver with phases (111), (200), (220) and (311). 5-FU did not contribute to the SAED pattern which recommend its complete encapsulation in the dendrimer interiors. Energy dispersive spectroscopy (EDS) confirmed the existence of Ag and F (of 5-FU) elements in the 5-FU@DsAgNCs **(Figure 4.2 e).** Structural characteristics of 5-FU@DsAgNCs were further interpreted by XRD and match with the above SAED findings **(Figure 4.3).** Appearance of crystallographic phases (111), (200), (220) and (311) in 5-FU@DsAgNCs confirm the formation of crystalline face centered cubic Ag (Matai et al., 2014a). No separate peaks of 5-FU were identified which confirms its complete encapsulation.

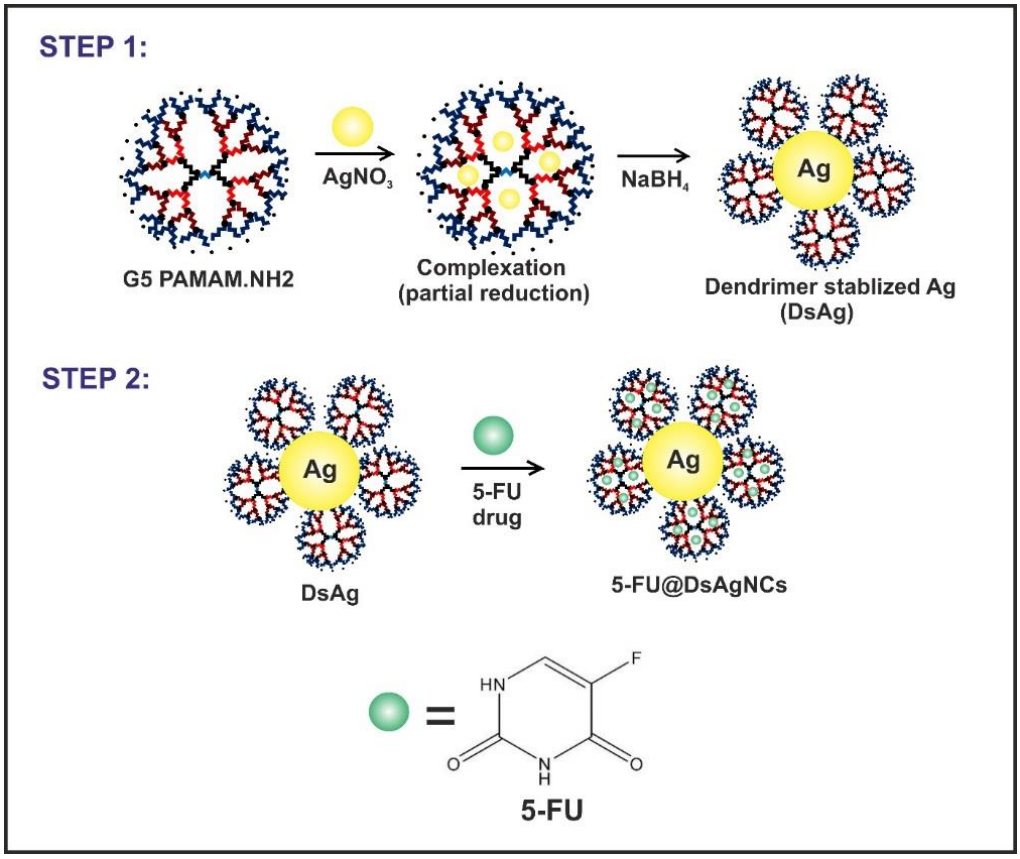

Scheme 4.0. Schematic description of formation of DsAgNPs (STEP 1) and 5-FU@DsAgNCs (STEP 2).

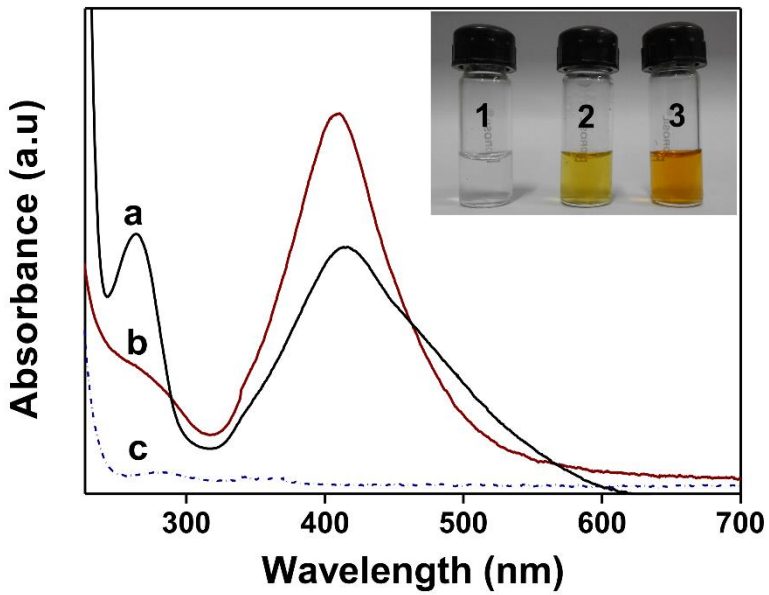

Figure 4.1. UV-vis spectra and corresponding digital photographs of G5 PAMAM (blue dotted line, 1), DsAgNPs (red line, 2) and 5-FU@DsAgNCs (black line, 3).

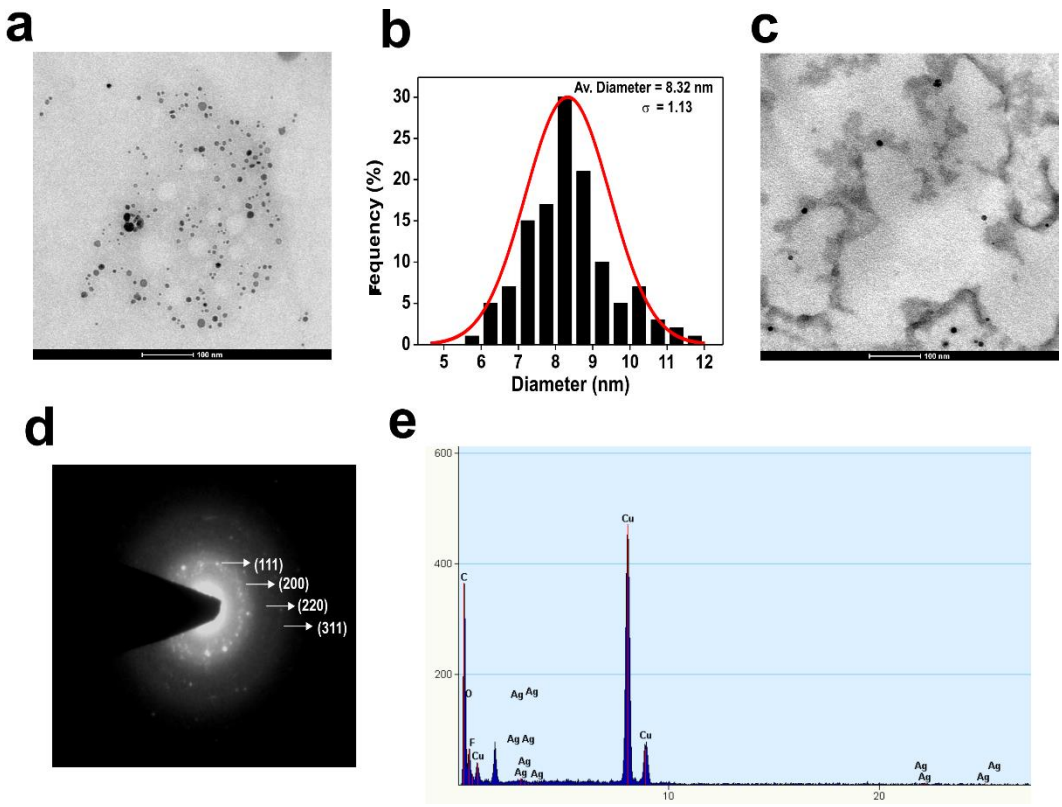

Figure 4.2. a) Representative TEM images of DsAgNPs and its corresponding (b) size distribution histogram, (c) TEM image of 5-FU@DsAgNCs after PTA staining, its corresponding (d) SAED pattern and (e) EDX spectra (Scale bar: 100 nm)

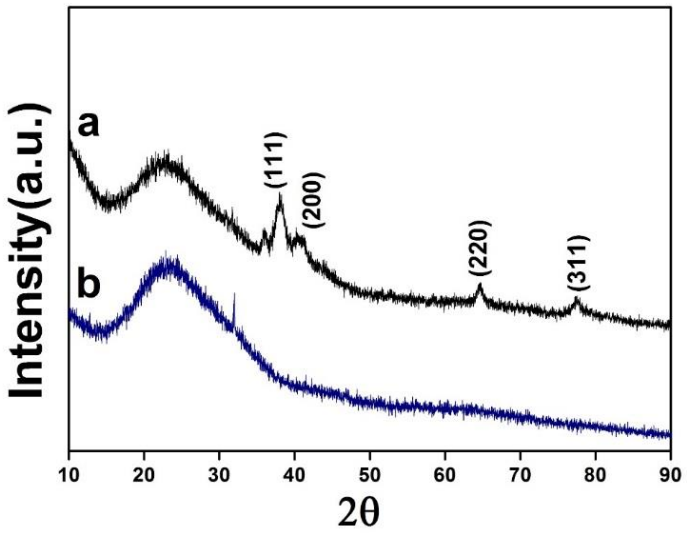

Figure 4.3. XRD spectra of a) 5-FU@DsAgNCs and b) blank G5 PAMAM dendrimer. Crystallographic phases (111), (200), (220) and (311) in (a) match closely with JCPDS card# 04-0783 corresponding to face centered cubic structure of Ag.

Accounting the stability of 5-FU@DsAgNCs under physiological conditions is of utmost importance for their biological applications. 5-FU@DsAgNCs in powder form were readily soluble in water and PBS with appreciable stability for at least 2 months at 4 °C. Changes in the surface charge potential with 5-FU encapsulation were recorded **(Figure 4.4).** As seen, Zeta potential (ζ) of G5 PAMAM was +49.6 mV which decreased to +44 mV with formation of dendrimer stabilized AgNPs. The slight reduction in charge can be ascribed to utilization of few terminal NH_2 groups for stabilizing the nanoparticle surface. Surprisingly, the ζ values increased to +45.6 mV with 5-FU encapsulation, explaining higher stability of 5-FU@DsAgNCs than DsAg. Liu et al., 2012b obtained similar results for 5-FU-SeNPs where surface decoration of 5-FU increased the stability of SeNPs. The high stability of 5-FU@DsAgNCs is essential for their future biomedical applications.

4.2.2. ^{1}H NMR analysis

The formation of DsAgNPs and 5-FU@DsAgNCs was further confirmed by ^{1}H NMR measurements. **Figure 4.5** represents the ^{1}H NMR spectra of G5 PAMAM, DsAgNPs and 5-FU@DsAgNCs. Significant difference in the chemical shift of protons related to DsAgNPs **(Figure 4.5 b)** and 5-FU@DsAgNCs **(Figure 4.5 c)** were observed compared to G5 PAMAM dendrimers **(Figure 4.5 a)**. Upon formation of DsAg, ^{1}H NMR signals related to 4, 5, 6 protons of G5 PAMAM shift downfield while remaining protons retain their original position. This signifies the interaction of dendrimer secondary and terminal amines with the surface of Ag nanoparticle (Shi et al., 2009). These interactions are predominantly involved in formation of amine terminated AgNPs. With 5-FU entrapment, only protons 1 and 3 of G5 PAMAM demonstrated a downfield chemical shift when compared to DsAg while the position of other protons remained unchanged. This presumably is due to strong complexation between secondary amines and amide groups with the 5-FU drug (Buczkowski et al., 2012b).

4.2.3. *In vitro* 5-FU release kinetics

Before moving to cellular environments we investigated the ability of PAMAM dendrimers to release the 5-FU payload under physiological conditions. **Figure 4.6 a** shows the release profiles of free 5-FU and 5-FU from 5-FU@DsAgNCs in PBS (pH 7.4).It can be seen that cumulative release of 5-FU from NCs was in a sustained manner. In contrast, about 90 % free 5-FU was released within 6 h while less than 30 % 5-FU released from 5-FU@DsAgNCs in the same time period. These nanocomposites were able to release 5-FU in a biphasic pattern, characterized by an initial faster release followed by a sustained release (Liao et al., 2014 and Zhang et al., 2014) The initial burst release can be owed to diffusion of loosely bound 5-FU molecules in the

dendrimer interiors or 5-FU adsorbed on the nanoparticle surface. **Figure 4.6 b** represents the schematic representation of the diffusion of bound 5-FU drug molecules from the dendrimer hydrophobic interiors with exposure to physiological environment.

4.2.4. Investigation of growth inhibition by 5-FU@DsAgNCs

4.2.4.1. *In vitro* cytotoxicity assay

The *in vitro* cytotoxicity of 5-FU@DsAgNCs was tested against A549 and MCF-7 cancer cells by MTT assay. Drug 5-FU and AgNPs as constituting elements of PAMAM nanocomposites exhibited growth inhibition in a dose-dependent manner **(Figure 4.7 a, b).** 5-FU@DsAgNCs synergistically induced cell death at far less dosage compared to DsAgNPs and 5-FU-D complexes in both cell lines. The half maximum inhibitory concentration (IC_{50}) of 5-FU@DsAgNCs recorded against A549 and MCF-7 was found to be 5 µg mL^{-1} and 1.5 µg mL^{-1}, respectively. However, PAMAM dendrimer showed minimal toxicity up to 20 µg mL^{-1} which indicate that the cell death was primarily due to combined action of 5-FU and AgNPs. Interestingly, cytotoxic effects of 5-FU@DsAgNCs were more pronounced in MCF-7 than A549 cells. These results indicate that the synergistic effects of 5-FU@DsAgNCs are cell-type specific. The selectivity in action could be attributed to different gene expression profiles of MCF-7 and A549 cells, involved in activation of different intracellular signalling pathways (Liu et al., 2012b).

4.2.4.2. Synergy analysis

The synergistic interaction between DsAgNPs and loaded drug (5-FU) was studied by isobologram examination. The IC_{50} values for 5-FU@DsAgNCs, DsAgNPs and 5-FU-D were found at 5, 15 and 30 µg mL^{-1} for A549 and 1.5, 5 and 20 µg mL^{-1} for MCF-7, respectively. Isobologram analysis revealed that viability inhibition of combined 5-FU and DsAgNPs treatment was strongly synergistic, as evidenced from the location of data point in isobologram being far below the additive line **(Figure 4.7 c, d).** The combination index (CI) of the IC_{50} value of 5-FU@DsAgNCs was calculated as 0.242 (for A549) and 0.178 (for MCF-7) which is less than one confirms the synergistic interaction between 5-FU and DsAgNPs (Tallarida et al., 2001, Joshi et al., 2011 and 2014). Collectively, our results clearly demonstrate that the strategy to combine 5-FU with DsAgNPs can effectively augment its anticancer potential.

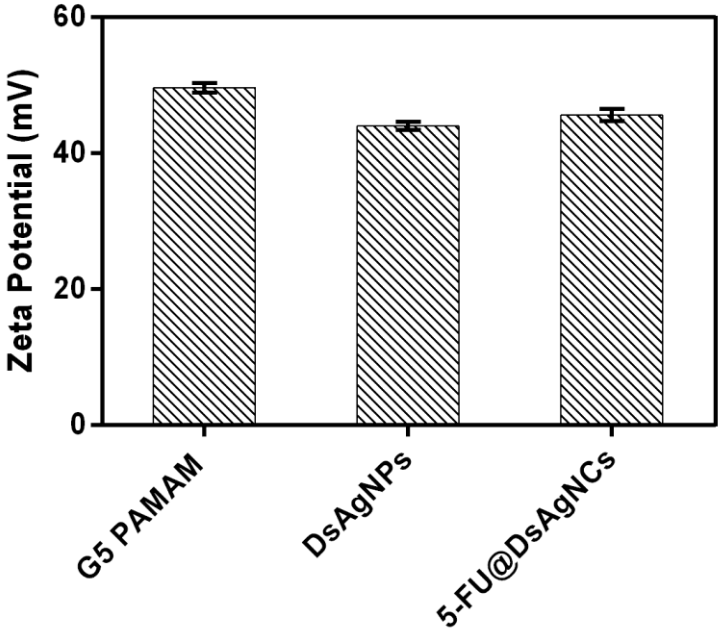

Figure 4.4. Zeta potential (ζ) measurements of G5 PAMAM, DsAgNPs and 5-FU@DsAgNCs.

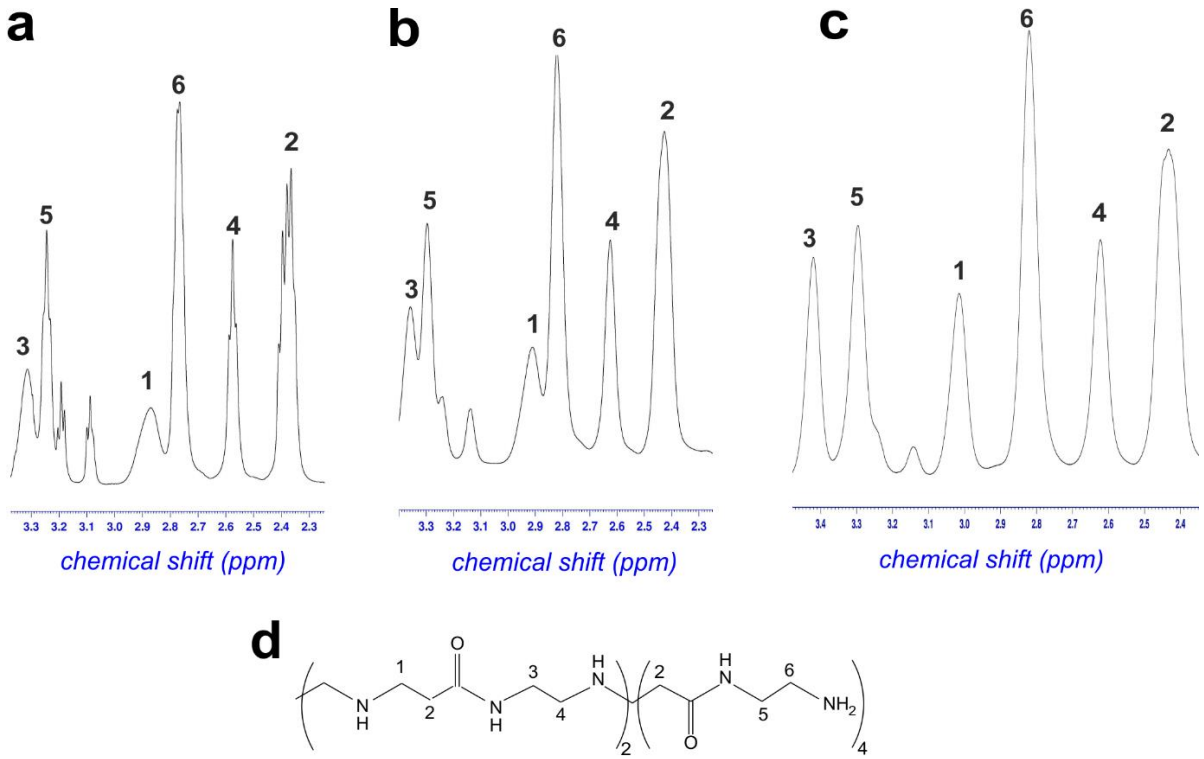

Figure 4.5. ^{1}H NMR spectra of a) G5 PAMAM, b) DsAgNPs and c) 5-FU@DsAgNCs. A schematic of the dendrimer structure used in NMR experiments is depicted in (d).

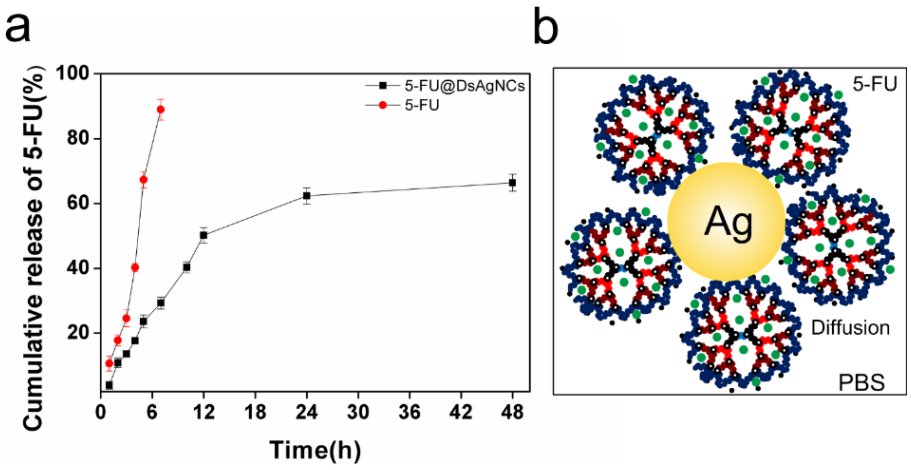

Figure 4.6. a) Cumulative release of 5-FU from 5-FU@DsAgNCs with time in PBS (pH = 7.4) (b) Schematic representation of 5-FU release from 5-FU@DsAgNCs.

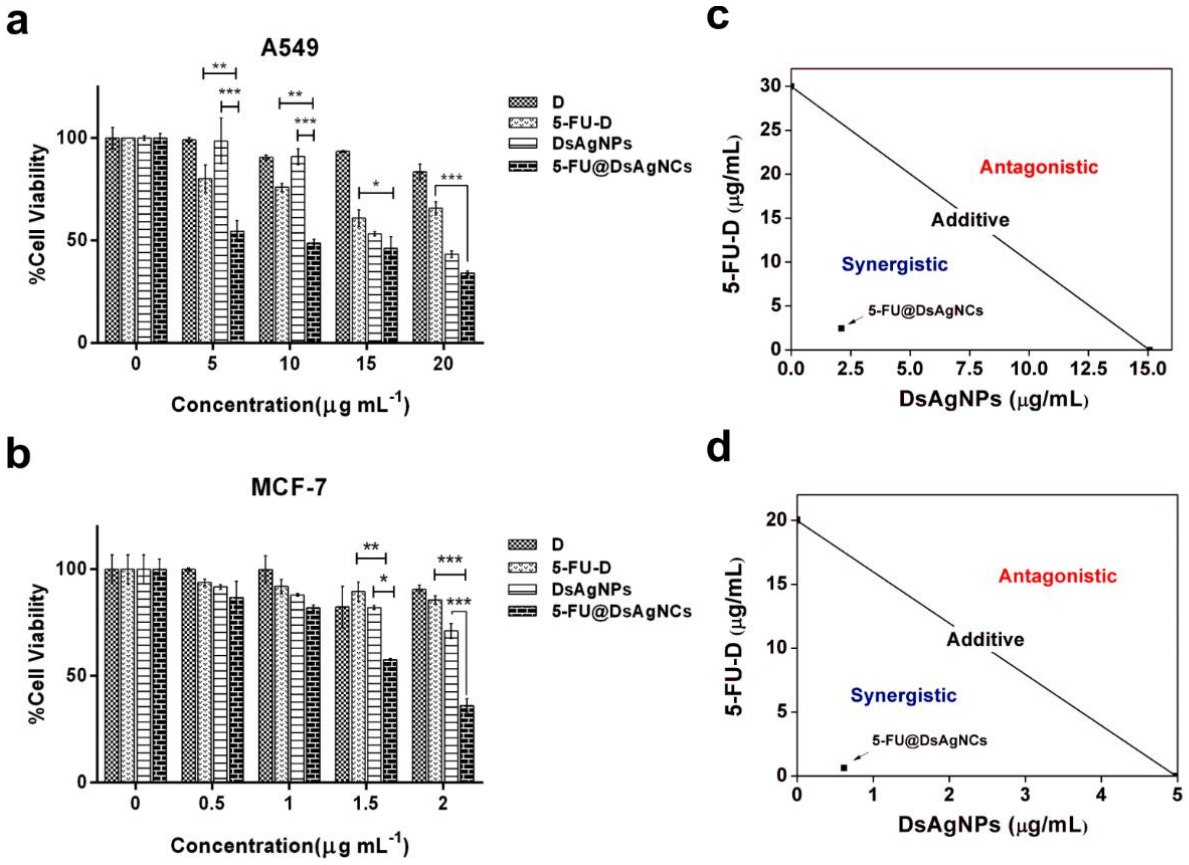

Figure 4.7. Cell viability of (a) A549 and (b) MCF-7 cells as calculated from the MTT assay. The cells were treated with blank PAMAM dendrimer (D), 5-FU-D, DsAgNPs and 5-FU@DsAgNCs (Concentration of Ag was equivalent to 5-FU in 5-FU@DsAgNCs sample). The values are represented as mean ± S.E.M (n =3). Two-way ANOVA with Bonferroni correction was done to determine multiple comparisons between the groups. Statistical significance between different samples is denoted by * ($p < 0.05$), ** ($p < 0.005$), and *** ($p < 0.001$). Synergy analysis between 5-FU and DsAgNPs as constituents of 5-FU@DsAgNCs and corresponding isobolograms of A549 and MCF-7 are shown in (c) and (d), respectively.

4.2.5. Quantification of intracellular uptake of Ag

AAS was used to quantify the cellular uptake of Ag in both A549 and MCF-7 cells treated with 5-FU@DsAgNCs for 3 h **(Figure 4.8).** Cellular uptake of Ag was found to increase in a concentration dependent manner for both the cell types. The results indicate that at the studied Ag concentrations, the amount of Ag uptake in MCF-7 is significantly higher than in A549 cells. Presumably more uptake of Ag or 5-FU@DsAgNCs in MCF-7 cells, can be held responsible for its higher cytotoxicity than A549 cells.

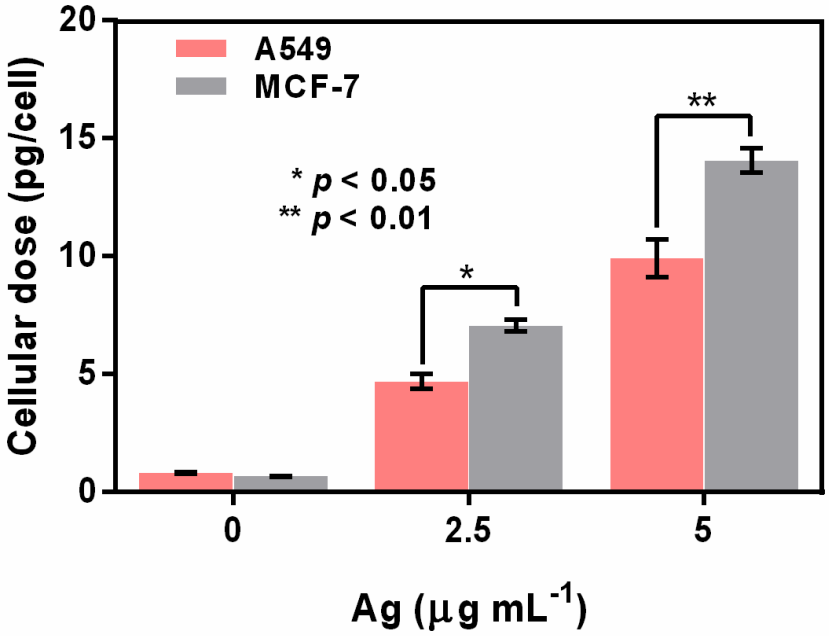

Figure 4.8. Cellular uptake of Ag in A549 and MCF-7 cells treated with different concentrations of 5-FU@DsAgNCs after 3 h. Data is represented as mean ± S.E.M (*n* =2).

4.2.6. Induction of apoptosis in cancer cells: AO/EB staining, FE-SEM and nuclear fragmentation studies

Apoptosis has been proposed as the main mechanism of anticancer action of 5-FU (Vargas et al., 2006 and Kumar et al., 2014) and Ag (Chairuangkitti et al., 2013 and Lee et al., 2014). So, in order to determine the mode of cancer cell death (viz. apoptosis or necrosis) by 5-FU@DsAgNCs, treated cells were stained with fluorescent DNA intercalating dyes namely AO/EB and observed under fluorescence microscope. AO dye can permeate all cell nucleus to emit green fluorescence on binding with double stranded DNA but EB can only enter the membrane compromised nucleus to emit orange-red fluorescence (Sharma et al., 2014). As evident from **Figure 4.9 a**, IC_{50} treated A549 and MCF-7 cells showed green and orange-stained condensed nuclei owing to both early and late apoptotic cells. While 2X IC_{50} treated cells,

displayed more number of late apoptotic cells and few necrotic cells. Thus, AO/EB staining signify apoptosis induction by 5-FU@DsAgNCs in both cancer cell types.

We next performed FE-SEM studies to monitor cell morphological changes associated with apoptosis. As seen in **Figure 4.9 b**, untreated cells have distinct shape and are well attached to the surface with no evidence of membrane constriction or leakage. Contrarily, IC_{50} treated cells were spherical and loosely-bound. Membrane blebbing and formation of apoptotic bodies, characteristics of apoptotic cell death (Rello et al., 2005), were clearly evident in 5-FU@DsAgNC treated cells. Following, elemental mapping detected the distribution profiles of elements, F (of 5-FU) and Ag in treated MCF-7 cells which verifies the apoptosis inducing ability of 5-FU@DsAgNCs **(Figure 4.10).**

Besides membrane blebbing, nuclear chromatin condensation and cytoplasmic shrinkage are key features of apoptotic cells (Wyllie et al., 1980, Cohen et al., 1992 and Martin et al., 1995). In this regard, time dependent induction of apoptosis in form of nuclear fragmentation and cytoskeleton compaction was studied at three time points i.e. at 6, 12 and 24 h using Hoechst 33342 and rho B dyes. Basically, Hoechst 33342 is a membrane permeant nuclear counterstain that emits blue fluorescence when bound to dsDNA. It can differentiate condensed pycnotic nuclei (nucleus with condensed chromatin) in apoptotic cells (Allen et al., 2001), while rho B stains the mitochondria and cytoplasmic compartments (Kumar et al., 2014). In the present case, as evident in **Figure 4.11 a**, with time course 5-FU@DsAgNC (IC_{50}) treated MCF-7 nuclei exhibited chromatin condensation in form of dark spots (marked with yellow arrows) and a significant reduction in cytoplasmic volume (white arrows). After 24 h, drastic reduction in cell number with very few rho B stained cells and appearance of many pycnotic nuclei suggest MCF-7 apoptotic cell death. Similar were the observations with 5-FU@DsAgNC (IC_{50}) treated A549 cells **(Figure 4.11 b)**.Taken together, these findings suggest that cell death induced by 5-FU@DsAgNCs is mainly caused by apoptosis.

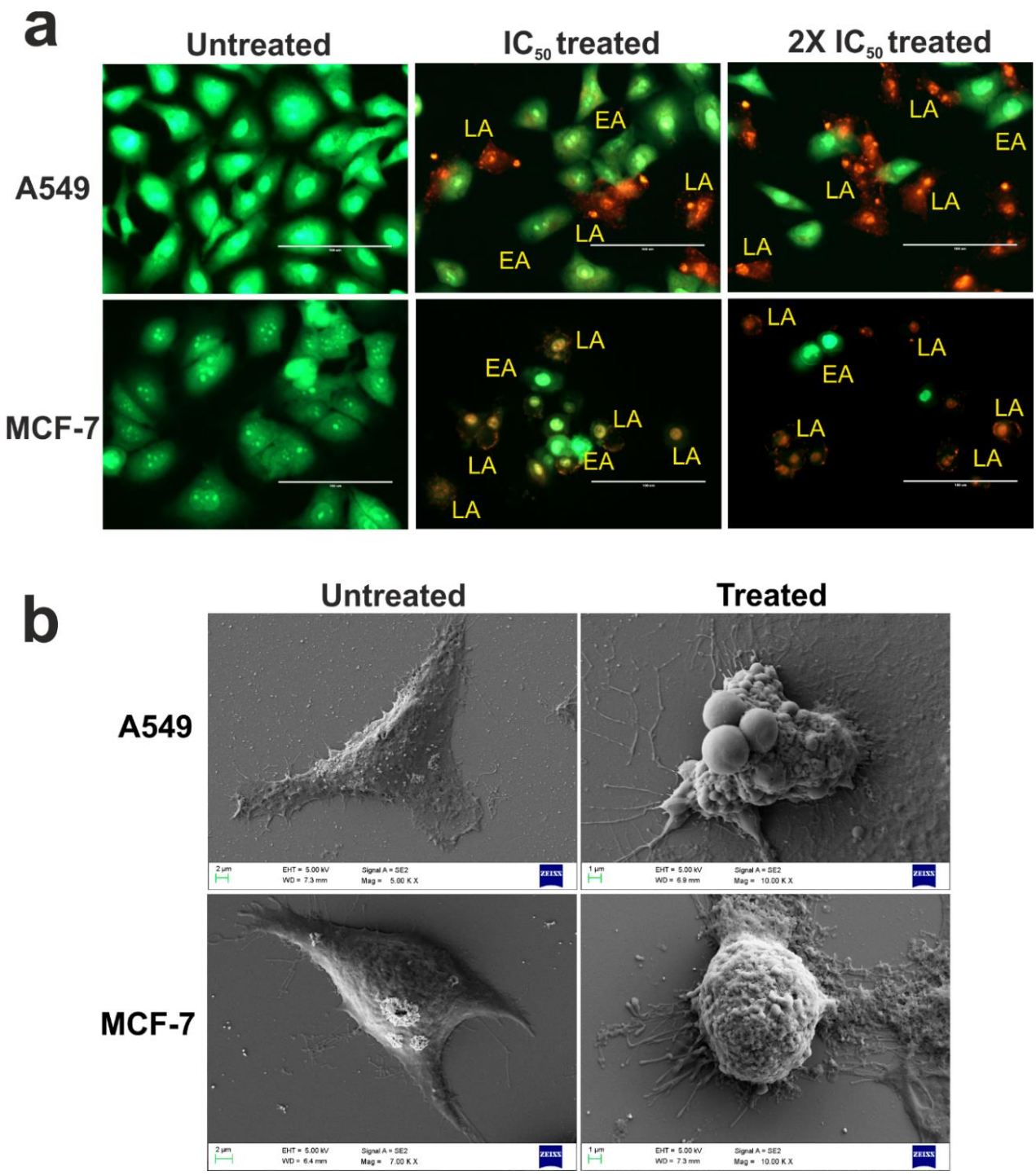

Figure 4.9. a) Representative AO/EB dual staining images of untreated, IC_{50} and 2X IC_{50} 5-FU@DsAgNC treated A549 and MCF-7 cells after 24 h. EA and LA represent early apoptotic and late apoptotic cells, respectively. Scale bar: 100 µm. b) FE-SEM images of untreated and IC_{50} 5-FU@DsAgNC treated A549 and MCF-7 cells, respectively.

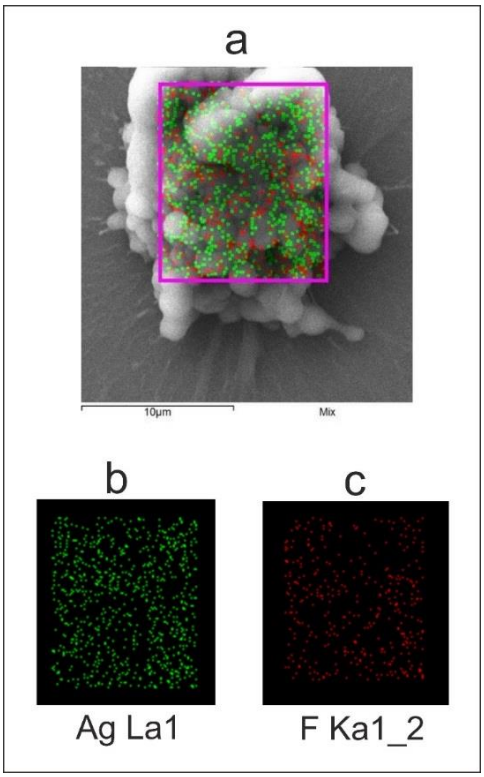

Figure 4.10. FE-SEM image of 5-FU@DsAgNC treated MCF-7 cell and color coded SEM/EDX dot maps. a) Overlay SEM image depicting elemental distributions in 5-FU@DsAgNC treated MCF-7 cell, b-c) Individual elemental distribution (green for silver and red for fluorine).

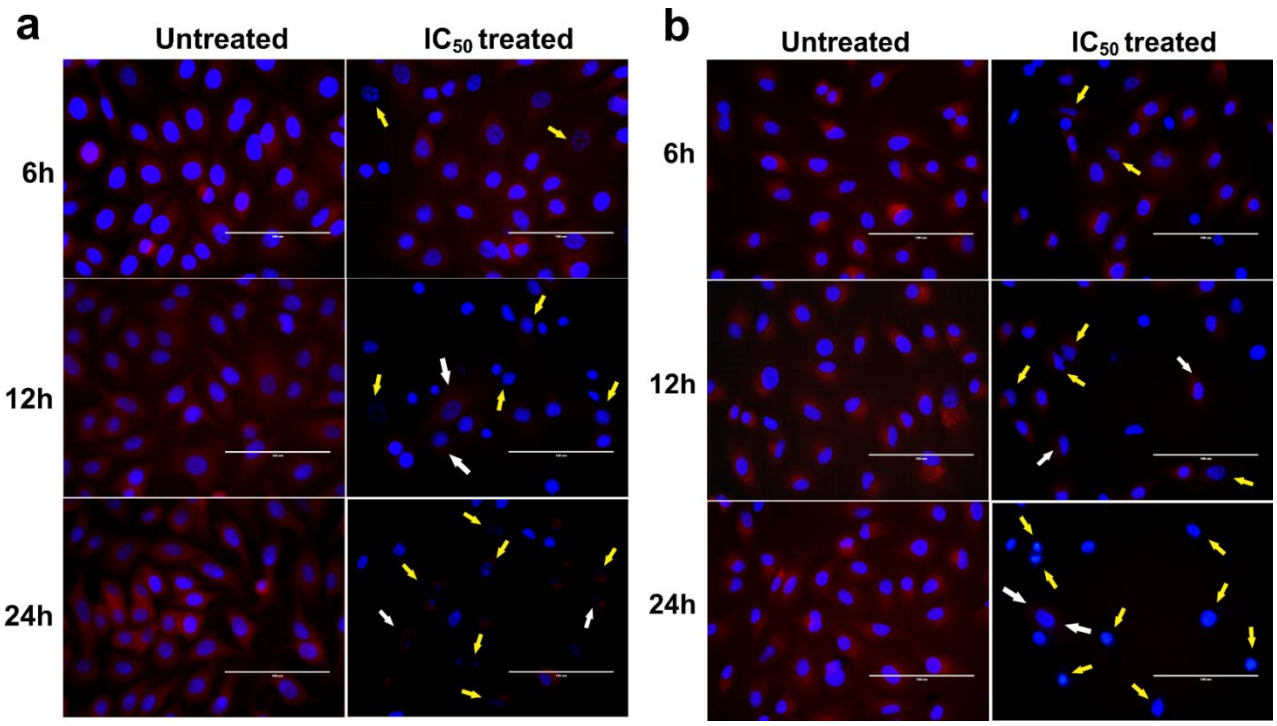

Figure 4.11. Time-dependent overlay images of untreated and 5-FU@DsAgNC (IC_{50}) treated (a) MCF-7 and (b) A549 cells stained with Hoechst 33342 (blue) and co-stained with rhodamine B (red). Yellow arrows indicate chromatin condensation (dark spots) and white arrows point towards cytoskeleton compaction. Scale bar: 100 µm.

4.2.7. 5-FU@DsAgNCs induce oxidative stress by evoking ROS

Oxidative stress has been considered to be one of the most crucial mechanisms of toxicity upon Ag nanoparticle exposure (Chairuangkitti et al., 2013 and Lee et al., 2014). Excessive generation of ROS result in disturbance of cells intrinsic antioxidant defence mechanisms and the induction of oxidative stress. This oxidative stress causes mitochondrial dysfunction, DNA damage and finally apoptotic cell death (Sanpui et al., 2011 and Sharma et al., 2014). To evaluate the potential role of oxidative stress mediated by 5-FU@DsAgNC exposure, ROS levels were measured using DCFH-DA assay. In MCF-7 cells, the percentage of ROS producing cells was 3.88 % in untreated cells which increased to 32.7 % (~8.5 times) in 1.5 µg mL^{-1} (IC_{50}) and to 41.1 % (~10.5 times) in 3 µg mL^{-1} (2X IC_{50}) treated cells **(Figure 4.12)**. Comparatively, in A549 cells, % population with ROS induction elevated from 2.48 % in untreated cells to 6.58 % (~2.5 times) in 5 µg mL^{-1} (IC_{50}) and to 19.9 % (~8 times) in 10 µg mL^{-1} (2X IC_{50}) treated cells **(Figure 4.13)**. Complementarily, fluorescent images showed a subsequent increase in number of cells with DCF fluorescence (green) with increase in 5-FU@DsAgNC dose for both MCF-7 and A549 cells **(Figure 4.12 and 4.13)**. These results suggest that 5-FU@DsAgNCs induced oxidative stress by evoking more ROS in MCF-7 than A549. Moreover, these findings match closely with the MTT results wherein MCF-7 cells were found to be more susceptible to 5-FU@DsAgNC treatment than A549 cells. Hence, MCF-7 cells were selected for elucidating the apoptotic gene expression induced by 5-FU@DsAgNCs.

4.2.8. 5-FU@DsAgNC treatment turns on p53 mediated gene signalling cascade

An RT-PCR analysis of 5-FU@DsAgNC (IC_{50}) treated and untreated MCF-7 cells was done to monitor the expression profiles of pro-apoptotic: p53, caspase 3, c myc, bax, bad and anti-apoptotic: bcl-xl, bcl-2 and β-actin (housekeeping) genes. The results indicated differential expression of various apoptotic genes **(Figure 4.14 a)**. Interestingly, it was observed that pro-apoptotic genes were up-regulated (depicted in figure by upward arrow) and anti-apoptotic genes were down-regulated (depicted in figure by downward arrow). Expression of β-actin remained unaltered. The fold difference in gene expression has been shown in **Figure 4.14 b**.

A schematic illustration of apoptotic pathway involved in 5-FU@DsAgNC treatment is represented in **Figure 4.14 c**. 5-FU@DsAgNC attachment causes membrane destabilization and ROS induction which activates intracellular signalling pathway and triggers activation of p53. Moreover, p53 is also considered as the main effector molecule involved in 5-FU toxicity (Vargas et al., 2006 and Cheng et al., 2012). 5-FU, principally acts as a thymidylate synthase (TS) inhibitor, an enzyme required for DNA replication and inhibits DNA synthesis. Herein, we have

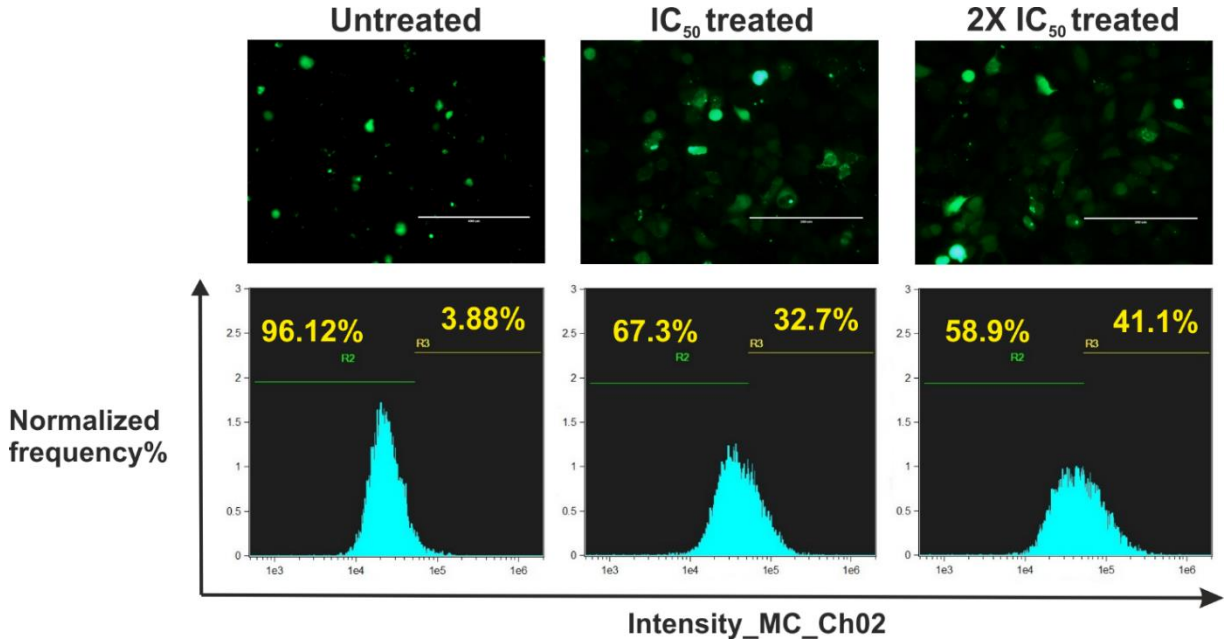

Figure 4.12. Microscopic and flow cytometric analysis of ROS production in MCF-7 cells treated with different concentrations of 5-FU@DsAgNCs for 3 h. Upper panel: Green DCF fluorescence indicates intracellular ROS generation. Scale bar: 100 µm. Lower panel: Corresponding flow cytometric quantitation.

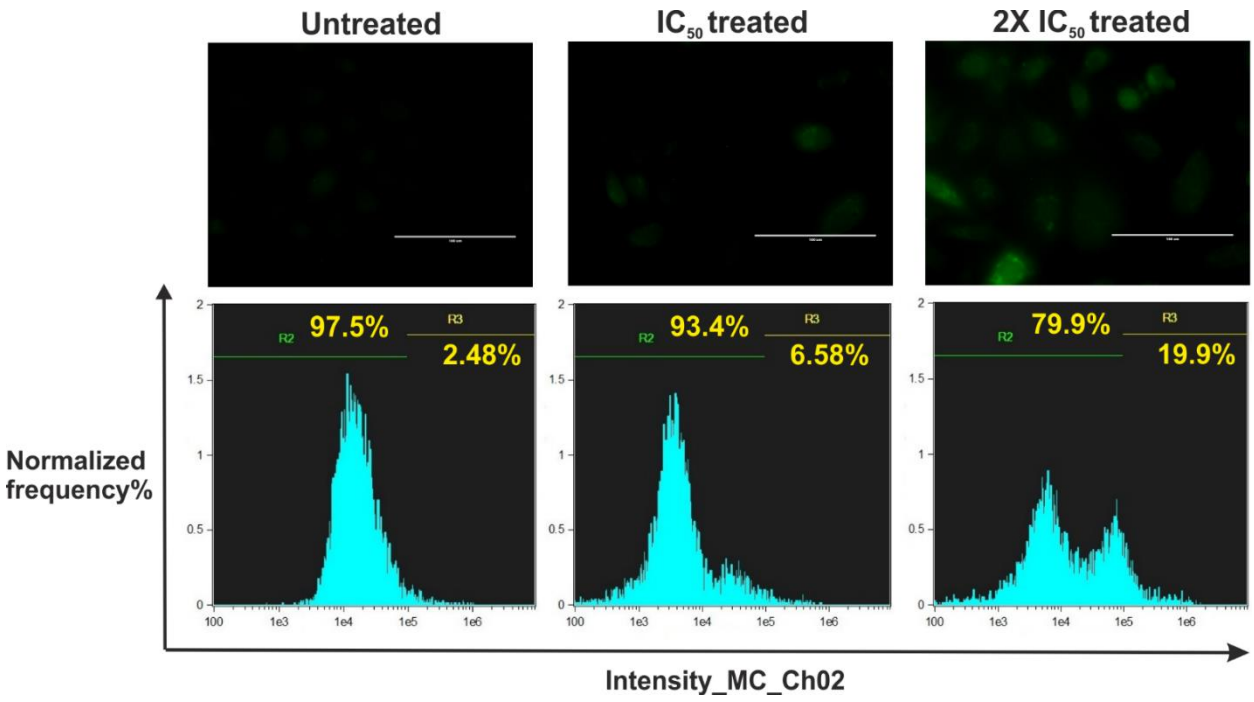

Figure 4.13. Microscopic and flow cytometric analysis of ROS production in 5-FU@DsAgNCs treated A549 cells for 3 h. Upper panel: Green DCF fluorescence indicates intracellular ROS generation. Scale bar: 100 µm. Lower panel: Corresponding flow cytometric quantitation.

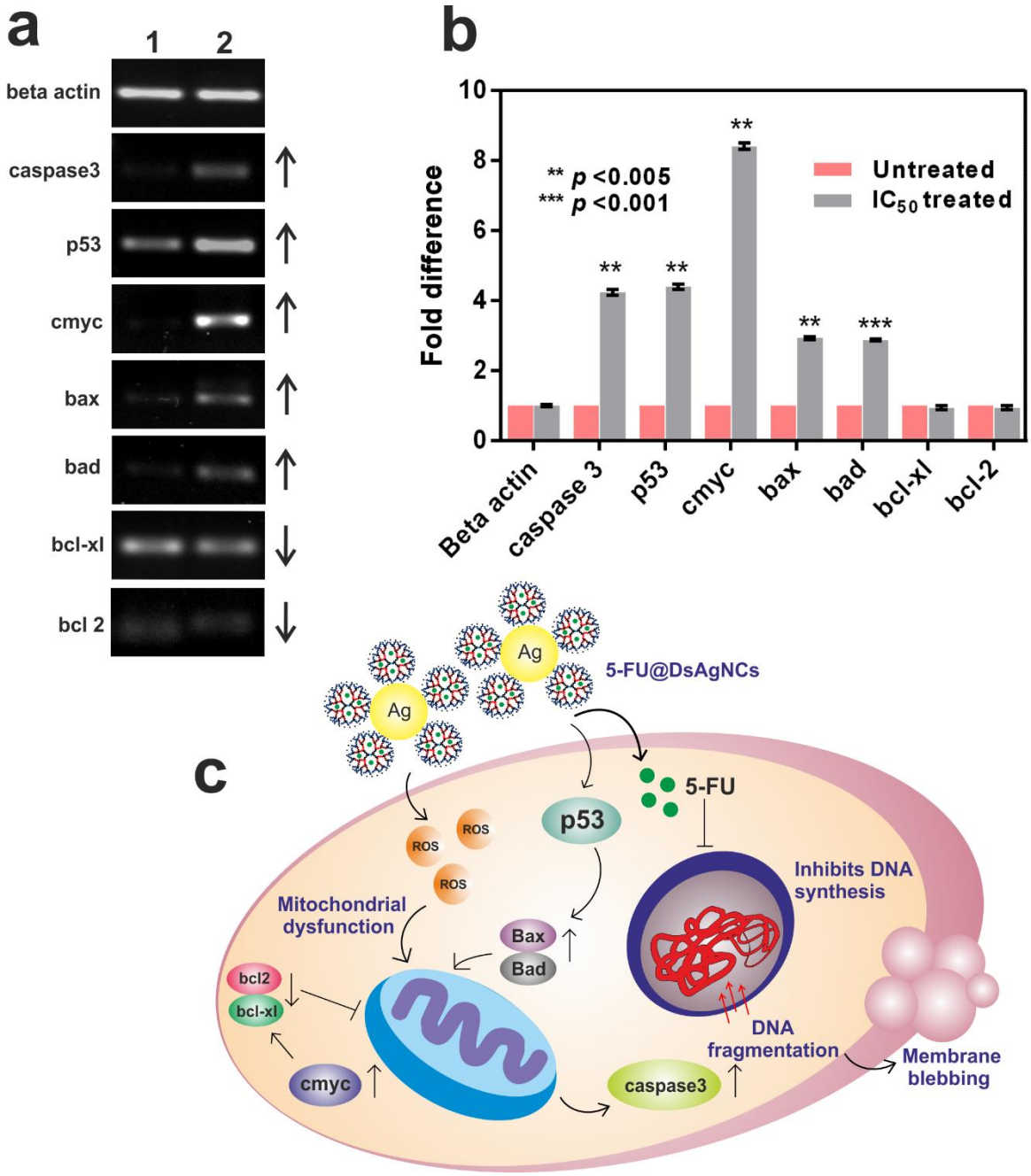

Figure 4.14. a) Semi-quantitative RT-PCR analysis of apoptotic signalling genes and their representative images. Lane 1 and 2: Untreated and 1.5 µg mL^{-1} 5-FU@DsAgNC (IC_{50}) treated MCF-7 cells. b) Fold difference in gene expression represented as mean ± S.E.M of individual experiments (*n* =3). c) Schematic representation of progressive apoptotic events involved in 5-FU@DsAgNCs treatment.

observed up-regulation of p53 gene which indicate activation of p53 mediated signalling cascade (Ng et al., 2011 and Setyawati et al., 2013). Anti-apoptotic bcl-2 (basal cell lymphoma 2) and bcl-xl (basal cell lymphoma-extra large) protects the cell from undergoing apoptosis and bad (bcl-2-associated death promoter) promotes apoptosis (Yang et al., 1995 and Chao et al., 1998). We observed down-regulation of bcl-2 and bcl-xl with up- regulation of bad, which suggests initiation of apoptosis. Further, p53 is known to up-regulate bax (bcl-2-associated X protein) (Wolter et al., 1997). An elevation in bax expression was seen which postulates the role of p53 in bax up-regulation upon 5-FU@DsAgNC treatment. Translocation of bax from cytosol to mitochondria has been associated with outer membrane permeabilization (MOMP) and formation of pores which allow cytochrome c release (Wolter et al., 1997). The released cytochrome c is identified to trigger caspase 3 (cysteine-aspartic acid proteases), the final agents leading to apoptosis which cause cellular DNA fragmentation and subsequently cell death (Liu et al., 1996 and Hengartner, 2000). We have observed increased expression of caspase 3, which prompts caspase 3 mediated apoptosis in 5-FU@DsAgNC treated cells. Consecutively, up-regulation of C-myc, a known inducer of apoptosis, promotes apoptotic genes and down-regulates anti-apoptotic genes, bcl-2 and bcl-xl, validating manifestation of cell blebbing and p53 mediated apoptotic cell death. Similar results have been reported by Gopinath et al., 2008 and Hsin et al., 2008. Such an understanding of the molecular underpinnings of 5-FU@DsAgNCs mediated cell death can primarily establish 5-FU@DsAgNCs as a potent anticancer weapon to prevent multidrug resistance and cancer recurrence.

In summary, the present work describes the construction of a novel G5 PAMAM dendrimer based multicomponent system for the simultaneous delivery of AgNPs and anticancer drug 5-FU to cancer cells. The drug 5-FU confined within dendrimer stabilized AgNP interiors circumvents the limitations associated with multidrug resistance in cancer cells at low dosage to emerge as a potential alternative to traditional chemotherapy.

CHAPTER 5

Formulation of Chemically Cross-linked Hybrid Nanogels of Alginate and PAMAM Dendrimers for Efficient Delivery of Anticancer Agents

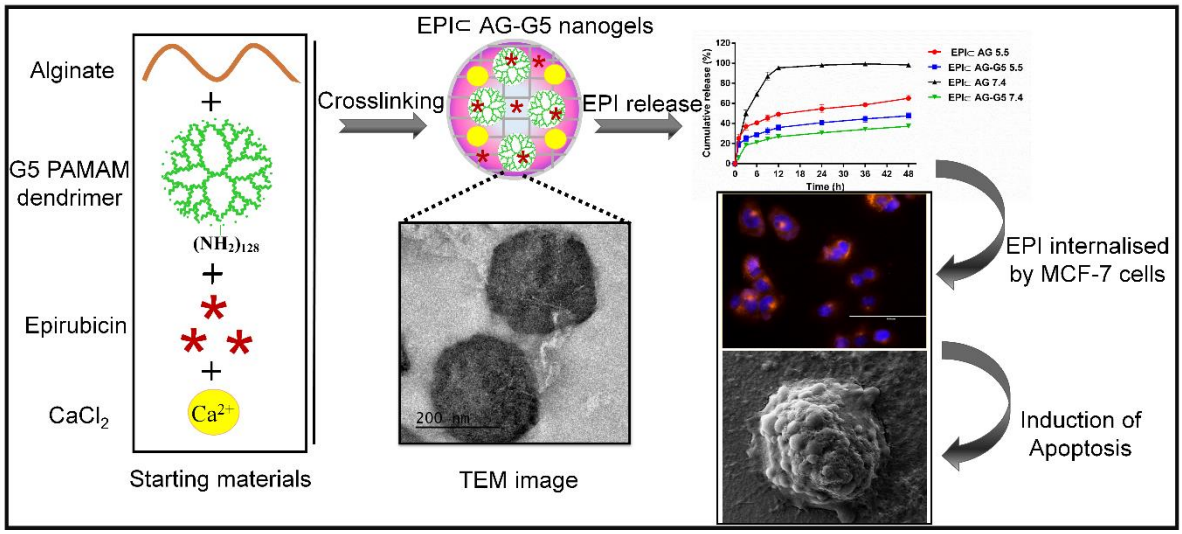

CHAPTER 5

FORMULATION OF CHEMICALLY CROSS-LINKED HYBRID NANOGELS OF ALGINATE AND PAMAM DENDRIMERS FOR EFFICIENT DELIVERY OF ANTICANCER AGENTS

5.1. Overview

Sodium alginate (AG) is a naturally occurring algal polysaccharide composed of consecutive units of (1–4) linked α-L-guluronate (G) and β-D-mannuronate (M) residues followed by alternating segments of M-G blocks (Balakrishnan et al., 2011 and Lee et al., 2012). The G blocks in alginate can ionically cross-link in presence of divalent cations such as calcium, barium and strontium to form the popular "egg-box" structure (Grant et al., 1973). Divalent calcium cations (Ca^{2+}) can form a bridge of intermolecular bonds between the deprotonated carboxylate groups of one G block with the two hydroxyl groups of another. However, pure Ca^{2+}-cross-linked AG nanogels lack stability and dissociate due to rapid exchange of Ca^{2+} with other cations in buffers like phosphate buffer saline (PBS) (LeRoux et al., 1999 and Li et al., 2011). Such abnormal behavior of pure Ca^{2+}-cross-linked AG nanogels refrains their utility as delivery vehicles for nanomedicine. Hence, a second component was required to interact with alginate and improve its structural stability under physiological conditions for drug delivery applications. PAMAM dendrimers are synthetic macromolecules which are known to ferry both hydrophobic and hydrophilic drugs (Matai et al., 2014b and Gopinath et al., 2015). These amine group bearing cationic dendrimers can electrostatically interact with anionic molecules such as alginate to develop polymer nanoparticles with improved properties. Moreover, nanogels formulated by this strategy are expected to possess enhanced stability, toughness and compact shape for tunable drug delivery applications. Till date, only one report exists on formation of alginate-dendrimer nanogels through double emulsion method for drug delivery to CAL-72 cells (Goncalves et al., 2014). In the present study, we have developed alginate-PAMAM dendrimer (AG-G5) hybrid nanogels for drug delivery to cancer cells using a facile synthetic approach. 1-ethyl-3-(3-

dimethylamino propyl) carbodiiamide hydrochloride (EDC), a zero length cross-linker was used to activate the carboxylate groups of alginate to covalently interact with PAMAM dendrimer amine groups (Lopez-Alonso et al., 2009). By this strategy, permanent irreversible amide bond formation can take place between alginate and PAMAM moieties. Finally, the remaining carboxylate groups were cross-linked using calcium chloride ($CaCl_2$). Such a unique combination of covalent and ionic interactions in alginate-dendrimer network imparts structural stability with high drug entrapment efficiencies. To ensure this, EPI was used as a model drug to investigate the physical and biological aspects related to AG-G5 nanogels. EPI is a stereoisomer of DOX and is known to exhibit comparable antitumor efficacy in breast cancer cells and low cardiotoxicity than DOX (Swarnakar et al., 2014). As a proof of concept, we examined the anticancer efficacy of EPI ⊂AG-G5 nanogels in human breast cancer (MCF-7) cells. By taking advantage of inherent red fluorescence of EPI, we could track intracellular distribution of EPI therein. This can be useful in fluorescence based evaluation of cancer progression and therapy. Overall, we suggest AG-G5 nanogels as suitable platforms for enhanced drug delivery to cancer cells.

5.2. RESULTS AND DISCUSSION

5.2.1. Design, preparation and characteristics of EPI loaded AG-G5 hybrid nanogels

Herein, AG-G5 hybrid nanogels were prepared by covalent cross-linking technique using EDC chemistry. The step-wise preparation of EPI⊂AG-G5 nanogels has been depicted in **Scheme 5.0**. The synthesis procedure involves various steps. Firstly, sodium alginate (SA) powder was completely dissolved in water to form a transparent hydrogel solution. Then, EDC was added to activate the –COOH groups of sodium alginate. With the dropwise addition of G5.0 PAMAM dendrimer, the viscosity of the activated alginate solution increased manifold. The increased viscosity indicate the interaction between the $–NH_2$ groups of PAMAM dendrimer and the –COOH groups of alginate to form amide bond. Thereafter, the red colored EPI solution was slowly added to entrap EPI molecules within the alginate-PAMAM dendrimer framework. The loaded EPI molecules imparts the nanogels with anticancer properties. Interestingly, the color of the hybrid solution changed from transparent to deep purple with incorporated EPI molecules. Finally, remaining –COOH groups of alginate were ionically cross-linked using divalent Ca^{2+} ions to obtain EPI⊂AG-G5 nanogels. **Figure 5.1 a-c** depicts the digital photographs of as-synthesized AG, AG-G5 and EPI⊂AG-G5 nanogels. The entrapment efficiency (E.E, %) for alone AG and AG-G5 hybrid nanogels indirectly estimated from the dose-absorption curve of

EPI was 69.6 ± 0.48 % and 93.3 ± 2.22 %, respectively. Thus, incorporation of G5 PAMAM dendrimer could improve the solubility and hence bioavailability of EPI in the nanogels.

The formation of EPI⊂AG-G5 nanogels can be first justified by ζ-potential measurements at pH 7.4. Blank AG nanogels had an average ζ-potential of -32.7 mV. The high negative charge can be assigned to the abundant carboxylic acid groups in the alginate structure. With addition of PAMAM dendrimer, the ζ-potential reduced to -19.1 mV. This reduction in ζ-potential of AG is due to strong covalent linking of dendrimer amines with the alginate carboxylic groups. Interestingly, the ζ-potential and hence stability of AG-G5 nanogels slightly increased to -21.1 mV after EPI entrapment. The probable explanation for improved stability of EPI⊂AG-G5 nanogels could be successful incorporation of EPI molecules within the AG-G5 structure modulating the cross-linking densities. The overall negative charge of AG-G5 nanogels suggests them as a suitable nanovehicle for drug delivery and other biomedical applications.

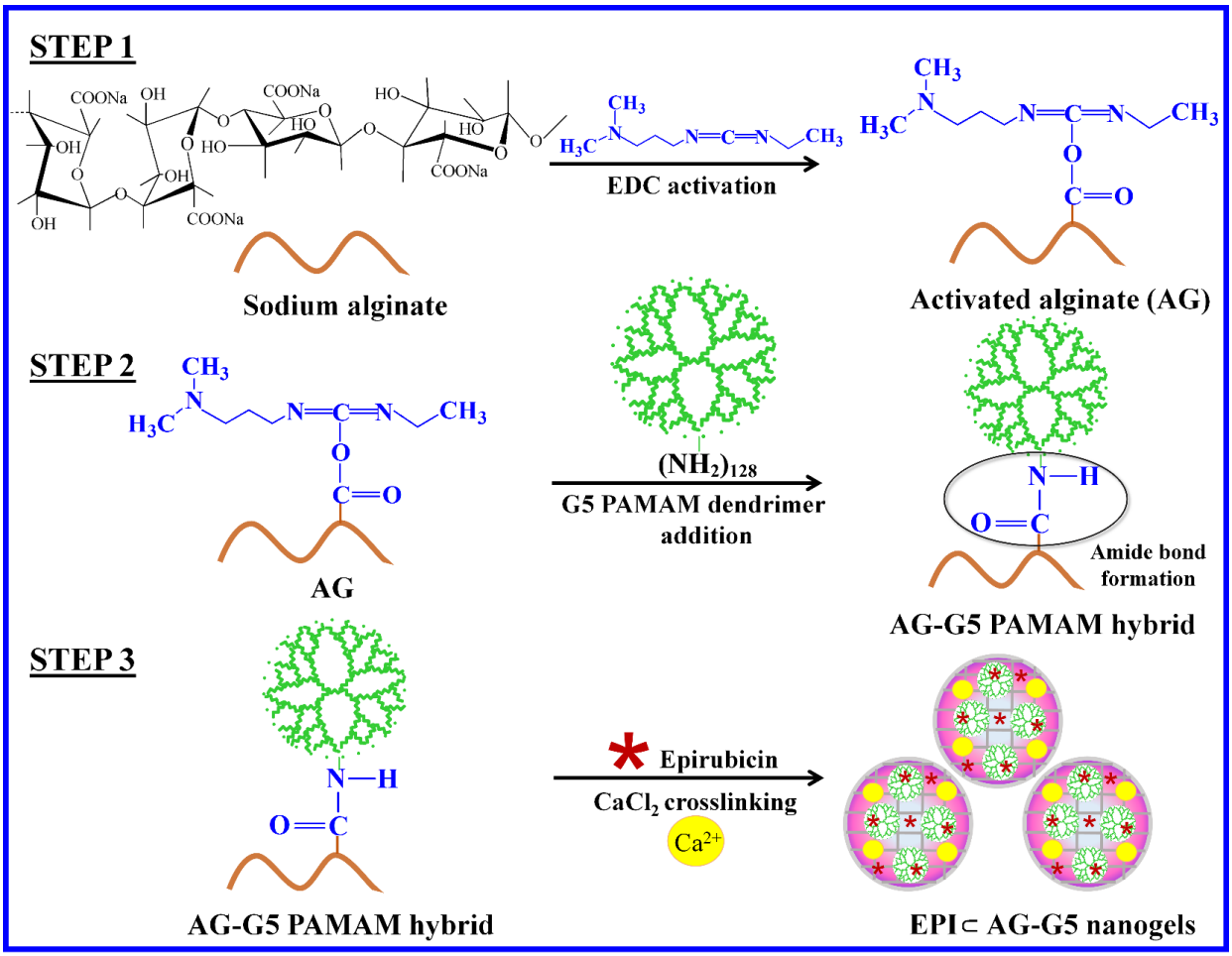

Scheme 5.0. Step-wise representation of synthesis scheme for EPI⊂AG-G5 nanogels.

With chemical cross-linking, AG-G5 nanogels are expected to have a more compact structure than alone AG nanogels. To verify this, morphology and size differences of freeze-dried nanogels were evaluated by FE-SEM. A marked difference was observed in the sizes of alone AG and cross-linked AG-G5 nanogels. As evident from **Figure 5.1 e**, AG-G5 nanogels had a quasi-tetrahedral morphology and appeared considerably small in size than AG nanogels **(Figure 5.1 d)**. Similarly, EPI⊂AG-G5 nanogels were uniformly distributed and looked compact in shape than AG-G5 nanogels **(Figure 5.1 f)**. Further, DLS measurements were recorded to estimate the hydrodynamic diameter of as-synthesized nanogels in PBS (pH 7.4). **Figure 5.1 g-i**, depicts the size distribution histograms of nanogels by DLS. The average hydrodynamic diameter of blank AG nanogels was 918.3 nm. The large size of AG nanogels can be assigned to the less physical entanglement among alginate polymeric chains after $CaCl_2$ cross-linking. Then, after chemical cross-linking with G5 PAMAM dendrimer the diameter of AG-G5 nanogels reduced to around 417.6 nm. Predominantly, covalent interactions between amino groups of dendrimer and alginate carboxyl groups results in formation of a permanent irreversible network (Ryu et al., 2010). With EPI loading, the hydrodynamic size of nanogels further reduced to 360.7 nm. This confirms the reduction in size of nanogels with increase in cross-link densities of the starting materials. It is noteworthy, that DLS predicts the overall hydrodynamic size of particles (Wang et al., 2013b). The DLS findings are in corroboration with the FE-SEM micrographs. This signifies the importance of cross-linking in designing well-defined and stable nanogels for drug delivery applications. Although the size of EPI⊂AG-G5 nanogels probed by DLS i.e. 360.7 nm is on the higher side for *in vivo* applications, still it can be effective for drug delivery to cancer cells. Tumor tissues with large pores are known to be more permeable in comparison to normal tissues, the well-established EPR effect. The cut off size of pores of tumor vessels is reported to be around 400 nm (Yuan et al., 1995). This suggests that EPI⊂AG-G5 nanogels could be internalized by cancer tissues, where in these can release the entrapped EPI molecules in a controlled and sustained manner. It was not possible to monitor the distribution of EPI molecules in the EPI⊂AG-G5 nanogels using FE-SEM due to size constraints and lack of differential contrast. To resolve this, nanogels were observed after negative staining by TEM. Also, the internal structure of EPI⊂AG-G5 nanogels was investigated. **Figure 5.2**, revealed TEM images of porous nanogels with near-spherical morphology with tiny dark domains (possibly associated with PAMAM dendrimer and EPI molecules) distributed in alginate-rich matrix with relatively low cross-link densities. Moreover, the average particle size of EPI⊂AG-G5 nanogels was estimated to be around 257.2 nm. The dried state diameter of EPI⊂AG-G5 nanogels measured by TEM was obviously smaller compared to its hydrodynamic diameter by DLS.

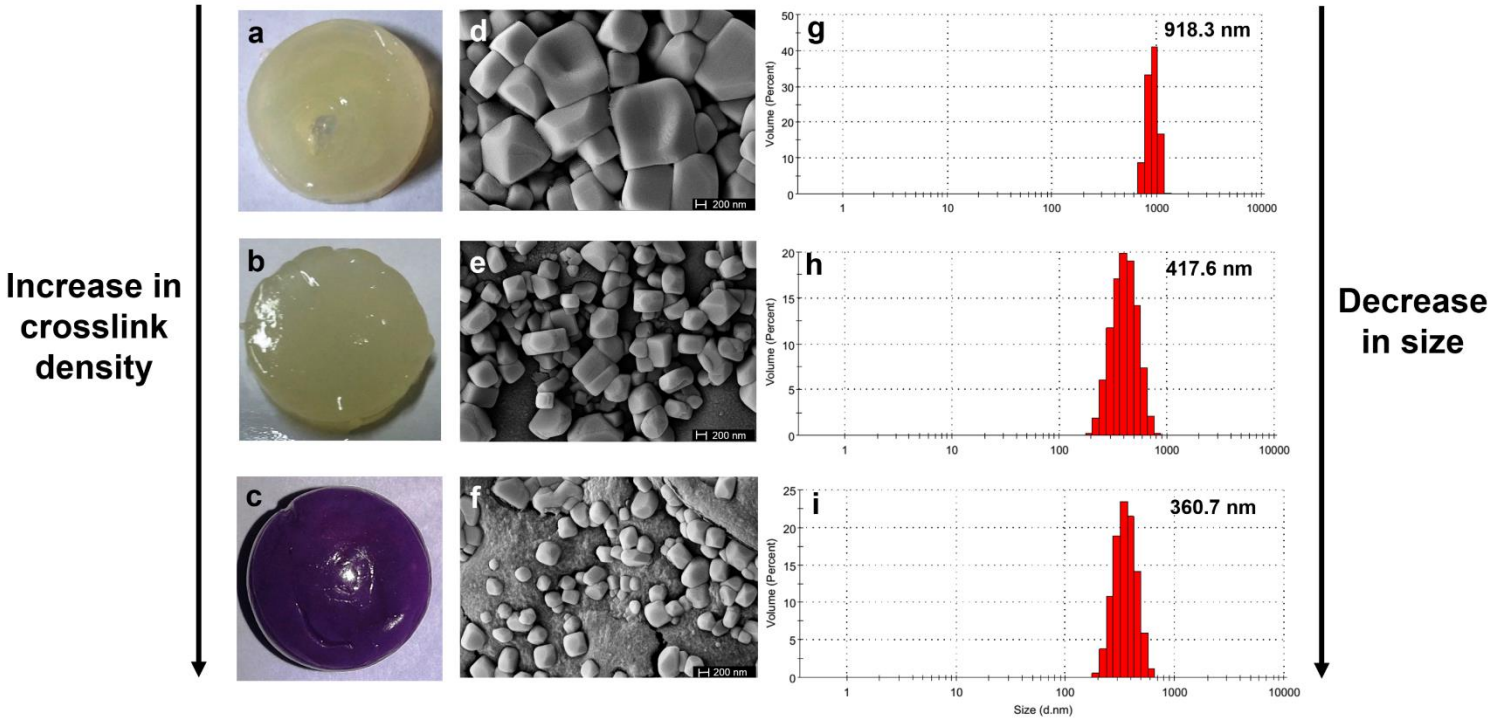

Figure 5.1. (a-c) Representative digital photographs and (d-f) FE-SEM images of AG, AG-G5 and EPI⊂AG-G5 nanogels (Scale bar: 200 nm); (g-i) corresponding size distribution histograms depicting average hydrodynamic diameter of nanogels.

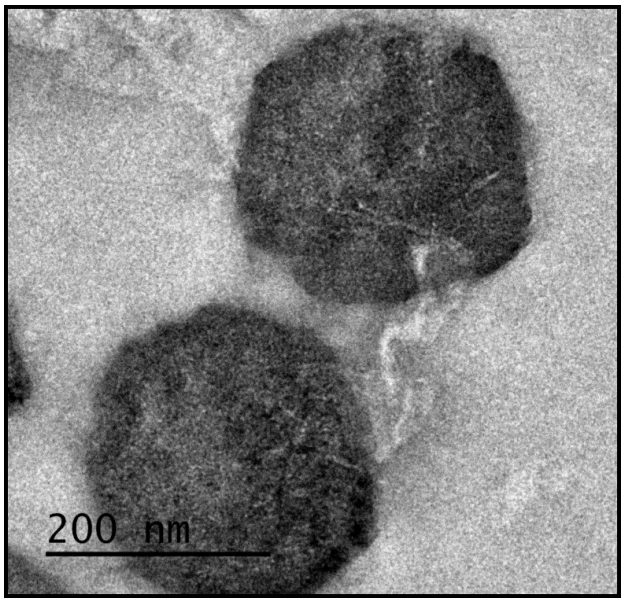

Figure 5.2. TEM image of as-synthesized EPI⊂AG-G5 nanogels after negative staining. (Scale bar: 200 nm).

This can be attributed to the swelling of the nanogels. It is imperative to mention that morphology of EPI⊂AG-G5 nanogels under TEM observation slightly varied from FE-SEM. The marginal variation was due to sonication of EPI⊂AG-G5 nanogels in PBS (pH 7.4) as a part of sample preparation for TEM analysis.

The chemical bonding involved in nanogels synthesis was interpreted by FTIR analysis. **Figure 5.3 A** shows the absorption bands from FTIR spectrum of pure SA, AG and AG-G5 nanogels. In the alginate spectra the peak at 3447 cm^{-1} corresponds to -OH stretching vibration, bands at 1627 and 1400 cm^{-1} can be attributed to asymmetric and symmetric COO^- stretching vibrations of carboxylate salt groups and peak at 1110 cm^{-1} (C-O-C stretching) is of saccharide structure of alginate (Sartori et al., 1997, Huang et al., 1999 and Lawrie et al., 2007). With $CaCl_2$ cross-linking, the antisymmetric carbonyl vibration at 1630 cm^{-1} was intensified and the symmetric carbonyl peak shifted to higher wavenumber (1430 cm^{-1}). While the –OH peak shifted to 3428 cm^{-1} (lower wavenumber). Appearance of peaks around 1300 and 800 cm^{-1} can be assigned to C-O stretching and bending vibrations, respectively (Sartori et al., 1997). All the observed spectral changes indicate existence of strong ionic interactions among alginate –COOH groups and Ca^{2+} ions. Upon chemical cross-linking with EDC, considerable changes were observed in the IR spectra of AG-G5 nanogels. The carbonyl peak at 1630 cm^{-1} red shifted to 1640 cm^{-1}. Moreover, a new band at 1580 cm^{-1} was observed corresponding to amide II (-CO-NH) linkage indicating bond formation between alginate –COOH and dendrimer $–NH_2$ groups (Pan et al., 2006). Prominent peaks at 1450 and 1410 cm^{-1} can be credited to the internal $–CH_2$ groups of PAMAM dendrimer (Fail et al., 2002). The sharp intense peaks at 1026 and 1143 cm^{-1} are of C-N vibrations, as amide group is introduced in AG-G5 structure (Pan et al., 2006). Rest peaks around 720 cm^{-1} are due to C-H bending vibrations of AG-G5 nanogels (Singh et al., 2008). Thus, the formation of cross-linked AG-G5 nanogels was be justified by FTIR analysis.

Further, alterations in thermal stability of nanogels with cross-linking and drug loading were monitored by TG analysis. The corresponding thermograms are depicted in **Figure 5.3 B**. According to TGA results, it is evident that AG, AG-G5 and EPI⊂AG-G5 nanogels follow multiple thermal-degradation stages. The observed weight losses till 100 ºC is attributed to loss of volatile products such as residual moisture content and dehydration of saccharide structure of alginate (Hua et al., 2009). Between 110-450 ºC, sharp weight loss occurred for AG nanogels due to rupturing and fragmentation of alginate network to its monomers (Laurienzo et al., 2005, Tripathi et al., 2012 and Mohy Eldin et al., 2015). For instance, at 200 ºC and 350 ºC, the weight

loss observed for AG nanogels was 25.6 % and 49.6 %, respectively. Comparing with AG, cross-linked AG-G5 nanogels showed much reduced weight loss within this temperature range. Only 19.1 % and 39.8 % weight loss was observed for AG-G5 nanogels at 200 ºC and 350 ºC, respectively. This suggests that introduction of G5 PAMAM dendrimer in the alginate network, restricts the availability of alginate chains for thermal degradation. This can be accredited to the chemical bonds between $–NH_2$ groups of dendrimer and –COOH groups of alginate. Beyond 450 ºC, the weight losses for both AG and AG-G5 nanogels are due to breakage of chemical linkages and formation of by-products. A slight reduction in stability of EPI⊂AG-G5 nanogels was observed compared to AG-G5, probably due to interference of EPI molecules with the alginate-dendrimer network. Swelling characteristics of freeze-dried nanogels was further evaluated to examine their behavior under slightly alkaline and acidic conditions. **Figure 5.4** represents the percent swelling of AG and AG-G5 nanogels at pH 5.5 and 7.4, respectively after 24 h. The percentage of swelling for AG and AG-G5 nanogels was estimated to be around 475±6.7 % and 302± 5.8 %, respectively. The greater swelling in AG nanogels is probably due to the strong electrostatic repulsive force between the ionized carboxyl groups ($-COO^-$) of alginate (pKa of alginate = 3.49) (Lin et al., 2005 and Lamelas et al., 2005). Upon conjugation, the carboxyl groups of alginate are bonded to dendrimer amine groups which increases the cross-linking density, thereby decreasing the swelling (Lin et al., 2005). Also, AG nanogels were found to disintegrate after swelling in PBS, while AG-G5 nanogels remained stable. Probably, rapid exchange of Ca^{2+} and Na^+ ions in AG nanogels can be held responsible for this (Pasparakis et al., 2006). Under acidic conditions, the observed swelling for AG and AG-G5 nanogels was 137±2.3 % and 130.9±3.7 %. Alginate chains tend to shrink under acidic environment which can be held responsive of reduced swelling of AG nanogels. Moreover, reduction in swelling of AG-G5 nanogels at pH 5.5 compared to pH 7.4 is attributed to enhanced cross-link density of anionic alginate with cationic dendrimers (Goncalves et al., 2014). Additionally, the reduced swelling in AG-G5 nanogels compared to AG nanogels is related to its reduced surface area. The specific surface area and pore volume of AG and AG-G5 nanogels were determined by BET measurements using N_2 adsorption-desorption isotherms **(Figure 5.5 A and Table 5.1)**. Surface areas of AG and AG-G5 nanogels measured by BJH method were 234.19 and 203.76 m^2/g, respectively indicating porous behavior of nanogels. Likewise, the pore volume of AG was 0.309 cc/g, which reduced to 0.271 cc/g in AG-G5 nanogels. Thus, BET results predicts a slight reduction in surface area and hence porosity of AG-G5 due to the increased cross-link density in AG-G5 when compared to AG nanogels. Overall, swelling and BET findings suggest the formation of rigid and stable AG-G5 nanogels network.

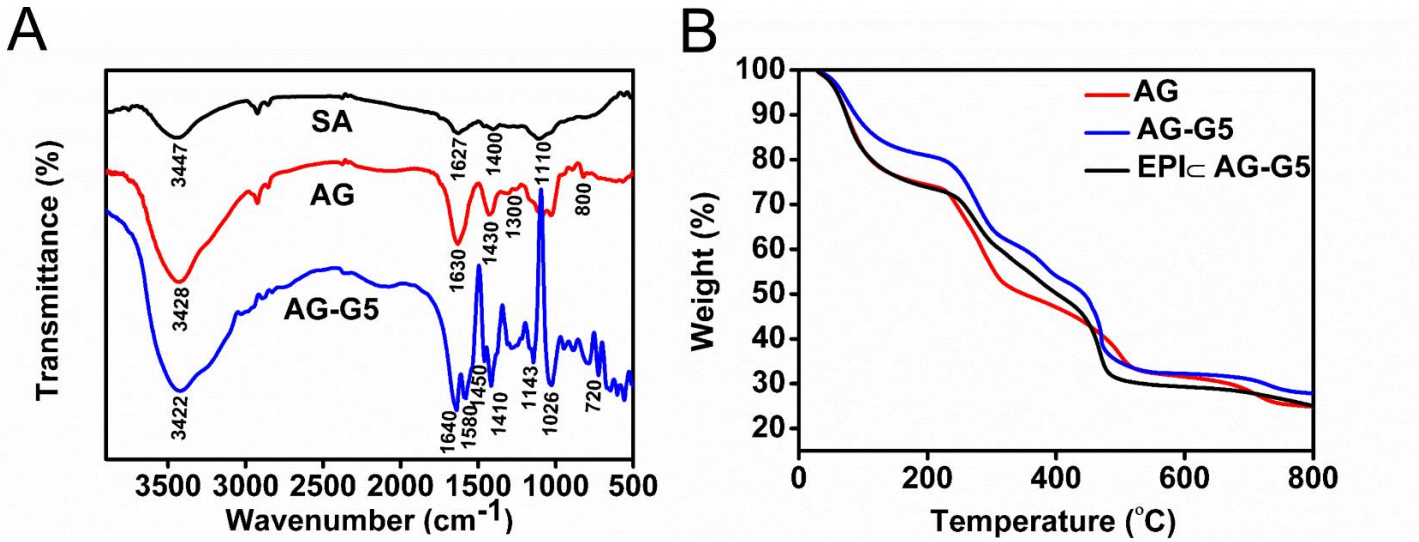

Figure 5.3. (A) FTIR spectra and (B) TGA plot of as-synthesized nanogels.

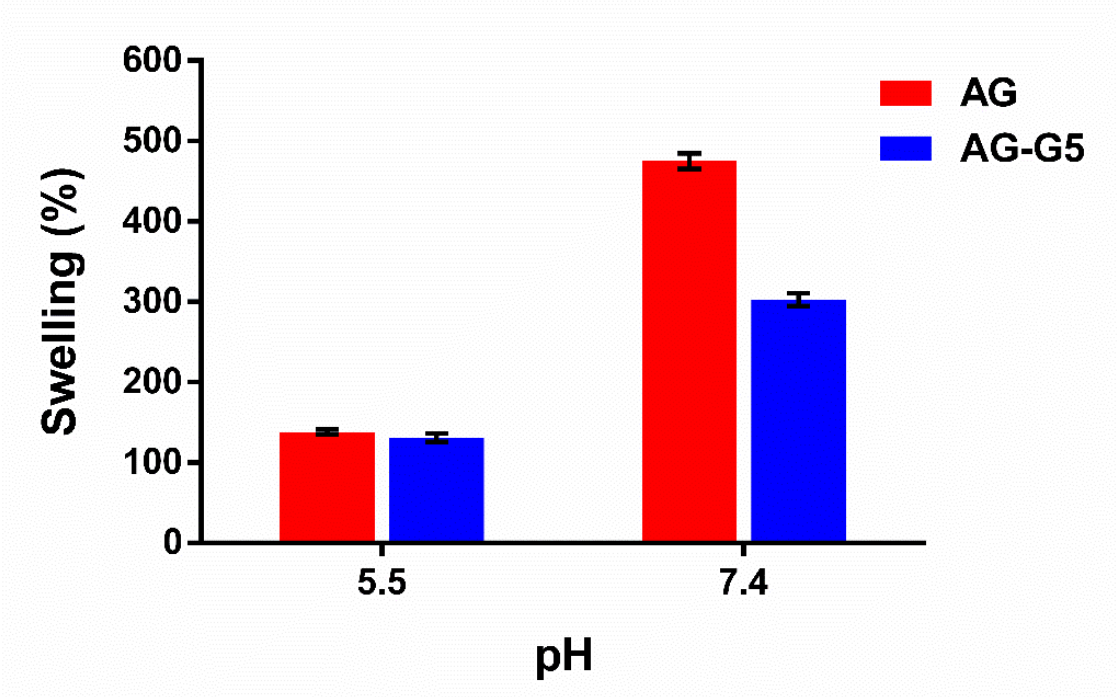

Figure 5.4. Swelling behavior of as-synthesized AG and AG-G5 nanogels as a function of pH after 24 h incubation. The experiments were performed in duplicate and values are expressed as mean ± S.E.M.

Besides this, mechanical strength of nanogels is one of the important factors for controlled and extended delivery of therapeutic cargo. Mechanical properties of materials varies with the cross-link density (Leenders et al., 2014). Chemically cross-linked nanogels with high cross-link densities usually exhibit improved mechanical properties than ionic cross-linked nanogels (Berger et al., 2004 and Xing et al., 2014). In line with this generic concept, tensile testing of nanogels was performed to evaluate their mechanical properties. The stress-strain plots of AG and AG-G5 nanogels are shown in **Figure 5.5 B**. The mechanical properties of nanogels in terms of ultimate tensile strength (UTS) and elongation at break is enlisted in **Table 5.2**. The UTS value of Ca^{2+} linked AG nanogels was estimated to be 7.34 MPa, which significantly increased to 10.89 MPa (~ 48 % more) in AG-G5 nanogels. Conversely, elongation at break has an inverse relationship with tensile strength. The elongation at break value for AG-G5 was far less than AG nanogels. Therefore, chemical cross-linking of alginate with PAMAM dendrimer can significantly alter the mechanical strength of AG-G5 nanogels.

5.2.2. *In vitro* drug release studies

The therapeutic utility of an ideal nanocarrier is expressed in its ability to release the drug in a controlled and prolonged manner (Banerjee et al., 2015). A sudden or burst drug release is undesirable as the excess drug can sensitize the nearby tissues causing unwanted side effects. Moreover, if the drug is released slowly from the carrier it can prevent the chances of recurrence of cancer growth and progression. Moreover, the nanocarrier should be able to release more drug under acidic environment (mimicking tumor microenvironment) compared to physiological conditions. In this context, we monitored the pH dependent drug release behavior of cross-linked EPI⊂AG-G5 nanogels *in vitro*. EPI⊂AG nanogels were evaluated for drug release in parallel as reference. **Figure 5.6** shows the time dependent release profiles of EPI drug from EPI⊂AG and EPI⊂AG-G5 nanogels at pH 5.5 and 7.4, respectively. At pH 7.4, burst release of EPI drug (95.4 %) from EPI⊂AG nanogels occurred within 12 h, while only 26.8 % of EPI was released from EPI⊂AG-G5 nanogels. The rapid and almost complete EPI release from EPI⊂AG nanogels can be ascribed to disintegration of AG nanogels due to exchange of Ca^{2+} with cations in PBS buffer (pH 7.4) (LeRoux et al., 1999, Li et al., 2011 and Goncalves et al., 2014). This indicates that PAMAM dendrimer imparts stability to AG nanogels after cross-linking to form a dense and rigid network. It is imperative to mention that PAMAM G5 dendrimers can entrap and stabilize the EPI drug in its hydrophobic cavities, to slow down its release rate from AG-G5 nanogels (Matai et al., 2015a,b). After 24 h, 30.7 % EPI was released from EPI⊂AG-G5 nanogels which sustained till 48 h (37.2 %).

However, when the pH was reduced to 5.5, the drug release rate of EPI from EPI⊂AG nanogels slowed down. A probable explanation could be shrinking of alginate chains under acidic conditions (Li et al., 2011). On the other hand, cross-linked EPI⊂AG-G5 nanogels were stable and continued to release EPI in a sustained manner under acidic conditions. Moreover, the release of EPI from EPI⊂AG-G5 nanogels was faster at pH 5.5 than 7.4. Within 48 h, 47.6 % EPI was released at pH 5.5 rather 37.2 % of EPI was released in PBS (pH 7.4). The improved delivery at acidic pH is probably due to protonation of $–NH_3^+$ groups of PAMAM dendrimers. Enhanced drug release at acidic pH (tumor milieu) than physiological conditions assigns specificity to EPI⊂AG-G5 nanogels for anticancer drug delivery. Thus, the benefit of PAMAM dendrimers and thereby cross-linking is clearly explained.

5.2.3. MTT assay

After drug release studies, we investigated the anticancer efficacy of nanogels against MCF-7 cells, *in vitro*. For this, the cytotoxicity of nanogels was measured using MTT assay. Appropriate controls were applied during the assay to ascertain the therapeutic effects of loaded EPI drug. As shown in **Figure 5.7 A**, MCF-7 cells treated with blank AG and cross-linked AG-G5 nanogels maintained a substantial cell viability (>70 %) at all treatment concentrations. This is in agreement with the criterion of a suitable drug nanocarrier. However, free EPI, EPI⊂AG and EPI⊂AG-G5 nanogels could significantly inhibit the cell proliferation with increase in dosage. Importantly, EPI⊂AG-G5 nanogels exhibited higher cytotoxicity than EPI⊂AG nanogels and free EPI. For instance, at 0.25 mg mL^{-1} dose ~ 59 % cells died with EPI⊂AG and around 49 % cells died with equivalent free EPI, respectively. While, cell viability drastically reduced to almost 25 % with EPI⊂AG-G5 treatment at similar nanogels concentration. The improved cytotoxic effects of EPI⊂AG-G5 nanogels compared to EPI⊂AG nanogels can be assigned to their high drug entrapment efficiency and structural stability which increases the drug circulation times. We also examined the inhibitory effects of nanogels on normal NIH3T3 cells **(Figure 5.7 B)**. Under the same tested concentrations, the nanogels exhibited some toxicity but overall the inhibitory effects were more distinct in MCF-7 cells.

After treatment, we monitored the morphology of MCF-7 cells when exposed to different samples by optical microscopy. The bright field images of MCF-7 cells incubated with blank and EPI loaded nanogels are shown in **Figure 5.8**. As evident, AG, AG-G5 nanogels exposed cells were elongated in shape and retained a healthy appearance, similar to untreated cells. While, exposure to either free EPI or EPI⊂AG/ EPI⊂AG-G5 nanogels affected the cell morphology.

The effect was more pronounced in EPI⊂AG-G5 and free EPI exposed cells. After treatment, many cells became sloppy in shape and were weakly adhered to the plate surface suggesting cytotoxicity. These observations match well with the MTT results. These findings indicate the utility of AG-G5 hybrid nanogels as carrier of EPI for achieving enhanced anticancer effects. Hence, EPI⊂AG-G5 nanogels were efficacious as a drug delivery vehicle for inhibiting and killing the breast cancer cells.

5.2.4. Cellular uptake of fluorescent nanogels

The intrinsic red fluorescence of EPI drug is proficient in monitoring its uptake in cells. Fluorescence microscopy was utilized to visualise the fluorescent signals related to cellular uptake of nanogels. **Figure 5.9** represents the microscopic images of MCF-7 cells incubated with different concentrations of EPI⊂AG-G5 nanogels and free EPI. Hoechst 33342 dye was used to label nucleus and emits blue fluorescence in DAPI channel (Allen et al., 2001). The red signals owing to EPI fluorescence were captured in RFP channel. The images revealed significant differences in trafficking of free EPI and EPI bound to nanogels. After incubation, free EPI molecules managed to penetrate the plasma membrane and reside in the nuclear region (Yordanov et al., 2013 and Matai et al., 2015b). This was apparent from the overlay of images with co-localized red and blue fluorescent signals **(Figure 5.9 b-d and j-l)**. Conversely at less dosage, EPI⊂AG-G5 nanogels were mostly localized in the cytoplasmic region **(Figure 5.9 f-h)**. However, with increase in nanogels concentration the red fluorescent signals became dense and shifted from cytoplasmic to nuclear region **(Figure 5.9 n-p)**. Moreover, reduction in cell size with increase in treatment concentrations of free EPI and EPI⊂AG-G5 nanogels was evident from the images acquired in bright illumination **(Figure 5.9 i,m)**. Overall, the constriction in cell size and alteration in EPI fluorescent signals epitomize induction of apoptosis in MCF-7 cells (Liu et al., 2010b). After cellular entry, it is important to investigate the location of nanogels in cancer cells to view their therapeutic outcomes. In this study, we identified the location of EPI⊂AG-G5 nanogels using lysotracker green, for fluorescence imaging of lysosomes. MCF-7 cells were incubated with EPI⊂AG-G5 nanogels for different time durations (1, 3 and 6 h) and were then stained with lysotracker green dye. As shown in **Figure 5.10**, the red fluorescence of EPI⊂AG-G5 nanogels increased in a time-dependent manner. Moreover, the fluorescent red signals of EPI colocalized with lysotracker green signals, with increment in time. These observations suggest, lysosomal uptake of EPI⊂AG-G5 nanogels after cellular internalization. Also, it is noteworthy that some nanogels managed to escape from lysosomes and released EPI in cytoplasm for nuclear entry.

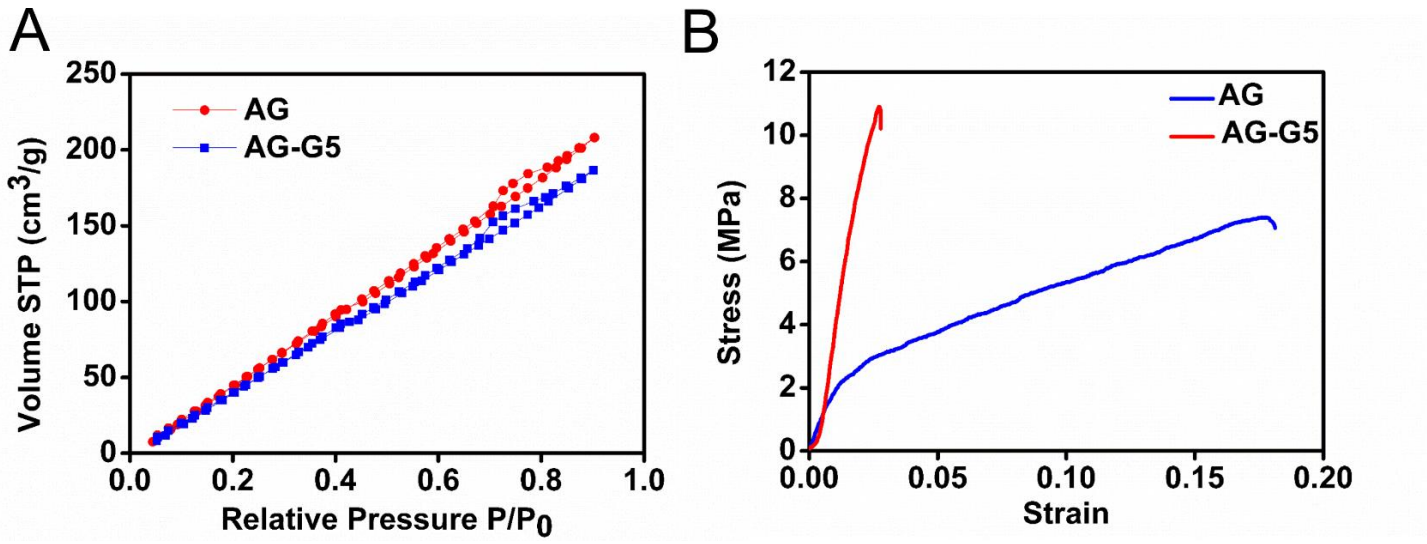

Figure 5.5. (A) N_2 absorption-desorption isotherms and (B) Stress vs strain plots of nanogels.

Nanogels	Surface area (m^2 g^{-1})	Pore volume (cc g^{-1})
AG	234.19	0.309
AG-G5	203.76	0.271

Table 5.1. Surface area and pore volume estimations of as-synthesized AG and AG-G5 nanogels from BET measurements.

Nanogels	Tensile strength (MPa)	Elongation at break (%)
AG	7.34	18.15
AG-G5	10.89	2.79

Table 5.2. Mechanical properties of as-synthesized AG and AG-G5 nanogels.

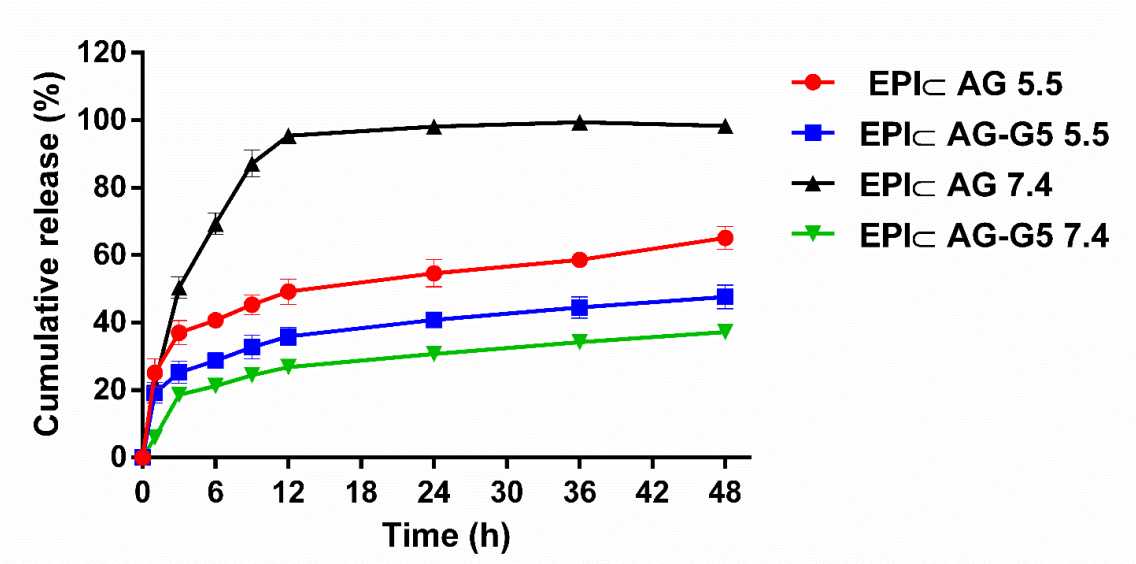

Figure 5.6. Time dependent cumulative release profiles of EPI from nanogels over 48 h at pH 5.5 in acetate buffer and at pH 7.4 in phosphate buffer saline (PBS). The experiments were performed at 37 °C.

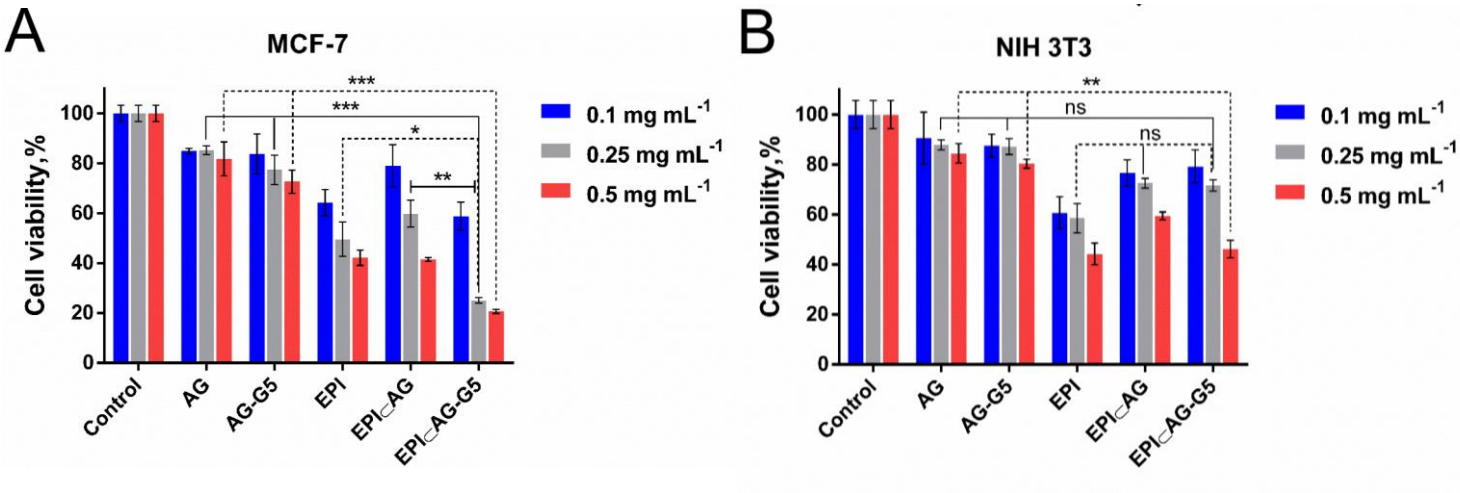

Figure 5.7. Cell viability of (A) MCF-7 and (B) NIH3T3 estimated by MTT assay after 48 h incubation with nanogels 0.1, 0.25 and 0.5 mg mL^{-1} corresponding to EPI concentration 0.84, 2.1 and 4.2 µg mL^{-1}. Free EPI, EPI⊂AG and EPI⊂AG-G5 nanogels had equivalent EPI concentrations. The experiments were conducted in triplicate and values are expressed as mean ± S.E.M. Statistical significance were carried out by Two-way ANOVA with Tukey's multiple comparisons test between groups using GraphPad Prism 6.0 software. Statistical significant values were denoted by * ($p < 0.05$), ** ($p < 0.005$), and *** ($p < 0.001$). Statistically insignificant values were represented by 'ns'.

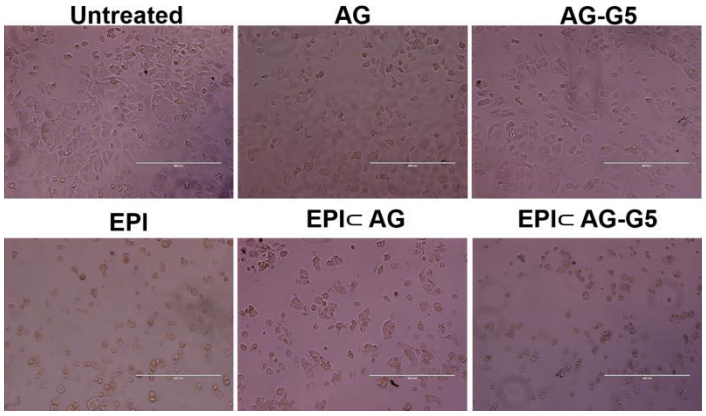

Figure 5.8. Bright field microscopic images of MCF-7 cells after 48 h incubation with different nanogel samples revealing cell morphology changes. (Scale bar = 400 µm).

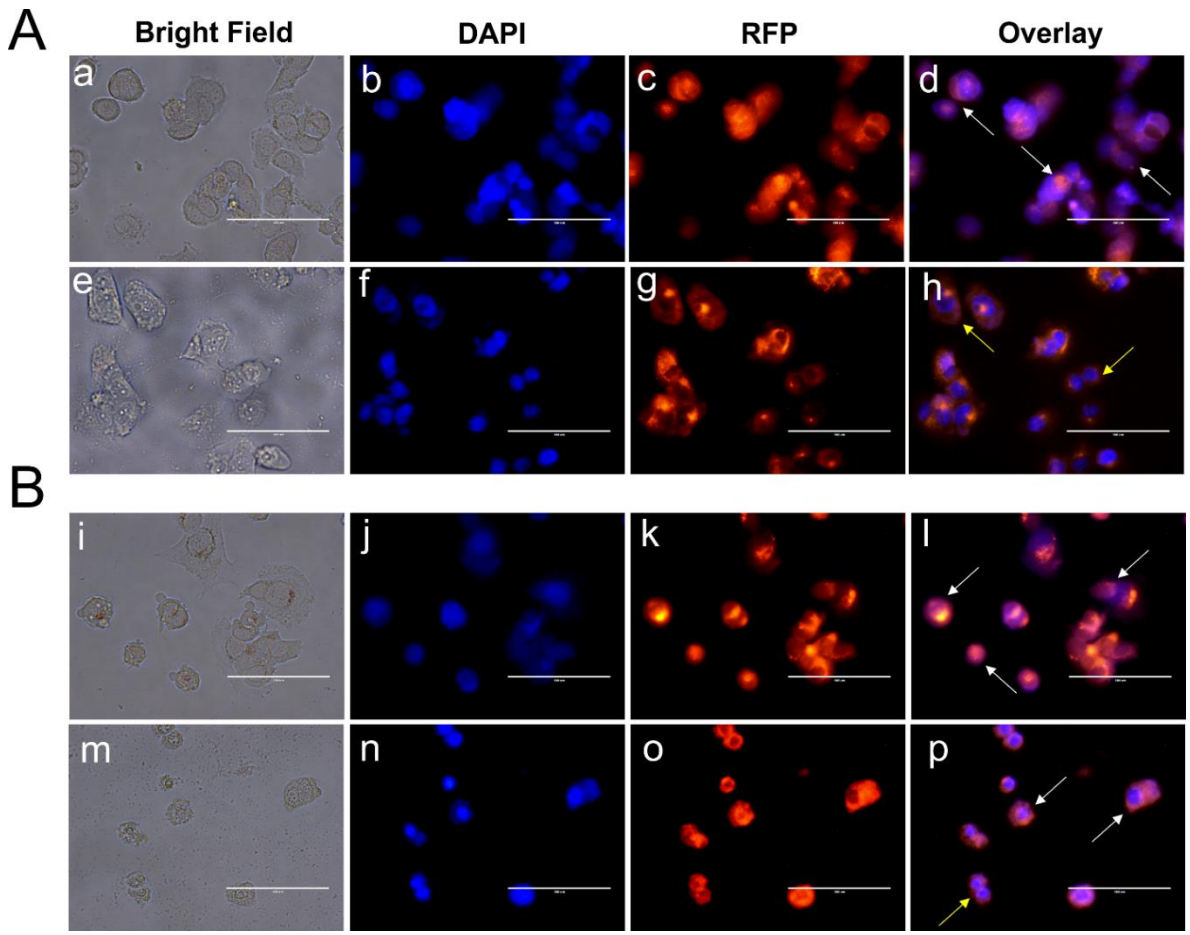

Figure 5.9. Fluorescence microscopic images of MCF-7 cells incubated with different concentrations of free EPI and EPI⊂AG-G5 nanogels after 24 h. (A) Cells treated with 0.84 µg mL^{-1} free EPI (a-d) and 0.1 mg mL^{-1} EPI⊂AG-G5 nanogels (e-h). (B) Cells treated with 2.1 µg mL^{-1} free EPI (i-l) and 0.25 mg mL^{-1} EPI⊂AG-G5 nanogels (m-p). The EPI⊂AG-G5 nanogels were used at equivalent concentrations of free EPI. White arrows indicate nuclear localization and yellow arrows indicate cytoplasmic localization. DAPI filter: λ_{ex} 360 nm, λ_{em} 447 nm; RFP filter: λ_{ex} 530 nm, λ_{em} 593 nm. (Scale bar = 100 µm).

To distinguish the pattern of cellular internalization between EPI⊂AG-G5 and EPI⊂AG nanogels, we also monitored the time dependent uptake of EPI⊂AG nanogels. Under similar treatment conditions, the fluorescence from EPI⊂AG nanogels was also found to increase with time. However, the red fluorescent signals were mostly distributed in the nuclear region and didn't merge with the green fluorescent signals of lysotracker **(Figure 5.11)**. Presumably, this could be devoted to rampant release of EPI from AG gels in cell medium (pH 7.4). This alteration in the cellular distribution pattern of EPI⊂AG-G5 nanogels can be accredited to PAMAM dendrimers as the chief constituent element of these hybrid nanogels. Hence, from the cellular uptake experiments it was clear that EPI⊂AG-G5 nanogels could be taken up by MCF-7 cells effectively wherein they resided in the lysosomes and released EPI molecules slowly which could inhibit the cell growth and induce apoptosis.

5.2.5. Cell cycle analysis and morphological changes

Next, we tried to examine the alterations in cell cycle stages of MCF-7 by PI staining, using a flow cytometer. Basically, PI is a fluorogenic compound capable of binding to nucleic acids stoichiometrically, and its fluorescence emission varies proportionally to the cell DNA content (Riccardi et al., 2006). To monitor the cell stages, MCF-7 cells were treated with AG-G5, EPI and EPI⊂AG-G5 nanogels (with equivalent EPI concentration) and were quantified by flow cytometry after PI staining. **Figure 5.12 A**, depicts the cell cycle distribution pattern of untreated and treated cells. Untreated and AG-G5 treated cells were primarily accumulated in G0/G1 phase. However, cells exposed to free EPI and EPI⊂AG-G5 nanogels exhibited a declined G0/G1 phase and increased G2/M phase arrest, i.e. ~ 39.3 % and 30.7 %, respectively, with respect to untreated cells (~ 8.2 %) (Hill et al., 1982, Bartkowiak et al., 1992). Additionally, a notable population of cells were accumulated in sub-G1 phase after treatment. Percentage of cells in sub-G1 phase increased from 1.3 % and 2.0 % in untreated and AG-G5 nanogels treated, to 15.1 % and 22.8 % in free EPI and EPI⊂AG-G5 treated cells, respectively. Increment in sub-G1 population with EPI⊂AG-G5 treatment, suggests induction of apoptotic death in MCF-7 cells (Darzynkiewicz et al., 1992 and Matai et al., 2015b).

We then observed the morphological changes related to apoptotic death by FE-SEM analysis. **Figure 5.12 B**, depicts the FE-SEM micrographs corresponding to untreated and EPI⊂AG-G5 nanogels treated MCF-7 cells. Untreated MCF-7 cells had a healthy appearance with no evidence of membrane constriction or leakage. Nevertheless, EPI⊂AG-G5 treated cells were round and loosely-bound to the surface. Membrane blebbing and formation of apoptotic bodies was clearly

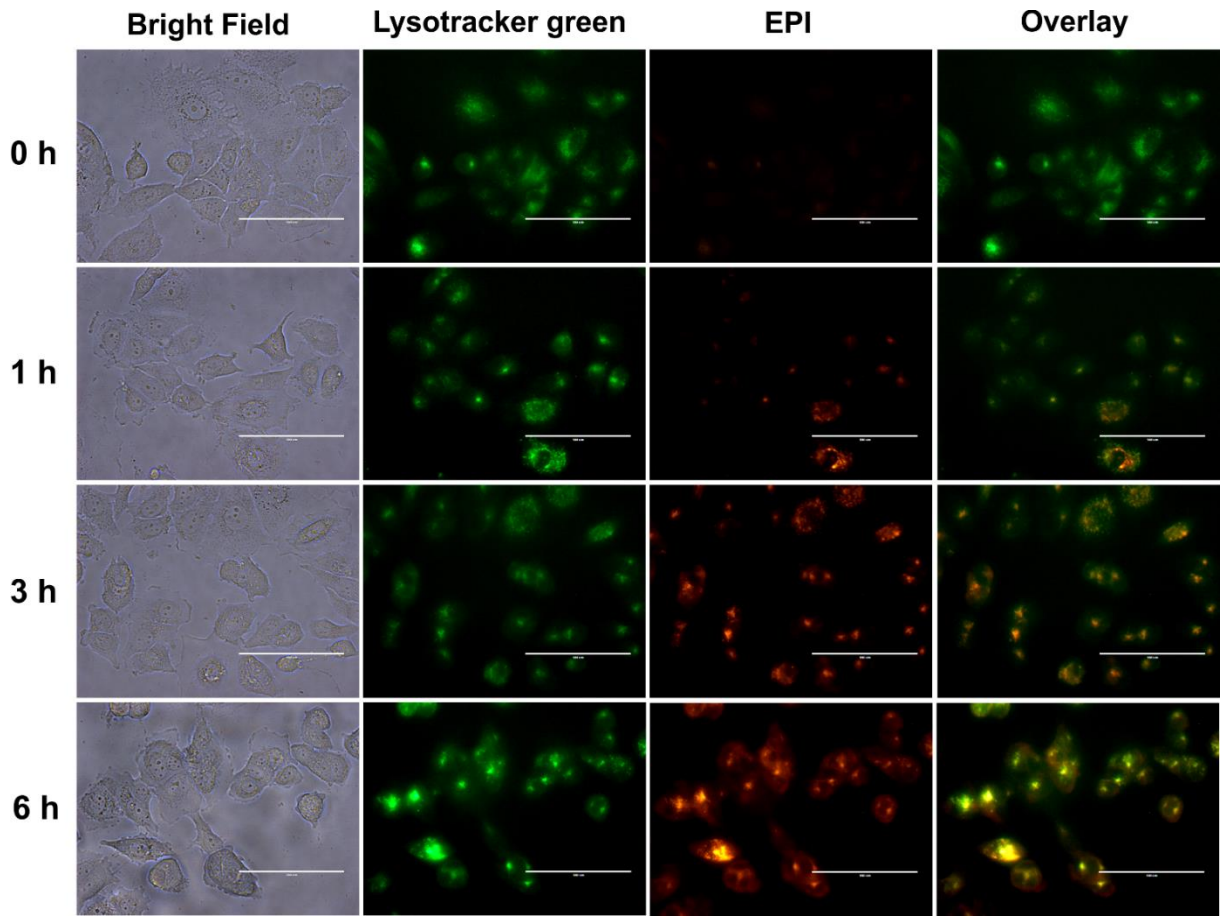

Figure 5.10. Fluorescence microscopic images of MCF-7 cells incubated with EPI⊂AG-G5 nanogels captured after different time intervals. The red fluorescence of EPI (under RFP filter) indicative of its intracellular distribution increased in a time-dependent manner and colocalized with the lysotracker green signals (under GFP filter). (Scale bar = 100 μm).

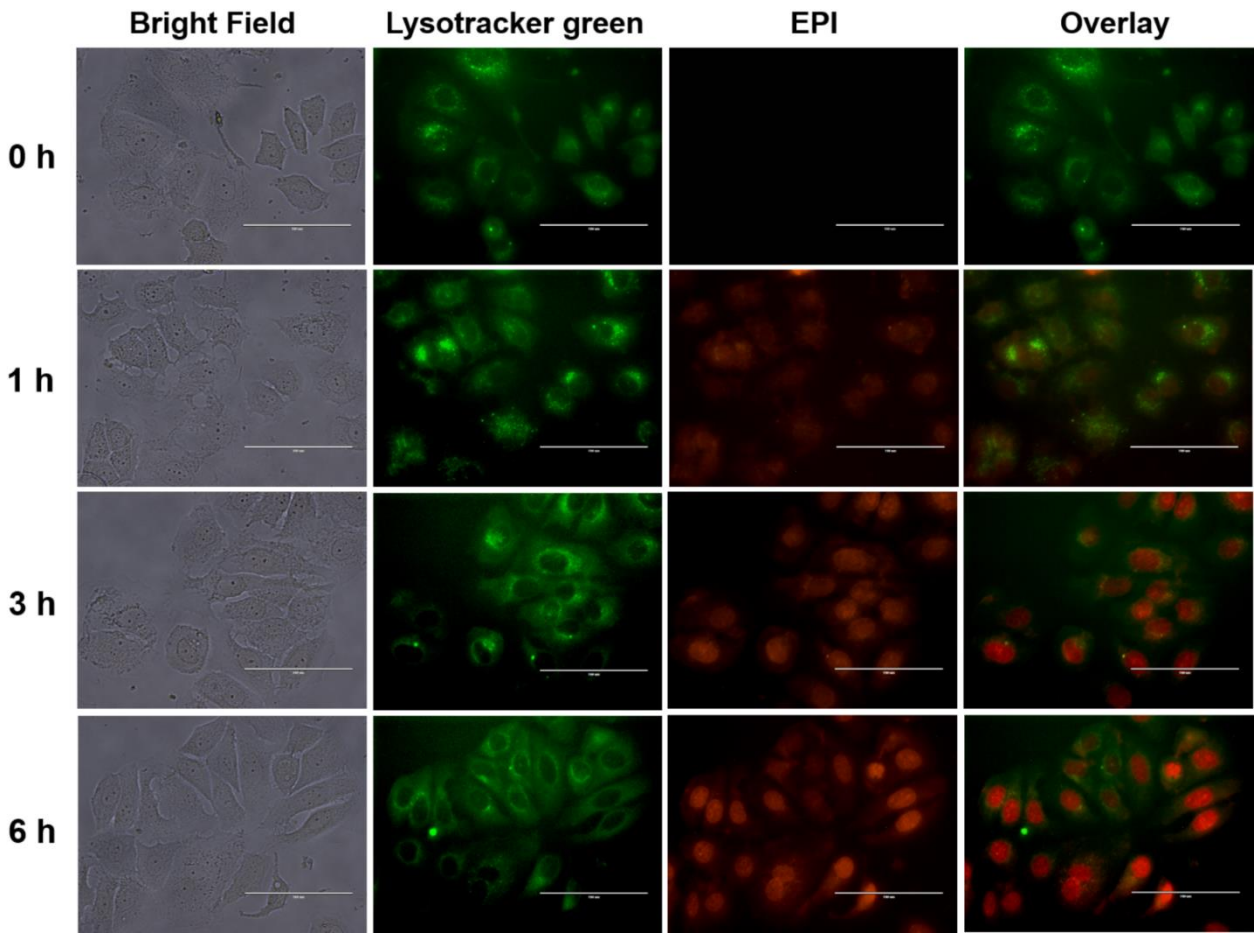

Figure 5.11. Fluorescence microscopic images of MCF-7 cells incubated with EPI⊂AG nanogels captured after different time intervals. The red fluorescence of EPI (under RFP filter) indicative of its intracellular distribution increased in a time-dependent manner. (Scale bar = 100 μm).

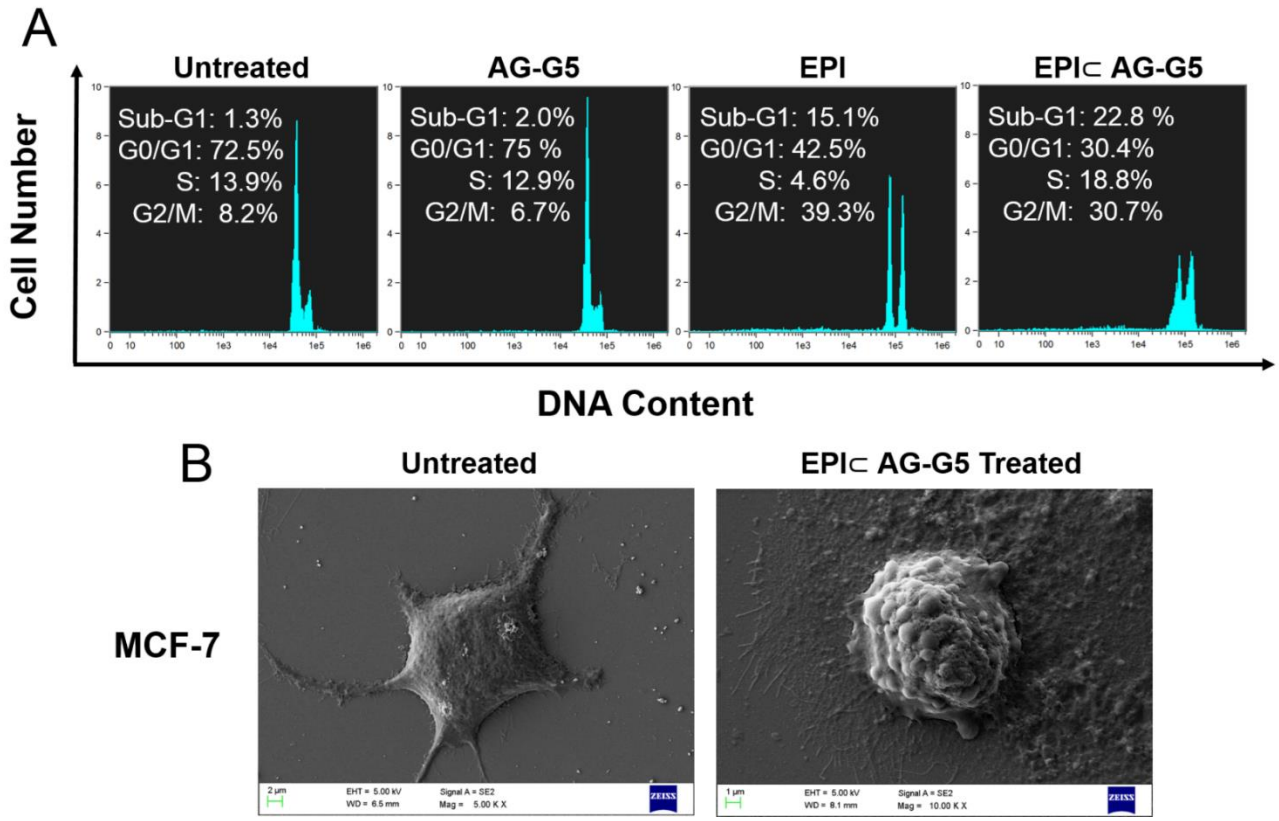

Figure 5.12. A) Flow cytometry analysis of different phases of untreated, AG-G5, EPI and EPI⊂AG-G5 nanogels treated MCF-7 cells. (B) FE-SEM images of untreated and EPI⊂AG-G5 nanogels treated MCF-7 cells.

apparent after treatment (Rello et al., 2005). These morphological alterations are typical of cells undergoing apoptosis.

In summary, AG-G5 hybrid nanogels linked through covalent interactions were designed following a novel and a facile route to serve as a carrier for anticancer drug EPI. Penetration of G5 PAMAM dendrimer within the AG network could significantly reduce the size of nanogels and impart superior stability, mechanical strength, and pH responsiveness than AG nanogels. Moreover, the performed cell-based assays justify the cytocompatibility of AG-G5 hybrid nanogels and excellent anticancer potential of EPI⊂AG-G5 nanogels. These EPI⊂AG-G5 nanogels were identified to induce apoptosis as the main mechanism of death in breast cancer cells. Proper knowledge of mode of cell death is pivotal in designing specialised drug loaded nanogels to attain enhanced anticancer effects.

CHAPTER 6

Hydrophobic Myristic acid Modified PAMAM Dendrimers for the Delivery of Anticancer Agents

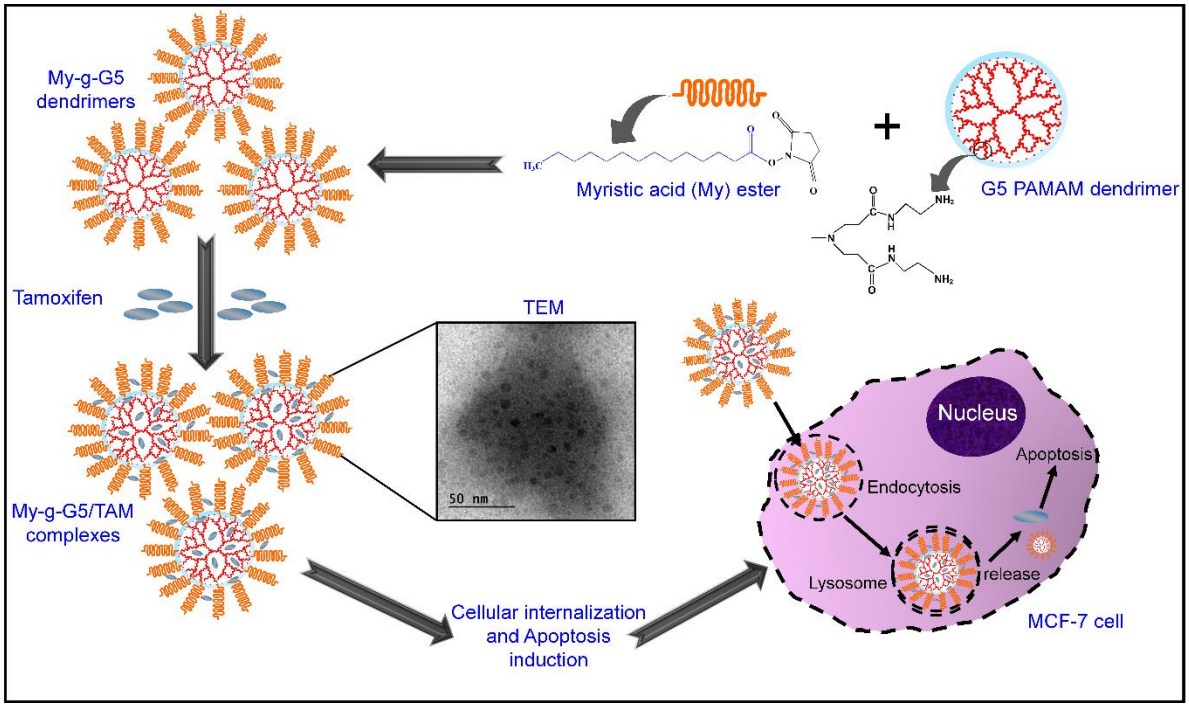

CHAPTER 6

HYDROPHOBIC MYRISTIC ACID MODIFIED PAMAM DENDRIMERS FOR THE DELIVERY OF ANTICANCER AGENTS

6.1. Overview

In the present study, cationic G5 PAMAM dendrimers were hydrophobically modified by grafting the surface with lipid-like myristic acid (My) tails to augment their potential as a drug delivery vector *in vitro*. Such modified dendritic entities comprise of backbone of PAMAM dendrimer with both amine groups and myristic acid tails at the periphery. These incorporated hydrophobic alkyl segments can act synergistically with the cationic core facilitating their interactions with cell membranes to effectively transport and deliver the therapeutic cargo (Liu et al., 2010c). Also, such hydrophobic dendrimers with shielded positive charges are expected to have diminished cytotoxicity than unmodified dendrimers (Jevprasesphant et al., 2003). Under physiological conditions, these myristic acid grafted dendrimers (My-*g*-G5) can enhance the solubility and bioavailability of poorly soluble/insoluble drugs. This can be attributed to the increased internal space in dendritic architecture after attaching lipid-like chains. For this study, medium generation G5 PAMAM dendrimers were chosen owing their higher amine content (>G4) and lower toxicity (<G6) than other available cationic PAMAM dendrimers (Naha et al., 2013). Thereafter, we conjugated the surface amine groups of PAMAM dendrimers with the carboxylic groups of myristic acid using carbodiimide chemistry in a stoichiometric manner. Such modified PAMAM dendrimers with hydrophobic tails associate the advantages of cationic dendrimers and lipids to interact with cell membranes. Furthermore, we evaluated the ability of My-*g*-G5 dendrimers as drug delivery vectors. Tamoxifen (TAM) an estrogen agonist, is a U.S. FDA approved nonsteroidal drug for treatment and prevention of breast cancer (Jain et al., 2011 and 2013). It binds to the estrogen hormone receptor (ER) expressed in breast cancer cells thereby blocking the binding site of estrogen (Taylor et al., 1984 and Devulapally et al., 2015). This eventually inhibits the tumor progression and reduces the risks of cancer recurrence (Zheng et al., 2007). Owing to these, we chose TAM as a model drug for encapsulation within the interiors of My-*g*-G5 dendrimers. Various biological assays were performed to interpret the

efficacy of My-*g*-G5 dendrimers to ferry TAM to inhibit and kill MCF-7 cells (human breast adenocarcinoma, ER positive) *in vitro*.

6.2. RESULTS AND DISCUSSION

6.2.1. Preparation and characterization of My-*g*-G5/TAM complexes

The main objective of this study was to combine the magnificent properties of PAMAM dendrimers and lipophilic moieties to realize a nanoscale delivery system with the desired biological features. With this idea, myristic acid (a fatty acid) chains chiefly hydrophobic in nature were linked to the periphery of G5 PAMAM dendrimers. EDC/NHS chemistry was employed to form amide linkage (–CONH–) between the terminal carboxyl group (–COOH) of myristate and amines ($–NH_2$) of dendrimers (Everaerts et al., 2008). After successful incorporation of myristic acid chains on the dendrimers, we evaluated My-*g*-G5 system as a carrier for encapsulating water insoluble TAM drug. G5 PAMAM dendrimers with hydrophobic cavities can stabilize and increase the water solubility of TAM (Wolinsky et al., 2008). This is primarily important to achieve the desired therapeutic benefits by enhancing the drug circulation times. The entire synthesis procedure of preparation of My-*g*-G5/TAM complexes has been depicted in **Scheme 6.0**. The as-synthesized My-*g*-G5/TAM samples were stored at -20 °C in powdered form and were found to be stable for several months without any loss in TAM activity. These My-*g*-G5 dendrimers were first characterized by ^{1}H NMR measurements to ascertain the extent of functionalization. **Figure 6.1** represents the ^{1}H NMR spectra of My, My-*g*-G5 and G5 dendrimers in DMSO-d_6 solvent. As seen, the characteristic proton peaks of myristic acid at 0.8 and 1.25 ppm of $–CH_3$ and $–CH_2$ groups were present in My-*g*-G5 along with its other main peaks (2.2–3.4 ppm). Based on integrals of proton peaks at 0.8 ppm (of myristic acid) and 2.3 ppm (of G5), ~29 myristic acid chains were present per dendrimer. Hence from ^{1}H NMR findings, the functionalization of dendrimer exterior with myristic acid chains was confirmed.

Subsequently, we evaluated the potential stability of My-*g*-G5 dendrimers by performing zeta potential measurements in acetate buffer, PBS and DMEM medium, respectively. **Figure 6.2 A**, shows the variation in the zeta potential profile of My-*g*-G5 dendrimers with change in medium. When added to acetate buffer (pH 5.5), the zeta potential of My-*g*-G5 was 41.3±1.18 mV suggesting their excellent stability in acidic conditions. While, the zeta potential value declined to 15.7±1.11 mV when added to PBS (pH 7.4). A flip in the charge of My-*g*-G5 dendrimer solution was observed when added to DMEM medium, it was -5.12±0.426 mV suggesting slight reduction in dendrimer stability owing to its obvious interaction with the medium constituents. However, with visual examination the My-*g*-G5 dendrimers (at 1 mg mL^{-1} concentration)

displayed good solubility in acetate buffer, PBS and DMEM medium and no aggregation was observed **(Figure 6.2 B)**. This suggests that even after attachment of some myristic chains on the dendrimer periphery, they retained their solubility properties. Thereafter complexation with TAM, we characterized the formed My-*g*-G5/TAM complexes by UV−visible spectroscopy. The absorption spectra of free TAM in methanol and blank My-*g*-G5 dendrimers were also recorded for comparison. As shown in **Figure 6.3**, TAM exhibits two characteristic peaks at 238 and 278 nm. After encapsulation, My-*g*-G5/TAM complexes exhibits a prominent peak ~278 nm when compared to blank My-*g*-G5 dendrimers. Presence of peak enhancement at 278 nm in My-*g*-G5/TAM complexes indicate successful encapsulation of TAM in My-*g*-G5 dendrimers. Estimated from UV-vis analysis and dose dependent TAM curve, the encapsulation efficiency was calculated to be ~55.6 %. Next, we visualized the morphology and size of My-*g*-G5/TAM complexes under TEM. **Figure 6.4** shows the TEM micrographs of My-*g*-G5/TAM complexes after negative staining with PTA. As evident from the results, My-*g*-G5/TAM complexes were uniform in distribution with near spherical morphology. The average size of these complexes were in range of 6-8 nm, larger than PAMAM G5 size (5.4 nm). This size increment is indicative of presence of myristic acid segments at the dendrimer surface.

6.2.2. *In vitro* TAM release studies

To monitor the ability of My-*g*-G5/TAM complexes to release the therapeutic payload, we exposed My-g-G5/TAM complexes to buffers with different pH and monitored the release of TAM with time. **Figure 6.5** depicts the cumulative release profile of TAM as a function of time at pH 5.5 and 7.4, respectively. As observed, My-*g*-G5 dendrimers were proficient to release TAM over a span of time with more release under acidic conditions (tumor microenvironment) than basic environments (physiological environment). For instance, after 48 h ~67 % TAM was released at pH 5.5 while only ~ 28 % drug was released at pH 7.4. The fast drug release at acidic pH can be owed to the protonation of the interior amines of My-*g*-G5 dendrimers (pKa~ 6.3) (Niu et al., 2003b). After *in vitro* testing, we estimated the anticancer properties of My-*g*-G5/TAM complexes under cellular conditions.

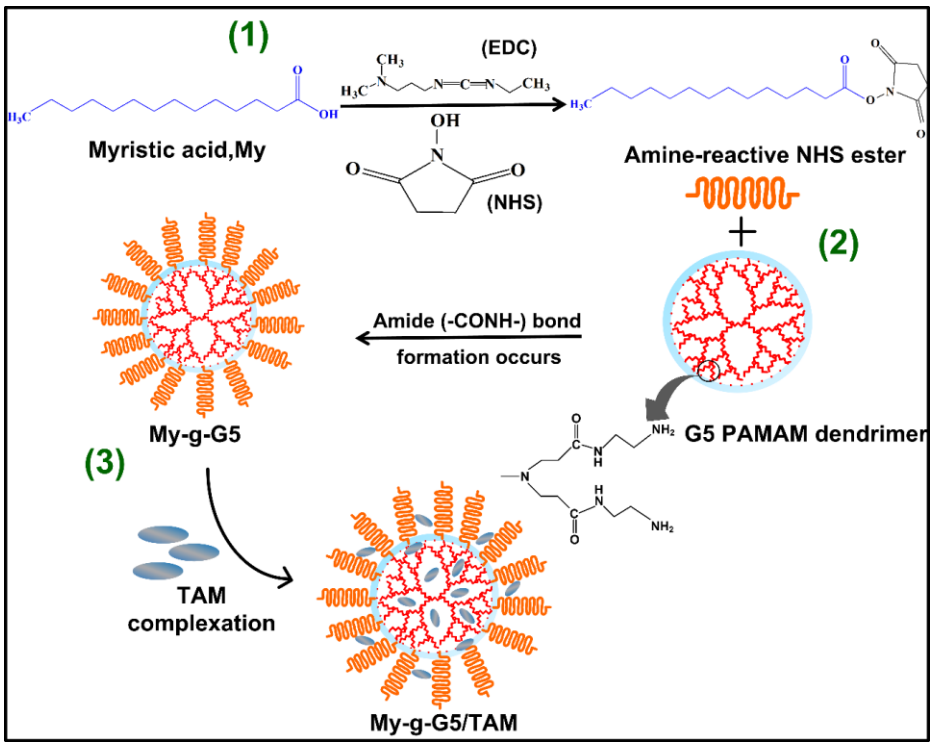

Scheme 6.0. Schematic representation of preparation of My-*g*-G5/TAM complexes. The entire synthesis scheme involves multiple steps which include: 1) EDC/NHS activation of myristic acid, 2) chemical reaction of activated myristic acid and G5 PAMAM dendrimers and 3) complexation of TAM in the internal spaces of My-*g*-G5 dendrimers to form My-*g*-G5/TAM complexes.

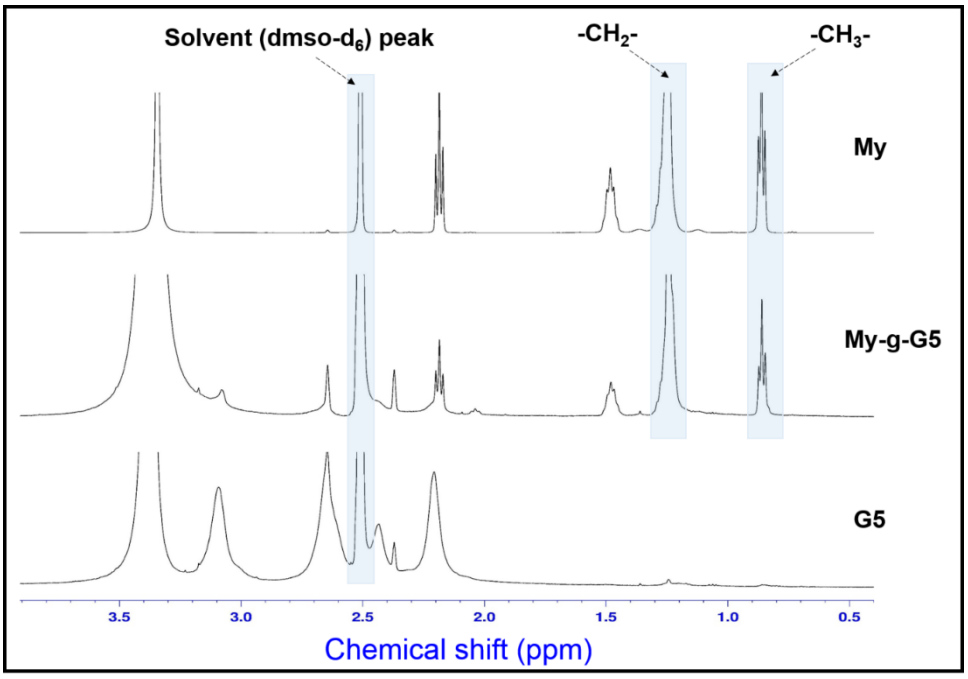

Figure 6.1. ^{1}H NMR spectra of different samples at RT. The blue highlighted portions reflect similar regions.

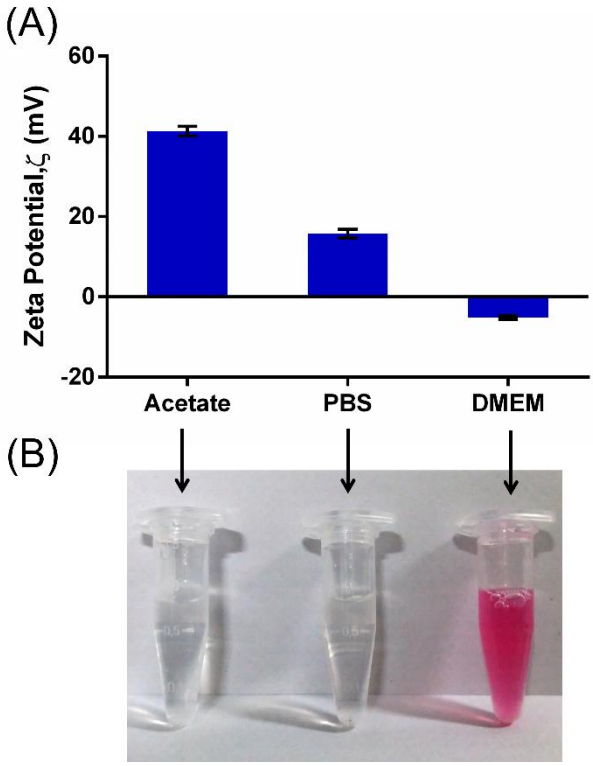

Figure 6.2. A) Zeta potential measurements of My-*g*-G5 dendrimers in acetate buffer (pH 5.5), PBS (pH 7.4) and DMEM medium, respectively. The values are expressed as mean ± SEM) (n=3). B) The corresponding digital photographs of My-*g*-G5 dendrimers in different medium under daylight.

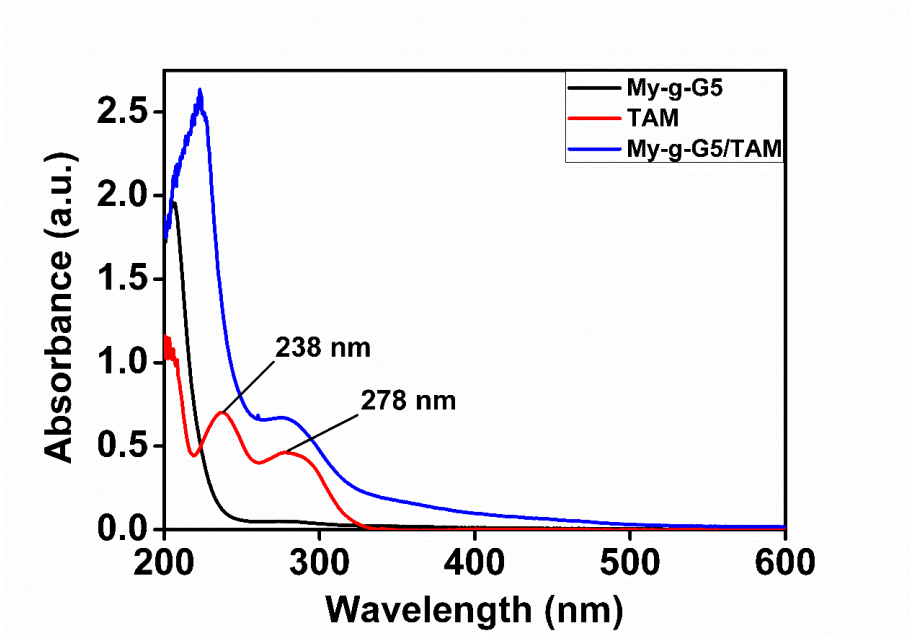

Figure 6.3. UV-vis absorption spectra of free TAM in methanol and aqueous solutions of My-*g*-G5 and My-*g*-G5/TAM complexes.

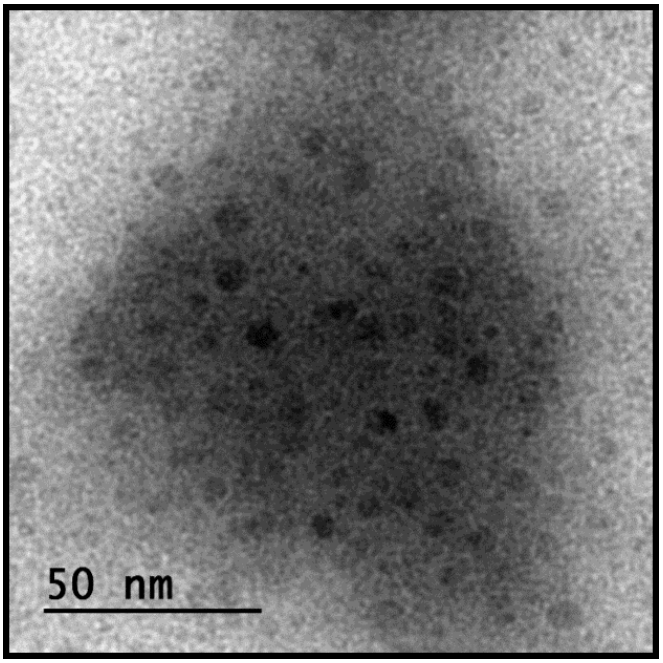

Figure 6.4. High resolution TEM image of My-*g*-G5/TAM complexes after negative staining. (Scale bar: 50 nm).

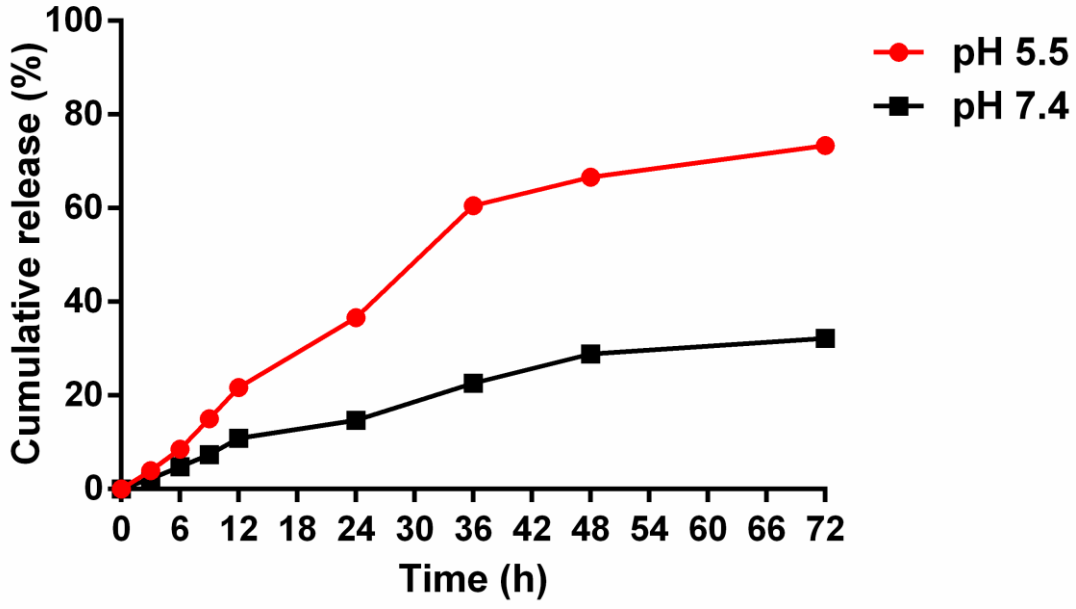

Figure 6.5. Cumulative release profile of TAM from My-*g*-G5/TAM complexes as a function of time at pH 5.5 (red) and 7.4 (black), respectively.

6.2.3. Effect of My-*g*-G5/TAM complexes on cell viability

The cytotoxic effects of as as-synthesized My-*g*-G5/TAM complexes were then tested *in vitro* in MCF-7 and NIH 3T3 cells by MTT assay. As shown in **Figure 6.6 A**, MCF-7 cells incubated with G5 and My-*g*-G5 were able to maintain a good cell viability (~80 %) at the tested drug concentrations (0.25-0.75 µM). A slight decrease in cell viability with My-*g*-G5 at 1 µM, may be due its enhanced interaction with the cells. Unmodified G5/TAM complexes didn't show any signs of cell inhibition and death at all the tested dosages. Contrarily, the My-*g*-G5/TAM complexes were found to significantly alter the MCF-7 survival and induce cell death. With increase in drug concentration from 0.25-1 µM, the cell viability drastically reduced from 83.8 % to 27.1 %. Since, within this concentration regime My-*g*-G5 dendrimers did not display much cytotoxicity, the plausible explanation to the reduced cell viability could be due to the action of the entrapped TAM molecules. Moreover, this observed cell viability was similar to that observed with free TAM (equivalent concentrations) (Karami-Tehrani et al., 2003). This suggests that My-*g*-G5 dendrimers were able to preserve the TAM activity in cellular environment to inhibit the ER positive cancer growth. Moreover, such significant difference in the cell viabilities of G5/TAM and My-*g*-G5/TAM complexes can be designated to the surface modification of dendrimers with lipophilic tails which enhanced the TAM stability and interaction with the breast cancer cell membranes.

We also evaluated the effects of My-*g*-G5/TAM complexes on normal NIH3T3 cells. As expected, under similar treatment conditions the cells incubated with G5 PAMAM dendrimers showed some cytotoxic effects and reduced the cell viability to nearly ~60 % **(Figure 6.6 B)**. However, cells in presence of My-*g*-G5 or My-*g*-G5/TAM complexes exhibited an appreciable cell viability (> 80 %). This recommends that introduction of myristoyl moieties on dendrimer surface reduces its cytotoxicity. Moreover, free TAM was found to inhibit the cell growth at high concentrations. These results conclude that at similar dosage, the inhibitory effects of My-*g*-G5/TAM complexes were more pronounced in MCF-7 than NIH3T3 cells. Hence, My-*g*-G5 dendrimers with hydrophobic corona are a more suitable alternative to unmodified G5 PAMAM dendrimers for TAM delivery and induction of breast cancer cell death *in vitro*.

6.2.4. Investigation of cellular uptake

An important parameter which affects the therapeutic outcome of most drugs is the effective cellular uptake of its carrier. Most nanocarriers tend to deliver their drug cargos by passively targeting and accumulating within the cancer cells (Yuan et al., 1995). Hence it is imperative to track the intracellular distribution of chemotherapeutics after its uptake. Since TAM is a

non-fluorescent drug, we prepared coumarin-6 loaded My-*g*-G5 dendrimers to monitor and quantitate the cellular uptake. MCF-7 cells were incubated with different concentrations of My-*g*-G5/C6 complexes for 6 h and viewed after fluorescent microscopic imaging. As evident from **Figure 6.7** the green fluorescence from MCF-7 cells increased in a dose-dependent manner. We then quantitated the intracellular fluorescence intensity using flow cytometry. As expected, with shift in the concentration of My-*g*-G5/C6 from 0.75-1 µM, the percentage of green positive cells indicating uptake of My-*g*-G5/C6 complexes increased from 66.6 % to 84.9 % **(Figure 6.7 b2,c2)**.The obtained results indicate fruitful internalization and accumulation of My-*g*-G5 dendrimers in cancer cells. Next we tried to track the localization of My-*g*-G5/C6 complexes in cancer cells using Hoechst 33342 as a marker for nuclei and lysotracker red for fluorescence imaging of lysosomes. As evident from **Figure 6.8** the green fluorescent signals increased with time and were distributed in the cytoplasm of cells. However, we did not observe any overlay of green and blue fluorescence which suggests that nuclei were not the cellular targets of My-*g*-G5/C6 complexes. On the contrary, the red fluorescence from lysosomes colocalized with the green fluorescence which eventually increased with time. These observations clearly demonstrate lysosomes as the residing compartment of My-*g*-G5/C6 complexes. It is important to mention that some My-*g*-G5/C6 managed to escape the lysosomes and were released in the cell cytoplasm. These results corroborate with the previously reported findings whereby PAMAM dendrimers target lysosomes after endocytosis and are released by the "proton-sponge effect" (Sonawane et al., 2003 and Thomas et al., 2009).

6.2.5. Induction of apoptotic cell death by My-*g*-G5/TAM complexes

We then tried to investigate the mode of death (viz. apoptosis or necrosis) after treatment with My-*g*-G5/TAM complexes using AO/EB dual dye. **Figure 6.9** shows that MCF-7 cells treated with 0.75 µM G5/TAM complexes **(Figure 6.9 b)** had uniform morphology and displayed green fluorescence similar to untreated ones **(Figure 6.9 a)**. A slight onset of apoptosis was viewed based on yellow-green fluorescence from cells treated with 1 µM G5/TAM **(Figure 6.9 c)**. However, upon treatment with My-*g*-G5/TAM complexes, both yellow-green and orange-red stained nuclei suggest early and late apoptosis, respectively **(Figure 6.9 d)**. The proportion of cells in late apoptotic stage increased when treated with 1 µM My-*g*-G5/TAM complexes **(Figure 6.9 e)**. Thus, AO/EB staining signifies manifestation of apoptosis in My-*g*-G5/TAM complexes treated MCF-7 cells.

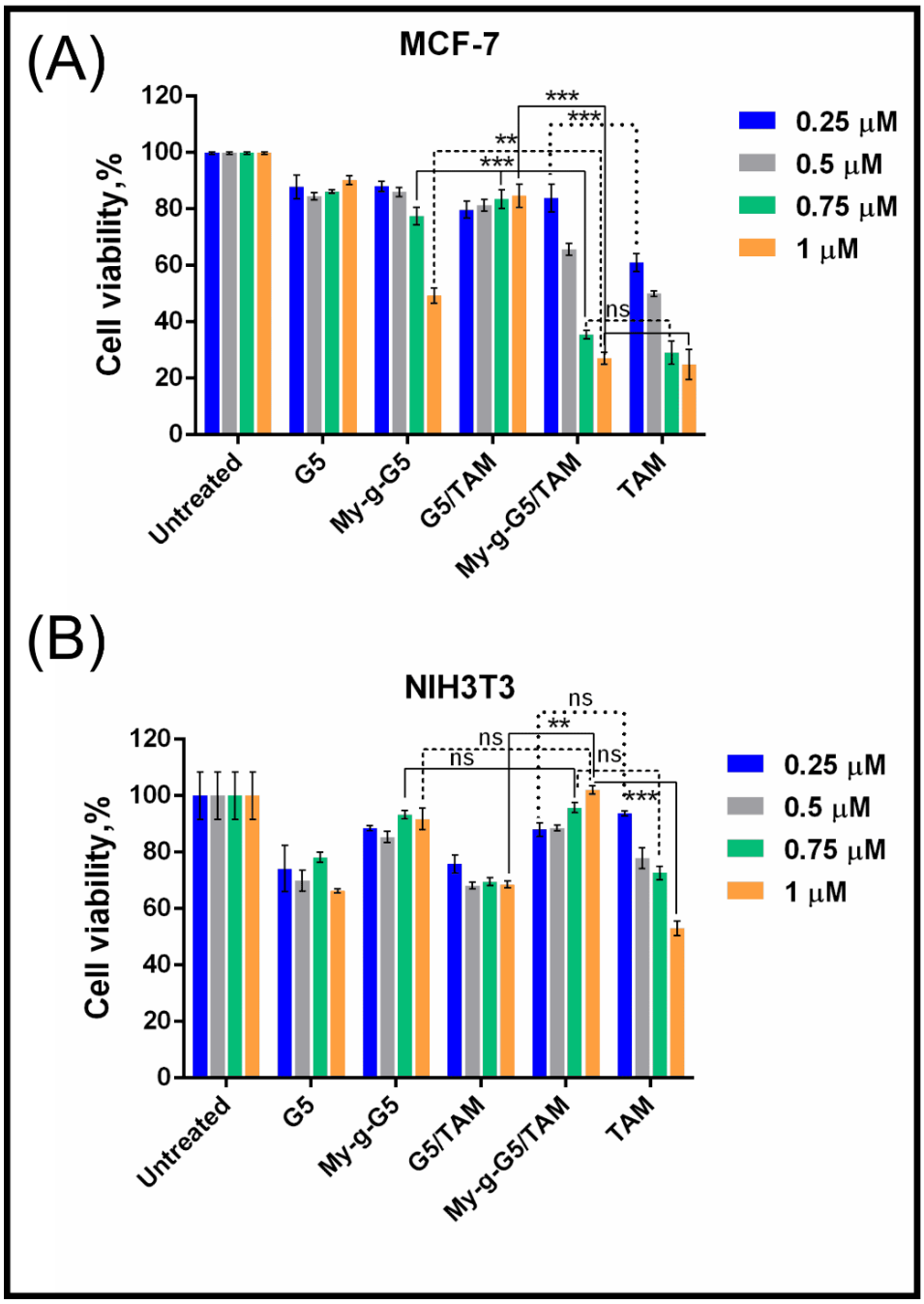

Figure 6.6. Viability of (A) MCF-7 and (B) NIH3T3 cells after treatment with different concentrations of G5, My-*g*-G5, G5/TAM, My-*g*-G5/TAM and free TAM after 48 h calculated from MTT assay. The values are expressed as mean ± standard error mean (SEM) (n=3). Two-way ANOVA with Tukey's multiple comparisons test was used to determine statistical difference between the group means (**$p < 0.005$, ***$p < 0.001$, ns: non-significant).

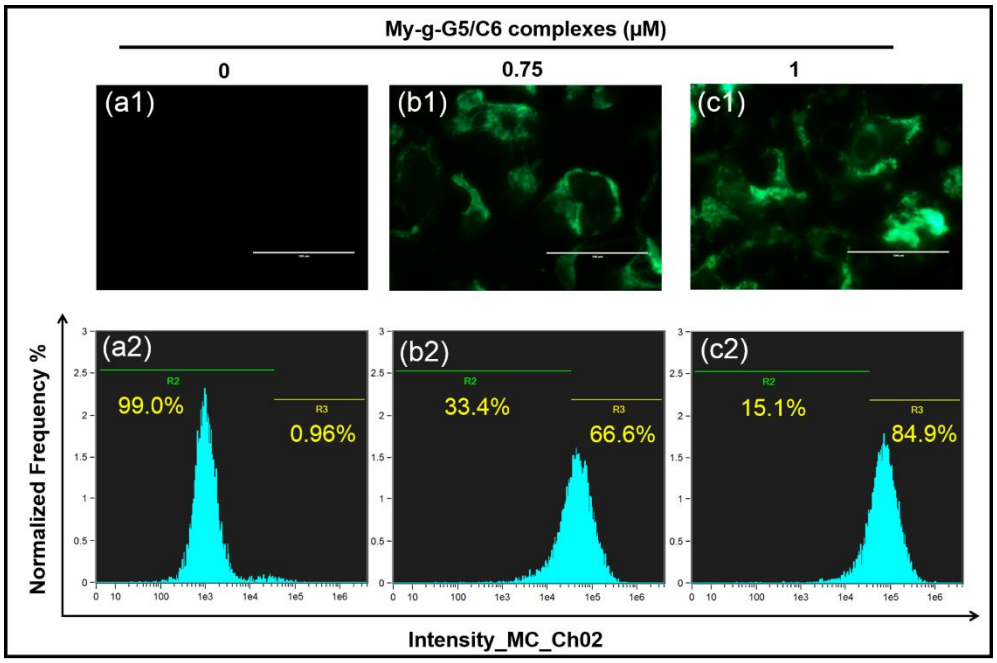

Figure 6.7. Fluorescence microscopic images of MCF-7 cells incubated with different concentrations of My-*g*-G5/C6 complexes (a1-c1) for 6 h and the corresponding quantitation of cellular uptake by flow cytometry (a2-c2). (Scale bar: 100 μm).

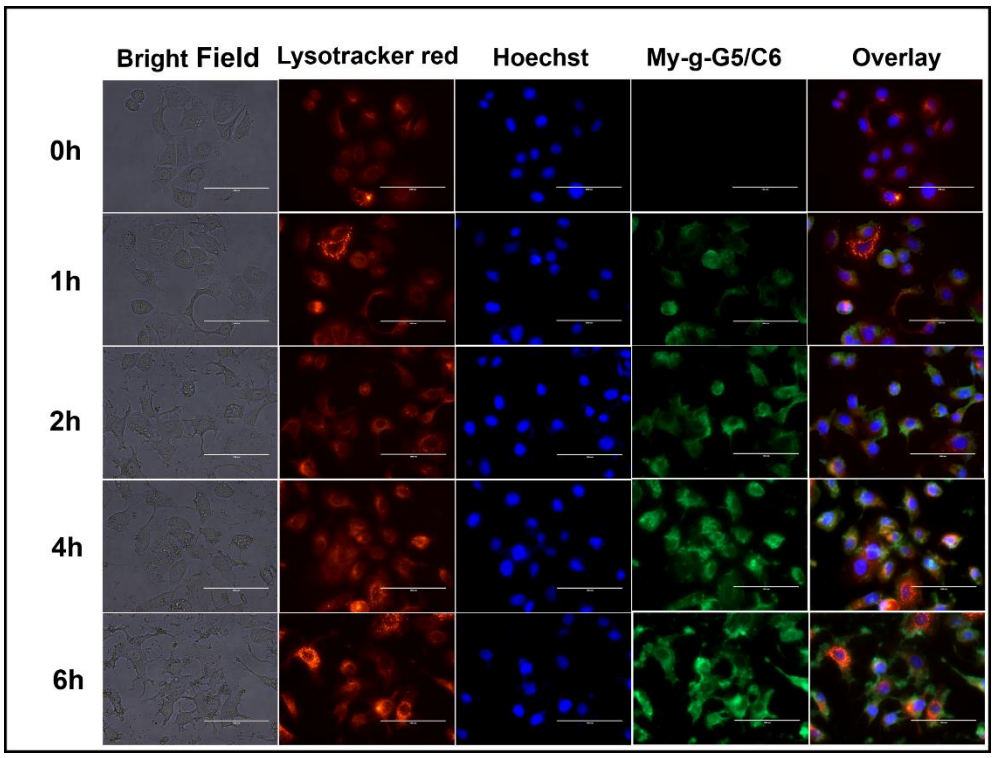

Figure 6.8. Fluorescence microscopic images revealing time dependent cellular uptake of My-*g*-G5/C6 complexes (0.75 μM) in MCF-7 cells under different filters. (Scale bar: 100 μm).

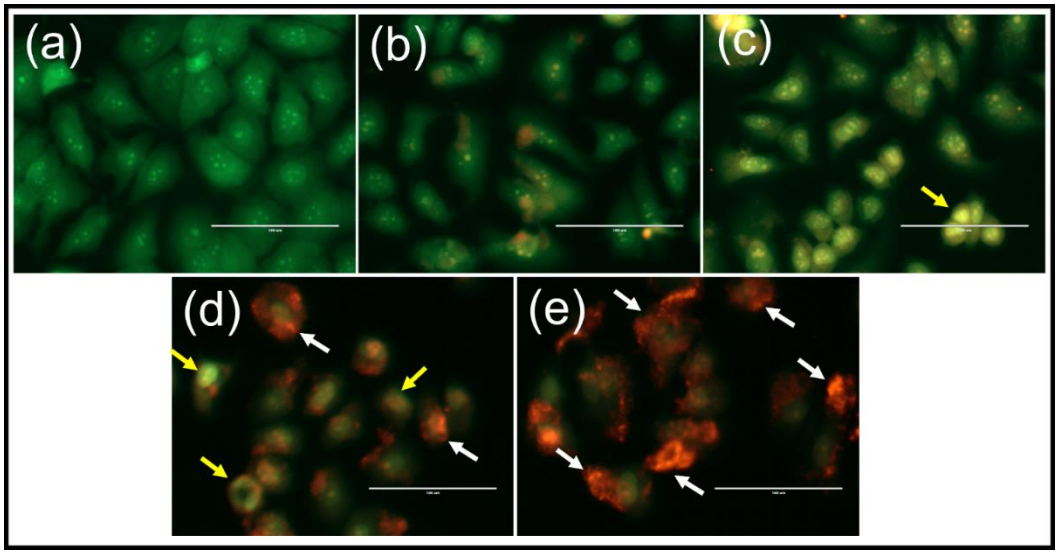

Figure 6.9. AO/EB stained images of (a) untreated, (b,c) G5/TAM and (d,e) My-*g*-G5/TAM (0.75 and 1 µM) treated MCF-7 cells after 24 h. Yellow arrows indicate cells undergoing early apoptosis and white arrows point towards the late apoptosis stages. (Scale bar: 100 µm).

6.2.6. Fluctuation in mitochondrial membrane potential (MMP)

Mitochondria is one of the key cell organelle affected during the apoptotic pathway of cell death. Change in the mitochondrial membrane permeability with a loss in MMP ($\Delta\Psi$) is an indicator of early apoptotic events (Ly et al., 2003). To explore whether the apoptosis induced by My-*g*-G5/TAM complexes involved the loss of mitochondrial integrity and hence $\Delta\Psi$, a cationic dye rhodamine 123 was used. Rhodamine 123 can rapidly diffuse inside the mitochondrial interior and can reflect the changes in MMP (Ren et al., 2012). MCF-7 cells exposed to different concentrations of G5/TAM and My-*g*-G5/TAM complexes were stained with Rhodamine 123 and its fluorescence intensity was observed. In MCF-7 cells treated with G5/TAM (0.75 and 1 µM) the intensity of red fluorescence was identical to the untreated cells **(Figure 6.10 a1-c1)** i.e., no loss in MMP was observed. In comparison, cells treated with My-*g*-G5/TAM (0.75 and 1 µM) displayed a significant decline in the red fluorescent signal, suggesting reduced uptake of rhodamine 123 or loss of $\Delta\Psi$ **(Figure 6.10 d1,e1)**. To support this observation, the percentage of cells with rhodamine 123 uptake were quantitated by flow cytometry. As evident, the percentage of red positive cells reduced from 61.1 % (without treatment) to 51.1 % and 37.3 % after My-*g*-G5/TAM (0.75 and 1 µM) and 1 µM) treatment, respectively **(Figure 6.10 a2,d2,e2)**. Whereas, the population of positive cells after G5/TAM exposure remained unaltered (70.4 % and 64.5 %). These results reveal a remarkable decline in MMP confirming induction of apoptosis in MCF-7 cells after My-*g*-G5/TAM treatment.

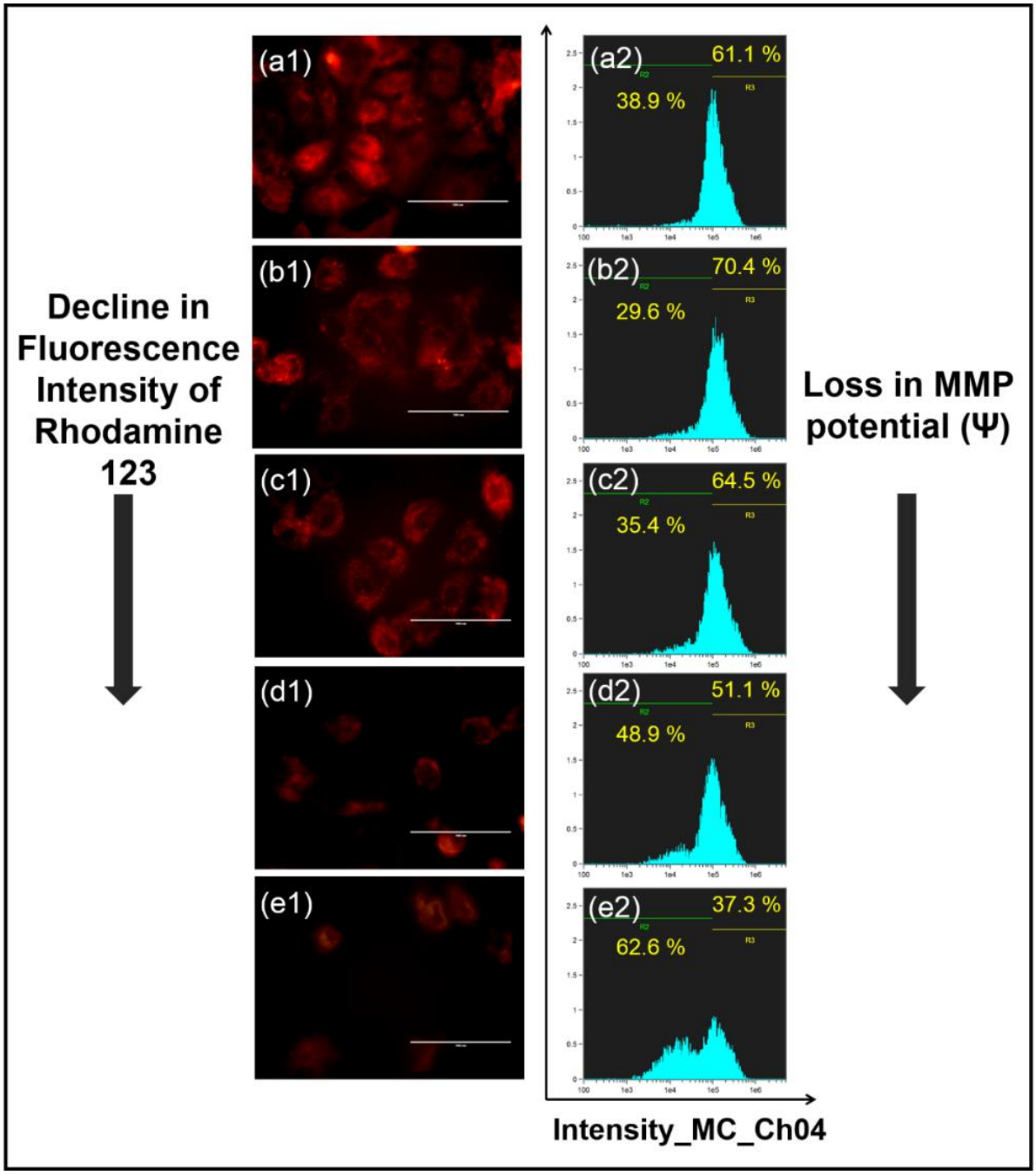

Figure 6.10. Fluorescence microscopic images of rhodamine 123 stained (a1) untreated, (b1,c1) G5/TAM and (d1,e1) My-*g*-G5/TAM (0.75 and 1 µM) treated MCF-7 cells after 24 h. (Scale bar: 100 µm). The other panel (a2-e2) depicts the corresponding flow quantitation. Decline in the fluorescence intensity of rhodamine 123 represents loss in mitochondrial membrane potential (MMP).

6.2.7. My-*g*-G5/TAM treatment triggers ROS production

An increase in the cellular ROS species or oxidative stress is known to elicit apoptotic cell death. The intracellular ROS production was evaluated in MCF-7 cells after exposure to different concentrations of My-*g*-G5/TAM (0.75 and 1 µM) complexes by DCFH-DA staining. The fluorescence images reveal an intensification in the DCF green fluorescence after treatment compared to untreated cells **(Figure 6.11 a1-c1)**. When quantified, the percentage of cells with ROS increased from 11.7 % (in untreated cells) to 29.6 % after My-*g*-G5/TAM (0.75 µM) treatment **(Figure 6.11 a2,b2)**. However, at higher concentration of My-*g*-G5/TAM (1 µM), the percentage of green positive cells reduced to 16.7 %, owing to their increased killing and leakage of ROS (Sharma et al., 2014).

6.2.8. Effect of My-*g*-G5/TAM treatment on cell cycle and gene expression profile

To probe the effect of My-*g*-G5/TAM treatment in altering the cell cycle stages, PI staining was performed and cells were thereafter quantitated. As shown in **Figure 6.12 A**, a dose dependent increase in cells arrested at sub G0/G1 stage was observed with My-*g*-G5/TAM treatment. These cells in the sub G0/G1 phase with sub-diploid DNA content primarily constitutes the apoptotic population (Darzynkiewicz et al., 2010 and Matai et al., 2015b). The % apoptotic cells reached to around 12.1 % and 22.9 % after My-*g*-G5/TAM treatment (0.75 and 1 µM), respectively. Moreover, the ability of anti-estrogen TAM to modulate the expression of genes involved in mitochondrial mediated apoptotic pathway is well-documented (Somai et al., 2003 and Kallio et al., 2005). In this context, we monitored the differential expression of pro-apoptotic p53, bax, bad, caspase 3 and anti-apoptotic bcl-xl genes. Beta actin (a housekeeping gene) was kept as an internal control. **Figure 6.12 B** shows the RT-PCR analysis of these apoptotic genes after My-*g*-G5/TAM treatment. The obtained data clearly depicts an up-regulation in the pro-apoptotic gene expression in a dose dependent manner. On the other hand, with increase in treatment concentration a significant down-regulation was observed in bcl-xl expression levels. The expression of beta actin remained unchanged. The prominent trigger of pro-apoptotic p53, bax, bad and caspase 3 mRNA levels suggests instigation of gene signalling cascade in MCF-7 cells. For comparative gene expression analysis, we exposed MCF-7 cells to G5/TAM and My-*g*-G5/TAM complexes (with equivalent TAM concentrations, 0.75 µM) under similar conditions. We observed that the expression of pro-apoptotic genes in response to G5/TAM were comparable to the untreated cells **(Figure 6.13)**. On the other hand, the same genes were found to be up-regulated with My-*g*-G5/TAM exposure compared to G5/TAM. The deviation in regulation of gene profile of apoptosis related genes suggest superiority of My-*g*-G5 dendrimers

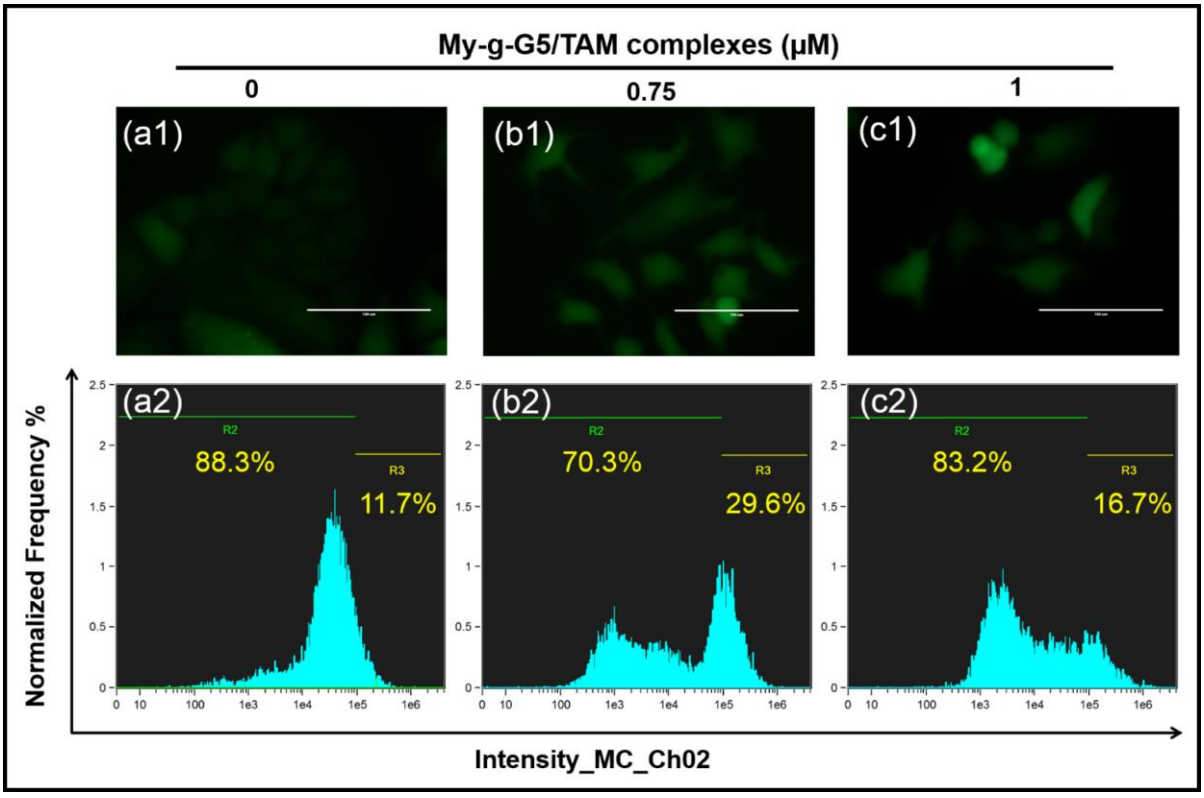

Figure 6.11. Microscopic and flow cytometric analysis of (a1,a2) untreated, My-*g*-G5/TAM treated MCF-7 cells with (b1,b2) 0.75 μM and (c1,c2) 1 μM, respectively for ROS generation after 24 h after DCFH-DA staining. (Scale bar: 100 μm).

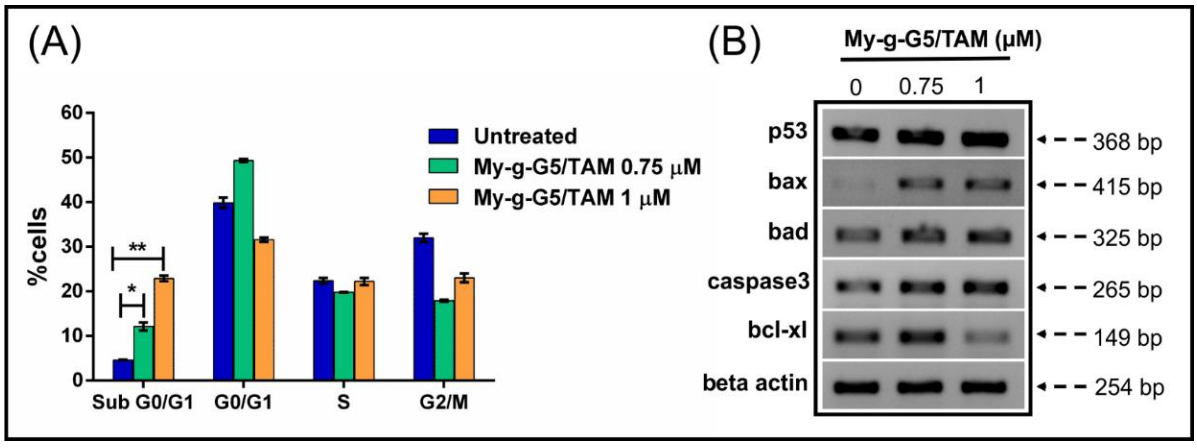

Figure 6.12. A) Cell cycle and B) Semi quantitative RT-PCR analysis of MCF-7 cells treated with different concentrations of My-*g*-G5/TAM complexes for 24 h. Multiple *t* tests using the Holm-Sidak method, was used to compute the statistical significance. (* $p < 0.05$, ** $p < 0.005$).

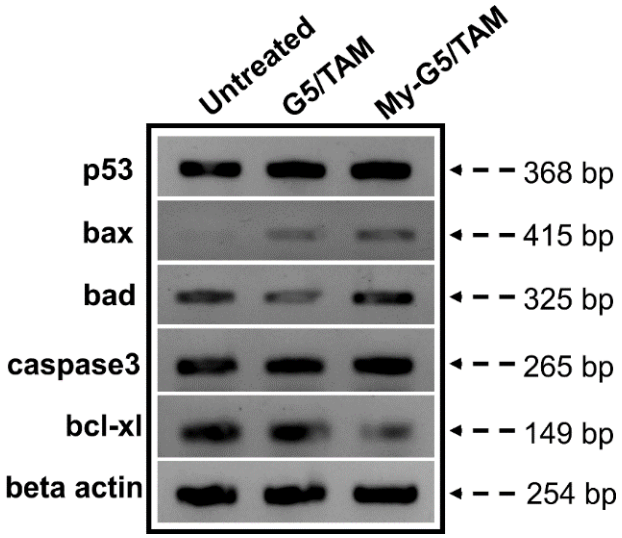

Figure 6.13. Comparative gene expression analysis of G5/TAM and My-*g*-G5/TAM treated MCF-7 cells.

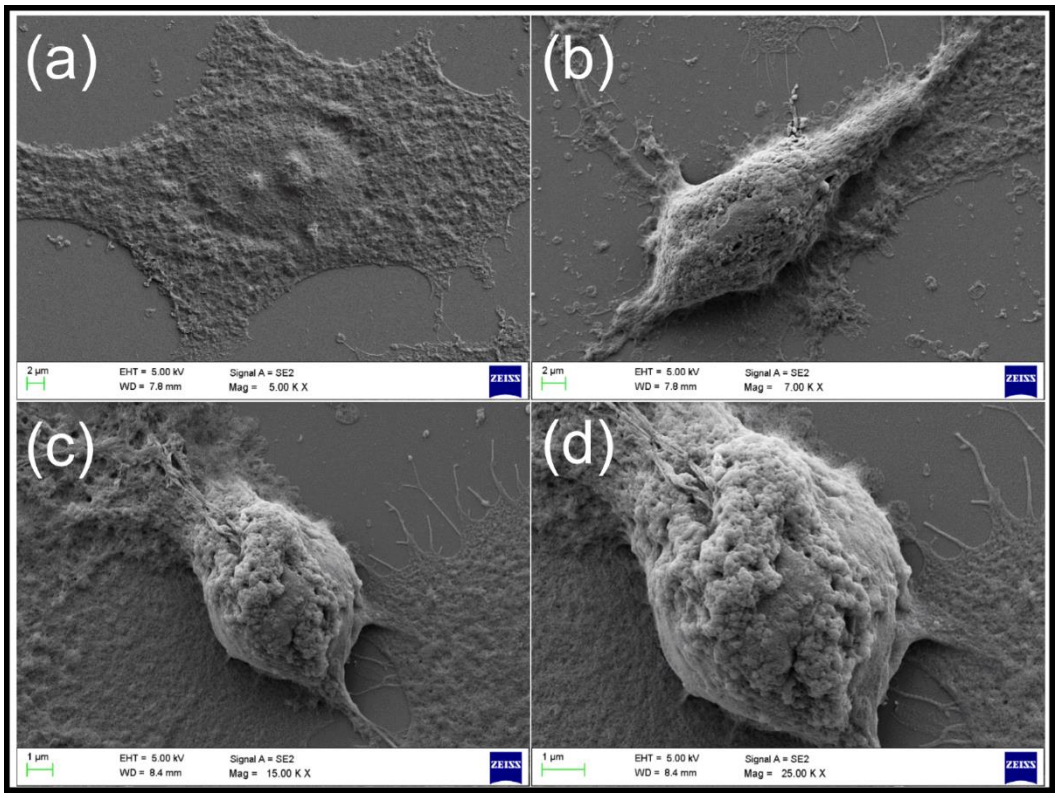

Figure 6.14. FE-SEM images of (a) untreated and (b,c) My-*g*-G5/TAM (0.75 and 1 µM) treated MCF-7 cells, respectively. d) Magnified view of (c) depicting apoptotic morphology of cells after 24 h.

over pristine G5 PAMAM dendrimers. These results signifies that My-*g*-G5/TAM complexes were effective enough to regulate the expression of genes directly involved in apoptotic pathway.

6.2.9. Morphological changes associated with My-g-G5/TAM treatment

We further analyzed the changes in cell morphology and appearance owing to apoptosis induction under FE-SEM. **Figure 6.14** depicts the typical FE-SEM micrographs of untreated and treated MCF-7 cells. Untreated MCF-7 cells appeared healthy and were well-attached to the surface **(Figure 6.14 a)**. At lower dose of My-*g*-G5/TAM (0.75 μM), membrane constriction and shrinkage was seen and cells were loosely-adhered to the surface **(Figure 6.14 b)**. Moreover at higher dose, the cells became round and typical morphological transformations related to apoptosis including membrane blebbing and appearance of apoptotic bodies were observed (**Figure 6.14 c,d)** (Rello et al., 2005, Matai et al., 2015 b, 2016). Such findings are valuable while designing nanocarriers for achieving the desired therapeutic benefits for cancer inhibition and prevention.

In summary, the present study explores the advantages of hydrophobically modified G5 PAMAM dendrimers for the delivery of anti-estrogen TAM over unmodified G5 PAMAM dendrimers. Random grafting of lipid-like myristic acid chains on the dendrimer surface significantly enhanced the stability and solubility of TAM in polar conditions. Moreover, introduction of myristoyl groups improved the cellular uptake and decreased the cytotoxicity of G5 PAMAM dendrimers. Different cell-based experiments elucidated apoptosis inducing ability of these My-*g*-G5/TAM complexes in MCF-7 cells. In totality, surface engineering of PAMAM dendrimers by randomly decorating myristoyl chains can be an intelligent strategy to design delivery vectors with improved benefits.

CHAPTER 7

Development of Self-Assembled Hybrids of Fluorescent Carbon Dots and PAMAM Dendrimers for Epirubicin Delivery and Intracellular Imaging

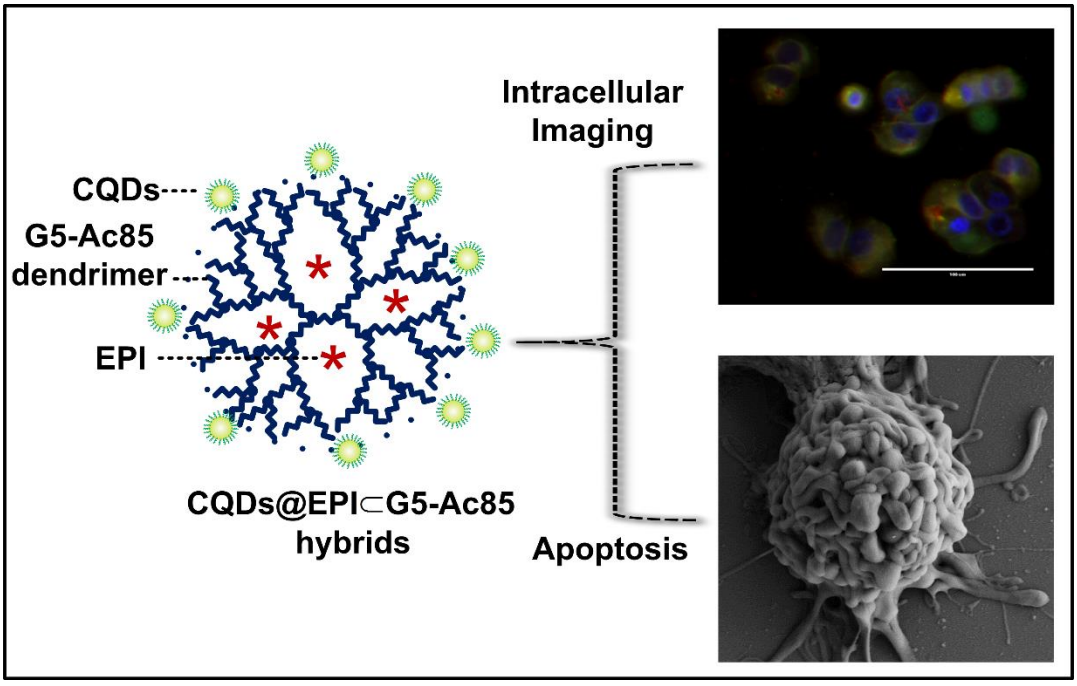

CHAPTER 7

DEVELOPMENT OF SELF-ASSEMBLED HYBRIDS OF FLUORESCENT CARBON DOTS AND PAMAM DENDRIMERS FOR EPIRUBICIN DELIVERY AND INTRACELLULAR IMAGING

7.1. Overview

Designing strategies for integrating imaging modalities with PAMAM dendrimers carrying anticancer drugs for concurrent intracellular tracking and therapy offer a new horizon in cancer treatment. Recently, carbon dots (CQDs) have been successfully employed for bioimaging of cancer cells. Macromolecules such as PAMAM dendrimers with abundant amine terminal groups can form hybrids with other nanomaterials such as low molecular weight CQDs via molecular self-assembly. CQDs with hydroxyl (-OH) surface groups can non-covalently interact with the cationic acetylated PAMAM dendrimers to form fluorescent hybrids. We intentionally adopted non-covalent pathway for hybrid formation for its several advantages: (i) relatively simple approach to a variety of hybrid assemblies, (ii) covalent conjugation by surface modification can quench CQDs fluorescence, and (iii) enhancement in CQDs fluorescence by PAMAM dendrimer via charge-transfer process (Datta et al., 2014 and Sachdev et al., 2015). Recently, Zhou and co-workers demonstrated use of negatively charged CQDs as caps on positive mesoporous silica nanoparticles (MSPs) for smart delivery of anticancer drug DOX (Zhou et al., 2013b). Zong and group reported photoluminescence (PL) enhancement of carbon dots in the vicinity of AuNPs conjugated through G4.0 PAMAM. NH_2 dendrimers (Zong et al., 2013). In the present study, G5 PAMAM dendrimers with large interiors than G4 dendrimers (~ 5.4 nm), and low cytotoxicity than G6 dendrimers were selected for hybrid formation. The surface of PAMAM dendrimers was altered by converting some cationic primary amine groups to neutral acetyl groups. This strategy is envisioned to be effective in reducing the inherent toxicity of PAMAM dendrimers. In addition, these partial acetylated dendrimers can enhance the solubility of EPI drug after encapsulation. Herein, self-assembled hybrids of CQDs and EPI⊂G5-Ac85 dendrimer complexes (85 refers to peripheral acetyl groups) as CQDs@EPI⊂G5-Ac85 acts as a multifunctional dual-emission and therapeutic system. The emission intensity of CQDs is

enhanced after non-covalent complexation with EPI⊂G5-Ac85 complexes. To the best of our knowledge, this is the first instance wherein CQDs have been used to visualize and quantitate the intracellular uptake of EPI⊂G5-Ac85 inclusion complexes by fluorescence microscopy and flow cytometry techniques. CQDs@EPI⊂G5-Ac85 hybrids illustrate pH dependent release of encapsulated EPI drug and served as imaging probes in the transport process to their target destination. Various cell based assays were performed to investigate the anticancer activity of EPI in encapsulated form in CQDs@EPI⊂G5-Ac85 hybrids in MCF-7 (breast cancer) and NIH3T3 (mouse embryonic fibroblast) cells. Further, elucidation of mode of cell death was done by monitoring the cell cycle distribution, ROS levels by flow cytometry and differential expression of apoptosis related genes by RT-PCR, respectively. Our results indicated that CQDs@EPI⊂G5-Ac85 hybrids could remarkably reduce the MCF-7 proliferation and induce apoptosis by oxidative DNA disintegration and trigger of mitochondrial pathway of apoptosis. The ability of CQDs@EPI⊂G5-Ac85 hybrids for synchronized bioimaging and drug delivery has been confirmed to achieve improved cancer diagnosis and therapy.

7.2. RESULTS AND DISCUSSION

7.2.1. Synthesis and characterization of CQDs@EPI⊂G5-Ac85 hybrids

Theoretically, G5 PAMAM dendrimer has 128 primary amine groups on its surface available for modification or functionalization. The chemistry of these terminal groups render dendrimer with unique properties of water-solubility and reactivity. Exploiting the potential of PAMAM dendrimers as delivery systems while reducing its cytotoxicity is highly appreciable. With this perspective, a fraction of primary amines were converted to neutral acetamide groups, to reduce its toxicity. In this study, the stoichiometric ratio of acetic anhydride: amine groups was kept 90:1 to achieve 70 % conversion of surface amines to acetamides. The ^{1}H NMR spectra of the acetyl-derivatized G5 PAMAM shows peak at 1.9 ppm corresponding to – CH_3 protons of acetyl group **(Figure 7.1)**. The peaks at 2.2-3.4 ppm can be assigned to the -CH_2-protons of G5 PAMAM (Majoros et al., 2003). Number of acetylated primary amines was determined by comparing the intensity of the -CH_3 protons of the acetyl groups to the sum of all -CH_2 peaks. From NMR integration, -CH_3/-CH_2-ratio was calculated and 85 primary amine groups were functionalized to acetamides to yield G5-Ac85 dendrimers. The obtained partially acetylated molecules are expected to be more compact and water soluble, compared to pristine dendrimers due to minimal charge-repulsion from reactive primary amines (Majoros et al., 2003).

Next, EPI.HCl was neutralized with triethylamine to form water-insoluble EPI to enable its efficient encapsulation within G5-Ac85 hydrophobic interiors. This new formulation of

EPI⊂G5-Ac85 complexes is expected to enhance the water-solubility and thus bioavailability of EPI. This drug-dendrimer formulation was stored in -20 °C and was stable for 1-2 months without any loss in EPI activity. Additionally, hydroxyl (-OH) functionalized carbon dots (CQDs) were synthesized hydrothermally using chitosan as carbon source and PEG-4000 polymer as the passivating agent. Use of a suitable passivating agent is known to enhance the fluorescence properties of CQDs (Sachdev et al., 2014). CQDs with –OH overhangs can form hybrids with cationic EPI⊂G5-Ac85 nanocomplexes through non-covalent linkages such as hydrogen-bonding and electrostatic interactions to track the intracellular distribution of EPI. Step-wise representation of synthesis of CQDs@EPI⊂G5-Ac85 hybrids is shown in **Scheme 7.0**. Such EPI loaded CQDs@G5-Ac85 hybrids are expected to act as multifunctional dual-emission delivery systems.

The formed CQDs@EPI⊂G5-Ac85 hybrids were characterized by UV-Vis spectroscopy. The absorption spectra of aqueous CQDs solution and EPI dissolved in methanol were also recorded for comparison. CQDs display a single absorption band at 255 nm, which can be attributed to π–π* transition of the conjugated C=C bond (Sachdev et al., 2014 and Dong et al., 2015) **(Figure 7.2 A)**. EPI exhibits a characteristic band at 481nm. Upon EPI encapsulation, G5-Ac85 complexes exhibit an absorption enhancement at 481nm peak when compared to blank G5-Ac85 dendrimers **(Figure 7.2 B)**. This suggests complete entrapment of EPI within the G5-Ac85 interiors. The amount of EPI payload in G5-Ac85 dendrimers was determined from the dose-absorption curve of EPI and encapsulation efficiency was calculated as 57.36 ± 1.5 %. With the formation of CQDs@EPI⊂G5-Ac85 hybrids, the absorption band of CQDs was slightly red shifted to 262 nm suggesting interaction between the terminal amines and -OH groups of CQDs. Additionally, the zeta potential (ζ) measurements were also recorded to study the surface charge and interactions among various components of nanocomplexes. The zeta potential of CQDs and G5-Ac85 dendrimers was -18.5 and +16 mV, respectively. After EPI encapsulation, the zeta of G5-Ac85 dendrimers reduced to +11.6 mV indicating its entrapment within the dendritic architecture. The interactions between the -COOH groups of EPI and interior tertiary amines of G5-Ac85 dendrimers can be held responsible for formation of EPI⊂G5-Ac85 complexes. After adding CQDs, the zeta potential further reduced to +8.74 mV, which indicate efficient grafting of anionic CQDs on the cationic EPI⊂G5-Ac85 surface. The overall positive charge of hybrids make them suitable candidates for bioapplications such as cellular imaging and for drug delivery (Liu et al., 2012a and Dong et al., 2015).

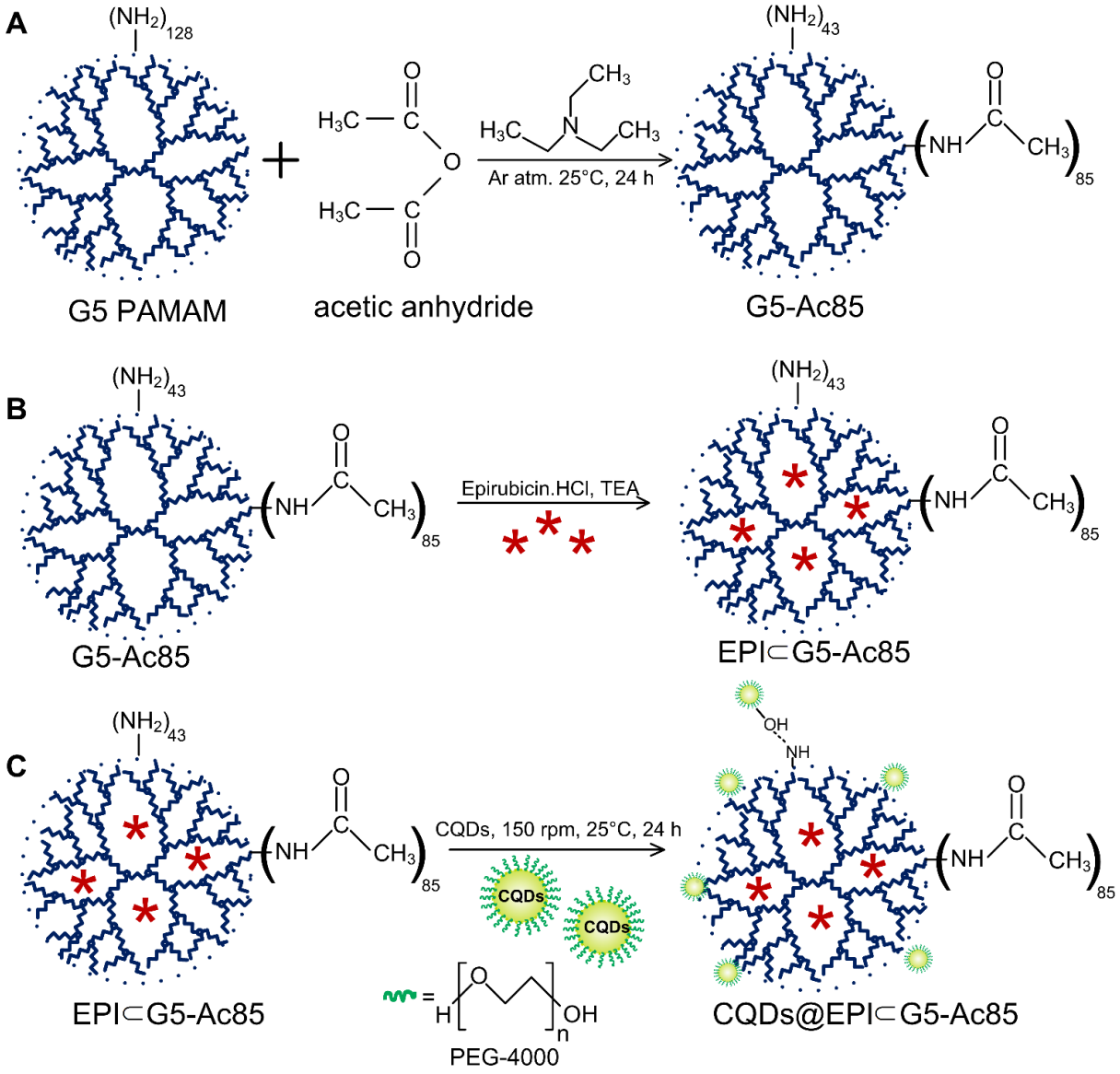

Scheme 7.0. Schematic representation of (A) Synthesis of partially acetylated G5 PAMAM dendrimers (G5-Ac85); (B) Encapsulation of anticancer drug epirubicin (EPI) in the cavities of G5-Ac85 dendrimers; (C) Synthesis of CQDs@EPI⊂G5-Ac85 hybrids via non-covalent interactions.

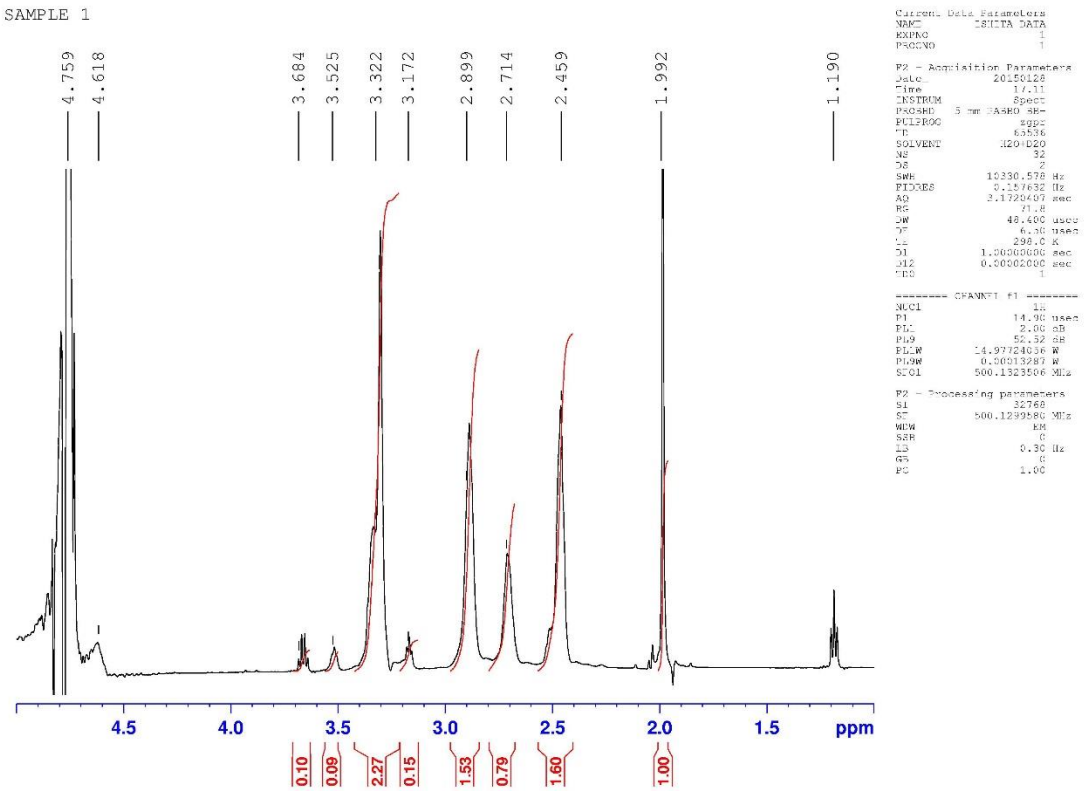

Figure 7.1. Typical ^{1}H NMR spectra of G5-acetylated dendrimers. Peaks around 4.7 ppm and 1.99 ppm are of the D_2O solvent and acetamides, respectively. Other peaks are of the structural protons of acetylated dendrimer.

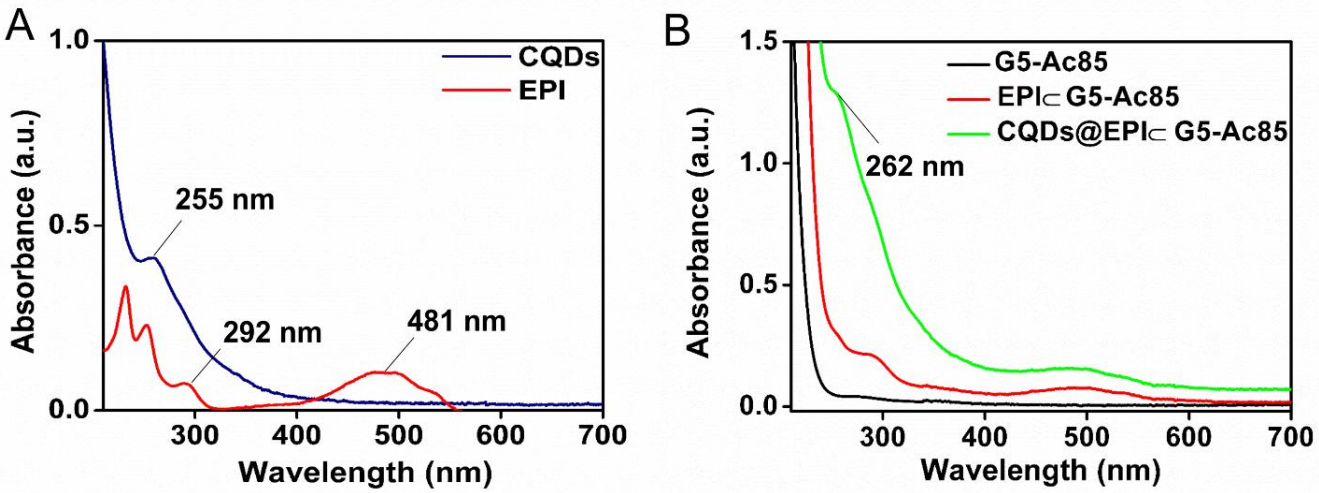

Figure 7.2. UV-visible spectrum of (A) CQDs in water and EPI in methanol; (B) aqueous solution of G5-Ac85, EPI⊂G5-Ac85 complexes and CQDs@EPI⊂G5-Ac85 hybrids, respectively.

Further, TEM investigation was done to predict the morphology and size of CQDs and CQDs@EPI⊂G5-Ac85 hybrids. The as-synthesized CQDs appeared nearly-spherical with average size 1.75 ± 0.474 nm **(Figure 7.3 A, B).** Negative staining with PTA revealed uniform EPI⊂G5-Ac85 complexes uniformly decorated with CQDs (black spots) to form CQDs@EPI⊂G5-Ac85 hybrids **(Figure 7.4 A).** DLS measurements showed that the hydrodynamic diameter of as-prepared hybrids was 6.9 ± 0.774 nm **(Figure 7.4 B).** It is important to mention that DLS predicts the complete hydrodynamic size of particles (Wang et al., 2013b).

7.2.2. ^{1}H NMR analysis

The formation of EPI⊂G5-Ac85 complexes and CQDs@EPI⊂G5-Ac85 hybrids was further confirmed by ^{1}H NMR measurements using D_2O as solvent **(Figure 7.5)**. TSP (3-(Trimethylsilyl) propionic-2, 2, 3, 3,-d_4 acid, sodium salt) was used as an internal standard. From **Figure 7.5 A**, peak at 1.99 ppm can be assigned to methyl protons of acetamides and peaks at 2.46 ppm, 2.71 ppm, 2.9 ppm, 3.17 ppm, 3.32 ppm and 3.52 ppm are representative of the structural protons in acetylated dendrimer (Majoros et al., 2006). With EPI encapsulation **(Figure 7.5 B)**, characteristic peaks of methyl protons of EPI at 1.3 ppm and 3.2 ppm were observed along with acetylated dendrimer proton peaks (Li et al., 2015a). Moreover, for the structural peaks assigned at ‘b’ and ‘c’ positions a slight upfield shift from 2.71 ppm to 2.65 ppm, and 2.9 ppm to 2.8 ppm appeared after EPI complexation reflecting interaction of EPI molecules with dendrimer secondary amines. The other peaks retained their original positions. With the formation of CQDs@EPI⊂G5-Ac85 hybrids, peaks at ~ 3.7 ppm and 1.93 ppm were seen in conjunction to the other peaks **(Figure 7.5 C)**. These can be attributed to methylene protons of PEG moiety and remnant acetic acid in CQDs (Huang et al., 2008). Presence of representative NMR peaks of EPI and CQDs, indicate the successful formation of EPI⊂G5-Ac85 complexes and CQDs@EPI⊂G5-Ac85 hybrids.

7.2.3. Fluorescence studies

The aqueous solution of CQDs display the molecular signature excitation dependent emission behavior (Sachdev et al., 2013 and 2014) **(Figure 7.6 A, B)**. Increment in excitation wavelength from 320 to 480 nm resulted in a progressive red shift in its maximum emission from 400 to 490 nm, with reduction in emission intensity. The maximum emission of CQDs was recorded at an excitation wavelength of 320 nm. It is worth mentioning that CQDs at 480 nm excitation have negligible emission, resulting in minimal interference with EPI emission signal. Interestingly, an enhancement in fluorescence of CQDs in CQDs@EPI⊂G5-Ac85 hybrids was encountered

compared to blank CQDs **(Figure 7.6 C)**. This can be ascribed to the electron charge transfer from G5-Ac85 dendrimers to CQDs (Zong et al., 2013 and Tong et al., 2015). To confirm this, the fluorescence lifetime decay curves for CQDs and CQDs@EPI⊂G5-Ac85 hybrids were recorded. The obtained data could be fitted to a triple-exponential decay curve and their average lifetimes were calculated **(Figure 7.6 D and Table 7.1)**. Average fluorescence lifetime of bare CQDs was 5.84 ns, which increased to 6.12 ns in CQDs@EPI⊂G5-Ac85 hybrids. Thus, grafting of negatively charged CQDs on the PAMAM surface could be a simple and an effective strategy for fluorescence enhancement of CQDs.

The effect of change in pH on fluorescence properties of CQDs and CQDs@EPI⊂G5-Ac85 hybrids was also investigated. The emission intensity of both bare CQDs and CQDs@EPI⊂G5-Ac85 hybrids varied with change in pH of medium **(Figure 7.7)**. The fluorescence intensity of CQDs increased steadily in the pH range of 4.0-10.0. However, a slight red shift in emission was monitored from pH 7.0 onwards **(Figure 7.7 A)**. With increase in pH, the terminal –OH groups of CQDs get ionized which influence electronic transitions resulting in such pH dependent behavior. Contrarily, for CQDs@EPI⊂G5-Ac85 hybrids maximum fluorescence was evident at acidic environment (pH 5.5) followed by neutral and alkaline conditions (pH 7.0-10.0) **(Figure 7.7 B)**. This can be attributed to the protonation of surface amino groups of PAMAM under acidic conditions and deprotonation under alkaline conditions (Maiti et al., 2005, Dong et al., 2012 and Sachdev et al., 2014). Their colloidal stability of bare CQDs and CQDs@EPI⊂G5-Ac85 hybrids was also affected with variation in pH **(Figure 7.8)**. Zeta potential of CQDs was maximum -21.64 mV at pH 10.0, but reduced to -18.5 mV at pH 7.0 and became low under acidic conditions. Conversely, CQDs@EPI⊂G5-Ac85 hybrids were found to exhibit maximum stability at pH 5.5 with zeta potential +28.9 mV. The pH dependent stability estimation of CQDs and CQDs@EPI⊂G5-Ac85 hybrids are in validation with the fluorescence results.

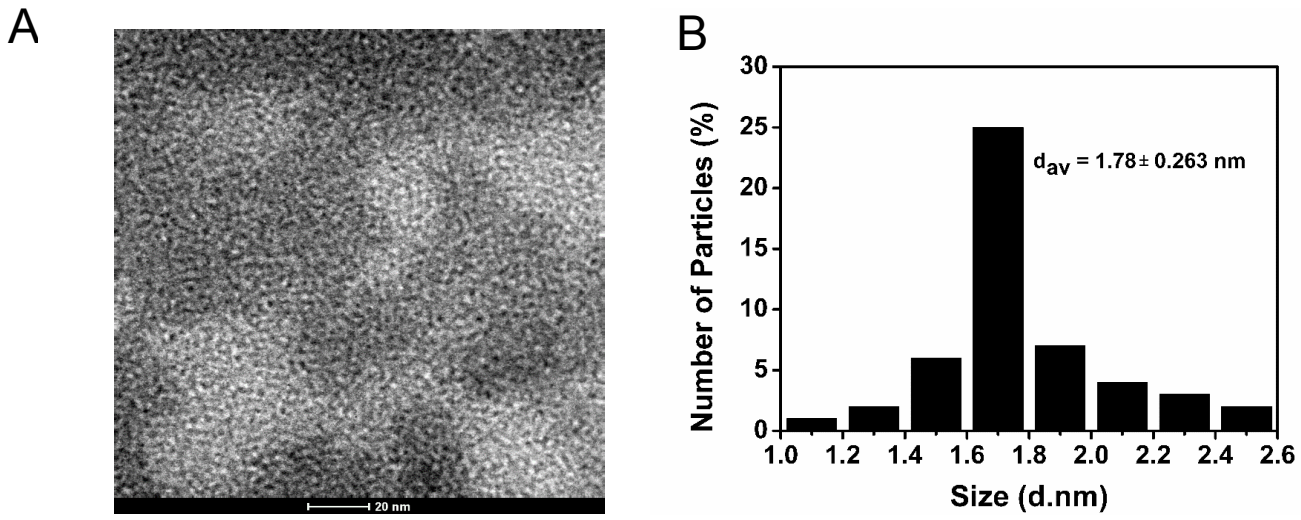

Figure 7.3. (A) Typical TEM image of as-synthesized CQDs, revealing formation of uniform dark dots with near spherical morphology and (B) size distribution pattern of CQDs. (Scale bar: 20 nm)

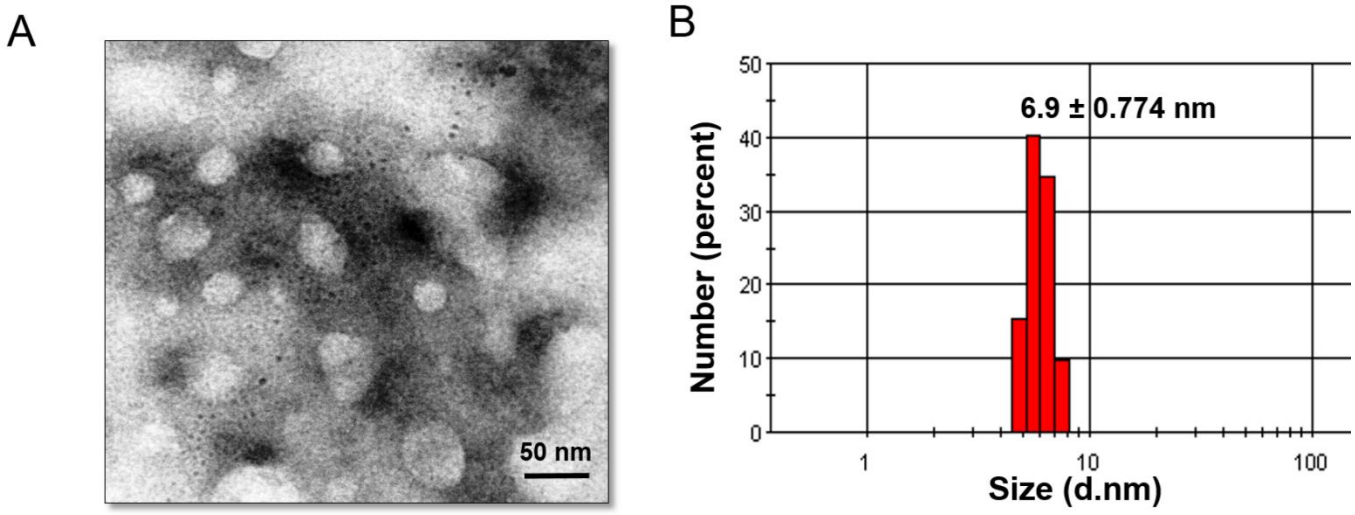

Figure 7.4. (A) TEM image of as-synthesized CQDs@EPI⊂G5-Ac85 hybrids (with 50 nm scale bar) and (B) Size distribution profile by DLS measurements at pH 7.0.

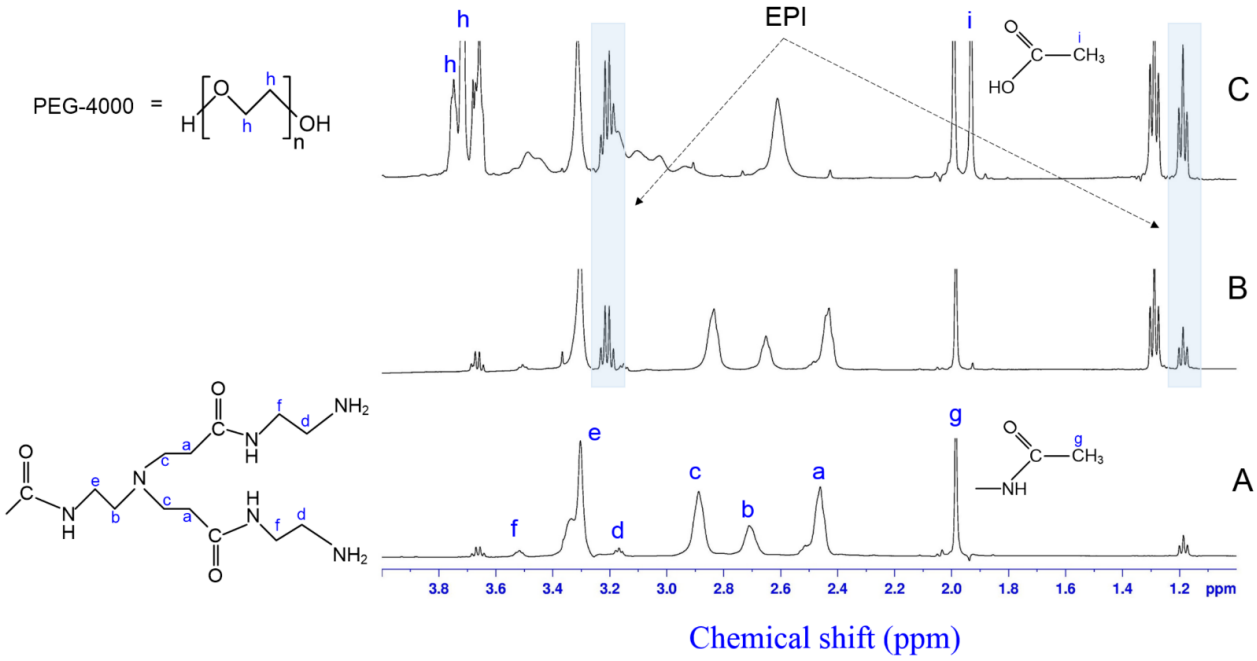

Figure 7.5. ^{1}H NMR spectra of (A) G5-Ac85, (B) EPI⊂G5-Ac85 complexes and (C) CQDs@EPI⊂G5-Ac85 hybrids in D_2O. The highlighted portions (blue) represent the characteristic peaks of EPI.

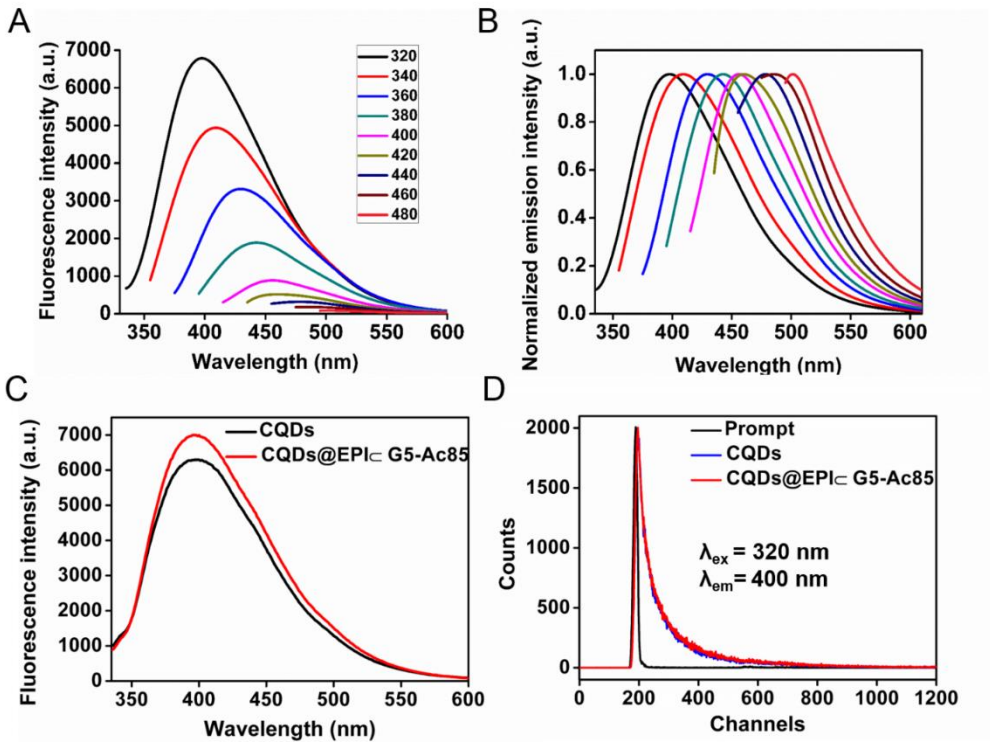

Figure 7.6. (A) Fluorescence emission spectra of CQDs in water at different excitation wavelengths; (B) Normalized emission spectra. (C) Comparative emission spectra and (D) Fluorescence decay profile of CQDs and CQDs@EPI⊂G5-Ac85 hybrids, respectively (λ_{ex} = 320 nm; λ_{em} = 400 nm).

Sample	a_1	τ_1(ns)	a_2	τ_2(ns)	a_3	τ_3 (ns)	τ_{av} (ns)	χ^2
CQDs	0.4743	3.2470	0.1390	0.6021	0.3867	10.91	5.8426	0.9896
CQDs@EPI⊂G5-Ac85	0.4296	3.1308	0.4453	10.59	0.1251	0.4759	6.1202	1.0731

Table 7.1. Tabular representation of lifetime data obtained from tri-exponential model for the fluorescence decay profile CQDs and CQDs@EPI⊂G5-Ac85 hybrids. (λ_{ex} = 320 nm; λ_{em} = 400 nm).

Average lifetime was calculated from the following equation:

$$\tau_{av} = a_1\tau_1 + a_2\tau_2 + a_3\tau_3$$

τ_1, τ_2 and τ_3 represent the first, second and third component of the decay time of CQDs and CQDs@EPI⊂G5-Ac85 hybrids and a_1, a_2 and a_3 are the corresponding relative weightings (emission %) of these components, respectively.

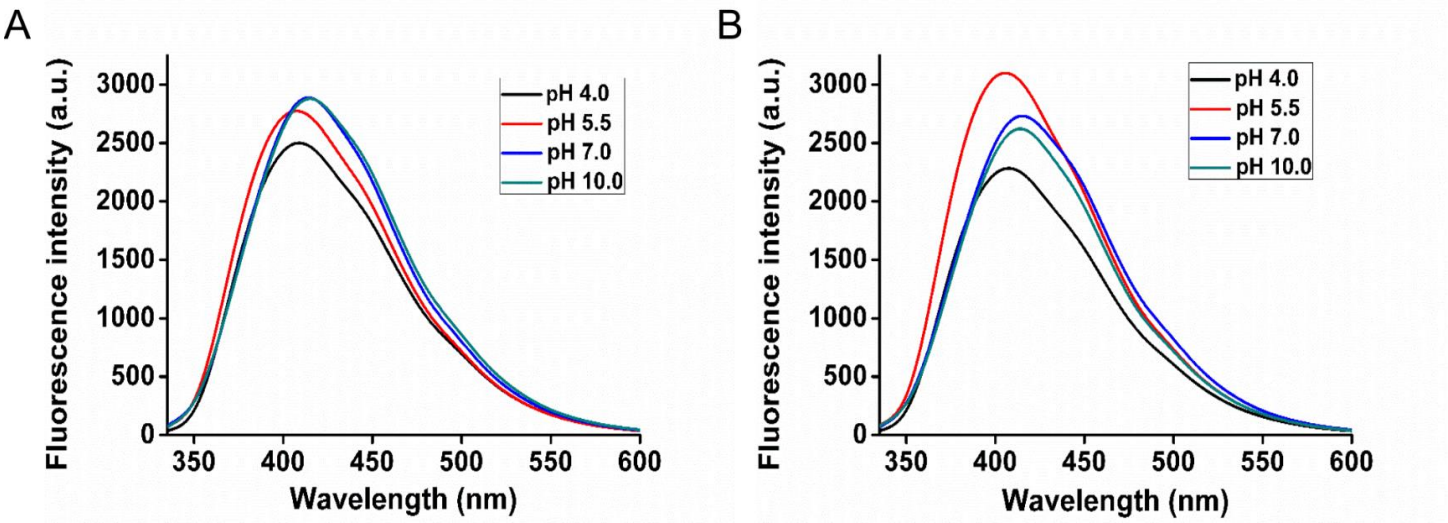

Figure 7.7. Fluorescence emission spectra of (A) CQDs and (B) CQDs@EPI⊂G5-Ac85 hybrids in the pH range of 4.0-10.0. (λ_{ex} = 320 nm). The shift in the emission spectra suggests the effect of change in pH on the peripheral functional groups which contribute to the fluorescence properties of CQDs and CQDs@EPI⊂G5-Ac85 hybrids.

7.2.4. *In vitro* EPI release studies

Another important parameter is the ability of CQDs@EPI⊂G5-Ac85 hybrids to release the EPI payload in a sustained manner. Before evaluating the anticancer activity, the pH controlled release of EPI by CQDs@EPI⊂G5-Ac85 hybrids was investigated *in vitro* at pH 5.5 and 7.4, respectively. The time-dependent release profiles of EPI are shown in **Figure 7.9**. These hybrids were able to release EPI in a biphasic pattern, characterized by an initial rapid release followed by sustained release. About 90 % of EPI was released after 48 h at pH 5.5, imitating the tumor microenvironment. While, around 51 % was released in the same time at pH 7.4, close to physiological conditions. The rapid EPI release under acid conditions may be due to weakened electrostatic interactions between protonated interior amines and –CONH- linkages of CQDs@G5-Ac85 hybrids with –COOH groups of EPI molecules (Maiti et al., 2005). The slow release of EPI from CQDs@G5-Ac85 hybrids at physiological pH than under acidic environment makes it a suitable candidate for specifically targeting the cancerous cells.

7.2.5. MTT assay

We further investigated the anticancer effects of released EPI from EPI⊂G5-Ac85 complexes and CQDs@EPI⊂G5-Ac85 hybrids *in vitro* first by performing MTT assay. As shown in **Figure 7.10 A**, MCF-7 cells treated with blank G5-Ac85 dendrimers exhibited a good cell viability at all tested concentrations. This suggests that introduction of a small acetyl moiety on the dendrimer peripheral surface could improve its cytocompatibility. Free CQDs were also able to maintain appreciable cell viability. Free EPI was found to significantly inhibit the cell growth at all studied doses. With increase in EPI concentration from 0.625 to 10 µM, the cell viability reduced to nearly 16 %. Importantly, CQDs@EPI⊂G5-Ac85 and EPI⊂G5-Ac85 hybrids were also able to inhibit cancer cell proliferation significantly. For instance, at an EPI concentration of 5 µM around 85 % cells died with free EPI and almost 70 % cells died with CQDs@EPI⊂G5-Ac85 and EPI⊂G5-Ac85 treatments. Since, G5-Ac85 dendrimers did not alter the cell survival, the toxicity was solely induced by the loaded EPI drug. Also, addition of CQDs to EPI⊂G5-Ac85 complexes did not affect significantly the exhibited toxic response. We also examined the effect of CQDs@EPI⊂G5-Ac85 hybrids on normal NIH3T3 cells. At similar dosage, the hybrids exhibited more inhibitory effect on MCF-7 cells compared to normal cells **(Figure 7.10 B)**. Based on the therapeutic profile of EPI⊂G5-Ac85 complexes and CQDs@EPI⊂G5-Ac85 hybrids, 5 µM EPI concentration was selected for further cell-based experiments.

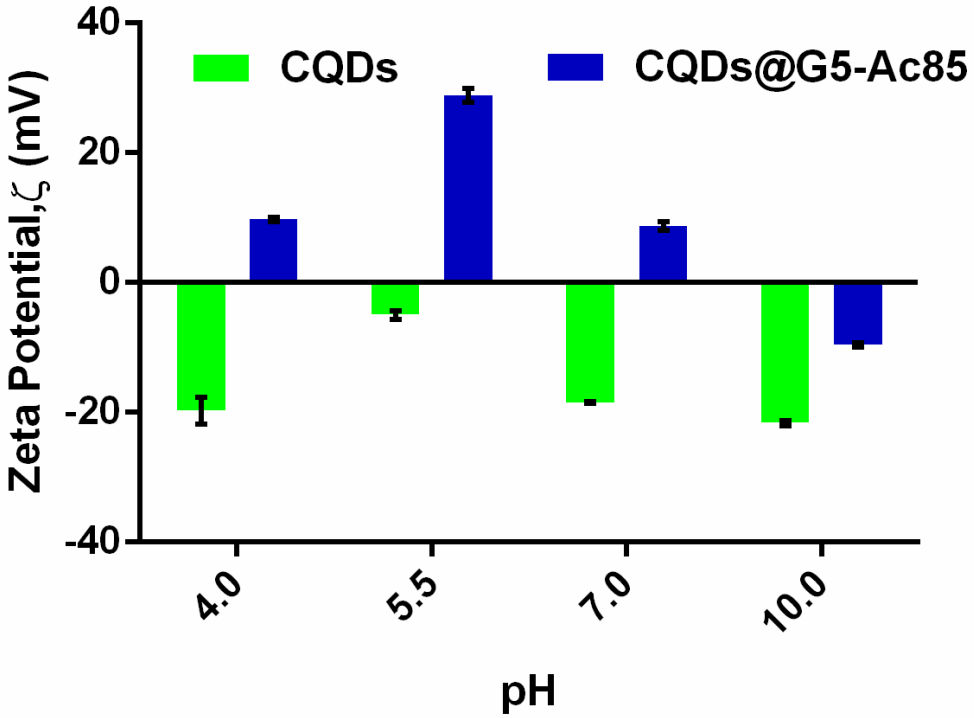

Figure 7.8. Zeta potential measurements as a function of pH (4.0-10.0) for CQDs and CQDs@G5-Ac85 hybrids. Experiments were performed in triplicate and values are expressed as mean ± S.E.M. The results indicate the overall surface charge and stability of CQDs and CQDs@G5-Ac85 hybrids with pH change.

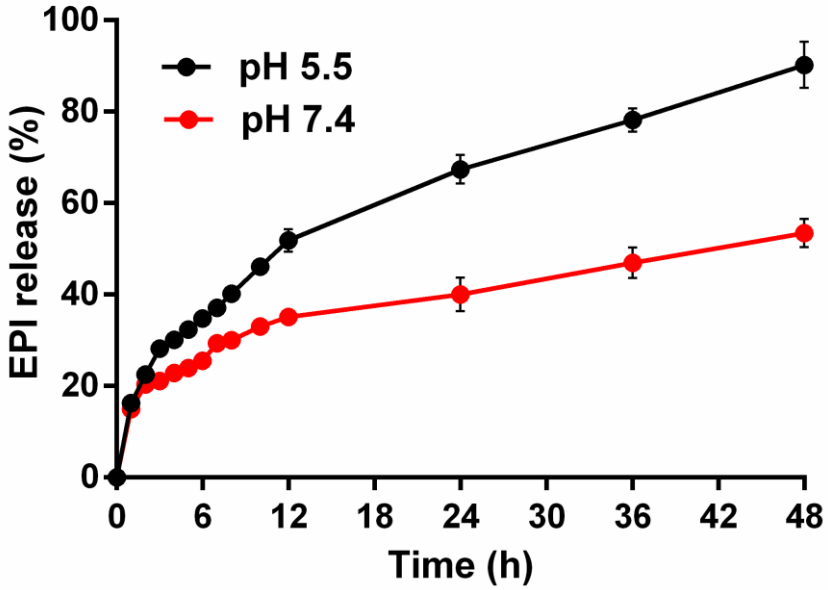

Figure 7.9. Time-dependent *in vitro* release profiles of EPI (in %) from CQDs@EPI⊂G5-Ac85 hybrids over 48 h in acetate buffer (pH 5.5, black) and in phosphate buffer saline (pH 7.4, red), respectively.

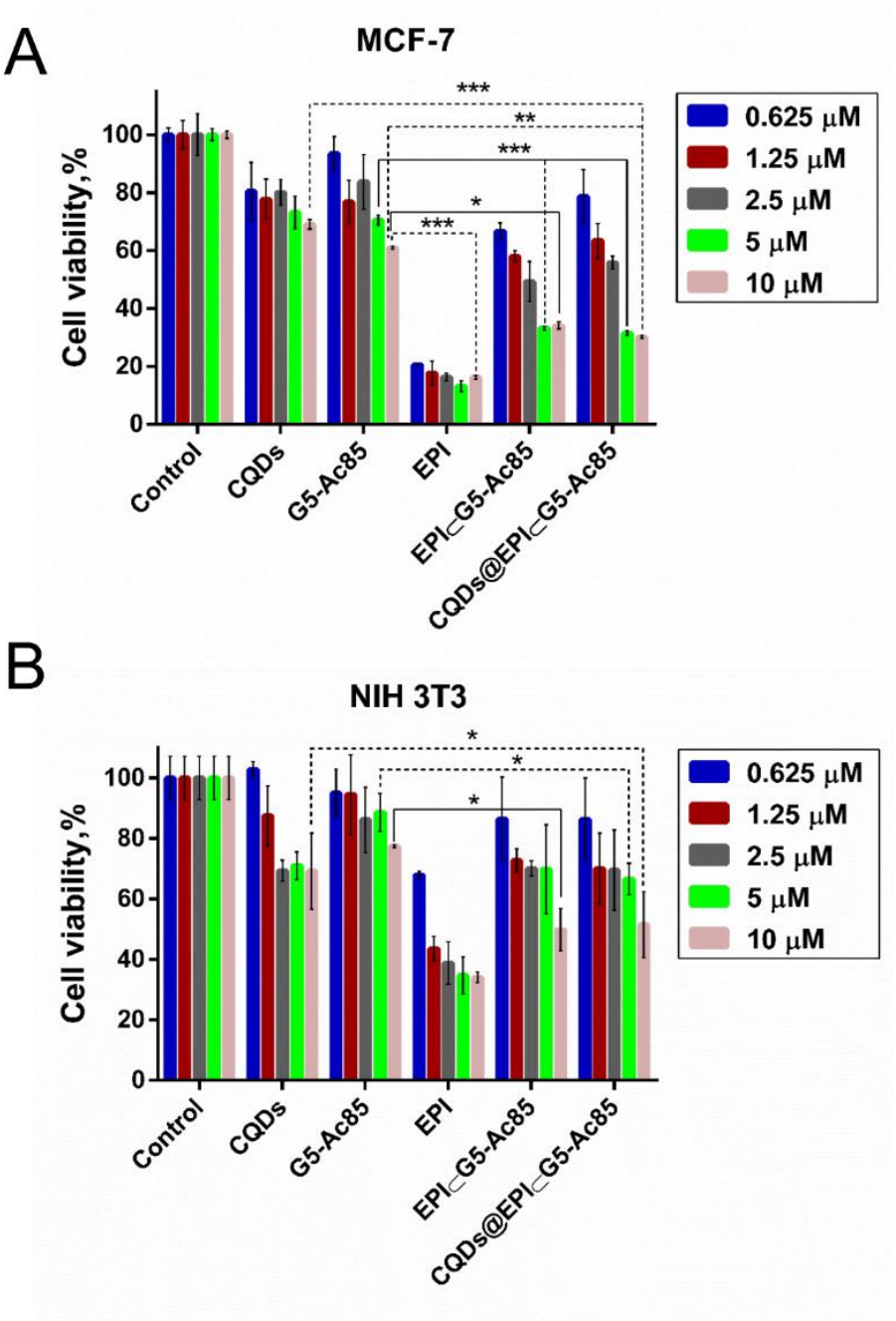

Figure 7.10. Viability of MCF-7 and NIH3T3 cells calculated by MTT assay after 48 h treatment with CQDs, G5-Ac85 dendrimers, EPI, EPI⊂G5-Ac85 complexes and CQDs@EPI⊂G5-Ac85 hybrids with varying EPI concentrations (0.625, 1.25, 2.5, 5 and 10 μM). EPI⊂G5-Ac85 complexes, CQDs@EPI⊂G5-Ac85 hybrids and free EPI had equivalent EPI concentrations. CQDs, G5-Ac85 and CQDs@EPI⊂G5-Ac85 hybrids had equivalent weight concentrations. Experiments were performed in triplicate. Two-way ANOVA with Tukey's multiple comparisons test was used to determine statistical difference between the group means (* $p < 0.05$, ** $p < 0.005$, *** $p < 0.001$).

7.2.6. Intracellular imaging

Next, CQDs were examined as fluorescent probes to monitor the intracellular trafficking of CQDs@EPI⊂G5-Ac85 hybrids in MCF-7 cells. Fluorescence microscope imaging is a promising technique to discern the cellular uptake of fluorescent nanomaterials. **Figure 7.11** shows the fluorescence microscopic images of MCF-7 cells incubated with CQDs, EPI, EPI⊂G5-Ac85 complexes and CQDs@EPI⊂G5-Ac85 hybrids under similar conditions. CQDs appeared intense green under blue illumination **(Figure 7.11 a)** and EPI emits red fluorescence under green light **(Figure 7.11 g)**. Hoechst 33342 dye was used as a fluorescence marker for nucleus and emitted blue fluorescence under UV light. After 12h incubation, CQDs were mostly internalized in the cell cytoplasm but could not enter the nucleus **(Figure 7.11 d)**.This suggests cytoplasmic region as the main cellular target of free CQDs (Wang et al., 2013b, Zhou et al., 2013b and Sachdev et al., 2015). Interestingly, there was a marked difference in the trafficking of free and encapsulated EPI. Free EPI molecules were mostly localized in the nuclear region as evident from the merged fluorescence image **(Figure 7.11 f-h)**. Probably, free EPI molecules penetrated through the plasma and nuclear membranes to enter the nuclei (Yordanov et al., 2013). Conversely, EPI⊂G5-Ac85 complexes were primarily found distributed in the cytoplasmic region **(Figure 7.11 j-l)**. Moreover, CQDs@EPI⊂G5-Ac85 hybrids were also traced in cell cytoplasm surrounding the nucleus and exhibited co-localization of green and red fluorescence (due to release of both CQDs and EPI, respectively) **(Figure 7.11 m-p)**.

The location of CQDs@G5-Ac85 hybrids in MCF-7 cells after internalization was visualized using lysotracker red, for fluorescence imaging of lysosomes. MCF-7 cells were incubated with CQDs@G5-Ac85 hybrids for 3 h and were then stained with lysotracker red. After incubation, green fluorescence of hybrids was clearly evident within cells which coincided with the lysotracker red fluorescence **(Figure 7.12)**. This observation indicated that CQDs@G5-Ac85 hybrids sufficiently accumulated in the cells after internalization and were thereafter transported to lysosomes. These findings suggest lysosomes as the target organelles of CQDs@G5-Ac85 hybrids. The obtained findings demonstrate the significance of luminescent CQDs as fluorescent tracers for cellular delivery of therapeutic agents. Surprisingly, from the fluorescent micrographs an enhancement in the intensity of green fluorescent signal of CQDs in CQDs@G5-Ac85 hybrids was monitored. This can be ascribed to the improved delivery and therefore enhanced uptake of CQDs bound to G5-Ac85 dendrimers.

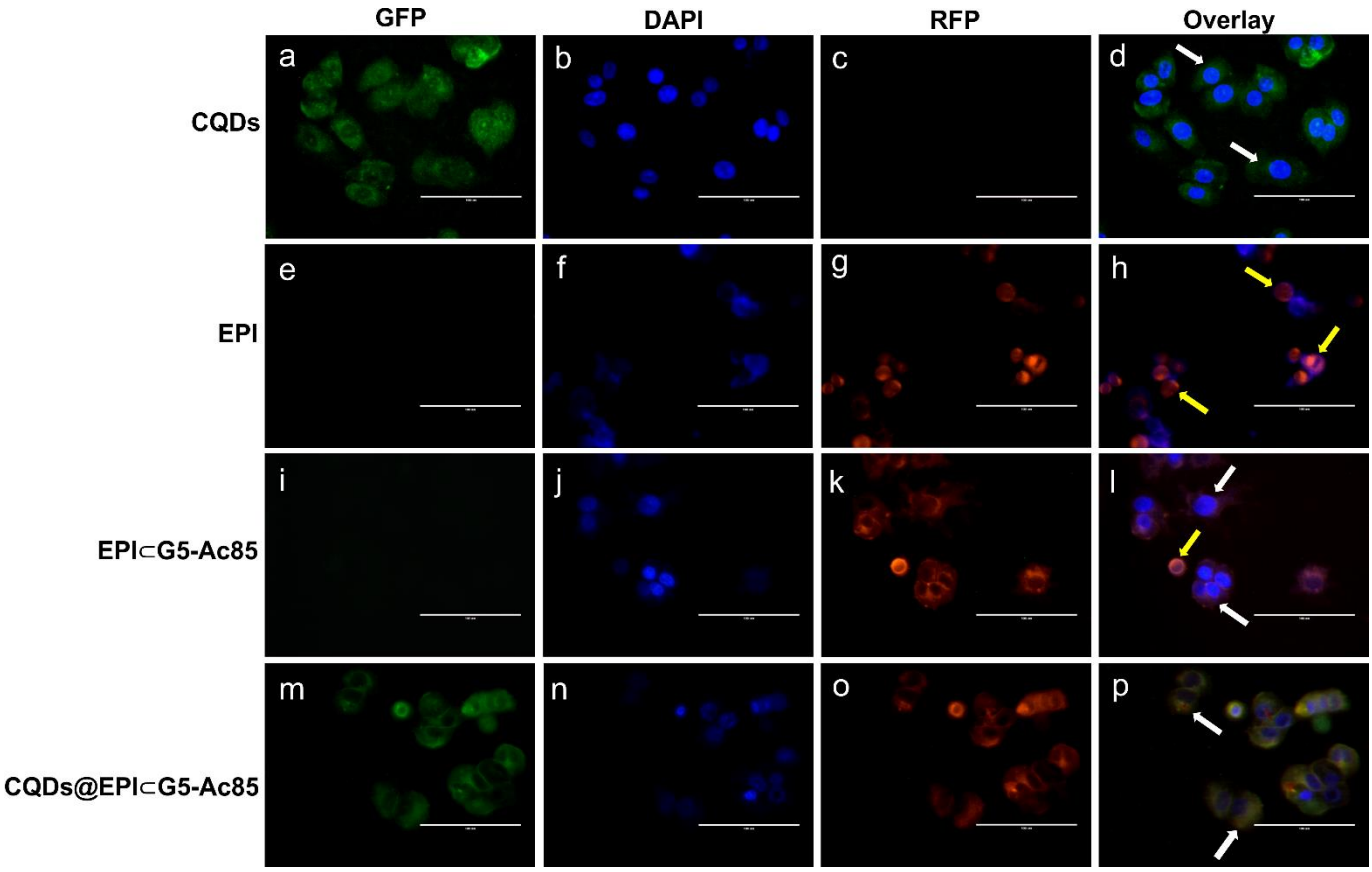

Figure 7.11. Fluorescence microscope images of MCF-7 cells incubated with free CQDs, free EPI, EPI⊂G5-Ac85 complexes and CQDs@EPI⊂G5-Ac85 hybrids (with equivalent EPI concentration 5 µM) after 12 h. Intracellular distribution of CQDs is shown in (a-d); (e-h) represent cells treated with EPI; (i-l) and (m-p) depicts cells treated with EPI⊂G5-Ac85 and CQDs@EPI⊂G5-Ac85 hybrids, respectively. Yellow arrows: nuclear localization; white arrows: cytoplasmic localization. (Scale bar = 100 µm).

7.2.7. Quantitating the cellular uptake

Further, experiments were conducted to quantitate the intracellular uptake of hybrids. For this, MCF-7 cells were incubated with free CQDs, EPI⊂G5-Ac85 complexes and CQDs@EPI⊂G5-Ac85 hybrids (with equivalent concentration of CQDs) for 3 h, under same conditions. After incubation, cells were analyzed using flow cytometry without use of any other dye. The cellular uptake was measured in terms of percentage of cells expressing green fluorescence (due to uptake of CQDs). The flow cytometric analysis revealed that CQDs were internalized by almost 70 % cells compared to cells incubated without CQDs (control). However, about 80 % cells could uptake CQDs@EPI⊂G5-Ac85 hybrids under same parameters **(Figure 7.13 A)**. For EPI⊂G5-Ac85 treated cells, the observed fluorescence (~ 17 %) can primarily be due to the autoflourescent signal of EPI. In a nutshell, both qualitative and quantitative results indicated that G5-Ac85 dendrimers could augment the intracellular distribution and uptake of CQDs. This aspect offers new horizon in development of dendrimer based multifunctional vehicles for delivery of imaging and anticancer agents. Although, the exact mechanism of cellular uptake and ultimate cellular fate of nanomaterials in cancer cells is still under investigation. Recent reports suggest clathrin dependent receptor-mediated endocytosis (CME) as the main pathway for internalization of positively charged nanoparticles in MCF-7 cells (Kitchens et al., 2007, 2008 and Sahay et al., 2010). For CQDs@EPI⊂G5-Ac85 hybrids carry an overall positive charge, the probable mechanism of internalization could be classical clathrin-mediated endocytosis.

7.2.8. Cell cycle and FE-SEM analysis

EPI is known to inhibit the topoisomerase II activity in MCF-7 cells with induction of oxidative DNA damage. Thereafter, cells with failed DNA repair mechanisms, undergo apoptosis. (Fornari et al., 1994, Olinski et al., 2002 and Lo et al., 2013). Subsequently, we examined the effect of EPI on cell cycle and hence DNA damage by PI staining using flow cytometer. **Figure 7.13 B** represents the cell cycle distribution pattern of MCF-7 cells incubated with CQDs, EPI⊂G5-Ac85 complexes and CQDs@EPI⊂G5-Ac85 hybrids (EPI concentration = 5 μM) for 48 h. The flow cytometric analysis showed that untreated and CQDs treated cells were arrested primarily in G0/G1 phase. Contrarily, EPI⊂G5-Ac85 complexes or CQDs@EPI⊂G5-Ac85 hybrids treated cells mainly accumulated in sub G0/G1 phase i.e., 65.9 ± 1.41 % and 75.7 ± 0.85 %, respectively with respect to untreated cells (17 ± 0.42 %). Moreover, a reduction in S phase was monitored upon EPI exposure. This implicates DNA damage by EPI⊂G5-Ac85 and CQDs@EPI⊂G5-Ac85 treatment. A substantial increase in sub G0/G1 phase and reduction in S phase population, is indicative of apoptotic mode of cell death (Darzynkiewicz et al., 1992 and Riccardi et al., 2006). After PI staining, CQDs@EPI⊂G5-Ac85 treated cells were examined under FE-SEM to monitor

cell morphology alterations. **Figure 7.13 C**, shows the typical morphology of healthy MCF-7 cells. The cells were well adhered to the surface with no signs of membrane constrictions or damage. However, CQDs@EPI⊂G5-Ac85 treated cells were round and loosely attached **(Figure 7.13 D)**. Membrane blebbing and appearance of apoptotic bodies in treated cells confirm the occurrence of apoptosis (Rello et al., 2005).

7.2.9. Intracellular ROS production

Manifestation of free radical generation can result in oxidative stress in cancer cells, causing apoptosis and finally cell death. The ability of free EPI to induce ROS production in breast cancer cells is well documented (Lo et al., 2013). As a proof of concept, we exposed MCF-7 cells to CQDs@EPI⊂G5-Ac85 hybrids with different EPI concentrations for ROS production. The percentage of cells expressing ROS were measured by DCF fluorescence. **Figure 7.14**, shows the flow cytometric images of cells with green DCF fluorescence. Each spot in the image reflects the cell expressing ROS. CQDs@EPI⊂G5-Ac85 hybrids were found to induce ROS production in a dose-dependent manner **(Figure 7.14 b-e)**. For instance, CQDs@EPI⊂G5-Ac85 hybrids with 5 μM EPI, could elevate the ROS levels by ~86.7 % with regard to untreated cells (0.61 %) **(Figure 7.14 a, e)**. Such increased cellular oxidative stress can be held responsible for causing DNA damage in cancer cells. It is imperative to mention that fluorescence of CQDs did not interfere during flow measurements owing to its relatively weak signal than commercial DCFH-DA dye. Furthermore, we used NIH3T3 cells to examine the ROS levels in normal cells when exposed to CQDs@EPI⊂G5-Ac85 hybrids. With increase in the hybrids concentration, the ROS levels in NIH3T3 cells increased from 5.2 % to 13.1 % **(Figure 7.15).** However, under similar treatment concentrations the intracellular ROS production was more in MCF-7 than NIH3T3 cells. Thus, CQDs@EPI⊂G5-Ac85 hybrids were proficient in inducing apoptosis by causing oxidative stress and thus, DNA damage in drug resistant breast cancer cells.

7.2.10. Gene expression studies

To ascertain the molecular signalling pathway involved in CQDs@EPI⊂G5-Ac85 hybrid mediated apoptosis, gene expression analysis was done. Semi-quantitative RT-PCR was utilized to validate the expression levels of apoptotic (p53, bax, bad, caspase 3, and c-myc) and anti-apoptotic (bcl-xl) genes, respectively. **Figure 7.16 A** shows the RT-PCR analysis of apoptosis related genes and the computed fold change **(Figure 7.16 B)**. Elevated mRNA expressions of p53, bax, bad and caspase-3 were observed with down regulation of c-myc and bcl-xl mRNA levels in EPI, EPI⊂G5-Ac85 and CQDs@EPI⊂G5-Ac85 treated samples compared to untreated/CQDs treated cells. The expression of β-actin remained unaltered.

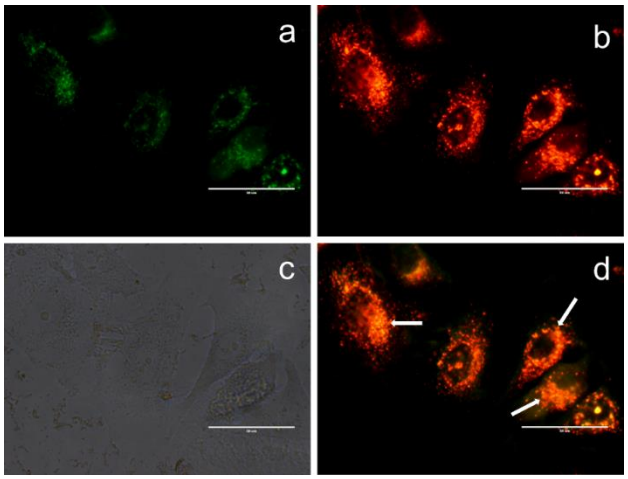

Figure 7.12. Fluorescence of MCF-7 cells after incubation with CQDs@G5-Ac85 hybrids. Fluorescence images of (a) CQDs@G5-Ac85 hybrids (green), (b) lysosomes (red), (c) bright field and (d) merged image. The white arrows in (d) indicate the overlay of CQDs@G5-Ac85 signals with the lysotracker red signals. The merged green and red signals appear yellow. (Scale bar = 50 µm)

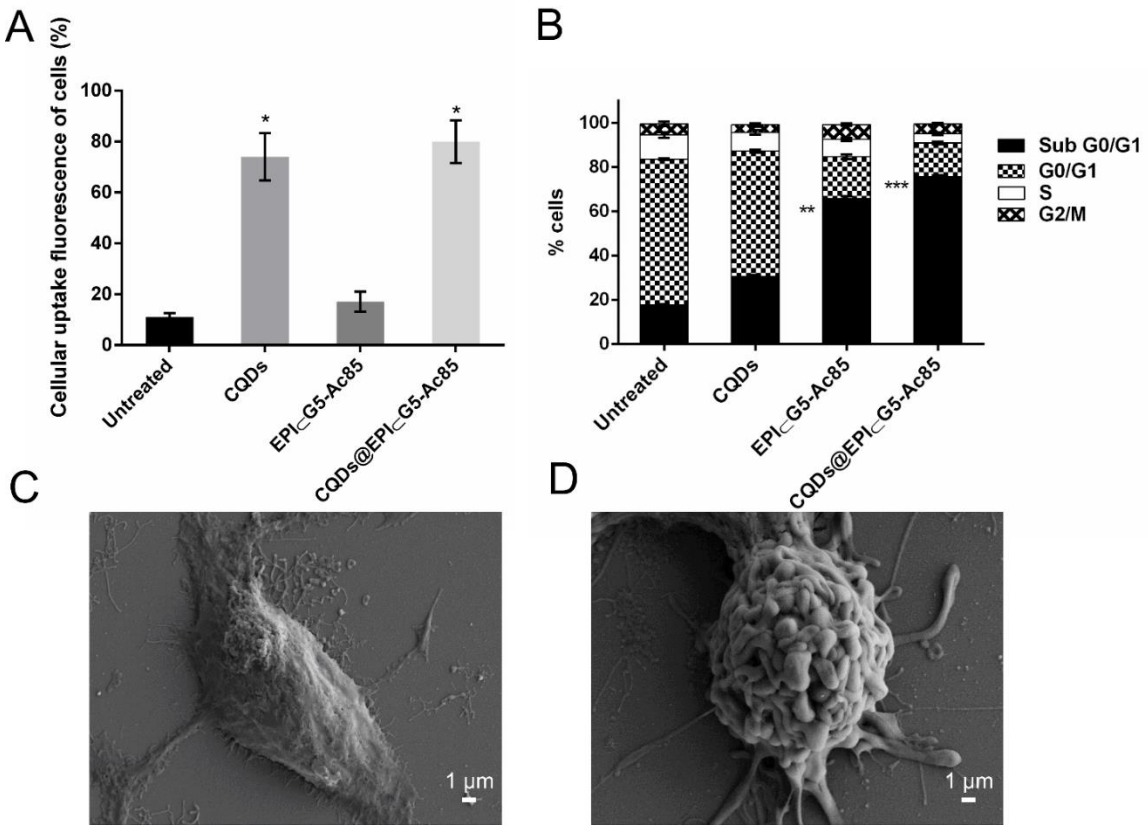

Figure 7.13. Quantitative cellular uptake in MCF-7 cells after 3 h by flow cytometer. The fluorescence intensity was recorded in channel 02 (505-560 nm). (B) Cell cycle distribution of different samples by flow cytometry. FE-SEM micrographs of (C) Untreated and (D) CQDs@EPI⊂G5-Ac85 hybrids treated MCF-7 cell indicating apoptotic cell death. (Scale bar = 1 µm). Statistical significance is denoted by * ($p < 0.05$), ** ($p < 0.005$), and *** ($p < 0.001$).

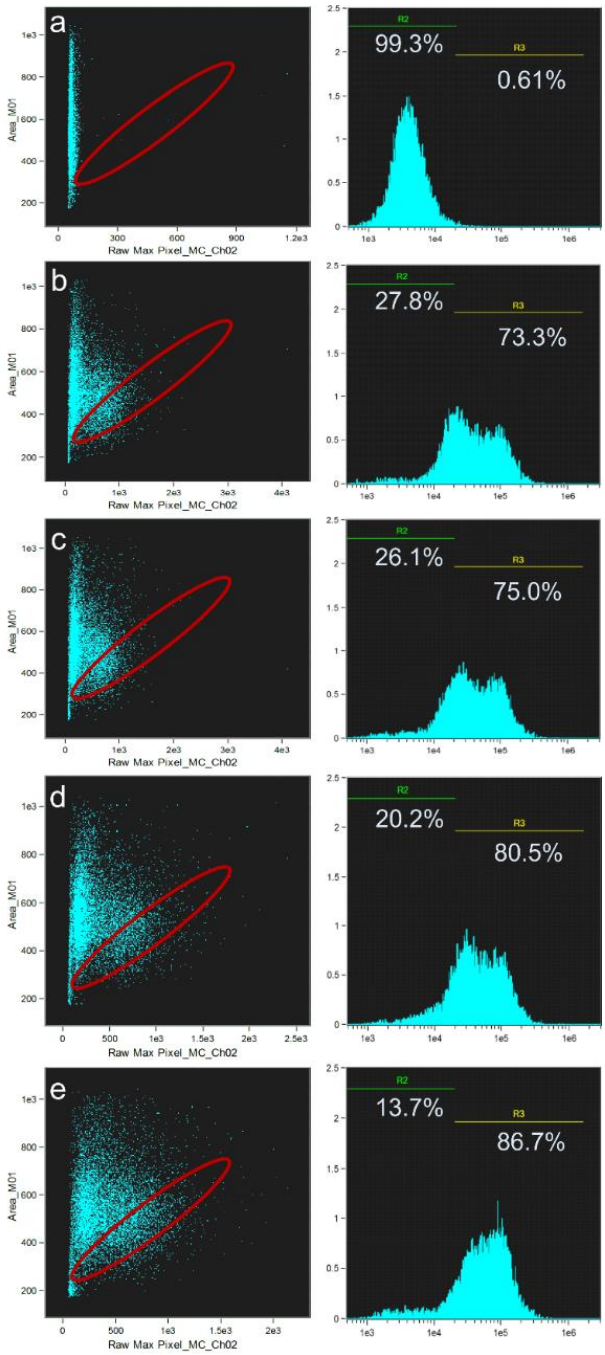

Figure 7.14. Flow cytometric analysis of ROS production in MCF-7 cells treated with CQDs@EPI⊂G5-Ac85 hybrids with varying concentrations of EPI. Untreated cells are shown in (a), (b-e) depicts cells treated with CQDs@EPI⊂G5-Ac85 hybrids with EPI concentration 0.625, 1.25, 2.5 and 5 μM, respectively. Left panel: dot plots of DCF fluorescence and right panel: corresponding fluorescence histogram.

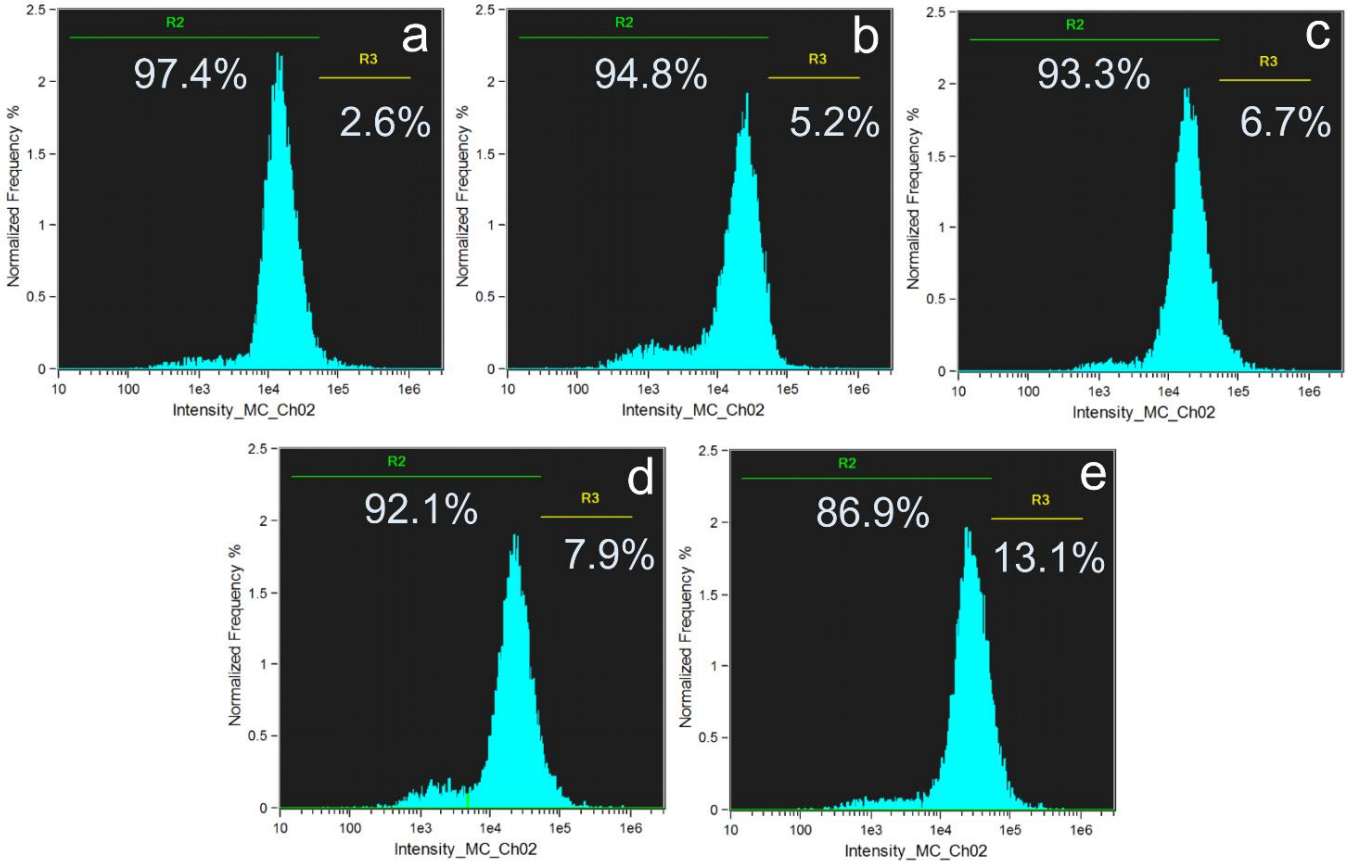

Figure 7.15. Flow cytometric analysis of ROS production in NIH3T3 cells treated with CQDs@EPI⊂G5-Ac85 hybrids with varying concentrations of EPI. Untreated cells are shown in (a), (b-e) depicts cells treated with CQDs@EPI⊂G5-Ac85 hybrids with EPI concentration 0.625, 1.25, 2.5 and 5 µM, respectively.

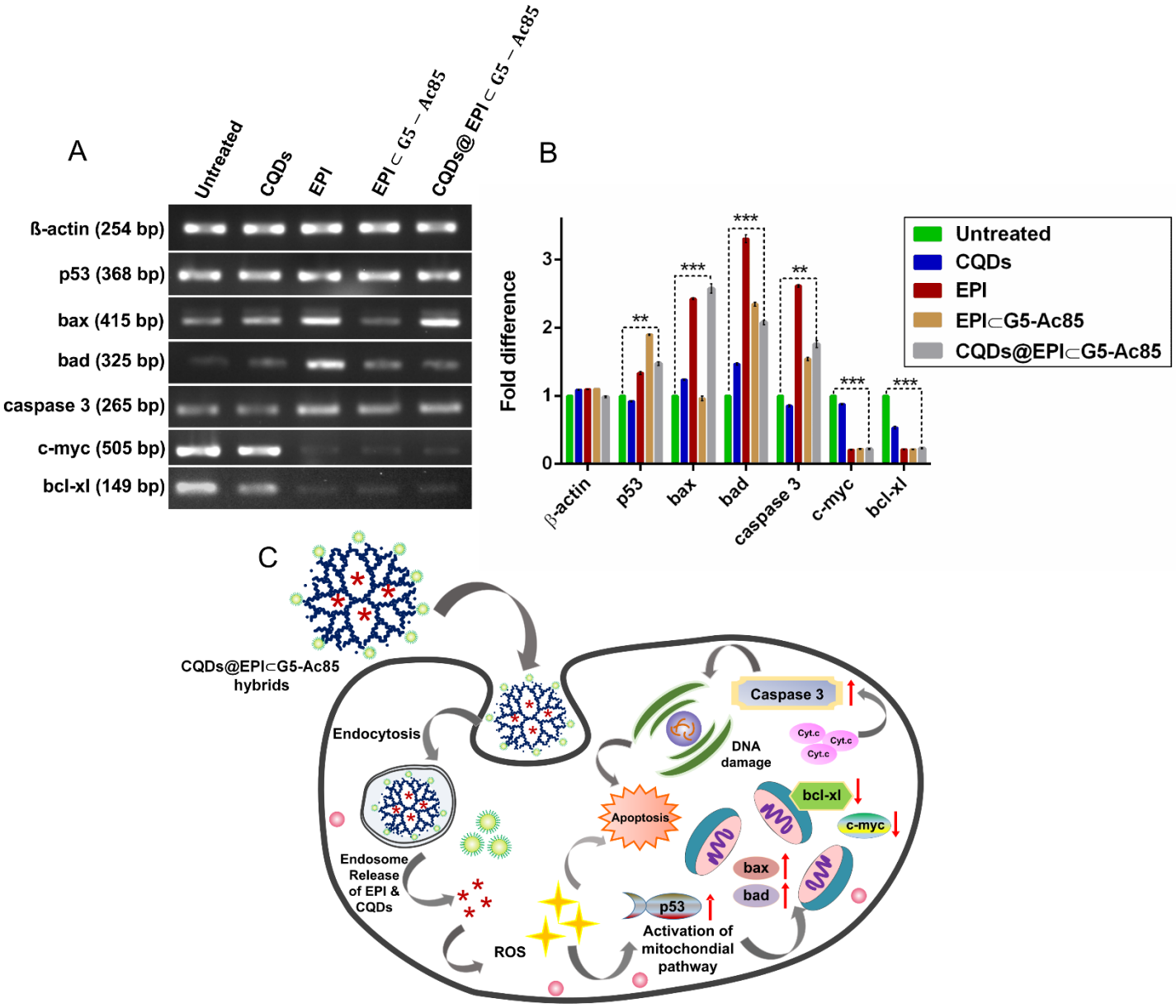

Figure 7.16 (A) Semi-quantitative RT-PCR analysis of apoptotic signalling genes, and (B) Fold difference in gene expression. Statistical significance between CQDs@EPI⊂G5-Ac85 treated vs untreated MCF-7 cells is denoted by ** ($p < 0.005$), and *** ($p < 0.001$). (C) Schematic illustration of cellular uptake and apoptotic events following CQDs@EPI⊂G5-Ac85 hybrid treatment.

A schematic illustration of the apoptotic events involved in CQDs@EPI⊂G5-Ac85 treatment is depicted in **Figure 7.16 C**. Internalization of CQDs@EPI⊂G5-Ac85 hybrids causes membrane destabilization and generation of ROS which in turn triggers activation of intrinsic/mitochondrial apoptosis pathway. EPI treatment results in transcriptional activation of p53 gene which is pivotal to promote apoptosis in tumor cells (Millour et al., 2011 and Hu et al., 2014). After treatment, the p53 mRNA levels significantly enhanced ($p < 0.005$) which indicate turning-on of p53 mediated gene signalling cascade. Bcl-xl, a member of bcl-2 family of proteins is known to protect cells from undergoing apoptosis. Hence, suppression of bcl-xl gene is essential for initiation of apoptotic events (Chao et al., 1998). A significant down regulation in bcl-xl gene ($p < 0.001$) in treated samples marks the onset of apoptosis. The transcription factor p53 further upregulates bax (bcl-2-associated X protein) and bad (bcl-2-associated death promoter) levels, which accelerates apoptosis (Wolter et al., 1997). Relocalization of bax from mitochondrial membrane to cytosol leads to outer membrane permeabilization (MOMP) and pore formation to allow cytochrome c (cyt. c) release. The released cyt.c triggers activation of cysteine-aspartic acid proteases (caspase 3) which are the key executioners of apoptosis (Liu et al., 1996). Caspase 3 is identified to induce various biochemical changes and morphological changes in cancer cells (Porter et al., 1999). In EPI treated cells a significant upregulation of caspase 3, ($p < 0.005$) co-relates with the observed DNA damage and formation of apoptotic bodies. Also, EPI is identified to supress the c-myc mRNA levels (Lee et al., 2013). We also observed drastically reduced c-myc mRNA levels, indicating EPI induced toxicity in breast cancer cells.

In summary, self-assembled CQDs@EPI⊂G5-Ac85 hybrids were synthesized for monitoring the cellular distribution of EPI in MCF-7 cells. The obtained findings strongly suggest that CQDs@EPI⊂G5-Ac85 hybrids induced apoptosis in breast cancer cells through oxidative DNA damage and trigger p53 mediated gene signalling cascade. Understanding of cellular and molecular mechanisms behind CQDs@EPI⊂G5-Ac85 mediated cell death can be vital in designing strategies for improved cancer therapy. Moreover, such complicated regulatory pathway necessitates the development of multifunctional nanovehicle like G5-Ac dendrimers for real-time delivery of anticancer agents and fluorescent probes such as CQDs for improved cancer diagnostics and therapy.

CHAPTER 8

CONCLUDING REMARKS

In this chapter the conclusions drawn from the present work are mentioned and the future scope of the work has been described.

CHAPTER 8

CONCLUDING REMARKS

8.1. Conclusions

The main aim of this thesis was to explore the *in vitro* capabilities of various PAMAM dendrimer based nanomaterials as carriers for anticancer applications. Considering the complete work, some significant conclusions can be drawn. PAMAM dendrimers (with EDA core and amine termini) are interesting nanomaterials to hold and deliver agents to cancer cells. Moreover, dendrimers with abundant terminal amine groups can serve as templates or can stabilize the surface of metal NPs. This is indeed remarkable as it discourages the need of unnecessary chemical reagents. Such dendrimer stabilized metal NPs (such as DsAgNPs) with free internal cavities can further act as hosts to encapsulate small drug molecules (either hydrophobic or hydrophilic, like 5-FU). By this strategy, a multicomponent system can be generated to exhibit synergistic anticancer effects. When different therapeutic agents are united in 'one system' the required dose to exert the anticancer effect is far below than when the agents are used singularly. Results from chapter 4, justify this claim wherein 5-FU@DsAgNCs in low concentrations could induce synergistic anticancer effects in lung and breast cancer cells. Therefore, such multicomponent dendrimer nanocomposites are advantageous to attain anticancer synergism.

PAMAM dendrimers can also serve as a durable component to develop hybrid nanogels with an oppositely charged polymer by forming permanent chemical bonds. By using carbodiimide chemistry, nanosized gels can be developed of sodium alginate and PAMAM dendrimers for delivery of anticancer agents. Results from chapter 5 clearly indicate high encapsulation efficiencies and better physical and drug release properties of EPI loaded AG-G5 hybrid nanogels than simple AG gels. These EPI⊂AG-G5 nanogels could accumulate in MCF-7 cells in a dose and time dependent manner. Subsequently, they could induce MCF-7 cell death by trigger of apoptosis.

A surface modification of G5 PAMAM dendrimers was carried out by adding lipid-like tails of myristic acid on the periphery. Such hydrophobically modified PAMAM dendrimers mimic closely the liposomes or biological membranes and can preserve and ferry the therapeutic cargo

across the cancer cell membranes suitably. Our results described in chapter 6, were a proof-of-concept to this hypothesis. Such My-*g*-G5 dendrimers could encapsulate the poorly water-soluble TAM, an anti-estrogen and enhanced its solubility manifold. By using a fluorescent dye coumarin-6, we found that My-*g*-G5 dendrimers could pave their way across the MCF- membranes to enter and sufficiently accumulate in the cellular cytoplasm. After cellular entry, the dendrimers released the TAM molecules to exert anticancer effects. Taking together our findings, such surface engineered PAMAM dendrimers behave as a unique nanoscale delivery system to combine the advantages of both lipid based carriers and dendritic systems for anticancer therapeutics.

Native PAMAM dendrimers (with amine termini) are associated with some inherent toxicities which makes it difficult to take dendrimer based nanomedicines to clinical trials despite incredible advantages. To resolve this, as described in chapter 7 the dendrimer surface was modified by partial acetylation (i.e. some acetyl groups were introduced on surface). This reduced the overall surface charge of dendrimers making them cytocompatible. Such partially acetylated dendrimers apart from being biocompatible had remarkable stability and aqueous solubility. Hydroxyl-functionalized CQDs could electrostatically interact with cationic acetylated dendrimers to form fluorescent hybrids. Such hybrids can track the uptake of chemotherapeutic agents. Our results demonstrated, that CQDs@G5-Ac85 hybrids could monitor the cellular distribution of EPI in MCF-7. Owing to the therapeutic profile of EPI, these hybrids also displayed appreciable killing of breast cancer cells. Overall, these PAMAM based hybrids were effective for theranostic applications.

8.2. Future scope of work

Taking in account the observed potential of PAMAM dendrimer based nanocarriers *in vitro* for anticancer applications, the biological performance of these nanoformulations can be next tested *in vivo*.

- For *in vivo* experiments, different mouse models bearing tumors can be developed. PAMAM dendrimer nanoformulations can then be administered through various routes to observe the tumor inhibition and biodistribution. Further, as discussed in Chapter 2 the pharmacokinetic profile of these drug loaded PAMAM nanocarriers can be investigated to study the ultimate fate of these nanomaterials.
- To attain target specificity, 5-FU@DsAgNCs, EPI⊂AG-G5 nanogels, CQDs@EPI⊂G5-Ac85 hybrids and My-g-G5/TAM complexes can be functionalized by conjugating cell-specific ligands such as antibodies, peptides, carbohydrate residues for active

targeting of cancer cells. The anticancer action of these dendrimer formulations can then be studied.

- Interactions between these dendrimer formulations and cellular membranes as well as their uptake mechanisms can also be studied by using specific endocytic-inhibitors. For instance, hypertonic sucrose, chlorpromazine and potassium depletion are inhibitors of clathrin dependent endocytosis; methyl-β-cyclodextrin (MβCD), filipin, nystatin and cholesterol oxidase are inhibitors for caveolae dependent endocytosis; amiloride, cytochalasin D and rottlerin can block macropinocytosis.
- PAMAM dendrimers (with amine termini) can further be used to deliver specific anticancer genes such as suicide gene (CD::UPRT) to cancer cells and can concurrently deliver the pro-drug 5-Fluorocytosine (5-FC). This can be another approach to inhibit cancer proliferation and instigate cell death.
- Various approaches directed towards the amelioration of toxicity of native PAMAM dendrimers can developed.

REFERENCES

1. Abbasi E., Aval S. F., Akbarzadeh A., Milani M., Nasrabadi H. T., Joo S. W., Hanifehpour Y., Nejati-Koshki K. and Pashaei-Asl R., Dendrimers: synthesis, applications, and properties. *Nanoscale Res. Lett.*, 9, 247 (2014).
2. Adeli M., Soleyman R., Beiranvanda Z. and Madani F., Carbon nanotubes in cancer therapy: a more precise look at the role of carbon nanotube–polymer interactions. *Chem. Soc. Rev*., 42, 5231-5256 (2013).
3. Adronov A. and Fréchet J.M. J., Light-harvesting dendrimers. *Chem. Commun*., 1701-1710 (2000).
4. Agashe H.B, Babbar A.K, Jain S., Sharma R.K, Mishra A.K., Asthana A., Garg M., Dutta T. and Jain N.K., Investigations on biodistribution of technetium-99m-labeled carbohydrate-coated poly(propylene imine) dendrimers. *Nanomedicine*., 3, 120-127 (2007).
5. Ahlers P., Frisch H., Spitzer D., Vobecka Z., Vilela F. and Besenius P., The synthesis of dendritic EDOT-peptide conjugates and their multistimuli-responsive self-assembly into supramolecular nanorods and fibers in water. *Chem. Asian J.*, 9, 2052-2057 (2014).
6. Al-Jamal K. T., Ramaswamy C. and Florence A. T.,Supramolecular structures from dendrons and dendrimers. *Adv. Drug Delivery Rev*., 57, 2238-2270 (2005).
7. Allen S., Sotos J., Sylte M. J. and Czuprynski C. J., Use of Hoechst 33342 staining to detect apoptotic changes in bovine mononuclear phagocytes infected with mycobacterium avium subsp. paratuberculosis. *Clin. Diagn. Lab. Immunol*., 8, 460-464 (2001).
8. Allen T.M. and Cullis P.R., Drug delivery systems: entering the mainstream. *Science*, 303, 1818-1822 (2004).
9. Allen T.M., Ligand-targeted therapeutics in anticancer therapy. *Nat. Rev. Cancer*, 2, 750-763 (2002).
10. American Cancer Society. Cancer Facts & Figures 2014. *American Cancer Society*, Atlanta (2014).
11. American Cancer Society. Global Cancer Facts & Figures 3rd Edition. *American Cancer Society*, Atlanta (2015).

12. Appel R., Fuchs J., Tyrrell S.M., Korevaar P.A., Stuart M.C.A., Voets I.K., Schönhoff M. and Besenius P., Steric constraints induced frustrated growth of supramolecular nanorods in water. *Chem. Eur. J.*, 21, 19257-19264 (2015).
13. AshaRani P. V., Low Kah Mun G., Hande M. P. and Valiyaveettil S.,Cytotoxicity and genotoxicity of silver nanoparticles in human cells. *ACS Nano*, 3, 279-290 (2009).
14. Balakrishnan B. and Banerjee R., Biopolymer-based hydrogels for cartilage tissue engineering. *Chem Rev.*, 111, 4453-4474 (2011).
15. Balasubramanian S., Girija A. R., Nagaoka Y., Fukuda T., Iwai S., Kizhikkilot V., Kato K., Maekawa T. and Nair Sakthikumar D. An 'all in one' approach for simultaneous chemotherapeutic, photothermal and magnetic hyperthermia mediated by hybrid magnetic nanoparticles. *RSC Adv*., 5, 25066-25078 (2015).
16. Banerjee R., Maiti S., Dey D. and Dhara D., Polymeric nanostructures with pH-labile core for controlled drug release. *J. Colloid Interface Sci*., 462, 176-182 (2016).
17. Banerjee R., Parida S., Maiti C., Mandal M. and Dhara D., pH-degradable and thermoresponsive watersoluble core cross-linked polymeric nanoparticles as potential drug delivery vehicle for doxorubicin. *RSC Adv*., 5, 83565-83575 (2015).
18. Barrett T., Ravizzini G., Choyke P.L. and Kobayashi H., Dendrimers application related to bioimaging. *IEEE Eng. Med. Biol. Mag*., 28, 12-22 (2009).
19. Bartkowiak D., Hemmer J. and Röttinger E., Dose dependence of the cytokinetic and cytotoxic effects of epirubicin *in vitro*. *Cancer Chemother. Pharmacol*., 30, 189-192 (1992).
20. Baselga. J., Manikhas A., Cortés J., Llombart A., Roman L., Semiglazov V. F., Byakhov M., Lokanatha D., Forenza S., Goldfarb R. H., Matera J., Azarnia N., Hudis C. A. and Rozencweig M., Phase III trial of nonpegylated liposomal doxorubicin in combination with trastuzumab and paclitaxel in HER2-positive metastatic breast cancer. *Ann. Oncol.*, 25, 592-598 (2014).
21. Bendtsen S. T. and Wei M., Synthesis and characterization of a novel injectable alginate−collagen−hydroxyapatite hydrogel for bone tissue regeneration. *J. Mater. Chem. B*, 3, 3081-3090 (2015).
22. Berger J., Reist M., Mayer J. M., Felt O., Peppas N. A. and Gurny R., Structure and interactions in covalently and ionically crosslinked chitosan hydrogels for biomedical applications. *Eur. J. Pharm. Biopharm.*, 57, 19-34 (2004).

23. Bertrand N., Wu J., Xu X., Kamaly N. and Farokhzad O.C., Cancer nanotechnology: the impact of passive and active targeting in the era of modern cancer biology. *Adv. Drug Deliv. Rev.*, 66, 2-25 (2014).
24. Besenius P., Heynens J.L., Straathof R., Nieuwenhuizen M.M., Bomans P.H., Terreno E., Aime S., Strijkers G.J., Nicolay K. and Meijer E.W., Paramagnetic self-assembled nanoparticles as supramolecular MRI contrast agents. *Contrast Media Mol. Imaging*, 7, 356-361 (2012).
25. Bhadra D., Bhadra S., Jain S. and Jain N.K., A PEGylated dendritic nanoparticulate carrier of fluorouracil. *Int. J. Pharm.*, 257, 111-124 (2003).
26. Bhushan B., Dubey P., Kumar S. U., Sachdev A., Matai I. and Gopinath P., Bionanotherapeutics: niclosamide encapsulated albumin nanoparticles as a novel drug delivery system for cancer therapy. *RSC Adv*., 5, 12078-12086 (2015).
27. Bhyrappa P., Young J. K., Moore J. S. and Suslick K. S., Dendrimer-metalloporphyrins: synthesis and catalysis. *J. Am. Chem. Soc.*, 118, 5708-5711 (1996).
28. Boas U., Christensen J. B. and Heegaard P. M. H., Dendrimers in medicine and biotechnology : new molecular tools. *RSC Publishing* (2006).
29. Bradshaw D. S. and Andrews D. L., Mechanisms of light energy harvesting in dendrimers and hyperbranched polymers. *Polymers*, 3, 2053-2077 (2011).
30. Brannon-Peppas L. and Blanchette J. O., Nanoparticle and targeted systems for cancer therapy. *Adv. Drug Deliv. Rev*., 56, 1649-1659 (2004).
31. Brigger I., Dubernet C. and Couvreur P., Nanoparticles in cancer therapy and diagnosis. *Adv. Drug Deliv Rev.*, 54, 631-651 (2002).
32. Buczkowski A., Urbaniak P. and Palecz B., Thermochemical and spectroscopic studies on the supramolecular complex of PAMAM-NH_2 G4 dendrimer and 5-fluorouracil in aqueous solution. *Int. J. Pharm*., 428, 178-182 (2012a).
33. Buczkowski A., Piekarski H. and Palecz B., Stoichiometry and equilibrium constant of the complex of PAMAM-NH_2 G4 and 5-fluorouracil. *J. Mol. Liq*., 173, 8-12 (2012b).
34. Buhleier E., Wehner W. and Vogtle F., Cascade and Nonskid-chain-like Synthesis of Molecular Cavity Topologies. *Synthesis*, 2, 155-158 (1978).
35. Caminade A. M. and Turrin C.O.,Dendrimers for drug delivery. *J. Mater. Chem. B*, 2, 4055-4066 (2014).
36. Cao W., Zhou J., Mann A., Wang Y. and Zhu L.,Folate-functionalized unimolecular micelles based on a degradable amphiphilic dendrimer-like star polymer for cancer cell-targeted drug delivery. *Biomacromolecules*, 12, 2697-2707 (2011).

37. Cattel L., Ceruti M. and Dosio F., From conventional to stealth liposomes: a new frontier in cancer chemotherapy. *Tumori.*, 89, 237-249 (2003).
38. Chairuangkitti P., Lawanprasert S., Roytrakul S., Aueviriyavit S., Phummiratch D., Kulthong K., Chanvorachote P. and Maniratanachote R., Silver nanoparticles induce toxicity in A549 cells via ROS-dependent and ROS-independent pathways. *Toxicol. In Vitro*, 27, 330-338 (2013).
39. Chang Y., Li Y., Meng X., Liu N., Sun D., Liu H. and Wang J., Dendrimer functionalized water soluble magnetic iron oxide conjugates as dual imaging probe for tumor targeting and drug delivery. *Polym. Chem.*, 4, 789-794 (2013).
40. Chao D. T. and Korsmeyer S. J., BCL-2 family: regulators of cell death. *Annu. Rev. Immunol*., 16, 395-419 (1998).
41. Chen H.T., Neerman M.F., Parrish A.R. and Simanek E.E., Cytotoxicity, hemolysis, and acute *in vivo* toxicity of dendrimers based on melamine, candidate vehicles for drug delivery. *J. Am Chem. Soc.*, 126, 10044-10048 (2004).
42. Chen Y., Wang G., Kong D., Zhang Z., Yang K., Liu R., Zhao W. and Xu Y.,Double-targeted and double-enhanced suicide gene therapy mediated by generation 5 polyamidoamine dendrimers for prostate cancer. *Mol. Carcinog.*, 52, 237-246 (2013a).
43. Chen Q., Li K., Wen S., Liu H., Peng C., Cai H., Shen M., Zhang G. and Shi X., Targeted CT/MR dual mode imaging of tumors using multifunctional dendrimer-entrapped gold nanoparticles. *Biomaterials*, 34, 5200-5209 (2013b).
44. Cheng M., He B., Wan T., Zhu W., Han J., Zha B., Chen H., Yang F., Li Q., Wang W., Xu H. and Ye T.,5-Fluorouracil nanoparticles inhibit hepatocellular carcinoma via activation of the p53 pathway in the orthotopic transplant mouse model. *PLoS One*, 7, 47115 (2012).
45. Cheng Y., Xu Z., Ma M. and Xu T.,Dendrimers as drug carriers: applications in different routes of drug administration. *J. Pharm. Sci.*, 97, 123-143 (2008).
46. Chiang W. H., Ho V. T., Huang W. C., Huang Y. F., Chern C. S. and Chiu H. C., Dual stimuli-responsive polymeric hollow nanogels designed as carriers for intracellular triggered drug release. *Langmuir*, 28, 15056-15064 (2012).
47. Chou T.C., Theoretical basis, experimental design, and computerized simulation of synergism and antagonism in drug combination studies. *Pharmacol Rev.*, 58, 621-681 (2006).
48. Cohen J. J., Duke R. C., Fadok V. A. and Sellins K. S., Apoptosis and programmed cell death in immunity. *Annu. Rev. Immunol*., 10, 267-293 (1992).

49. Crooks R.M., Zhao M., Sun L., Chechik V. and Yeung L.K., Dendrimer-encapsulated metal nanoparticles: synthesis, characterization, and applications to catalysis. *Acc. Chem. Res*., 34, 181-190 (2001).
50. D'Emanuele A. and Attwood D., Dendrimer-drug interactions. *Adv. Drug Deliv. Rev.*, 57, 2147-2162 (2005).
51. Dandliker P. J., Diederich F., Zingg A., Gisselbrecht J.P., Gross M., Louati, A. and Sanford E., Dendrimers with porphyrin cores: synthetic models for globular heme proteins. *Helv. Chim. Acta*, 80, 1773-1801 (1997).
52. Darzynkiewicz Z., Bruno S., Del Bino G., Gorczyca W., Hotz M. A., Lassota P. and Traganos F., Features of apoptotic cells measured by flow cytometry. *Cytometry*, 13, 795-808 (1992).
53. Datta K. K. R., Kozak O., Ranc V., Havrdova M., Bourlinos´ A. B., Šafař ovaˇ K., Hola´ K., Toma´nkova´ K., Zoppellaro G.,´Otyepkaa M. and Zboril R., Quaternized carbon dot-modified grapheneˇoxide for selective cell labelling−controlled nucleus and cytoplasm imaging. *Chem. Commun.*, 50, 10782-10785 (2014).
54. DeFever R.S., Geitner N.K., Bhattacharya P., Ding F., Ke P.C. and Sarupria S., PAMAM dendrimers and graphene: materials for removing aromatic contaminants from water. *Environ. Sci. Technol.*, 49, 4490-4497 (2015).
55. Denkewalter R.G., Kolc J. and Lukasavage W.J., Macromolecular highly branched homogenous compound based on lysine units. *US patent* 4, 289, 872 (1981).
56. Desai N., Trieu V. and Yao R., Increased endothelial transcytosis of nanoparticle albumin-bound paclitaxel (ABI-007) by endothelial gp60 receptors: a pathway inhibited by Taxol. *Proc SABCS*, 1071 (2004).
57. Desai N., Trieu V., Yao Z., Louie L., Ci S., Yang A., Tao C., De T., Beals B., Dykes D., Noker P., Yao R., Labao E., Hawkins M. and Soon-Shiong P.,Increased antitumor activity, intratumor paclitaxel concentrations, and endothelial cell transport of cremophor-free, albumin-bound paclitaxel, ABI-007, compared with cremophor-based paclitaxel. *Clin. Cancer Res.*, 12, 1317-1324 (2006).
58. Devulapally R., Sekar T. V. and Paulmurugan R., Formulation of anti-miR-21 and 4-hydroxytamoxifen co-loaded biodegradable polymer nanoparticles and their antiproliferative effect on breast cancer cells. *Mol. Pharmaceutics*, 12, 2080-2092 (2015).

59. Dong W., Zhou S., Dong Y., Wang J., Ge X. and Sui L., The preparation of ethylenediamine-modified fluorescent carbon dots and their use in imaging of cells. *Luminescence*, DOI: 10.1002/bio.2834 (2015).
60. Dong X. and Mumper R.J.,Nanomedicinal strategies to treat multidrug-resistant tumors: current progress.*Nanomedicine (Lond).*, 5, 597-615 (2010).
61. Dong Y., Wang R., Li H., Shao J., Chi Y., Lin X. and Chen G., Polyamine-functionalized carbon quantum dots for chemical sensing. *Carbon*, 50, 2810-2815 (2012).
62. Dufès C., Uchegbu I. F. and Schätzlein A. G., Dendrimers in gene delivery. *Adv. Drug Deliv. Rev.*, 57, 2177-2202 (2005).
63. Dutta S., Samanta P. and Dhara D., Temperature, pH and redox responsive cellulose based hydrogels for protein delivery. *Int. J. Biol. Macromol.*, 87, 92-100 (2016).
64. Eckmann D. M., Composto R. J., Tsourkas A. and Muzykantov V. R., Nanogel carrier design for targeted drug delivery. *J. Mater. Chem. B*, 2, 8085-8097 (2014).
65. Elemans J.A., Boerakker M.J., Holder S.J., Rowan A.E., Cho W.D., Percec V. and Nolte R.J., Plastic- and liquid-crystalline architectures from dendritic receptor molecules. *Proc. Natl. Acad. Sci. U S A.*,99, 5093-5098 (2002).
66. Elzoghby A. O., Samy W. M. and Elgindy N. A., Protein-based nanocarriers as promising drug and gene delivery systems. *J. Control Release.*, 161, 38-49 (2012).
67. Endo T., Yoshimura T. and Esumi K., Synthesis and catalytic activity of gold-silver binary nanoparticles stabilized by PAMAM dendrimer. *J. Colloid Interface Sci.*, 286, 602-609 (2005).
68. Esfand R. and Tomalia D.A.,Poly(amidoamine) (PAMAM) dendrimers: from biomimicry to drug delivery and biomedical applications. *Drug Discov. Today.*, 6, 427-436 (2001).
69. Esumi K., Suzuki A., Yamahira A. and Torigoe K., Role of poly(amidoamine) dendrimers for preparing nanoparticles of gold, platinum, and silver. *Langmuir*, 16, 2604-2608 (2000).
70. Everaerts F., Torrianni M., Hendriks M. and Feijen J., Biomechanical properties of carbodiimide crosslinked collagen: influence of the formation of ester crosslinks. *J. Biomed. Mater. Res., Part A.*, 85, 547-555 (2008).
71. Fail C. A., Evenson S. A., Ward L. J., Schofield W. C. E. and Badyal J. P. S., Controlled attachment of PAMAM dendrimers to solid surfaces. *Langmuir*, 18, 264-268 (2002).

72. Fant K., Esbjörner E.K., Jenkins A., Grossel M.C., Lincoln P. and Nordén B., Effects of PEGylation and acetylation of PAMAM dendrimers on DNA binding, cytotoxicity and *in vitro* transfection efficiency. *Mol. Pharmaceutics*, 7, 1734-1746 (2010).
73. Feynman R.P., There's plenty of room at the bottom. *Eng. Sci. (CalTech)*, 23, 22-36 (1960).
74. Fischer D., Li Y., Ahlemeyer B., Krieglstein J. and Kissel T., *In vitro* cytotoxicity testing of polycations: influence of polymer structure on cell viability and hemolysis. *Biomaterials*, 24, 1121-1131 (2003).
75. Fornari F. A., Randolph J. K., Yalowich J. C., Ritke M. K. and Gewirtz D. A., Interference by doxorubicin with DNA unwinding in MCF-7 breast tumor cells. *Mol. Pharmacol.*, 45, 649-656 (1994).
76. Funkhouser J., Reintroducing pharma: Theranostic revolution. *Curr. Drug Discovery*, 2 (2002).
77. Gandhi S. S., Yan H. and Kim C., Thermoresponsive gelatin nanogels. *ACS Macro Lett.*, 3, 1210-1214 (2014).
78. Garcia M.E., Baker L.A. and Crooks R.M., Preparation and characterization of dendrimer-gold colloid nanocomposites. *Anal. Chem.*, 71, 256-258 (1999).
79. Gillies E.R., Dy E., Fréchet J.M. and Szoka F.C.,Biological evaluation of polyester dendrimer: poly(ethylene oxide) "bow-tie" hybrids with tunable molecular weight and architecture. *Mol. Pharmaceutics*, 2, 129-138 (2005a).
80. Gillies E. R. and Frechet J. M. J., Dendrimers and dendritic polymers in drug delivery. *Drug Discov. Today.*, 10, 35-43 (2005b).
81. Gliga A. R., Skoglund S., Wallinder I. O., Fadeel B. and Karlsson H. L., Size-dependent cytotoxicity of silver nanoparticles in human lung cells: the role of cellular uptake, agglomeration and Ag release. *Part. Fibre Toxicol.*, 11, 11 (2014).
82. Goller R., Vors J.P., Caminade A.M. and Majoral J.P., Phosphorus dendrimers as new tools to deliver active substances. *Tetrahedron Lett.*, 42, 3587-3590 (2001).
83. Goncalves M., Maciel D., Capelo D., Xiao S., Sun W., Shi X., Rodrigues J., Tomas H. and Li Y., Dendrimer-assisted formation of fluorescent nanogels for drug delivery and intracellular imaging. *Biomacromolecules*, 15, 492-499 (2014).
84. Gopidas K. R., Whitesell J. K. and Fox M. A., Synthesis, characterization, and catalytic applications of a palladium-nanoparticle-cored dendrimer. *Nano Lett.*, 3, 1757-1760 (2003).

85. Gopinath P., Gogoi S. K., Chattopadhyay A. and Ghosh S. S., Implications of silver nanoparticle induced cell apoptosis for *in vitro* gene therapy. *Nanotechnology*, 19, 075104 (2008).
86. Gopinath P., Gogoi S. K., Sanpui P., Paul A., Chattopadhyay A. and Ghosh S. S., Signaling gene cascade in silver nanoparticle induced apoptosis. *Colloids Surf., B,* 77, 240-245 (2010).
87. Gopinath P., Uday S.K., Matai I., Bhushan B., Malwal D., Sachdev A. and Dubey P., Cancer Nanotheranostics. *Springer briefs in applied science and technology,* 1-93 (2015).
88. Gordon A.N., Fleagle J.T, Guthrie D., Parkin D.E., Gore M.E. and Lacave A.J.,Recurrent epithelial ovarian carcinoma: A randomized phase III study of pegylated liposomal doxorubicin versus topotecan. *J. Clin. Oncol*., 19, 3312-3332 (2001).
89. Gordon A.N., Granai C.O., Rose P.G., Hainsworth J., Lopez A., Weissman C., Rosales R. and Sharpington T.,Phase II study of liposomal doxorubicin in platinum- and paclitaxel-refractory epithelial ovarian cancer. *J. Clin. Oncol*., 18, 3093-3100 (2000).
90. Goswami S., Thiyagarajan D., Das G., and Ramesh A., A biocompatible nanocarrier fortified with a dipyridinium-based amphiphile for eradication of biofilm. *ACS Appl. Mater. Inter.*, 6, 16384-16394 (2014).
91. Grant G. T., Morris E. R., Rees D. A., Smith P. J. C. and Thom D., Biological interactions between polysaccharides and divalent cations: the egg-box model. *FEBS Lett.*, 32, 195-198 (1973).
92. Grayson S.M. and Fréchet J.M.,Convergent dendrons and dendrimers: from synthesis to applications. *Chem. Rev*., 101, 3819-3867 (2001).
93. Griffiths J.R., Are cancer cells acidic? *Br. J. Cancer,* 64, 425-427 (1991).
94. GuhaSarkar S. and Banerjee R., Intravesical drug delivery: challenges, current status, opportunities and novel strategies. *J. Control. Rel.*, 148, 147-159 (2010).
95. Guillaudeu S.J., Fox M.E., Haidar Y.M., Dy E.E., Szoka F.C. and Fréchet J.M.,PEGylated dendrimers with core functionality for biological applications. *Bioconjugate Chem.*, 19, 461-469 (2008).
96. Gupta U., Agashe H.B., Asthana A. and Jain N.K.,Dendrimers: novel polymeric nanoarchitectures for solubility enhancement. *Biomacromolecules,* 7, 649-658 (2006).
97. Hawker C. J. and Frechet J. M. J.,Preparation of polymers with controlled molecular architecture. A new convergent approach to dendritic macromolecules. *J. Am. Chem. Soc*., 112, 7638-7647 (1990).

98. He H., Li Y., Jia X.R., Du J., Ying X., Lu W.L., Lou J.N. and Wei Y., PEGylated Poly(amidoamine) dendrimer-based dual-targeting carrier for treating brain tumors. *Biomaterials*, 32, 478-487 (2011).
99. He X., Alves C.S., Oliveira N., Rodrigues J., Zhu J., Bányai I., Tomás H. and Shi X., RGD peptide-modified multifunctional dendrimer platform for drug encapsulation and targeted inhibition of cancer cells. *Colloids Surf., B.*, 125, 82-89 (2015).
100. Hecht S. and Fréchet J.M.J., Dendritic encapsulation of function: applying nature's site isolation principle from biomimetics to materials science. *Angew. Chem., Int. Ed. Engl*., 40, 74-91 (2001).
101. Hengartner M. O., The biochemistry of apoptosis. *Nature*, 407, 770-776 (2000).
102. Hill B. T. and Whelan R. D., A comparison of the lethal and kinetic effects of doxorubicin and 4′-epi-doxorubicin *in vitro*. *Tumori*, 68, 29-37 (1982).
103. Holland C., Terry A.E., Porter D. and Vollrath F., Natural and unnatural silks, *Polymer*, 48, 3388-3392 (2007).
104. Hong S., Bielinska A.U., Mecke A., Keszler B., Beals J.L., Shi X., Balogh L., Orr B.G., Baker JR Jr. and Banaszak Holl M.M., Interaction of poly(amidoamine) dendrimers with supported lipid bilayers and cells: hole formation and the relation to transport. *Bioconjug Chem.*, 15, 774-782 (2004).
105. Hong H., Shi J., Yang Y., Zhang Y., Engle J.W., Nickles R.J., Wang X. and Cai W., Cancer-targeted optical imaging with fluorescent zinc oxide nanowires. *Nano Lett.*, 11, 3744-3750 (2011).
106. Hsin Y. H., Chen C. F., Huang S., Shih T. S., Lai P. S. and Chueh P. J., The apoptotic effect of nanosilver is mediated by a ROS- and JNK-dependent mechanism involving the mitochondrial pathway in NIH3T3 cells. *Toxicol. Lett*., 179, 130-139 (2008).
107. Hu D. G., Rogers A. and Mackenzie P. I., Epirubicin upregulates UDP glucuronosyltransferase 2B7 expression in liver cancer cells via the p53 pathway. *Mol. Pharmacol.*, 85, 887-897 (2014).
108. Hu J., Su Y., Zhang H., Xu T. and Cheng Y., Design of interior-functionalized fully acetylated dendrimers for anticancer drug delivery. *Biomaterials*, 32, 9950-9959 (2011).
109. Hua S. and Wang A., Synthesis, characterization and swelling behaviors of sodium alginate-g-poly(acrylic acid)/sodium humate superabsorbent. *Carbohydr. Polym*., 75, 79-84 (2009).

110. Huang C.H., Nwe K., Zaki A.A., Brechbiel M.W. and Tsourkas.A., Biodegradable polydisulfide dendrimer nanoclusters as MRI contrast agents. *ACS Nano*, 6, 9416-9424 (2012).
111. Huang R. Y. M., Pal R. and Moon G. Y., Characteristics of sodium alginate membranes for the pervaporation dehydration of ethanolwater and isopropanol-water mixtures. *J. Membr. Sci.*, 160, 101-113 (1999).
112. Huang R., Ke W., Liu Y., Jiang C. and Pei Y., The use of lactoferrin as a ligand for targeting the polyamidoamine-based gene delivery system to the brain. *Biomaterials*, 29, 238-246 (2008).
113. Jain A.K., Swarnakar N.K., Godugu C., Singh R.P. and Jain S., The effect of the oral administration of polymeric nanoparticles on the efficacy and toxicity of tamoxifen. *Biomaterials*, 32, 503-515 (2011).
114. Jain A.K., Thanki K. and Jain S., Co-encapsulation of tamoxifen and quercetin in polymeric nanoparticles: implications on oral bioavailability, antitumor efficacy, and drug-induced toxicity. *Mol. Pharmaceutics*, 10, 3459-3474 (2013).
115. Jain S., Jain R., Das M., Agrawal A. K., Thanki K. and Kushwah V., Combinatorial bio-conjugation of gemcitabine and curcumin enables dual drug delivery with synergistic anticancer efficacy and reduced toxicity. *RSC Adv*., 4, 29193-29201 (2014).
116. Janib S.M., Moses A.S. and MacKay J.A., Imaging and drug delivery using theranostic nanoparticles. *Adv. Drug Deliv. Rev*., 62, 1052-1063 (2010).
117. Jansen J.F., de Brabander-van den Berg E.M. and Meijer E.W., Encapsulation of guest molecules into a dendritic box. *Science.*, 266, 1226-1229 (1994).
118. Jevprasesphant R., Penny J., Attwood D., McKeown N. B. and D'Emanuele A., Engineering of dendrimer surfaces to enhance transepithelial transport and reduce cytotoxicity. *Pharm. Res*., 20, 1543-1550 (2003).
119. Ji S.R., Liu C., Zhang B., Yang F., Xu J., Long J., Jin C., Fu D.L., Ni Q.X. and Yu X.J., Carbon nanotubes in cancer diagnosis and therapy. *Biochim Biophys Acta.*, 1806, 29-35 (2010).
120. Jiang D.L. and Aida T., A dendritic iron porphyrin as a novel haemoprotein mimic: effects of the dendrimer cage on dioxygenbinding activity. *Chem. Commun*., 1523-1524 (1996).
121. Jolly A. M. and Bonizzoni M., Intermolecular forces driving encapsulation of small molecules by PAMAM dendrimers in water. *Macromolecules*, 47, 6281-6288 (2014).

122. Jolly A. M. and Bonizzoni M., PAMAM dendrimers as supramolecular hosts through non-covalent interactions. *Supramol. Chem*., 27, 151-160 (2015).
123. Joshi N., Shanmugam T., Kaviratna A. and Banerjee R., Proapoptotic lipid nanovesicles: synergism with paclitaxel in human lung adenocarcinoma A549 cells. *J. Control Release*, 156, 413-420 (2011).
124. Joshi N., Shanmugam T., Deshmukh A. and Banerjee R., Apoptotic cascade inspired lipid nanovesicles show synergism with encapsulated paclitaxel in chemoresistant colon carcinoma. *Nanomedicine (Lond.)*, 9, 1789-1805 (2014).
125. Kabanov A. V. and Vinogradov S. V., Nanogels as pharmaceutical carriers: finite networks of infinite capabilities. *Angew. Chem., Int. Ed.*, 48, 5418-5429 (2009).
126. Kallio A., Zheng A., Dahllund J., Heiskanen K. M. and Harkonen P., Role of mitochondria in tamoxifen-induced rapid death of MCF-7 breast cancer cells. *Apoptosis*, 10, 1395-1410 (2005).
127. Kaminskas L.M., Boyd B.J., Karellas P., Krippner G.Y., Lessene R., Kelly B. and Porter C.J., The impact of molecular weight and PEG chain length on the systemic pharmacokinetics of PEGylated poly l-lysine dendrimers. *Mol. Pharmaceutics*, 5, 449-63 (2008).
128. Kaminskas L.M., McLeod V.M., Ascher D.B., Ryan G.M., Jones S., Haynes J.M., Trevaskis N.L., Chan L.J., Sloan E.K., Finnin B.A., Williamson M., Velkov T., Williams E.D., Kelly B.D., Owen D.J. and Porter C.J., Methotrexate-conjugated PEGylated dendrimers show differential patterns of deposition and activity in tumor-burdened lymph nodes after intravenous and subcutaneous administration in rats. *Mol. Pharmaceutics*, 12, 432-443 (2015).
129. Karami-Tehrani F. and Salami S., Cell kinetic study of tamoxifen treated MCF-7 and MDA-MB 468 breast cancer cell lines. *Iran. Biomed. J*., 7, 51-56 (2003).
130. Kedar U., Phutane P., Shidhaye S. and Kadam V., Advances in polymeric micelles for drug delivery and tumor targeting. *Nanomedicine*, 6, 714-729 (2010).
131. Kelkar S.S. and Reineke T.M., Theranostics: combining imaging and therapy. *Bioconjugate Chem*., 22, 1879-1903 (2011).
132. Kesharwani P., Jain K. and Jain N. K., Dendrimer as nanocarrier for drug delivery. *Prog. Polym. Sci*., 39, 268-307 (2014).
133. Kim K., Bae B., Kang Y. J., Nam J. M., Kang S. and Ryu J. H., Natural polypeptide-based supramolecular nanogels for stable noncovalent encapsulation. *Biomacromolecules*, 14, 3515-3522 (2013).

134. Kim Y., Klutz A. M. and Jacobson K. A., Systematic investigation of polyamidoamine dendrimers surface-modified with poly(ethylene glycol) for drug delivery applications: synthesis, characterization, and evaluation of cytotoxicity. *Bioconjugate Chem*., 19, 1660-1672 (2008).
135. Kitchens K. M., Foraker A. B., Kolhatkar R. B., Swaan P. W. and Ghandehari H., Endocytosis and interaction of poly (amidoamine) dendrimers with Caco-2 cells. *Pharm. Res.*, 24, 2138-2145 (2007).
136. Kitchens K. M., Kolhatkar R. B., Swaan P. W. and Ghandehari H., Endocytosis inhibitors prevent poly(amidoamine) dendrimer internalization and permeability across Caco-2 cells. *Mol. Pharmaceutics*, 5, 364-369 (2008).
137. Klajnert B. B., Pikala S. and Bryszewska M., Haemolytic activity of polyamidoamine dendrimers and the protective role of human serum albumin. *Proc. R. Soc. A*, 466, 1527-1534 (2010).
138. Klajnert, B. and Bryszewska M., Dendrimers in medicine. *Nova Science Publishers* (2007).
139. Kobayashi H. and Brechbiel M. W., Nano-sized MRI contrast agents with dendrimer cores. *Adv. Drug Deliv Rev*., 57, 2271-2286 (2005).
140. Kojima C., Regino C., Umeda Y., Kobayashi H. and Kono K., Influence of dendrimer generation and polyethylene glycol length on the biodistribution of PEGylated dendrimers. *Int. J. Pharm.*, 383, 293-296 (2010).
141. Kolhatkar R.B., Kitchens K.M., Swaan P.W. and Ghandehari H., Surface acetylation of polyamidoamine (PAMAM) dendrimers decreases cytotoxicity while maintaining membrane permeability. *Bioconjugate Chem*., 18, 2054-2060 (2007).
142. Kolhatkar R.B., Swaan P. and Ghandehari H., Potential oral delivery of 7-ethyl-10-hydroxy-camptothecin (SN-38) using poly(amidoamine) dendrimers. *Pharm. Res*., 25, 1723-1729 (2008).
143. Kolishetti N., Dhar S., Valencia P. M., Lin L. Q., Karnik R., Lippard S. J., Langer R. and Farokhzad O. C., Engineering of self-assembled nanoparticle platform for precisely controlled combination drug therapy. *Proc. Natl. Acad. Sci. U. S. A*., 107, 17939-17944 (2010).
144. Kumar P., Bolshette N., Jamdade V., Mundhe N., Thakur K., Saikia K. and Lahkar M., Breast cancer status in India: an overview. *Biomed. Prev. Nutr*., 3, 177-183 (2013).
145. Kumar S. U., Matai I., Dubey P., Bhushan B., Sachdev A. and Gopinath P., Differentially cross-linkable core–shell nanofibers for tunable delivery of anticancer

drugs: synthesis, characterization and their anticancer efficacy. *RSC Adv*., 4, 38263-38272 (2014).

146. Kutty R. V., Tay C. Y., Lim C. S., Feng Si-S. and Leong D. T., Anti-migratory and increased cytotoxic effects of novel dual drug loaded complex hybrid micelles in triple negative breast cancer cells. *Nano Research*, 8, 2533-2547 (2015).
147. Lamelas C., Avaltroni F., Benedetti M., Wilkinson K. J. and Slaveykova V. I., Quantifying Pb and Cd complexation by alginates and the role of metal binding on macromolecular aggregation. *Biomacromolecules*, 6, 2756-2764 (2005).
148. Laurienzo P., Malinconico M., Motta A. and Vicinanza A., Synthesis and characterization of a novel alginate−poly(ethylene glycol) graft copolymer. *Carbohydr. Polym.*, 62, 274-282 (2005).
149. Lawrie G., Keen I., Drew B., Chandler-Temple A., Rintoul L., Fredericks P. and Grøndahl L., Interactions between alginate and chitosan biopolymers characterized using FTIR and XPS. *Biomacromolecules*, 8, 2533-2541 (2007).
150. Lee C. C., MacKay J. A., Fréchet J. M. J. and Szoka F.C., Designing dendrimers for biological applications. *Nat. Biotechnol.*, 23, 1517-1526 (2005).
151. Lee H. and Larson R. G., Lipid bilayer curvature and pore formation induced by charged linear polymers and dendrimers: the effect of molecular shape. *J. Phys. Chem. B*, 112, 12279-12285 (2008).
152. Lee K. Y. and Mooney D. J., Alginate: properties and biomedical applications. *Prog. Polym. Sci*., 37, 106-126 (2012).
153. Lee Y. H., Cheng F. Y., Chiu H. W., Tsai J. C., Fang C. Y., Chen C. W. and Wang Y. J., Cytotoxicity, oxidative stress, apoptosis and the autophagic effects of silver nanoparticles in mouse embryonic fibroblasts. *Biomaterials*, 35, 4706-4715 (2014).
154. Lee Y. K., Lin T. H., Chang C. F. and Lo Y. L., Galectin-3 silencing inhibits epirubicin-induced ATP binding cassette transporters and activates the mitochondrial apoptosis pathway via β-catenin/GSK-3β modulation in colorectal carcinoma. *PLoS One*, 8, 82478 (2013).
155. Leenders C. M. A., Mes T., Baker M. B., Koenigs M. M. E., Besenius P., Palmans A. R. A. and Meijer E. W., From supramolecular polymers to hydrogel materials. *Mater. Horiz.*, 1, 116-120 (2014).
156. LeRoux M. A., Guilak F.and Setton L. A., Compressive and shear properties of alginate gel: effects of sodium ions and alginate concentration. *J. Biomed. Mater. Res.*, 47, 46-53 (1999).

157. Lesniak W. G., Mishra M. K., Jyoti A., Balakrishnan B., Zhang F., Nance E., Romero R., Kannan S. and Kannan R. M., Biodistribution of fluorescently labeled PAMAM dendrimers in neonatal rabbits: effect of neuroinflammation. *Mol. Pharmaceutics*, 10, 4560-4571 (2013).

158. Li X., Gao C., Wu Y., Cheng C. Y., Xiac W. and Zhang Z., Combination delivery of adjudin and doxorubicin via integrating drug conjugation and nanocarrier approaches for the treatment of drug-resistant cancer cells. *J. Mater. Chem. B*, 3, 1556-1564 (2015a).

159. Li Y., Maciel D., Rodrigues J., Shi X. and Tomas H., Biodegradable´polymer nanogels for drug/nucleic acid delivery. *Chem. Rev.*, 115, 8564-8608 (2015b).

160. Li Y., Maciel D., Tomas H., Rodrigues J., Ma H. and Shi, X., pH´sensitive Laponite/alginate hybrid hydrogels: swelling behaviour and release mechanism. *Soft Matter*, 7, 6231-6238 (2011).

161. Li Z., Huang P., He R., Lin J., Yang S., Zhang X., Ren Q. and Cui D., Aptamer-conjugated dendrimer-modified quantum dots for cancer cell targeting and imaging. *Mater. Lett*., 64, 375-378 (2010).

162. Liang X. and Bonizzoni M., Boronic acid-modified poly (amidoamine) dendrimers as sugar-sensing materials in water. *J. Mater. Chem. B,* DOI: 10.1039/C5TB02530C (2016).

163. Liao H., Liu H., Li Y., Zhang M., Tomas H., Shen M. and Shi X., Antitumor efficacy of doxorubicin encapsulated within PEGylated poly(amidoamine) dendrimers. *J. Appl. Polym. Sci*., 131, 40358 (2014).

164. Lin Y. H., Liang H. F., Chung C. K., Chen M. C. and Sung H. W., Physically crosslinked alginate/N,O-carboxymethyl chitosan hydrogels with calcium for oral delivery of protein drugs. *Biomaterials*, 26, 2105-2113 (2005).

165. Liu C., Zhang P., Zhai X., Tian F., Li W., Yang J., Liu Y., Wang H., Wang W. and Liu W., Nano-carrier for gene delivery and bioimaging based on carbon dots with PEI-passivation enhanced fluorescence. *Biomaterials*, 33, 3604-3613 (2012a).

166. Liu G. and An Z., Frontiers in the design and synthesis of advanced nanogels for nanomedicine. *Polym. Chem*., 5, 1559-1565 (2014a).

167. Liu W., Li X., Wong Y. S., Zheng W., Zhang Y., Cao W. and Chen T., Selenium nanoparticles as a carrier of 5-fluorouracil to achieve anticancer synergism. *ACS Nano*, 6, 6578-6591 (2012b).

168. Liu H., Wang H., Xu Y., Guo R., Wen S., Huang Y., Liu W., Shen M., Zhao J., Zhang G. and Shi X., Lactobionic acid-modified dendrimer-entrapped gold nanoparticles for targeted computed tomography imaging of human hepatocellular carcinoma. *ACS Appl. Mater. Interfaces*, 6, 6944-6953 (2014b).
169. Liu H., Wang H., Guo R., Cao X., Zhao J., Luo Y., Shen M., Zhang G. and Shi X., Size-controlled synthesis of dendrimer-stabilized silver nanoparticles for X-ray computed tomography imaging applications. *Polym. Chem*., 1, 1677-1683 (2010a).
170. Liu L., Yu M., Duan X. and Wang S., Conjugated polymers as multifunctional biomedical platforms: anticancer activity and apoptosis imaging. *J. Mater. Chem*., 20, 6942-6947 (2010b).
171. Liu Z., Zhang Z., Zhou C. and Jiao Y.,Hydrophobic modifications of cationic polymers for gene delivery. *Prog. Polym. Sci*., 35, 1144-1162 (2010c).
172. Liu H., Shen M., Zhao J., Zhu J., Xiao T., Cao X., Zhang G. and Shi X., Facile formation of folic acid-modified dendrimer-stabilized gold-silver alloy nanoparticles for potential cellular computed tomography imaging applications. *Analyst*, 138, 1979-1987 (2013).
173. Liu M. and Fréchet J.M., Designing dendrimers for drug delivery. *Pharm. Sci. Technolo. Today*, 2, 393-401 (1999).
174. Liu M., Kono K. and Fréchet J. M., Water-soluble dendritic unimolecular micelles: their potential as drug delivery agents. *J. Control Release*, 65, 121-131 (2000).
175. Liu X., Kim C. N., Yang J., Jemmerson R. and Wang X.,Induction of apoptotic program in cell-free extracts: requirement for dATP and cytochrome c. *Cell*, 86, 147-157 (1996).
176. Liu Y., Miyoshi H. and Nakamura M., Nanomedicine for drug delivery and imaging: a promising avenue for cancer therapy and diagnosis using targeted functional nanoparticles. *Int. J. Cancer.*, 120, 2527-2537 (2007).
177. Lo Y. L. and Wang W., Formononetin potentiates epirubicin induced apoptosis via ROS production in Hela cells *in vitro*. *Chem. Biol. Interact*., 205, 188-197 (2013).
178. Longmire M., Choyke P.L. and Kobayashi H., Dendrimer-based contrast agents for molecular imaging. *Curr. Top. Med. Chem*., 8, 1180-1186 (2008).
179. Lopez-Alonso J. P., Diez-García F., Font J., Ribo´ M.,´Vilanova M., Scholtz J. M., Gonzalez C., Vottariello F., Gotte G.,´Libonati M. and Laurents D. V., Carbodiimide EDC induces cross-links that stabilize RNase A C-dimer against dissociation: EDC adducts can affect protein net charge, conformation, and activity. *Bioconjugate Chem*., 20, 1459-1473 (2009).

180. Ly J. D., Grubb D. R. and Lawen A., The mitochondrial membrane potential (deltapsi(m)) in apoptosis; an update. *Apoptosis*, 8, 115-128 (2003).
181. Lynch Jr.T. J., Kass F., Kalish L. A., Elias A. D., Strauss G., Shulman L. N., Sugarbaker D. J., Skarin A. and Frei E., Cisplatin, 5-fluorouracil, and etoposide for advanced non-small cell lung cancer. *Cancer*, 71, 2953-2957 (1993).
182. Maciel D., Figueira P., Xiao S., Hu D., Shi X., Rodrigues J., Tomas H. and Li Y., Redox-responsive alginate nanogels with enhanced anticancer cytotoxicity. *Biomacromolecules*, 14, 3140-3146 (2013).
183. Maeda H., Wu J., Sawa T., Matsumura Y. and Hori K., Tumor vascular permeability and the EPR effect in macromolecular therapeutics: a review. *J. Control Release*, 65, 271-284 (2000).
184. Maiti P. K., Cagin T., Lin S. T. and Goddard W. A., Effect of solvent and pH on the structure of pamam dendrimers. *Macromolecules*, 38, 979-991 (2005).
185. Majoros I. J., Keszler B., Woehler S., Bull T. and Baker J. R., Acetylation of poly(amidoamine) dendrimers. *Macromolecules*, 36, 5526-5529 (2003).
186. Majoros I.J., Thomas T.P., Mehta C.B. and Baker J.R. Jr., Poly(amidoamine) dendrimer-based multifunctional engineered nanodevice for cancer therapy. *J. Med. Chem.*, 48, 5892-5899 (2005).
187. Majoros I. J., Myc A., Thomas T., Mehta C. B. and Baker Jr. J. R., PAMAM dendrimer-based multifunctional conjugate for cancer therapy: synthesis, characterization, and functionality. *Biomacromolecules*, 7, 572-579 (2006).
188. Malecki M., Frontiers in Suicide Gene Therapy of Cancer. *J. Genet. Syndr. Gene Ther.* 2012, 3, (2012).
189. Malik N., Wiwattanapatapee R., Klopsch R., Lorenz K., Frey H., Weener J.W., Meijer E.W., Paulus W. and Duncan R., Dendrimers: relationship between structure and biocompatibility *in vitro*, and preliminary studies on the biodistribution of 125I-labelled polyamidoamine dendrimers *in vivo*. *J. Control Release*, 65, 133-148 (2000).
190. Markman J.L., Rekechenetskiy A., Holler E. and Ljubimova J.Y.,Nanomedicine therapeutic approaches to overcome cancer drug resistance. *Adv. Drug Deliv. Rev.*, 65, 1866-1879 (2013).
191. Martin S. J. and Green D. R.,Apoptosis and cancer: the failure of controls on cell death and cell survival. *Crit. Rev. Oncol./Hematol.*, 18, 137-153 (1995).

192. Matai I., Sachdev A., Dubey P., Kumar S. U., Bhushan B. and Gopinath P., Antibacterial activity and mechanism of Ag–ZnO nanocomposite on S. aureus and GFP-expressing antibiotic resistant E. coli. *Colloids Surf., B*, 115, 359-367 (2014a).
193. Matai I., Sachdev A., Uday S. K., Dubey P., Bhushan B. and Gopinath P., Dendrimer: a promising nanocarrier for cancer therapy. *Nanotechnology: Recent Trends, Emerging Issues and Future Direction Nanotechnology: Recent Trends, Emerging Issues and Future Directions; Nova Publishers*: New York, 127-156 (2014b).
194. Matai I., Sachdev A. and Gopinath P., Multicomponent 5-fluorouracil loaded PAMAM stabilized-silver nanocomposites synergistically induce apoptosis in human cancer cells. *Biomater. Sci*., 3, 457-468 (2015a).
195. Matai I., Sachdev A. and Gopinath P., Self-assembled hybrids of fluorescent carbon dots and PAMAM dendrimers for epirubicin delivery and intracellular imaging. *ACS Appl. Mater. Interfaces*, 7, 11423-11435 (2015b).
196. Matai I. and Gopinath. P., Chemically cross-linked hybrid nanogels of alginate and pamam dendrimers as efficient anticancer drug delivery vehicles. *ACS Biomater. Sci. Eng*., 2, 213-223 (2016).
197. Mathew A., Maekawa T. and Sakthikumar D., Aptamers in targeted nanotherapy. *Curr. Top Med. Chem*., 15, 1102-1114 (2015).
198. McCarthy T.D., Karellas P., Henderson S.A., Giannis M., O'Keefe D.F., Heery G., Paull J.R., Matthews B.R. and Holan G., Dendrimers as drugs: discovery and preclinical and clinical development of dendrimer-based microbicides for HIV and STI prevention. *Mol. Pharmaceutics*, 2, 312-318 (2005).
199. Mecke A., Majoros I. J., Patri A. K., Baker J. R. Jr., Banaszak Holl M. M. and Orr B. G., Lipid bilayer disruption by polyamidoamine dendrimers: the role of generation and capping group. *Langmuir*, 21, 10348-10354 (2005).
200. Mei M., Ren Y., Zhou X., Yuan X. B., Li F., Jiang L. H., Kang C. S. and Yao Z.,Suppression of breast cancer cells *in vitro* by polyamidoamine-dendrimer-mediated 5-fluorouracil chemotherapy combined with antisense micro-RNA 21 gene therapy. *J. Appl. Polym. Sci*., 114, 3760-3766 (2009).
201. Menjoge A.R., Kannan R.M. and Tomalia D.A.,Dendrimer-based drug and imaging conjugates: design considerations for nanomedical applications. *Drug Discov. Today*, 15, 171-185 (2010).

202. Milhem O.M., Myles C., McKeown N.B., Attwood D. and D'Emanuele A., Polyamidoamine starburst dendrimers as solubility enhancers. *Int. J. Pharm.*, 197, 239-241 (2000).
203. Millour J., de Olano N., Horimoto Y., Monteiro L. J., Langer J. K., Aligue R., Hajji N. and Lam E. W., ATM and p53 regulate FOXM1 Expression via E2F in breast cancer epirubicin treatment and resistance. *Mol. Cancer Ther*., 10, 1046-1058 (2011).
204. Miyahara T., Nyan M., Shimoda A., Yamamoto Y., Kuroda S., Shiota M., Akiyoshi K. and Kasugai S., Exploitation of a novel polysaccharide nanogel cross-linking membrane for guided bone regeneration (GBR). *J. Tissue Eng. Regener. Med*., 6, 666-672 (2012).
205. Miyake Y., Kimura Y., Ishikawa S., Tsujita H., Miura H., Narazaki M., Matsuda T., Tabata Y., Yano T., Toshimitsu A. and Kondo T., Synthesis and functional evaluation of chiral dendrimer–triamine-coordinated Gd complexes as highly sensitive MRI contrast agents. *Tetrahedron Lett*., 53, 4580-4583 (2012).
206. Mo C., Holland C., Porter D., Shao Z. and Vollrath F., Concentration state dependence of the rheological and structural properties of reconstituted silk. *Biomacromolecules*, 10, 2724-2728 (2009).
207. Moghimi S. M., Hunter A. C. and Murray J. C.,Nanomedicine: current status and future prospects. *FASEB J.*, 19, 311-330 (2005).
208. Mohy Eldin M. S., Kamoun E. A., Sofan M. A. and Elbayomi S. M., L-Arginine grafted alginate hydrogel beads: A novel pH-sensitive system for specific protein delivery. *Arabian J. Chem.*, 8, 355-365 (2015).
209. Morgan M.T., Carnahan M.A., Immoos C.E., Ribeiro A.A., Finkelstein S., Lee S.J. and Grinstaff M.W., Dendritic molecular capsules for hydrophobic compounds. *J. Am. Chem. Soc.*, 125, 15485-15489 (2003).
210. Morgan M.T., Carnahan M.A., Finkelstein S., Prata C.A., Degoricija L., Lee S.J. and Grinstaff M.W., Dendritic supramolecular assemblies for drug delivery. *Chem. Commun*., 34, 4309-4311 (2005).
211. Morgan M.T., Nakanishi Y., Kroll D.J., Griset A.P., Carnahan M.A., Wathier M., Oberlies N.H., Manikumar G., Wani M.C. and Grinstaff M.W., Dendrimer-encapsulated camptothecins: increased solubility, cellular uptake, and cellular retention affords enhanced anticancer activity *in vitro*. *Cancer Res.*, 66, 11913-11921 (2006).
212. Morigi V., Tocchio A., Pellegrini C. B., Sakamoto J. H., Arnone M. and Tasciotti E., Nanotechnology in medicine: from inception to market domination. *J. Drug Delivery*, 2012, 1-7 (2012).

213. Morimoto N., Hirano S., Takahashi H., Loethen S., Thompson D. H. and Akiyoshi K., Self-assembled pH-sensitive cholesteryl pullulan nanogel as a protein delivery vehicle. *Biomacromolecules*, 14, 56-63 (2013).
214. Mortimer B., Drodge D. R., Dragnevski K. I., Siviour C. R. and Holland C., In situ tensile tests of single silk fibres in an environmental scanning electron microscope (ESEM). *J. Mater. Sci*., 48, 5055-5062 (2013).
215. Mortimer B., Guan J., Holland C., Porter D. and Vollrath F., Linking naturally and unnaturally spun silks through the forced reeling of *Bombyx mori*. *Acta Biomater*., 11, 247-255 (2015).
216. Mukherjee S.P., Lyng F.M., Garcia A., Davoren M. and Byrne H.J., Mechanistic studies of *in vitro* cytotoxicity of poly(amidoamine) dendrimers in mammalian cells. *Toxicol. Appl. Pharmacol.*, 248, 259-268 (2010).
217. Muthu M. S., Leong D. T., Mei L. and Feng Si-S., Nanotheranostics - application and further development of nanomedicine strategies for advanced theranostics. *Theranostics*, 4, 660-677 (2014).
218. Naha P.C., Davoren M., Casey A. and Byrne H.J., An ecotoxicological study of poly(amidoamine) dendrimers-toward quantitative structure activity relationships. *Environ. Sci. Technol.*, 43, 6864-6869 (2009).
219. Naha P.C., Davoren M., Lyng F.M. and Byrne H.J., Reactive oxygen species (ROS) induced cytokine production and cytotoxicity of PAMAM dendrimers in J774A.1 cells. *Toxicol Appl Pharmacol.*, 246, 91-99 (2010).
220. Naha P. C. and Byrne H. J., Generation of intracellular reactive oxygen species and genotoxicity effect to exposure of nanosized polyamidoamine (PAMAM) dendrimers in PLHC-1 cells *in vitro. Aquat. Toxicol*., 132-133, 61-72 (2013).
221. Nair B.G., Varghese S.H., Nair R., Yoshida Y., Maekawa T. and Kumar D.S., Nanotechnology platforms; an innovative approach to brain tumor therapy. *Med Chem.*, 7, 488-503 (2011).
222. Najlah M., Freeman S., Attwood D. and D'Emanuele A., *In vitro* evaluation of dendrimer prodrugs for oral drug delivery. *Int. J. Pharm.*, 336, 183-190 (2007).
223. Natarajan J., Madras G. and Chatterjee K., Tailoring the degradation rate and release kinetics from poly (galactitol sebacate) by blending with chitosan, alginate or ethyl cellulose. *Int. J. Biol. Macromol*., http://dx.doi.org/10.1016/j.ijbiomac.2016.02.039 (2016).

224. Newkome G.R., Yao Z., Baker G.R. and Gupta V.K.,. Micelles. Part 1.Cascade molecules: a new approach to micelles A[27]-arborol. *J. Org. Chem*., 50, 2003-2004 (1985).

225. Ng K.W., Khoo S.P., Heng B.C., Setyawati M.I., Tan E.C., Zhao X., Xiong S., Fang W., Leong D.T. and Loo J.S., The role of the tumor suppressor p53 pathway in the cellular DNA damage response to zinc oxide nanoparticles. *Biomaterials*, 32, 8218-8225 (2011).

226. Nicolas J., Mura S., Brambilla D., Mackiewicz N. and Couvreur P., Design, functionalization strategies and biomedical applications of targeted biodegradable/biocompatible polymer-based nanocarriers for drug delivery. *Chem. Soc. Rev*., 42, 1147-1235 (2013).

227. Nigavekar S.S., Sung L.Y., Llanes M., El-Jawahri A., Lawrence T.S., Becker C.W., Balogh L. and Khan M.K., 3H dendrimer nanoparticle organ/tumor distribution. *Pharm Res.*, 21, 476-483 (2004).

228. Nishikawa M., Takakura Y. and Hashida M., Pharmacokinetic evaluation of polymeric carriers. *Adv. Drug Delivery Rev.*, 21, 135-155 (1996).

229. Niu Y. and Crooks R. M., Dendrimer-encapsulated metal nanoparticles and their applications to catalysis. *C. R. Chimie*, 6, 1049-1059 (2003a).

230. Niu Y., Sun L. and Crooks R. M., Determination of the intrinsic proton binding constants for poly(amidoamine) dendrimers via potentiometric pH titration. *Macromolecules*, 36, 5725-5731 (2003b).

231. Noriega-Luna B., Godínez L. A., Rodríguez F. J., Rodríguez A., Zaldívar-Lelo de Larrea G., Sosa-Ferreyra C. F., Mercado-Curiel R. F., Manríquez J. and Bustos E., Applications of dendrimers in drug delivery agents, diagnosis, therapy, and detection. *J. Nanomater*., 2014, 1-19 (2014).

232. O' Brian M.E., Wigler N., Inbar M., Rosso R., Grischke E., Santoro A., Catane R., Kieback D.G., Tomczak P., Ackland S.P., Orlandi F., Mellars L., Alland L., Tendler C. and CAELYX Breast Cancer Study Group.,Reduced cardiotoxicity and comparable efficacy in a phase III trial of pegylated liposomal doxorubicin HCl (CAELYX/Doxil) versus conventional doxorubicin for first-line treatment of metastatic breast cancer. *Ann. Oncol.*, 15, 440-449 (2004).

233. Oishi M., Sumitani S. and Nagasaki Y., On-off regulation of 19F magnetic resonance signals based on pH-sensitive PEGylated nanogels for potential tumor-specific smart 19F MRI probes. *Bioconjugate Chem*., 18, 1379-1382 (2007).

234. Olinski R., Gackowski D., Foksinski M., Rozalski R., Roszkowski K. and Jaruga P., Oxidative DNA damage: assessment of the role in carcinogenesis, atherosclerosis, and acquired immunodeficiency syndrome. *Free Radical Biol. Med.*, 33, 192-200 (2002).
235. Ooya T., Lee J. and Park K., Hydrotropic dendrimers of generations 4 and 5: Synthesis, characterization, and hydrotropic solubilization of paclitaxel. *Bioconjug. Chem.*, 15, 1221-1229 (2004).
236. Ornelas C., Pennell R., Liebes L.F. and Weck M., Construction of a well-defined multifunctional dendrimer for theranostics. *Org Lett*., 13, 976-979 (2011).
237. Pan B., Cui D., Gao F. and He R., Growth of multi-amine terminated poly(amidoamine) dendrimers on the surface of carbon nanotubes. *Nanotechnology*, 17, 2483-2489 (2006).
238. Pardeike J., Hommoss A. and Müller R.H., Lipid nanoparticles (SLN, NLC) in cosmetic and pharmaceutical dermal products. *Int. J. Pharm.*, 366, 170-184 (2009).
239. Park H. S., Lee J. E., Cho M. Y., Hong J. H., Cho S. H. and Lim Y. T., Hyaluronic acid/poly(β-amino ester) polymer nanogels for cancer-cell-specific NIR fluorescence switch. *Macromol. Rapid Commun.*, 33, 1549-1555 (2012).
240. Pasparakis G. and Bouropoulos N., Swelling studies and *in vitro* release of verapamil from calcium alginate and calcium alginatechitosan beads. *Int. J. Pharm*., 323, 34-42 (2006).
241. Patri A.K., Kukowska-Latallo J.F. and Baker J.R. Jr., Targeted drug delivery with dendrimers: comparison of the release kinetics of covalently conjugated drug and non-covalent drug inclusion complex. *Adv. Drug Deliv. Rev*., 57, 2203-2214 (2005).
242. Peer D., Karp J. M., Hong S, Farokhzad O. C., Margalit R. and Langer R.,Nanocarriers as an emerging platform for cancer therapy. *Nat. Nanotechnol.*, 2, 751-760 (2007).
243. Peng F., Su Y., Ji X., Zhong Y., Wei X. and He Y., Doxorubicin-loaded silicon nanowires for the treatment of drug-resistant cancer cells. *Biomaterials*, 35, 5188-5195 (2014).
244. Peng H. S., Stolwijk J. A., Sun L. N., Wegener J. and Wolfbeis O. S., A nanogel for ratiometric fluorescent sensing of intracellular pH values. *Angew. Chem., Int. Ed*., 49, 4246-4249 (2010).
245. Pillai G., Nanomedicines for cancer therapy: an update of FDA approved and those under various stages of development. *SOJ Pharm. Pharm Sci.*, 1, 13 (2014).
246. Pittelkow M., Moth-Poulsen K., Boas U. and Christensen J. B., Poly(amidoamine)-dendrimer-stabilized Pd(0) nanoparticles as a catalyst for the suzuki reaction. *Langmuir*, 19, 7682-7684 (2003).

247. Porter A. G. and Janicke R. U., Emerging roles of caspase-3 in apoptosis. *Cell Death Differ.*, 6, 99-104 (1999).

248. Pu Y., Chang S., Yuan H., Wang G., He B. and Gu Z., The anti-tumor efficiency of poly(Lglutamic acid) dendrimers with polyhedral oligomeric silsesquioxane cores. *Biomaterials*, 14, 3658-3666 (2013).

249. Rahman A.M., Yusuf S.W. and Ewer M.S., Anthracycline-induced cardiotoxicity and the cardiac sparing effect of liposomal formulation. *Int. J. Nanomedicine*, 2, 567-583 (2007).

250. Rapoport N., Physical stimuli-responsive polymeric micelles for anti-cancer drug delivery. *Prog. Polym. Sci.*, 32, 962-990 (2007).

251. Raveendran S., Palaninathan V., Nagaoka Y., Fukuda T., Iwai S., Higashi T., Mizuki T., Sakamoto Y., Mohanan P.V., Maekawa T. and Kumar D.S., Extremophilic polysaccharide nanoparticles for cancer nanotherapy and evaluation of antioxidant properties. *Int. J. Biol. Macromol*., 76, 310-319 (2015).

252. Rello S., Stockert J. C., Moreno V., Gámez A., Pacheco M., Juarranz A., Caňete M. and Villanueva A., Morphological criteria to distinguish cell death induced by apoptotic and necrotic treatments. *Apoptosis*, 10, 201-208 (2005).

253. Ren J., Cheng H., Xin W. Q., Chen X. and Hu K., Induction of apoptosis by 7-piperazinethylchrysin in HCT-116 human colon cancer cells. *Oncol. Rep.*, 28, 1719-1726 (2012).

254. Riccardi C. And Nicoletti I., Analysis of apoptosis by propidium iodide staining and flow cytometry. *Nat. Protoc.*, 1, 1458-1461 (2006).

255. Ryu J. H., Jiwpanich S., Chacko R., Bickerton S. and Thayumanavan S., Surface-functionalizable polymer nanogels with facile hydrophobic guest encapsulation capabilities. *J. Am. Chem. Soc.*, 132, 8246-8247 (2010).

256. Sachdev A., Matai I. and Gopinath P. Implications of surface passivation on physicochemical and bioimaging properties of carbon dots. *RSC Adv.*, 4, 20915-20921 (2014).

257. Sachdev A., Matai I. and Gopinath P., Dual-functional carbon dots−silver@zinc oxide nanocomposite: *in vitro* evaluation of cellular uptake and induction of apoptosis. *J. Mater. Chem. B*, 3, 1217-1229 (2015).

258. Sachdev A., Matai I., Kumar S. U., Bhushan B., Dubey P. and Gopinath, P., A novel one-step synthesis of PEG passivated multicolour fluorescent carbon dots for potential biolabeling application. *RSC Adv.*, 3, 16958-16961 (2013).

259. Sadekar S. and Ghandehari H., Transepithelial transport and toxicity of PAMAM dendrimers: implications for oral drug delivery. *Adv. Drug Deliv. Rev.*, 64, 571-588 (2012).
260. Saha B., Saikia J. and Das G., Correlating enzyme density, conformation and activity on nanoparticle surfaces in highly functional bio-nanocomposites. *Analyst*, 140, 532-542 (2015).
261. Sahay G., Alakhova D. Y. and Kabanov A. V., Endocytosis of nanomedicines. *J. Controlled Release*, 145, 182-195 (2010).
262. Sahoo B., Devi K.S., Dutta S., Maiti T.K., Pramanik P. and Dhara D., Biocompatible mesoporous silica-coated superparamagnetic manganese ferrite nanoparticles for targeted drug delivery and MR imaging applications. *J Colloid Interface Sci*., 431, 31-41 (2014).
263. Saikia J., Sikdar Yeasin, Saha B. and Das G., Malachite nanoparticle: a potent surface for the adsorption of Xanthene dyes. *J. Env. Chem. Engg*., 1, 1166-1173 (2013).
264. Sanpui P., Chattopadhyay A. and Ghosh S. S., Induction of apoptosis in cancer cells at low silver nanoparticle concentrations using chitosan nanocarrier. *ACS Appl. Mater. Interfaces*, 3, 218-228 (2011).
265. Sarkar K., Meka S. R. K., Madras G. and Chatterjee K., A self-assembling polycationic nanocarrier that exhibits exceptional gene transfection efficiency. *RSC Adv*., 5, 91619-91632 (2015a).
266. Sarkar K., Madras G. and Chatterjee K., Dendron conjugation to graphene oxide using click chemistry for efficient gene delivery. *RSC Adv*., 5, 50196-50211 (2015b).
267. Sarkar K., Banerjee S. L., Kundu P. P., Madras G. and Chatterjee K., Biofunctionalized surface-modified silver nanoparticles for gene delivery. *J. Mater. Chem. B*, 3, 5266-5276 (2015c).
268. Sartori C., Finch D. S., Ralph B. and Gilding K., Determination of the cation content of alginate thin films by FTi.r. spectroscopy. *Polymer*, 38, 43-51 (1997).
269. Setyawati M.I., Tay C.Y. and Leong D.T., Effect of zinc oxide nanomaterials-induced oxidative stress on the p53 pathway. *Biomaterials*, 34, 10133-10142 (2013).
270. Sezaki H., Takakura Y. and Hashida M.,. Soluble macromolecular carriers for the delivery of antitumor drugs. *Adv. Drug. Deliv. Rev*., 3, 247-266 (1989).
271. Sharma S., Chockalingam S., Sanpui P., Chattopadhyay A. and Ghosh S. S.,Silver nanoparticles impregnated alginate-chitosan-blended nanocarrier induces apoptosis in human glioblastoma cells. *Adv. Healthc Mater*., 3, 106-114 (2014).

272. Shi X., Majoros I. J., Patri A. K., Bi X., Islam M. T., Desai A., Ganser T. R. and Baker J. R., Molecular heterogeneity analysis of poly (amidoamine) dendrimer-based mono- and multifunctional nanodevices by capillary electrophoresis. *Analyst*, 131, 374-381 (2006).
273. Shi X., Lee I. and Baker Jr. J. R.,Acetylation of dendrimer-entrapped gold and silver nanoparticles. *J. Mater. Chem*., 18, 586-593 (2008).
274. Shi X., Sun K. and Baker Jr. J. R., Spontaneous formation of functionalized dendrimer-stabilized gold nanoparticles. *J. Phys. Chem. C Nanomater. Interfaces*, 112, 8251-8258 (2009).
275. Siegel R. L., Miller K. D. and Jemal A., Cancer statistics, 2015. *CA Cancer J. Clin*., 65, 5-29 (2015).
276. Silva G.A., Introduction to nanotechnology and its applications to medicine. *Surg. Neurol.*, 61, 216-220 (2004).
277. Singer J. W., Bhatt R., Tulinsky J., Buhler K. R., Heasley E., Klein P. and Vries P. D., Water-soluble poly-(L-glutamic acid)-Gly-camptothecin conjugates enhance camptothecin stability and efficacy *in vivo*. *J. Control Release*, 74, 243-247 (2001).
278. Singh P., Gupta U., Asthana A. and Jain N. K., Folate and folate PEG-PAMAM dendrimers: synthesis, characterization, and targeted anticancer drug delivery potential in tumor bearing mice. *Bioconjugate Chem*., 19, 2239-2252 (2008).
279. Sk U.H. and Kojima C., Dendrimers for theranostic applications. *Biomol Concepts*., 6, 205-217 (2015).
280. Somaï S., Chaouat M., Jacob D., Perrot J-Y., Rostène W., Forgez P. and Gompel A., Antiestrogens are pro-apoptotic in normal human breast epithelial cells. *Int. J. Cancer*, 105, 607-612 (2003).
281. Sonawane N. D., Szoka Jr. F. C. and Verkman A. S., Chloride accumulation and swelling in endosomes enhances DNA transfer by polyamine-DNA polyplexes. *J. Biol. Chem*., 278, 44826-44831 (2003).
282. Sun J-T., Hong C-Y. and Cai-Y. P., Surface modification of carbon nanotubes with dendrimers or hyperbranched polymers. *Polym. Chem*., 2, 998-1007 (2011).
283. Svenson S. and Tomalia D. A., Dendrimers in biomedical applications-reflections on the field. *Adv. Drug Deliv. Rev*., 4, 102-115 (2012).
284. Swarnakar N.K., Thanki K. and Jain S., Enhanced antitumor efficacy and counterfeited cardiotoxicity of combinatorial oral therapy using Doxorubicin- and Coenzyme Q10-

liquid crystalline nanoparticles in comparison with intravenous Adriamycin. *Nanomedicine*, 10, 1231-1241 (2014).

285. Swierczewska M., Han H.S., Kim K., Park J.H.and Lee S., Polysaccharide-based nanoparticles for theranostic nanomedicine. *Adv. Drug Deliv. Rev*., 99,70-84 (2016).
286. Tallarida R. J.,Drug synergism: its detection and applications. *J. Pharmacol. Exp. Ther*., 298, 865-872 (2001).
287. Tannock I.F. and Rotin D., Acid pH in tumors and its potential for therapeutic exploitation. *Cancer Res*., 49, 4373-4384 (1989).
288. Taratula O., Schumann C., Naleway M.A., Pang A.J., Chon K.J. and Taratula O., A multifunctional theranostic platform based on phthalocyanine loaded dendrimer for image-guided drug delivery and photodynamic therapy. *Mol. Pharmaceutics*, 10, 3946-3958 (2013).
289. Taylor C. M., Blanchard B. and Zava D. T., Estrogen receptor-mediated and cytotoxic effects of the antiestrogens tamoxifen and 4-hydroxytamoxifen. *Cancer Res*., 44, 1409-1414 (1984).
290. Teo B. M., Hosta-Rigau L., Lynge M. E. and Stadler B., Liposome-containing polymer films and colloidal assemblies towards biomedical applications. *Nanoscale*, 6, 6426-6433 (2014).
291. Thomas T. P., Majoros I., Kotlyar A., Mullen D., Holl M. M. B. and Baker Jr. J. R., Cationic poly(amidoamine) dendrimer induces lysosomal apoptotic pathway at therapeutically relevant concentrations. *Biomacromolecules*, 10, 3207-3214 (2009).
292. Thomas T.P., Huang B., Choi S.K., Silpe J.E., Kotlyar A., Desai A.M., Zong H., Gam J., Joice M., Baker J.R. Jr., Polyvalent dendrimer-methotrexate as a folate receptor-targeted cancer therapeutic. *Mol. Pharmaceutics*, 9, 2669-2676 (2012).
293. Tomalia D. A., Baker H., Dewald J., Hall M., Kallos G., Martin S., Roeck J., Ryder J. and Smith P., A new class of polymers: starburst-dendritic macromolecules. *Polym J*., 17, 117-132 (1985).
294. Tomalia D.A., Brothers II H.M., Piehler L.T., Durst H.D. and Swanson D.R., Partial shell-filled core-shell tecto(dendrimers): A strategy to surface differentiated nano-clefts and cusps. *Proc. Natl. Acad. Sci. U.S.A*., 99, 5081-5087 (2002).
295. Tomalia D.A., Huang B., Swanson D.R., Brothers II H.M. and Klimash J.W., Structure control within poly(amidoamine) dendrimers: size, shape and regio-chemical mimicry of globular proteins. *Tetrahedron*, 59, 3799-3813 (2003).

296. Tomalia D. A., Birth of a new macromolecular architecture: dendrimers as quantized building blocks for nanoscale synthetic polymer chemistry. *Prog. Polym. Sci*., 30, 294-324 (2005).
297. Tomalia D.A., Reyna L.A. and Svenson S., Dendrimers as multi-purpose nanodevices for oncology drug delivery and diagnostic imaging. *Biochem. Soc. Trans*., 35, 61-67 (2007).
298. Tong G., Wang J., Wang R., Guo X., He L., Qiu F., Wang Ge., Zhu B., Zhu X. and Liu T., Amorphous carbon dots with high twophoton fluorescence for cellular imaging passivated by hyperbranched poly(amino amine). *J. Mater. Chem. B*, 3, 700-706 (2015).
299. Toporkiewicz M., Meissner J., Matusewicz L., Czogalla A. and Sikorski A.F., Toward a magic or imaginary bullet? Ligands for drug targeting to cancer cells: principles, hopes, and challenges. *Int. J. Nanomedicine*., 10, 1399-1414 (2015).
300. Torre L. A., Bray F., Siegel R. L., Ferlay J., Lortet-Tieulent J. and Jemal A. Global Cancer Statistics 2012. *CA Cancer J. Clin*., 65, 87-108 (2015).
301. Tran N. Q., Nguyen C. K. and Nguyen T. P., Dendrimer-based nanocarriers demonstrating a high efficiency for loading and releasing anticancer drugs against cancer cells *in vitro* and *in vivo*. *Adv. Nat. Sci.: Nanosci. Nanotechnol*., 4, 045013 (2013).
302. Tripathi R. and Mishra B., Development and evaluation of sodium alginate−polyacrylamide graft−co-polymer-based stomach targeted hydrogels of famotidine. *AAPS PharmSciTech.*, 13, 1091-1102 (2012).
303. Uday S. P., Thiyagarajan D., Goswami S., Adhikari M. D., Das G. and Ramesh A., Amphiphile-mediated enhanced antibiotic efficacy and development of a payload nanocarrier for effective killing of pathogenic bacteria. *J. Mater. Chem. B*, 2, 5818-5827 (2014).
304. Uner M. and Yener G., Importance of solid lipid nanoparticles (SLN) in various administration routes and future perspectives. *Int. J. Nanomedicine*, 2, 289-300 (2007).
305. Vargas H. H., Ballestar E., Saez P. C., Kobbe C. V., Rodriguez I. B., Esteller M., Bueno G. M. and Palacios J., Transcriptional profiling of MCF7 breast cancer cells in response to 5-Fluorouracil: Relationship with cell cycle changes and apoptosis, and identification of novel targets of p53. *Int. J. Cancer*, 119, 1164-1175 (2006).
306. Veeranarayanan S., Poulose A. C., Mohamed M. S., Nagaoka Y., Kashiwada S., Maekawa T. And Kumar D. S., FITC/suramin harboring silica nanoformulations for

cellular and embryonic imaging/anti-angiogenic theranostics. *J. Mater. Chem. B*, 3, 8079-8087 (2015).

307. Ventola C.L., The nanomedicine revolution: part 2: current and future clinical applications. *P T.*, 37, 582-591 (2012).
308. Visser G. W., Gorree G. C., Peters G. J. and Herscheid J. D., Tissue distribution of [18F]-5-fluorouracil in mice: effects of route of administration, strain, tumour and dose. *Cancer Chemother. Pharmacol*., 26, 205-209 (1990).
309. Waite C.L., Sparks S.M., Uhrich K.E. and Roth C.M., Acetylation of PAMAM dendrimers for cellular delivery of siRNA. *BMC Biotechnol*., 9, 38 (2009).
310. Wang H., Zheng L., Peng C., Shen M., Shi X. and Zhang G., Folic acid-modified dendrimer-entrapped gold nanoparticles as nanoprobes for targeted CT imaging of human lung adencarcinoma. *Biomaterials*, 34, 470-480 (2013a).
311. Wang Q., Huang X., Long Y., Wang X., Zhang H., Zhu R., Liang L., Teng P. and Zheng H., Hollow luminescent carbon dots for drug delivery. *Carbon*, 59, 192-199 (2013b).
312. Wei T., Chen C., Liu J., Liu C., Posocco P., Liu X., Cheng Q., Huo S., Liang Z., Fermeglia M., Pricl S., Liang X.J., Rocchi P. and Peng L., Anticancer drug nanomicelles formed by self-assembling amphiphilic dendrimer to combat cancer drug resistance. *Proc. Natl. Acad. Sci. U S A.*, 112, 2978-2983 (2015).
313. Wen S., Liu H., Cai H., Shen M. and Shi X., Targeted and pH-responsive delivery of doxorubicin to cancer cells using multifunctional dendrimer-modified multi-walled carbon nanotubes. *Adv. Healthc. Mater*., 2, 1267-1276 (2013a).
314. Wen S., Li K., Cai H., Chen Q., Shen M., Huang Y., Peng C., Hou W., Zhu M., Zhang G. and Shi X., Multifunctional dendrimer-entrapped gold nanoparticles for dual mode CT/MR imaging applications. *Biomaterials*., 34, 1570-1580 (2013b).
315. Weyermann P., Gisselbrecht J.P., Boudon C., Diederich F. and Gross M., Dendritic iron porphyrins with tethered axial ligands: new model compounds for cytochromes. *Angew. Chem. Int. Ed. Engl*., 38, 3214-3219 (1999).
316. Whitesides G.M.,Nanoscience, nanotechnology, and chemistry.*Small.*, 1, 172-179 (2005).
317. Winne K. D., Seymour L. W. and Schacht E. H., A new amino-masking group capable of pH-triggered amino-drug release. *Eur. J. Pharm Sci.*, 24, 315-323 (2005).
318. Wolinsky J. B. and Grinstaff M.W., Therapeutic and diagnostic applications of dendrimers for cancer treatment. *Adv. Drug Delivery Rev*., 60, 1037-1055 (2008).

319. Wolter K. G., Hsu Y. T., Smith C. L., Nechushtan A., Xi X. G. and Youle R. J., Movement of Bax from the cytosol to mitochondria during apoptosis. *J. Cell Biol.*, 139, 1281-1292 (1997).

320. Wu P., Feldman A. K., Nugent A. K., Hawker C. J., Scheel A., Brigitte V., Pyun J., Frechet J. M. J., Sharpless K. B. and Fokin V. V., Efficiency and fidelity in a click-chemistry route to triazole dendrimers by the copper (i)-catalyzed ligation of azides and alkynes. *Angew Chem. Int. Ed. Engl.*, 43, 3928-3932 (2004).

321. Wu W., Aiello M., Zhou T., Berliner A., Banerjee P. and Zhou S., In-situ immobilization of quantum dots in polysaccharide-based nanogels for integration of optical pH-sensing, tumor cell imaging, and drug delivery. *Biomaterials*, 31, 3023-3031 (2010).

322. Wyllie A. H., Kerr J. F. R. and Currie A. R., Cell death: the significance of apoptosis. *Int. Rev. Cytol*., 68, 251-306 (1980).

323. Xing Q., Yates K., Vogt C., Qian Z., Frost M. C. and Zhao F., Increasing mechanical strength of gelatin hydrogels by divalent metal ion removal. *Sci. Rep.*, 4, 4706 (2014).

324. Xu Y. and Zhao D., Removal of copper from contaminated soil by use of poly(amidoamine) dendrimers. *Environ. Sci. Technol*., 39, 2369-2375 (2005).

325. Yamaoka T., Tabata Y., and Ikada Y., Distribution and tissue uptake of poly(ethylene glycol) with different molecular weights after intravenous administration to mice. *J. Pharm. Sci*., 83, 601-601 (1994).

326. Yang E., Zha J., Jockel J., Boise L. H., Thompson C. B. and Korsmeyer S. J., Bad, a heterodimeric partner for Bcl-XL and Bcl-2, displaces Bax and promotes cell death. *Cell*, 80, 285-291 (1995).

327. Yellepeddi V.K., Kumar A., Maher D.M., Chauhan S.C., Vangara K.K. and Palakurthi S., Biotinylated PAMAM dendrimers for intracellular delivery of cisplatin to ovarian cancer: role of SMVT. *Anticancer Res*., 31, 897-906 (2011).

328. Yiyun C., Tongwen X. and Rongqiang F., Polyamidoamine dendrimers used as solubility enhancers of ketoprofen. *Eur. J. Med. Chem*., 40 ,1390-1393 (2005).

329. Yordanov G., Evangelatov A. and Skrobanska R., Epirubicin loaded to pre-polymerized poly(butyl cyanoacrylate) nanoparticles: preparation and *in vitro* evaluation in human lung adenocarcinoma cells. *Colloids Surf., B*, 107, 115-123 (2013).

330. Yuan F., Dellian M., Fukumura D., Leunig M., Berk D. A., Torchilin V. P. and Jain R. K., Vascular permeability in a human tumor xenograft: molecular size dependence and cutoff size. *Cancer Res.*, 55, 3752-3756 (1995).

331. Yuan X., Wen S., Shen M. and Shi X., Dendrimer-stabilized silver nanoparticles enable efficient colorimetric sensing of mercury ions in aqueous solution. *Anal. Methods*, 5, 5486-5492 (2013).
332. Zhang M., Guo R., Keri M., Banyai I., Zheng Y., Cao M., Cao X. and Shi X., Impact of dendrimer surface functional groups on the release of doxorubicin from dendrimer carriers. *J. Phys. Chem. B*, 118, 1696-1706 (2014).
333. Zhang Y., Thomas T.P., Lee K.H., Li M., Zong H., Desai A.M., Kotlyar A., Huang B., Holl M.M. and Baker J.R. Jr., Polyvalent saccharide-functionalized generation 3 poly(amidoamine) dendrimer-methotrexate conjugate as a potential anticancer agent. *Bioorg. Med. Chem.*, 19, 2557-2564 (2011).
334. Zhao L., Zhu J., Cheng Y., Xiong Z., Tang Y., Guo L., Shi X. and Zhao J., Chlorotoxin-conjugated multifunctional dendrimers labeled with radionuclide 131I for single photon emission computed tomography imaging and radiotherapy of gliomas. *ACS Appl. Mater. Interfaces*, 7, 19798-19808 (2015).
335. Zheng A., Kallio A. and Harkonen P., Tamoxifen-induced rapid death of MCF-7 breast cancer cells is mediated via extracellularly signal-regulated kinase signaling and can be abrogated by estrogen. *Endocrinology*, 148, 2764-2777 (2007).
336. Zhou S., Dou H., Zhang Z., Sun K., Jin Y., Dai T., Zhouc G. and Shen Z., Fluorescent dextran-based nanogels: efficient imaging nanoprobes for adipose-derived stem cells. *Polym. Chem*., 4, 4103-4112 (2013a).
337. Zhou L., Li Z., Liu Z., Ren J. and Qu X., Luminescent carbon dot-gated nanovehicles for pH-triggered intracellular controlled release and imaging. *Langmuir*, 29, 6396-6403 (2013b).
338. Zhu S., Hong M., Zhang L., Tang G., Jiang Y. and Pei Y., PEGylated PAMAM dendrimer-doxorubicin conjugates: *in vitro* evaluation and *in vivo* tumor accumulation. *Pharm. Res*., 27, 161-174 (2010).
339. Zhu J., Zheng L., Wen S., Tang Y., Shen M., Zhang G. and Shi X., Targeted cancer theranostics using alpha-tocopheryl succinate-conjugated multifunctional dendrimer-entrapped gold nanoparticles. *Biomaterials*, 35, 7635-7646 (2014).
340. Zhu J., Xiong Z., Shen M. and Shi X., Encapsulation of doxorubicin within multifunctional gadolinium-loaded dendrimer nanocomplexes for targeted theranostics of cancer cells. *RSC Adv*., 5, 30286-30296 (2015).
341. Zong J., Yang X., Trinchi A., Hardin S., Cole I., Zhu Y., Li C., Muster T. and Wei G., Photoluminescence enhancement of carbon dots by gold nanoparticles conjugated via PAMAM dendrimers. *Nanoscale*, 5, 11200-11206 (2013).